Utilising genetic interaction networks to elucidate the anticancer and diabetogenic activities of statins

By

Cintya Elizabeth del Rio Hernandez

A thesis
submitted to the Victoria University of Wellington
in fulfilment of the requirements for the degree of
Doctor of Philosophy
In Cell and Molecular Biosciences

2022

Abstract

Discovered over 40 years ago, statins are one of the most prescribed drugs in the world that have saved millions of lives. Beyond their main cholesterol-lowering purpose, statins exert anticancer activity. However, statins have also shown diabetogenic action, a major concern because more than 200 million people take statins worldwide. The aim of this thesis is to elucidate the genetic mechanisms, specifically genetic, chemical genetic and conditional interactions, by which statins act on cancer and diabetes.

The target of statins is 3-hydroxy-3-methylglutaryl-CoA reductase (HMGCR), the rate-limiting enzyme in the well characterised mevalonate pathway integral to the synthesis of cholesterol that has several branches at farnesyl diphosphate (FPP) to other outcomes potentially affecting diabetes and cancer. My hypothesis is there are many genetic, chemical genetic and conditional interactions mediating the anticancer and pro-diabetogenic activities of statins. Since defining complex genetics may be achieved by building interactive gene networks utilising genome-wide deletion libraries that do not yet exist in human cells, I used the genetic model Baker's yeast (*Saccharomyces cerevisiae*) in three genetic backgrounds (S288C, UWOPS87-2421, and Y55).

In Chapter 2, genetic and chemical genetic interactions with the mevalonate pathway were investigated via a genome-wide analysis of 25,800 double deletion strains treated with atorvastatin, each lacking a gene in the statin pathway (*HMG1* or *BTS1*) and a second gene in the yeast genome. Atorvastatin-hypersensitive mutants were validated in serial dilution spot assays and examined in the context of a multi-layer network comprising genetic and physical interactions. Functional subnetworks (modules) in the multi-layer network were identified and evaluated for network centrality as well as pathway enrichment, which identified the importance of specific genes mediating actin, ageing, unfolded protein response (UPR) and autophagy. I propose a model whereby deregulated actin may inhibit endocytosis and induce UPR, resulting in autophagic cell death. I also identified combination therapies of statins with other compounds that may enhance the anticancer activity of atorvastatin.

In Chapter 3, genetic and chemical genetic interactions mediating the diabetogenic activity of atorvastatin were investigated via a genome-wide analysis in the background of the established yeast models of anorexia and obesity. I generated 51,600 triple deletion strains, each lacking either the *TGL3* and *TGL4* genes required for triacylglyceride (fat) degradation (the obese model) or the *DGA1* and *LRO1* triacylglyceride synthesis genes (the anorexia model) and a third gene in the yeast genome, and measured growth of these triple deletion strains in the presence and absence of atorvastatin. Atorvastatin-hypersensitive mutants were validated in serial dilution spot assays and examined in the

context of a multi-layer network comprising genetic and physical interactions. Functional subnetworks (modules) in the multi-layer network were identified and evaluated for network centrality as well as pathway enrichment, which confirmed the importance of specific genes involved in ER-to-Golgi vesicle transport, UPR and autophagy as buffering mechanisms in these lipotoxic yeast models. Furthermore, I propose that lipotoxicity itself is a mechanism for atorvastatin-induced insulin resistance. This may occur via accumulation of acetyl-CoA as well as fatty acids and other lipotoxic intermediates that induce insulin resistance. I also identified potential combination therapies of statin with other compounds that may reduce the diabetogenic activity of atorvastatin.

In Chapter 4, conditional genetic and conditional chemical genetic interactions mediating hypoxia-specific mechanisms were investigated to further understand the molecular basis by which atorvastatin could elicit anticancer activity in hypoxic tumours. I screened 12,900 single deletion and 12,900 double deletion strains with a statin-related query gene deletion (*BTS1*) in the presence and absence of hypoxia. Atorvastatin-hypersensitive single and double mutants were validated in serial dilution spot assays and examined in the context of a multi-layer network comprising genetic and physical interactions. Functional subnetworks (modules) in the multi-layer network were identified and evaluated for network centrality as well as pathway enrichment, which identified the importance of specific genes involved in mitophagy and ubiquitination for hypoxia-specific atorvastatin activity. I also identified potential compounds that may specifically enhance the anticancer activity of statins in hypoxic tumours.

In summary, my results comprise a novel integration of methods for characterising complex genetics using methods that include epistasis in genetic effects. My results reveal the genetic, chemical genetic and conditional regulation underlying the anticancer and diabetogenic activity of atorvastatin in yeast that identify novel combination therapies and molecular mechanisms to further investigate in human cells and clinical trials.

Contents

List of Figures

List of Tables

Acknowledgements

It has been a great journey since the day I decided I was going on an adventure. So many challenges to overcome and so many lessons to learn. So many friends to be made and so many helping hands to be offered and received. I am very grateful for all the invaluable experiences I have lived over the past years and for the plentiful help I have received from friends and organisations.

I would first like to thank the New Zealand Cancer Society for the scholarship and the Maurice Wilkins Centre for the funding support to this project, which allowed me to see its completion. I would also like to thank the Faculty Research Strategy Grant committee and the New Zealand Cancer Research Trust for the grants that made my attendance to the Yeast Lipid Conference in Slovenia possible.

I would like to thank my supervisors, Dr Andrew Munkacsi and Professor Paul Atkinson, whose guidance and support was crucial for the completion of this thesis. Andrew, thank you for letting me be part of the Chemical Genetics lab, it has been an honour to belong to such a great group. I really appreciate all I learned from you on how to approach my writing in better ways. Paulito, your input in the computational analyses and your infinite patience throughout my writing was fundamental, and I am sure your thorough reviews have made this thesis something I feel proud of. Also thank you to Dr Melanie McConnell for your advice on reading literature about hypoxia-activated prodrugs and hypoxic vs normal tissue, which helped me to expand my understanding and interpret my data in a more focused way.

I would also like to thank all the people in the Chem Gen lab with whom I have shared so many experiences, victories and defeats. Thank you for your friendship, help and kindness throughout the years. Tim, you being there for the first part of this journey is something I will always cherish, you made me smile every single day I saw you or read a sticky note you had left on my desk. Tamin, you have always been an inspiration to stand and fight against all. I will always appreciate you teaching me what we are capable of. Jeffrey, my little genius, I will be eternally grateful for your help with coding, for saving the day when I had my ‘Latex crises’ and for the silly chats we often had that made the hard days more bearable. Natalie, thank you for all the great memories of our trip to Europe that I will always treasure and for always being so supporting and caring. Joey, you always made me feel that I had a little brother to take care of and I will never forget the great brewing experience. Storm, thank you for being the first one to teach me all I had to know to survive in Chem Gen, I so much enjoyed being your bench neighbour. Dr Woolner, I will always appreciate all the pleasant chats I had with you and that you always had a smile for everyone. Pegah, you always made me feel that someone else understood

how hard it is to be far from home speaking a language that at times seemed so hard to understand. Aidan, all your tips and tricks using the Singer and the DGAT strains certainly made my life easier, and your unconditional help and friendly face will always be remembered. Also a special thank you to the Singer RoToR robot for so many hours of hard work and for the entertaining hours trying to fix you. I can confidently say that without you this project would have been impossible, hand-pinning hundreds of plates would not have been as fun.

I would also like to thank my family and friends for their support and understanding over the years, I know how much I have neglected you, thank you for still being there in my life. Brother, you were a constant reminder that no matter how dark life gets at times, there is always hope. Mom and Javier, you believing in me and your cheerful words sure gave me strength along this journey. Dad, thank you for showing me that it is possible to look for your dreams outside your comfort zone. Mrs. Tere Orea, your excitement from the beginning to the end of this project always made me feel that this was the right decision. Thank you to all other members of the family and my friends in Mexico and the US who also believed this was possible and were constantly cheering me up, cuñado, Almita, Blanquita, Noje, Carlitos, Dianis, Fede, Manihuis, Sinu, Vicky, Marthita, cousins, aunts and uncles, I hope I have made you proud. I am also thankful for having such great friends in New Zealand, Carito, Shona, Sally, Smita, Shailesh, Claudita and Hermes, all those drinks and dinners sure made of this a happy journey. Also thank you to my dearest friends Ilse and Dr Ever Forever for guiding me towards becoming a molecular biologist and Dr Kay Vopel for everything you taught me, I cannot imagine how hard this journey would have been without all I learned from you.

Dedication

This thesis is dedicated to my best friend, soulmate, partner in life and beyond, Christian Morales. Thank you for believing in me and for supporting this crazy decision that I know at times put you in difficult situations. Thank you for making me laugh in the toughest times and for holding me tight when I needed it the most. Above all, thank you for teaching me that life is about collecting memories as this unexpected journey has given me plenty of the greatest kind. I would not be here without you. It's gone, it's done. I found my edge.

Chapter 1

Literature Review

Quoting the pharmacologist and Nobel laureate James Black, “the most fruitful basis for the discovery of a new drug is to start with an old drug” (Raju 2000). Finding novel applications to already existing and commercialised drugs, namely drug repurposing, is a continuously growing field that has the potential for saving years of research time, associated costs and patients’ lives. The discovery of new therapeutic drugs takes between 10 and 17 years from target identification to its placing in the market and often fails to reach this ultimate purpose due to failed clinical trials (Nosengo 2016; Zhang et al. 2020). In fact, only about 5% of the drug molecules that are trialled in phase I of clinical trials are commercialised despite all the years of research and millions invested (Petsko 2010). Drug repurposing is thus an attractive strategy whereby many steps can be bypassed or shortened halving the time of *de novo* discovery and development as well as reducing costs from about $2.5 billion to an estimate of $300 million USD (Bertolini et al. 2015; Nosengo 2016; Zhang et al. 2020).

Repurposing of drugs has brought successful stories over the years, the anticancer therapeutics field included (Pushpakom et al. 2019). Raloxifene, for instance, originally intended to treat osteoporosis, got FDA approval in 2007 for the treatment of breast cancer (Eli Lilly 2007). One group of therapeutics that are currently in clinical trials for their anticancer properties, including phase III trials testing their potential as adjuvants for chemotherapy and improved prognosis are statins (https://clinicaltrials.gov/ct2/results?cond=cancer&term=statin). Statins discovered more than 40 years ago (Endo et al. 1976b) are indicated for hypercholesterolemia and have saved millions of lives by preventing cardiovascular disease since 1994 (Scandinavian Simvastatin Survival Study Group 1994).

One key advantage of drug repurposing is that the toxicity, tolerated doses and adverse effects of the drug being repurposed are well characterised after having passed all phases of clinical trials

and post-marketing drug surveillance. In the case of statins, one of the known risks associated with its consumption is the development of new onset type 2 diabetes (Betteridge and Carmena 2016; Coleman et al. 2008), a risk that the FDA advised inclusion in the product label (FDA 2012). The benefit-risk balance of statins, however, is clearly in favour of its life-saving efficacy in cardiovascular disease and their potential to become anticancer adjuvant therapeutics.

The anticancer and diabetogenic activity of statins are only partially understood and there is a necessity for more research to understand the underlying molecular mechanisms. Cancers are complex (many genes involved) and therapies usually include drug combinations to target multiple pathways that interact (Zhang et al. 2020). To investigate such compensatory pathways, large-scale experimental and computational approaches are used including phenotypic screening, network pharmacology, and signature matching (matching of one drug in combination with another drug based on genomics, proteomics, chemistry, etc.) (Pushpakom et al. 2019).

In this literature review, I will address the current understanding of the mechanisms behind the anticancer and diabetogenic activities of statins, and will describe the experimental and computational approaches used in this thesis to contribute to the elucidation of these mechanisms. Understanding such molecular mechanisms should aid in the identification of combination therapies to enhance the anticancer and reduce the diabetogenic activity of statins.

1.1 Statins have anticancer activity

1.1.1 A brief history of statins

Since its first identification in gallstones in 1769 by Poulletier de la Salle (Dam 1958), cholesterol has captivated the attention of many scientists with 13 Nobel Prizes awarded to major contributions on our understanding towards its synthesis and regulation (Brown and Goldstein 1986). Cholesterol is an essential structural component of all cells and a precursor of important cellular compounds, such as oxysterols, bile acids, lipoproteins and hormones. A connection between atherosclerosis and cholesterol was found in the early 1910's (Anitschkow 1913; Goldstein and Brown 2003) and high levels of cholesterol were linked to heart attacks in the early 1950's (Gofman et al. 1949; Gorman and Lindgren 1950; Gofman 1956), opening a new research field in the search for cholesterol-lowering drugs.

Inspired by the high rates of coronary heart disease in the US, the Japanese biochemist Akira Endo noted the causal effect of too much cholesterol (Endo 2010). Endo sought an inhibitor of the synthesis

of cholesterol, and particularly, of HMG-CoA reductase (HMGCR) (Endo 2008) that had been found to be the rate-limiting enzyme in the mevalonate pathway (Siperstein and Fagan 1966) (Figure 1.1). In 1971, Endo chose to investigate fungi as producers of antibiotics that might target the mevalonate pathway (Endo 2010) and identified the compound 'compactin' isolated from the fungus *Penicillium citrinum*, a potent competitive inhibitor of HMGCR (Endo et al. 1976a; Endo et al. 1976b) (Figure 1.2). Compactin proved to be a potent cholesterol-lowering drug in hens, dogs and monkeys (Endo et al. 1979; Endo 1992), yet only progressed to Phase II clinical trials in 1978-1979 due to safety concerns from side-effects (Endo 2010).

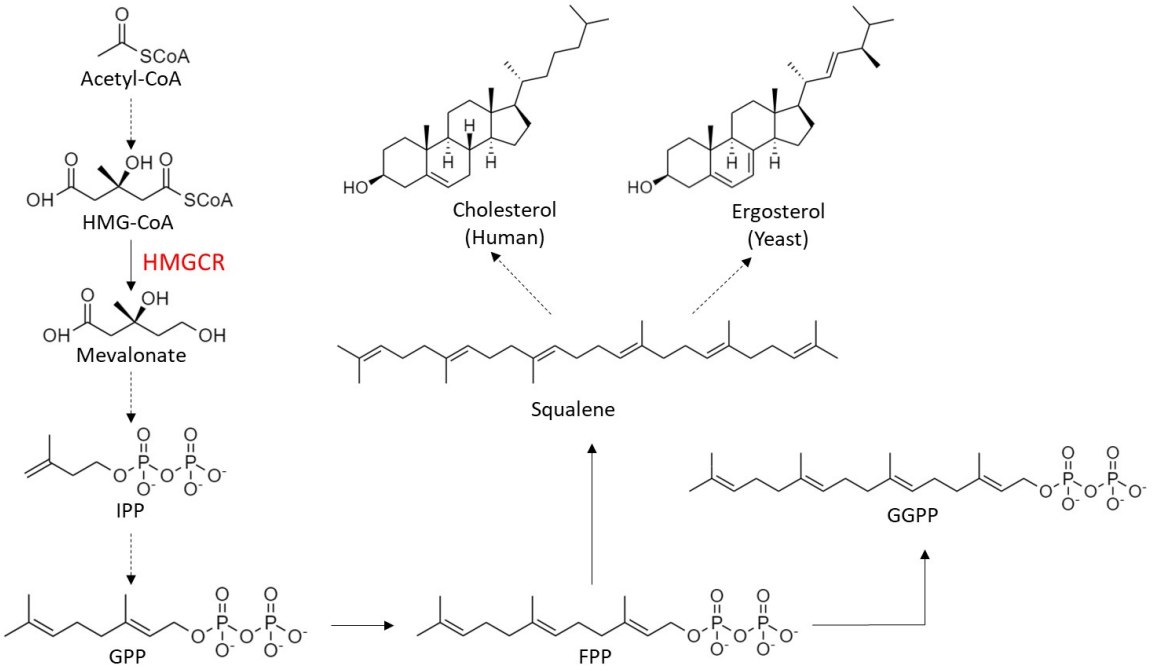

Figure 1.1: **HMGCR is the rate limiting enzyme in the mevalonate pathway.** HMGCR catalyses the formation of mevalonate from HMG-CoA in the mevalonate pathway. The end-product of this metabolic pathway is cholesterol in mammals and ergosterol in yeast.

Around the same time, Alberts and colleagues in an independent study identified lovastatin, which was isolated from *Aspergillus terreus* (Alberts et al. 1980). Lovastatin entered Phase I of clinical trials, but this was also suspended because of safety concerns. Clinical trials resumed in 1984 producing evidence of both efficacy and safety, which resulted in lovastatin being approved by the FDA in 1987 as the first FDA-approved statin (Steinberg 2006).

Discovery of nature-derived statins continued over the years with simvastatin and pravastatin as well as the generation of synthetic statins, fluvastatin, cerivastatin, atorvastatin, rosuvastatin and pitavastatin (Figure 1.2). Except for cerivastatin, which was discontinued due to strong myopathic

adverse effects, all other statins continue to be prescribed worldwide. Atorvastatin, developed in 1985 by Bruce Roth, became the highest-selling drug of all time under the name of Lipitor with yearly sales exceeding $12 billion USD (Wenner Moyer 2010).

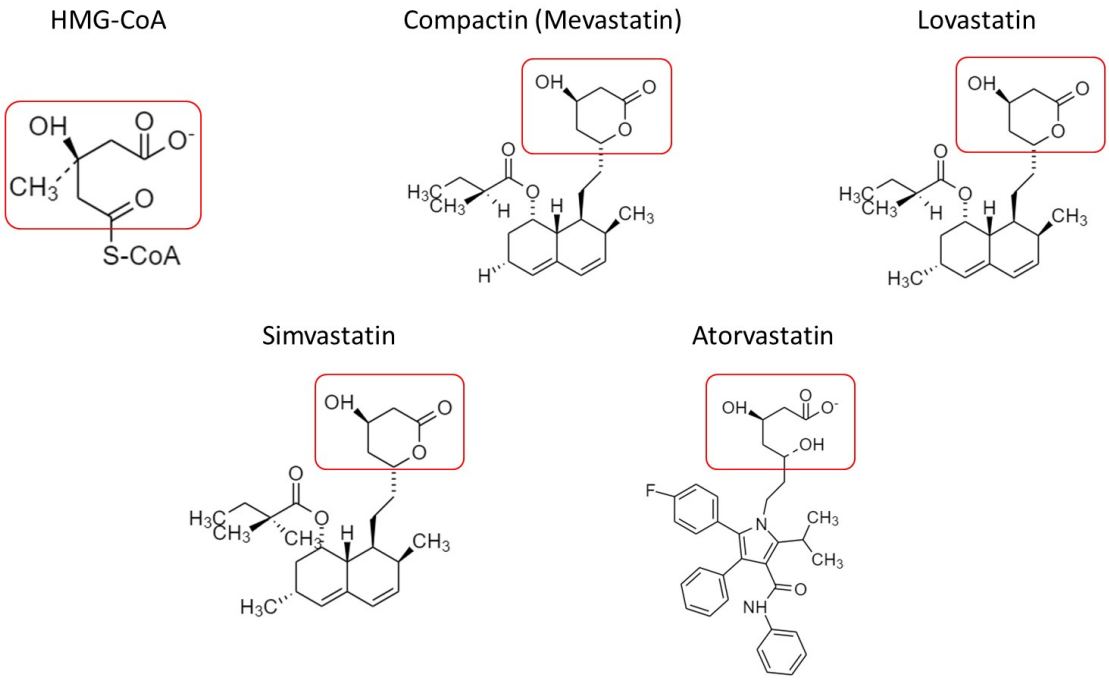

Figure 1.2: **Chemical structure of compactin, lovastatin, simvastatin and atorvastatin.** Statins are competitive inhibitors of HMGCR given its structure similar to that of HMG-CoA as shown inside red squares.

Since the early 1990's, evidence has grown to show that apart from being effective at preventing cardiovascular disease, statins have anticancer properties. The first studies in this regard showed that lovastatin induced growth inhibition and apoptosis in malignant glioma cells (Jones et al. 1994). Simvastatin proved in 1994 to reduce cardiovascular disease-related mortality (Scandinavian Simvastatin Survival Study Group 1994) and reduced cancer deaths by about 25% compared to the placebo group (Pedersen et al. 2000), which was further confirmed in a follow-up analysis (Strandberg et al. 2004). Initial experiments with atorvastatin showed a modest cytotoxic effect in acute myeloid leukaemia cells compared to cerivastatin (Wong et al. 2001), albeit this study was published the same year cerivastatin was retired from the market due to elevated toxicity risks (Furberg and Pitt 2001). More compelling evidence from the anticancer activity of atorvastatin emerged in 2003 where atorvastatin (and other statins) decreased proliferation of breast cancer cells (Seeger et al. 2003) and multiple papers to date have shown its anticancer properties including the sensitisation of lymphoma models to radiotherapy (Kim et al. 2020). Figure 1.3 summarises the history of statins explained in this section.

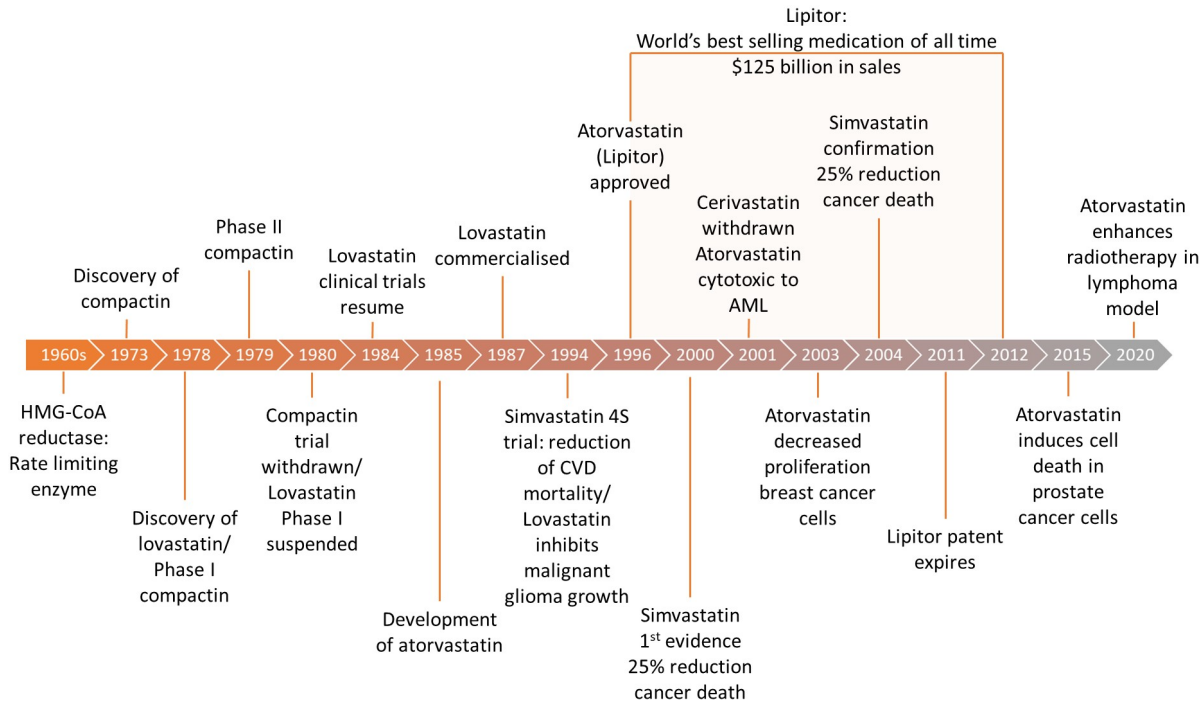

Figure 1.3: **Statins have consistently exhibited cholesterol-lowering and anticancer activities over the years.** First developed in the 1970's, statins quickly proved to be life-saving therapeutics by preventing cardiovascular disease (CVD) and later exhibited potential as anticancer agents. From its approval to the expiry of its patent, atorvastatin under the commercial name Lipitor was considered the world's best-selling medication of all time. AML, acute myeloid leukaemia.

1.1.2 Statins are inhibitors of the mevalonate pathway

As mentioned in the previous section, statins are competitive inhibitors of HMGCR, the enzyme that catalyses the rate-limiting step in the mevalonate pathway (Siperstein and Fagan 1966). However, the mevalonate pathway besides being a well conserved metabolic pathway for the synthesis of cholesterol, it provides the branch points for several other basic pathways such as the biosynthesis of dolichol, ubiquinone and isoprenoids (Figure 1.4).

The mevalonate pathway is an anabolic pathway that starts with the condensation of three molecules of acetyl-CoA (through acetoacetyl-CoA) into HMG-CoA mediated by HMGC-CoA synthase (Rudney and Ferguson 1959) that is coded by HMGCS1 in humans and *ERG13* in yeast (Figure 1.4). It then follows the rate-limiting step of the pathway, the reduction of HMG-CoA into mevalonate (Durr and Rudney 1960), catalysed by the enzyme HMGCR, the target of statins, that is coded by HMGCR in humans and the paralogues *HMG1* and *HMG2* in yeast.

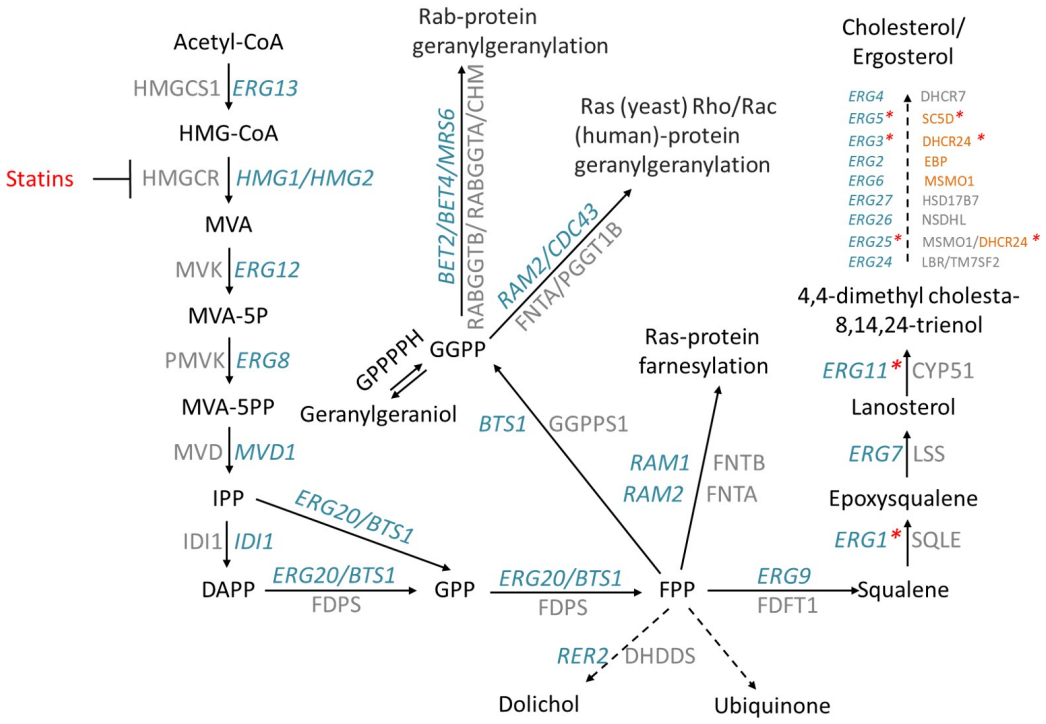

Figure 1.4: **Statins inhibit the synthesis of HMGCR and downstream products in the mevalonate pathway.** Statins are competitive inhibitors of HMGCR encoded by *HMG1* and *HMG2* in yeast and HMGCR in humans. A critical step in the mevalonate pathway is mediated by FPP, where the mevalonate pathway branches off to either the synthesis of cholesterol, isoprenes, dolichol or ubiquinone. Genes in blue are yeast genes and genes in grey are their human orthologues. Red asterisks in yeast genes indicate oxygen-dependent steps of the pathway. Human genes in orange at the end of the cholesterol pathway are less conserved with yeast and do not correspond to the yeast gene to the left.

Mevalonate is then phosphorylated twice through the action of two enzymes. First, the mevalonate kinase coded by MVK in humans and *ERG12* in yeast (Karst and Lacroute 1977; Tchen 1958), phosphorylates mevalonate using ATP as the phosphate donor, producing ADP and mevalonate-5 phosphate. The second phosphorylation is conducted by phosphomevalonate kinase (PMVK in humans, *ERG8* in yeast) (Hellig and Popják 1961; Karst and Lacroute 1977), which uses a second molecule of ATP to transform the mevalonate-5-phosphate into mevalonate-5-diphosphate and ADP (Figure 1.4). The enzyme mevalonate diphosphate decarboxylase (human MVD, yeast *MVD1*) (Bergès et al. 1997; Cherry et al. 2012) then mediates the ATP-dependent decarboxylation of mevalonate-5-diphosphate to form isopentenyl-5-diphosphate (IPP). IPP is then isomerised by the isopentenyl diphosphate isomerase (human IDI1, yeast *IDI1*) (Anderson et al. 1989; Mayer et al. 1992) to form dimethylallyl diphosphate. IPP and dimethylallyl diphosphate are then condensed to form farnesyl diphosphate in a two-step reaction catalysed by the farnesyl pyrophosphate synthase (FDPS in humans, *ERG20* in yeast) (Anderson et al. 1989; Chambon et al. 1991). First, the enzyme condenses

two units of isopentenyl diphosphate and dimethylallyl diphosphate to form geranyl diphosphate followed by a second condensation whereby geranyl diphosphate is condensed with another unit of isopentenyl diphosphate to form farnesyl diphosphate (Figure 1.4).

The steps that follow the synthesis of farnesyl diphosphate are of high importance because FPP is the substrate for numerous enzymes (UniProt Consortium 2021; Kanehisa et al. 2021). The farnesyl diphosphate farnesyltransferase 1 enzyme that is coded by FDFT1 in humans and *ERG9* (Karst and Lacroute 1977; Soltis et al. 1995) in yeast catalyses the reaction to transform FPP into squalene, which is the main branch of the mevalonate pathway, results in the synthesis of cholesterol in humans and ergosterol in yeast (Figure 1.4). If FPP, however, serves as substrate for the enzyme geranylgeranyl diphosphate synthase (GGPPS1 in humans *BTS1* in yeast) (Jiang et al. 1995; Kainou et al. 1999), it is condensed with IPP to form geranylgeranyl diphosphate (GGPP), a key mediator of isoprenylation and a key mediator of the anticancer activity of statins (Pandyra et al. 2015).

Other possible fates of FPP (UniProt Consortium 2021; Kanehisa et al. 2021) are the reaction with the enzyme ditrans,polycis-polyprenyl diphosphate synthase encoded mainly by the yeast gene *RER2* (Nishikawa and Nakano 1993) and the human gene DHDDS (Endo et al. 2003), which leads to the synthesis of dolichol, an important compound involved in the essential modification of proteins known as *N*-glycosylation that has a role in ageing (Bergamini et al. 2004; Chojnacki and Dallner 1988). FPP can also react with *RAM1/RAM2* in yeast and FNTA/FNTB in humans for the farnesylation of Ras GTPase-proteins (Andres et al. 1993; He et al. 1991). Lastly, FPP is transformed into ubiquinone, a precursor of the oxidative phosphorylation through a series of reactions with *COQ* genes in yeast and UBI genes in humans (UniProt Consortium 2021; Stefely and Pagliarini 2017).

1.1.3 Regulation of HMGCR

HMGCR encodes an 888 amino acid enzyme with two domains where the non-catalytic domain is embedded in the ER membrane and the C-terminal end facing the cytosol contains the catalytic unit (Gil et al. 1985; Liscum et al. 1985) (Figure 1.5). HMGCR is regulated by multiple feedback mechanisms at the degradation, transcriptional, and translational level. Although the enzyme is conserved between yeast and humans, its regulation is mediated by different sterol and non-sterol metabolites that are summarised below (Brown and Goldstein 1980; Jo and Debose-Boyd 2010; Roitelman and Simoni 1992).

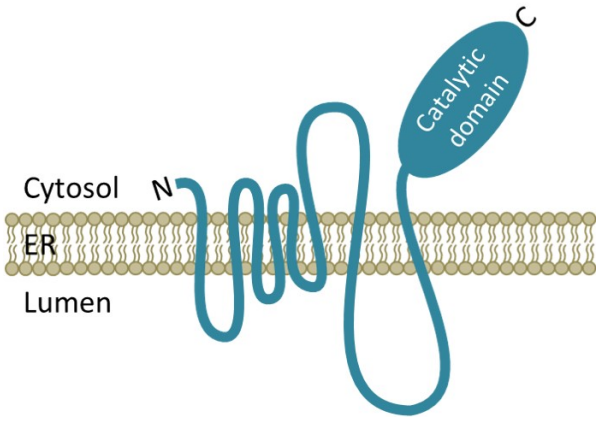

Figure 1.5: **HMGCR is a transmembrane enzyme of the ER.** The enzyme HMG CoA reductase contains two main domains. The non-catalytic domain comprises eight ER-membrane-spanning regions with the N-terminus facing the cytosol while the catalytic domain faces the cytosol on the C-terminal side.

HMGCR degradation regulation in humans

The levels of sterols are sensed by the ER-embedded domain of HMGCR, namely the sterol-sensing domain (Gil et al. 1985; Skalnik et al. 1988). ER-membrane proteins named INSIG1 and INSIG2 (collectively termed as INSIGs) bind to the sterol-sensing domain (Sever et al. 2003) and signal for ubiquitination of cytosolic lysine residues of the catalytic domain via the ubiquitin-conjugating enzyme Ubc7 (Kostova et al. 2007) and the ubiquitin ligase Gp78 (Song et al. 2005). HMGCR is then released from the ER by VCP/p97 and geranylgeraniol, and then delivered to the proteasome for degradation (Inoue et al. 1991) (Figure 1.6).

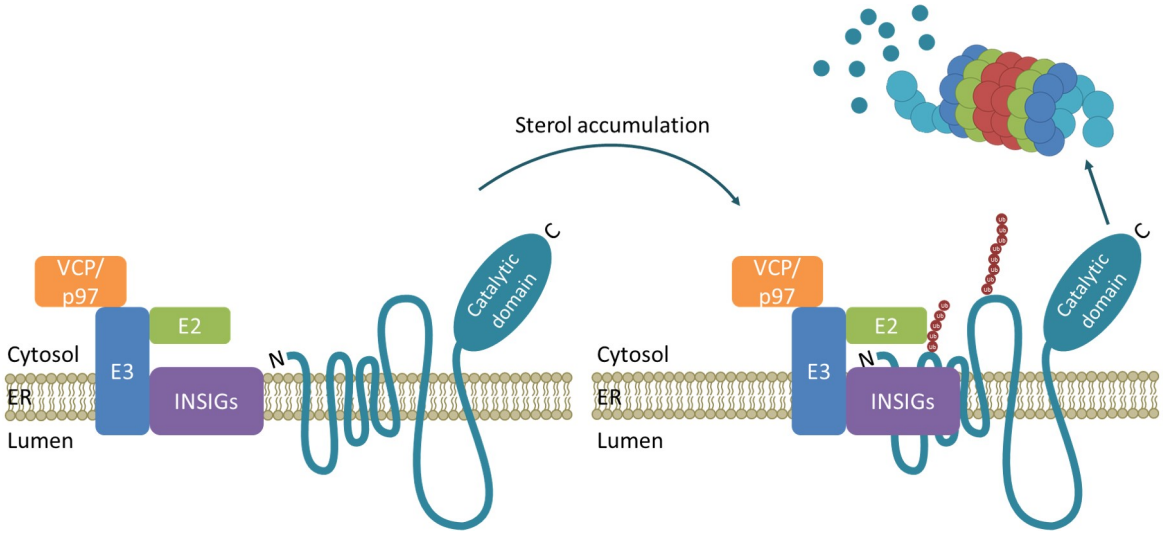

Figure 1.6: **Sterol-mediated and ER-associated degradation of HMGCR in humans.** The signal for degradation of HMGCR in humans is the accumulation of sterols in the cell; this triggers the binding of INSIGs and subsequent ubiquitination of the catalytic domain that tags it for ER-associated degradation (ERAD) by the proteasome.

HMGCR degradation regulation in yeast

In yeast, HMGCR comprises two enzymes and only the isozyme *HMG2* is regulated through ERAD. This degradation is regulated by GGPP and mediated by the E3 ligase Hrd1 and the E2 ubiquitin conjugating enzyme Ubc7 (Figure 1.7). Accumulation of GGPP changes the conformation of Hmg2 and triggers the HRD complex for proteasomal degradation. Accumulation of oxysterols also signals the HRD complex to ubiquitinate Hmg2 (Gardner et al. 2001; Garza et al. 2009). There are no equivalent studies on the regulation of *HMG1* degradation in yeast.

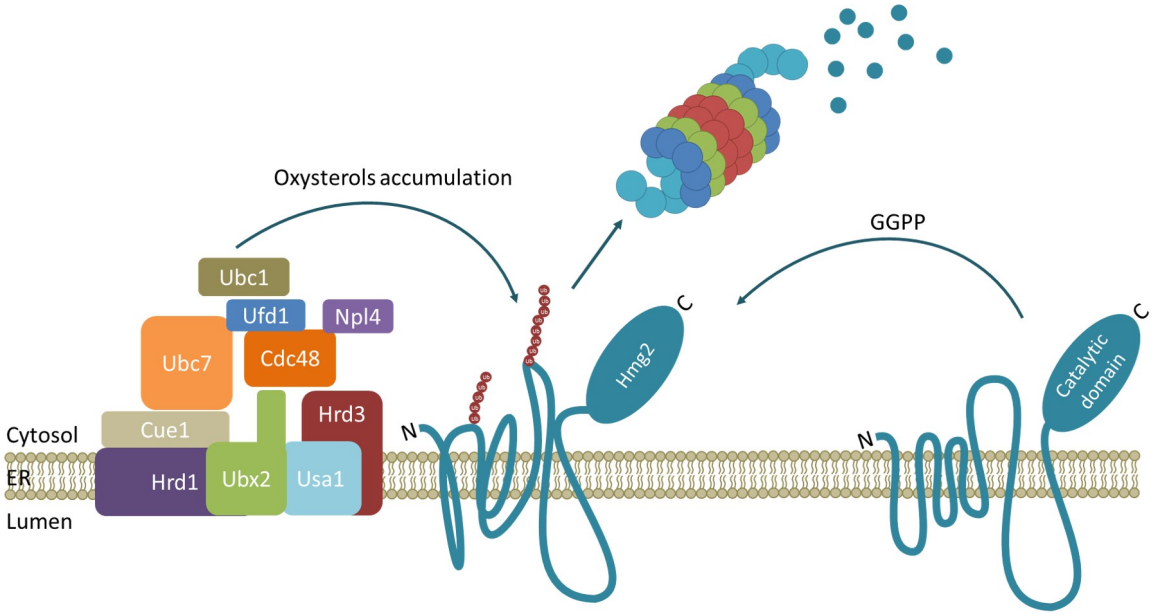

Figure 1.7: **Sterol-mediated HMGCR ERAD in yeast.** Similar to human, HMGCR is ubiquitinated for degradation. Only the isozyme synthesised from *HMG2*, however, is regulated through this pathway. Unlike human regulation, the signals for ubiquitination and degradation are mediated by the accumulation of GGPP and oxysterols.

Regulation of HMGCR transcription in humans

When sterol levels are high, sterol regulatory-element binding proteins (SREBPs) localise to the ER membrane and form a complex with SREBP cleavage-activating protein (SCAP), which has a sterol-sensing domain conserved with that of HMGCR and also binds to INSIGs (Figure 1.8). Sterols maintain the integrity of this complex bound to INSIGs, and SCAP dissociates from INSIGs when sterols are low. This dissociation allows the coat protein complex II (COPII) to bind to SCAP, thus triggering the vesicle-mediated transport of the whole complex (SCAP-COPII-SREBP) to the Golgi membrane. Once translocated, SREBPs are cleaved by the membrane bound transcription factor peptidases, S1P and S2P. The cleaved SREBPs homodimerise and translocate to the nucleus, where they bind to the promoter of HMGCR (and other target genes, such as LDLR and fatty acid synthase)

at the sterol-response elements (SRE) region to initiate its transcription (Amemiya-Kudo et al. 2002; Hua et al. 1993; Yokoyama et al. 1993).

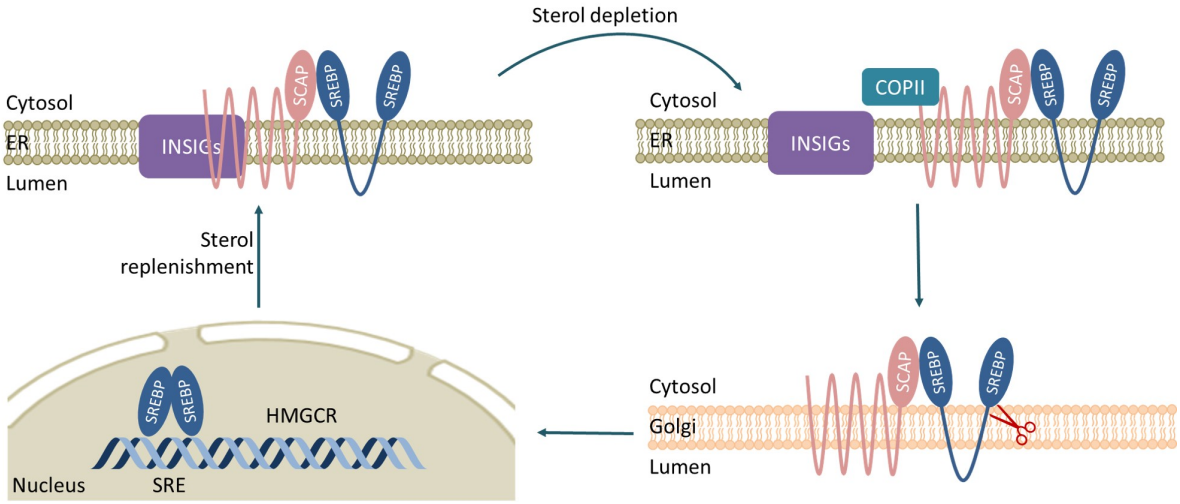

Figure 1.8: **Sterol-mediated HMGCR transcription.** The transcription of HMGCR is mediated by a sterol-sensing system with the participation of INSIGs, SREBPs and SCAP. SREBP dimers bind to the sterol regulatory element (SRE) promoter region to initiate the transcription of HMGCR.

HMGCR transcription regulation in yeast is oxygen-dependent

The feedback inhibition regulation of the synthesis of both yeast paralogues (*HMG1* and *HMG2*) that encode for HMGCR, use different regulators. The predominant paralogue that has more than 80% of the activity under aerated conditions is *HMG1* (Basson et al. 1986). When oxygen is present, the synthesis of heme is promoted and heme activates the transcription factor *HAP1*, which promotes the transcription of *HMG1* (Thorsness et al. 1989) (Figure 1.9).

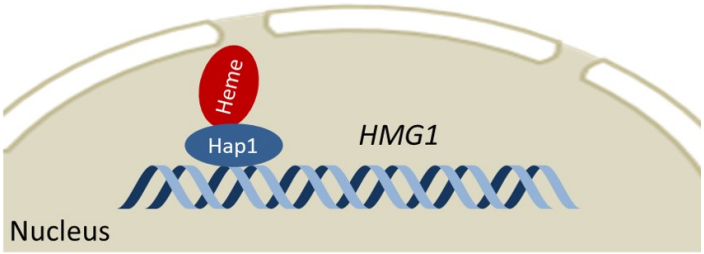

Figure 1.9: **Heme-mediated HMGCR transcription.** Oxygen promotes the synthesis of heme, which in turn activates the transcription factor Hap1 that promotes the transcription of *HMG1*.

In aerated conditions, the expression of *HMG2* is repressed by the Rox1 repressor of hypoxic genes (genes that are differentially expressed in hypoxia). When oxygen is present, Rox1 is expressed through a heme-activated Hap1 mechanism, similar to that of *HMG1* (Figure 1.10). In hypoxia, heme

is no longer synthesised, Rox1 is repressed and thus the hypoxic genes repressed by Rox1, including *HMG2*, are expressed (Thorsness et al. 1989; Zitomer et al. 1997) (Figure 1.10).

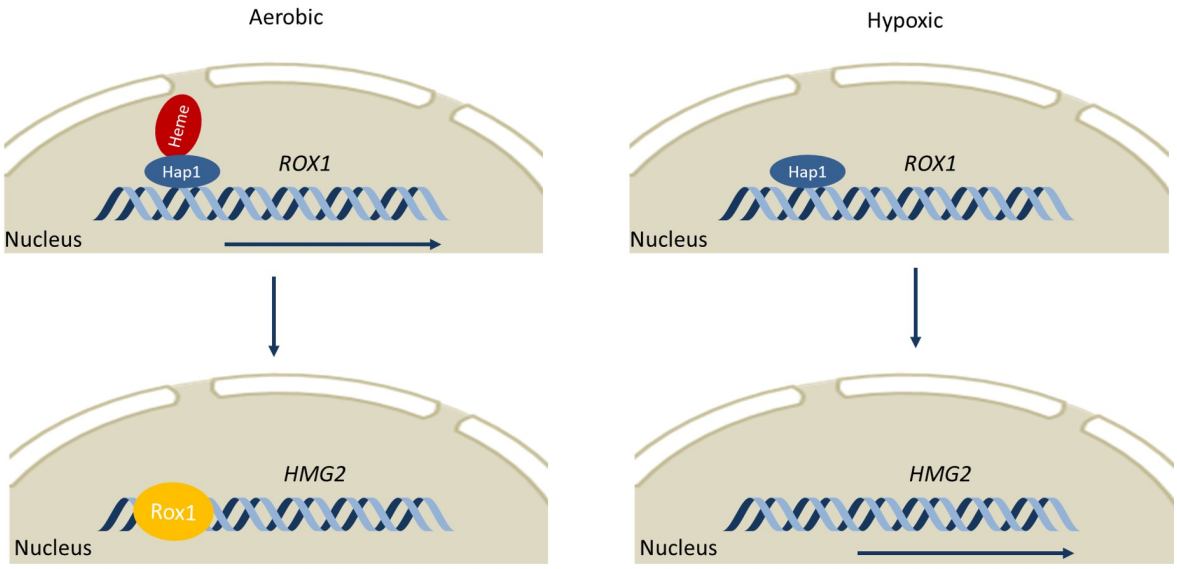

Figure 1.10: **De-repression of *HMG2* in hypoxia.** *ROX1* is a repressor of *HMG2* and its transcription is controlled by heme. In the presence of oxygen, *ROX1* is transcribed and represses the transcription of *HMG2*. As the transcription of *ROX1* is inhibited in hypoxia, it no longer represses the transcription of *HMG2*.

Oxygen-dependent regulation of HMGCR in humans

Humans also have a form of regulation dependent on oxygen, but it is not at the transcriptional level yet rather at the degradation level. The degradation of HMGCR in hypoxia is regulated by two mechanisms in humans. The deprivation of oxygen inhibits demethylation of lanosterol and 24,25-dihydrolanosterol resulting in their accumulation and in the INSIGs-mediated degradation of HMGCR (Nguyen et al. 2007) (Figure 1.11). INSIGs also accumulate due to the hypoxia-inducible factor (HIF1A), the oxygen-sensitive transcription factor that mediates the transcription of many genes in response to hypoxia (Hwang et al. 2017) and these bind to HMGCR to mediate its degradation (Figure 1.11). More detail about the HIF1A-mediated response to hypoxia is given in Section 1.1.6.

Regulation of HMGCR translation in humans

The mechanism by which the translation of HMGCR is regulated in humans is not extensively elucidated but it is known to be inhibited by an isoprenoid (Nakanishi et al. 1988). High dietary cholesterol inhibits the synthesis of HMGCR (Chambers and Ness 1998) as evidenced by accumulation of its mRNA molecules and a low number of associated polysomes (Kandutsch et al. 1978). The regulation of translation also seems to be mediated by oxy-lanosterol as an oxy-lanosterol binding

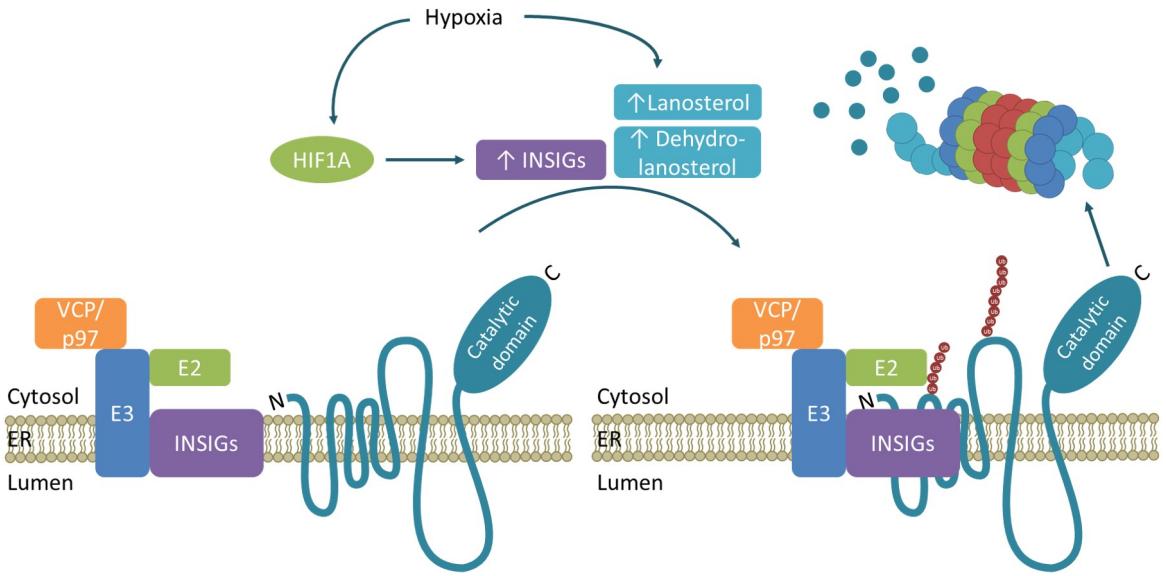

Figure 1.11: **Regulation of human HMGCR in hypoxia.** Hypoxia induces the degradation of HMGCR in humans through accumulation of lanosterol and 24,25-dihydrolanosterol and through the HIF1A-mediated transcription of INSIGs.

protein interfered with polysome loading upon binding with an oxy-lanosterol, thus decreasing the synthesis of HMGCR protein but not its turnover nor the amount of mRNA (Ness et al. 1985; Ness et al. 1998; Ness 2015; Trzaskos et al. 1993; Trzaskos 1995) (Figure 1.12).

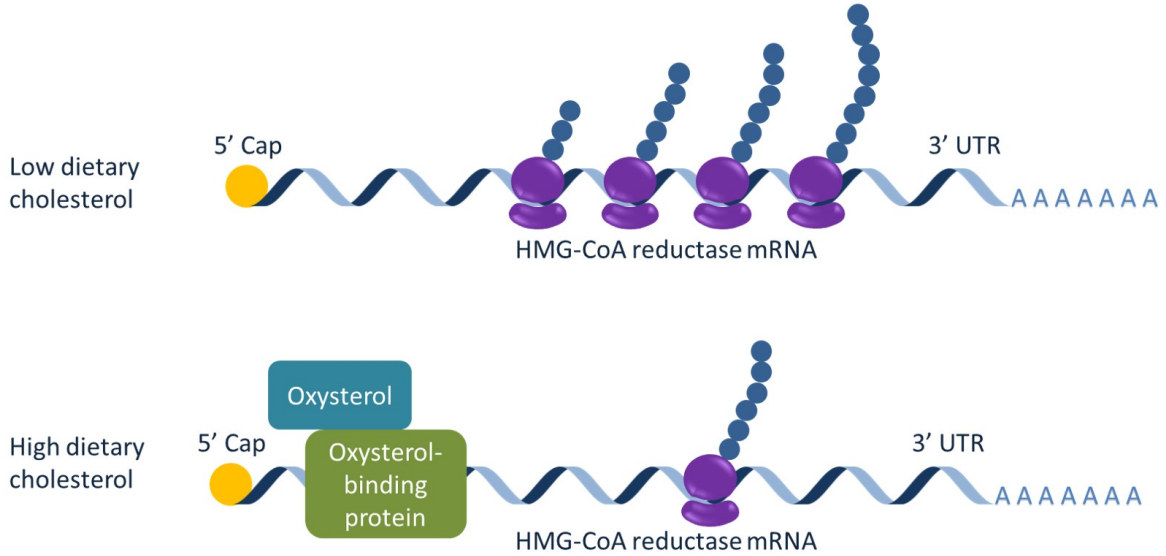

Figure 1.12: **Dietary cholesterol-mediated HMGCR translation.** In low dietary cholesterol conditions, HMGCR is translated. When the diet is high in cholesterol, oxysterols inhibit the translation of HMGCR mRNA likely through reduced binding of ribosomes.

Regulation of HMGCR translation in yeast

At the translational level, only *HMG1* is known to be regulated through a negative feedback mechanism that involves the activity of mevalonate (Dimster-Denk et al. 1994). The mechanism has not been elucidated but depletion of mevalonate increased activity of HMGCR upon mevalonate starvation without affecting the levels of mRNA (Figure 1.13) (Burg and Espenshade 2011).

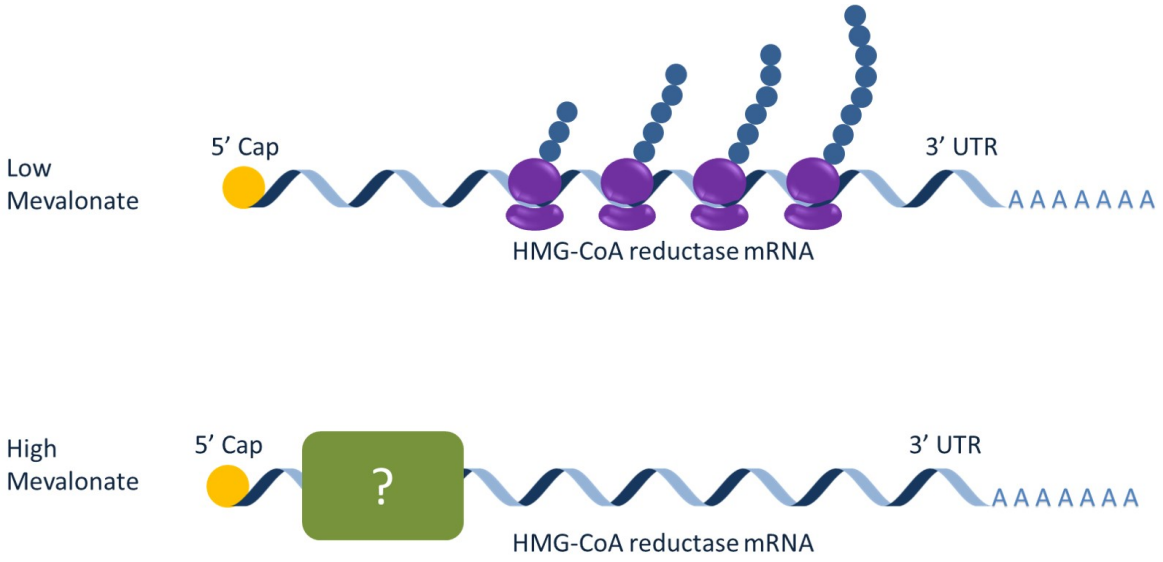

Figure 1.13: **Mevalonate-mediated HMGCR translation.** Similar to translation regulation in humans, yeast regulate translation of HMGCR via the concentration of mevalonate rather than ergosterol.

1.1.4 Statins inhibit proliferation and metastasis of cancer cells

Cancer cells require metabolites from the mevalonate pathway for survival, proliferation and metastasis (Mullen et al. 2016). The levels of cholesterol are elevated in cancer cells potentially protecting them from immune response and hence inhibiting synthesis of cholesterol may render them more vulnerable (Li et al. 2003; Novak et al. 2013). Moreover, elevated levels of IPP activated the response of a specific type of T-cells, namely gamma/delta T cells, which promoted the accumulation of the latter to improve clinical outcomes (Dieli et al. 2007; Meraviglia et al. 2010). FPP and GGPP are essential for tumour survival, for instance, inhibition of the isoprenylation of small GTPases induced apoptosis of cancer cells that was reversed upon addition of GGPP, and under certain conditions, FPP (Wong et al. 2007). Direct inhibition of GGPP, however, was toxic to healthy cells (Cox et al. 2014), emphasising the need to identify drugs for less essential enzyme targets that might inhibit GGPP synthesis in cancer cells. This may be a general strategy governing drug discovery in complex diseases like cancer and may be the reason that existing cancer drugs that are not highly specific have useful

outcomes by indirect mechanisms. As detailed in this chapter, multiple differential points in metabolic pathways could present opportunities for intervention.

There are two other downstream products of FPP that are known to be dysregulated in cancers. One of them is dolichol, which is a precursor of the *N*-glycosylation of newly synthesised peptides and aberrant glycosylation as overexpression and other modifications of glycans have been linked to tumour progression and metastasis (Pinho and Reis 2015). The other one is ubiquinone, a precursor for oxidative phosphorylation that is upregulated in cancer cells and also responsive to chemotherapeutics as a mechanism of defence (Brea-Calvo et al. 2006; Kaymak et al. 2020).

Targeting the mevalonate pathway branch-points to treat cancer is thus a promising area, and despite some studies showing conflicting evidence (Baron 2010; Desai et al. 2018; Wang et al. 2019b), many studies have shown evidence of statins reducing mortality and improving prognosis in different types of cancer such as breast and prostate (Ahern et al. 2011; Boudreau et al. 2014; Chae et al. 2011; Peltomaa et al. 2021; Tan et al. 2016a). Statins are also known to differentially induce apoptosis in other types of cancer including acute myeloid leukaemia, glioblastoma, lung adenocarcinoma (Chou et al. 2019; Dimitroulakos et al. 1999; Yanae et al. 2011). The metabolic processes and pathways by which statins are known to exert anticancer activity are summarised here.

Cancer cells are known to upregulate HMGCR and the mevalonate pathway in general to overexpress metabolites for their own benefit (Mullen et al. 2016). Breast cancer cell lines resistant to atorvastatin and simvastatin treatment, for instance, have shown enhanced SREBP-mediated induction of HMGCR compared to cell lines sensitive to atorvastatin and simvastatin (Göbel et al. 2019). Similarly, prostate cancer cell lines resistant to fluvastatin treatment were overcome by knocking down or silencing SREBPs (Longo et al. 2019).

A canonical pathway in cancer is the PI3K-AKT signalling pathway that is negatively regulated by the phosphatase and tensin homolog PTEN gene, and this pathway is an activator of the mevalonate pathway. PI3K-AKT induces mRNA and protein expression of SREBPs (Fleischmann and Iynedjian 2000; Luu et al. 2012) and prevents their proteasomal degradation (Sundqvist et al. 2005). Downstream to this signalling pathway is mTORC1, which is a mediator of cell growth and proliferation as well as an inhibitor of autophagy. mTORC1 activity is inhibited by AKT, and thus inhibition of AKT activates autophagy. Simvastatin has been shown to suppress PI3K/Akt/mTOR signalling by activating PTEN and dephosphorylating AKT, thus inducing apoptosis and inhibiting cell proliferation of breast cancer cell lines (Wang et al. 2016) (Figure 1.14).

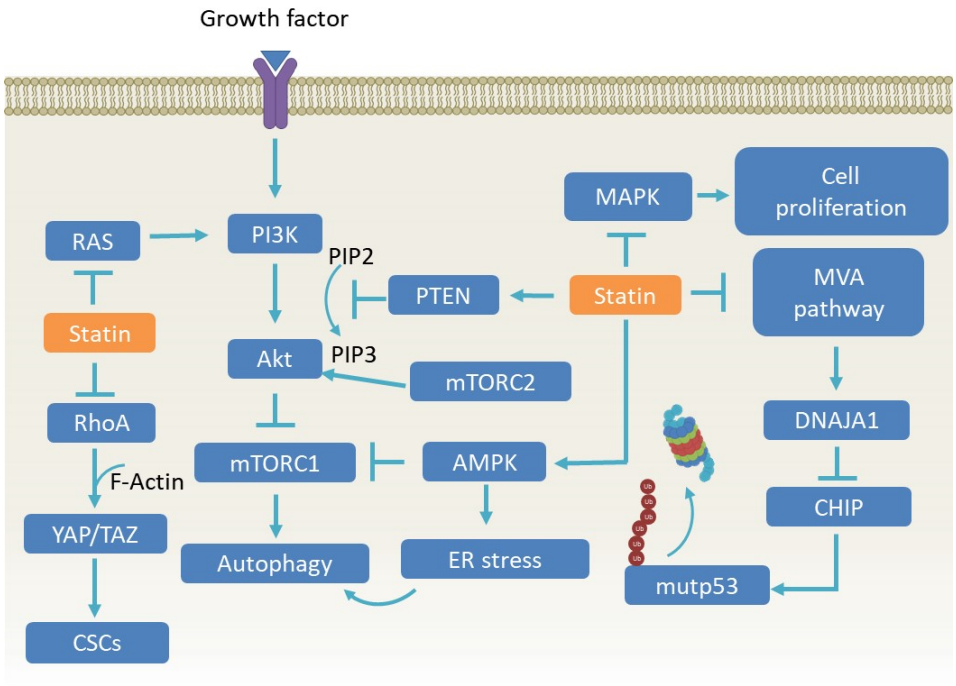

Figure 1.14: **Indirect mechanisms of the anticancer activity of statins may lead to viable drugs.** Statins can exert their anticancer properties through autophagic and apoptotic pathways. Such pathways are activated by inhibition of the mevalonate pathway, such as the prenylation of Ras and Rho GTPases, or inhibition of other metabolic pathways such as MAPK, PI3K/AKT and AMPK signalling pathways.

Atorvastatin also induces the AMPK signalling pathway (Figure 1.14), which in turn induces the expression of p21. This leads to ER stress that can induce autophagy (Yang et al. 2010), meaning the concentrations of drugs could be lessened to offset toxicity. The combination therapy with an inhibitor of autophagy, bafilomycin A1, enhanced the cytotoxic and apoptotic effect of atorvastatin (Yang et al. 2010). Fluvastatin has also been found to inhibit the mTOR pathway through activation of AMPK (Okubo et al. 2020), which enhanced the anticancer activity of vorinostat, a histone deacetylase inhibitor with a mechanism of action that includes mTOR pathway activation.

Another known mechanism for the anticancer activity of statins is apoptosis via the tumour-suppressor gene p53, which is the most commonly mutated gene in cancer (Brosh and Rotter 2009). In fact, repression of the mevalonate pathway suppresses p53 (Moon et al. 2019). Simvastatin, for instance, increased apoptosis and inhibited cell growth of mutant p53 lung cancer cells via the promotion of p53 degradation (Chou et al. 2019). Furthermore, some mutations in p53 upregulate the mevalonate pathway and treatment with rosuvastatin of p53 gain-of-function mutant animal models with clinically advanced T-cell lymphoma showed antitumour activity. This effect was not seen in a model expressing a different mutation nor in mice lacking p53 (Tutuska et al. 2020). Additionally, mevalonate kinase (Figure 1.4) inhibited degradation of mutant p53 and stabilised this oncogene (Parrales et al.

2016). Together, these results led to the hypothesis that statins induce degradation of mutant p53 (Freed-Pastor and Prives 2016) (Figure 1.14).

The MAPK signalling pathway has also been proposed as part of the anticancer mechanism of statins (Figure 1.14). Statins inhibit MAPK signalling which in turn inhibits cancer cell proliferation (Chang et al. 2013; Wang et al. 2016). Further, inhibited prenylation of RhoA GTPases leads to inhibition of the F-actin dependent transcriptional regulators YAP and TAZ (Zanconato et al. 2016), which mediate tumour initiation, growth, metastasis and chemoresistance and have a particular role in stemness and self-renewal of tumours.

1.1.5 Clinical trials prove the potential of statins as a therapeutic against cancer

There are nearly 150 active clinical trials investigating the use of statins to treat cancer (https://clinicaltrials.gov/ct2/results?cond=cancer&term=statin) (Table 1.1). Of the clinical trials that have published results, statins have proven beneficial in treating prostate cancer (NCT01821404, NCT01992042), colorectal cancer (NCT02026583), and have shown general cancer prevention (NCT00110448). Atorvastatin decreased the levels of serum and prostatic lipids that are essential for the adaptation of prostatic cells to hypoxia (NCT01821404) (Raittinen et al. 2020). Fluvastatin treatment prior to radical prostatectomy was associated with apoptosis of prostate cancer cells (NCT01992042) (Longo et al. 2020). Simvastatin improved efficacy of chemotherapy in patients with metastatic colorectal cancer (NCT02026583) (Kim et al. 2019). In a follow-up study of a clinical trial investigating the effect of aspirin on the prevention of atherosclerosis in Japanese patients with type 2 diabetes (NCT01821404), an association between the use of statins and a decreased incidence and mortality of cancer was identified (Okada et al. 2021). Statins, however, seem to not exert enhanced anticancer activity in patients with advanced cancer. For instance, simvastatin had no effect on capecitabine-cisplatin treatment in patients with advanced gastric cancer (NCT01099085) (Kim et al. 2014) and combination of pravastatin with sorafenib did not improve survival in advanced hepatocellular carcinoma patients (NCT01075555) (Jouve et al. 2019). More studies are needed as no statin therapy against cancer has been approved to date.

Clinical trial	Title	Status	Conditions	Statin or combination	Phases	Last Update Posted
NCT00433498	Etoposide and Cisplatin or Carboplatin as First-Line Chemotherapy With or Without Pravastatin in Treating Patients With Small Cell Lung Cancer	Completed	Lung Cancer	Pravastatin + Etoposide and Cisplatin or Carboplatin	Phase 3	3/12/2014
NCT01075555	Sorafenib Tosylate With or Without Pravastatin in Treating Patients With Liver Cancer and Cirrhosis	Completed	Liver Cancer	Pravastatin + sorafenib tosylate	Phase 3	30/3/2020
NCT01099085	Trial of XP (Capecitabine/CDDP) Simvastatin in Advanced Gastric Cancer Patients	Completed	Gastric Cancer	Simvastatin	Phase 3	17/2/2017
NCT01821404	Atorvastatin Before Prostatectomy and Prostate Cancer (ESTO1)	Completed	Prostatic Neoplasms	Atorvastatin	Phase 2	7/5/2018
NCT01903694	Randomized Trial Sorafenib-Pravastatin Versus Sorafenib Alone for the Palliative Treatment of Child-Pugh A Hepatocellular Carcinoma	Completed	Child-Pugh A Hepatocellular Carcinoma	Pravastatin + Sorafenib	Phase 3	13/5/2014
NCT01992042	Novel Window of Opportunity Trial to Evaluate the Impact of Statins to Oppose Prostate Cancer	Completed	Prostate Cancer	Fluvastatin + Pimonidazole	Phase 2	26/10/2017
NCT02026583	A Single Arm, Phase II Study of Simvastatin Plus XELOX and Bevacizumab as First-line Chemotherapy in Metastatic Colorectal Cancer Patients	Completed	Colorectal Cancer	Simvastatin	Phase 2	17/1/2018
NCT02201381	Study of the Safety, Tolerability and Efficacy of Metabolic Combination Treatments on Cancer	Not yet recruiting	Cancer Overall Survival	Atorvastatin	Phase 3	10/2/2021
NCT03024684	Statin for Preventing Hepatocellular Carcinoma Recurrence After Curative Treatment	Recruiting	Hepatocellular Carcinoma	Atorvastatin	Phase 4	9/6/2020
NCT03134157	The Effect of Simvastatin on Uterine Leiomyoma Development and Growth in Infertile Women	Recruiting	Infertility	Simvastatin (benign tumour)	Phase 3	6/10/2020
NCT03819101	Trial of Acetylsalicylic Acid and Atorvastatin in Patients With Castrate-resistant Prostate Cancer	Not yet recruiting	Prostate Cancer	Atorvastatin + Acetylsalicylic acid	Phase 3	28/1/2019
NCT03971019	Survival Benefits of Statins in Breast Cancer Patients	Recruiting	Breast Cancer Female	Simvastatin, Atorvastatin	Phase 3	14/8/2019
NCT04026230	Impact of Atorvastatin on Prostate Cancer Progression During ADT	Recruiting	Metastatic Prostate Cancer Recurrent Prostate Cancer	Atorvastatin	Phase 3	11/9/2019
NCT04385433	A Comparative Study of Pravastatin vs Placebo as Primary Prevention of Severe Subcutaneous Breast Fibrosis in Hyper-radiosensitive Identified Patients With Breast Cancer	Recruiting	Breast Cancer	Pravastatin	Phase 3	2/2/2021
NCT04601116	The MASTER Study (MAmmary Cancer STatin ER Positive Study)	Recruiting	Breast Cancer Female|Estrogen Receptor Positive Tumor	Atorvastatin	Phase 3	14/1/2021
NCT04705909	Efficacy of Statin Addition to Neo-adjuvant Chemotherapy Protocols for Breast Cancer	Not yet recruiting	Breast Cancer	Pitavastatin	Phase 2/ Phase 3	12/1/2021
NCT04776889	The Prognosis of Lipid Reprogramming With Rosuvastatin, in Castrated Egyptian Prostate Cancer Patients	Completed	Prostate Cancer Metastatic	Rosuvastatin	Phase 4	2/3/2021

Table 1.1: **Active and recently completed clinical trials testing the anticancer activity of statins.**

1.1.6 Hypoxic tumours prevent success of anticancer therapeutics

Drugs that progress past phase I clinical trials that assess toxicity will largely fail due to lack of efficacy (Petsko 2010). In advanced anticancer clinical trials where thousands of people are subjected to the treatment, treatments can be effective for some yet modest to not effective in many other people and this is due to the complex biology behind cancer, individual genetic variability and environmental effects.

The tumour microenvironment, for instance, is influenced by many factors and one such factor is tumour hypoxia. Hypoxia, the low availability of oxygen, confers resistance of some tumours to chemo- and radio-therapy. This has led to efforts to identify combination therapies that sensitise hypoxic tumours through alleviating hypoxia or become differentially expressed in hypoxia such as hypoxia-activated prodrugs (Diepart et al. 2012; Gallez et al. 2017; Graham and Unger 2018; Kelly et al. 2014; Zeman et al. 1986). Hypoxia decreases drug penetration because most anticancer therapeutics diffuse through capillaries. The principal mediator of the response to hypoxia in mammalian cells is the HIF family of hypoxia-inducible transcription factors, mainly of HIF1A (Semenza 2010). HIF1A is degraded through the ubiquitin-proteasome system in aerobic conditions. In hypoxia, HIF1A promotes the transcription of genes such as INSIGs, involved in cell proliferation, apoptosis and migration (Figure 1.15).

Moreover, the unfolded protein response (UPR) and mTOR pathways are oxygen-sensitive mediators of the hypoxic response of tumours (Wouters and Koritzinsky 2008) that interact with HIFs to promote tumour growth and survival (Figure 1.16). Interestingly, all three mechanisms of coping with hypoxia (HIF1A, mTOR and UPR) converge on autophagy (Daskalaki et al. 2018). Hypoxia inhibits mTOR through a number of pathways that promote both tumourigenesis and treatment resistance of advanced tumours (Wouters and Koritzinsky 2008). Inhibition of mTOR has two main outcomes in hypoxic tumours. It downregulates proapoptotic factors thus conferring increased survival of tumour cells and resistance to anticancer treatments (Erler et al. 2004) and it activates autophagy possibly conferring survival of hypoxic tumours (Tan et al. 2016b). Overall, hypoxia causes proteins to be misfolded because protein folding is dependent on oxygen, but the exact mechanism by which UPR mediates cell survival of hypoxic tumours has been poorly characterised (Chipurupalli et al. 2019).

Statins have been linked to the enhanced response of hypoxic tumours to anticancer treatments (Alupei et al. 2014; Chen et al. 2017; Zhou et al. 2016). The cytotoxic activity of statins in melanoma, for instance, has been linked to inhibition of HIF1A (Alupei et al. 2014) and atorvastatin

inhibits hypoxia-induced radiosensitivity in prostate cancer cells by inhibition of HIF1A expression (Chen et al. 2017). Statins have also been shown to ameliorate hypoxia-induced resistance to the chemotherapeutic sorafenib by enhancing the apoptotic activity of sorafenib in hepatocyte xenograft tumour growth (Zhou et al. 2016).

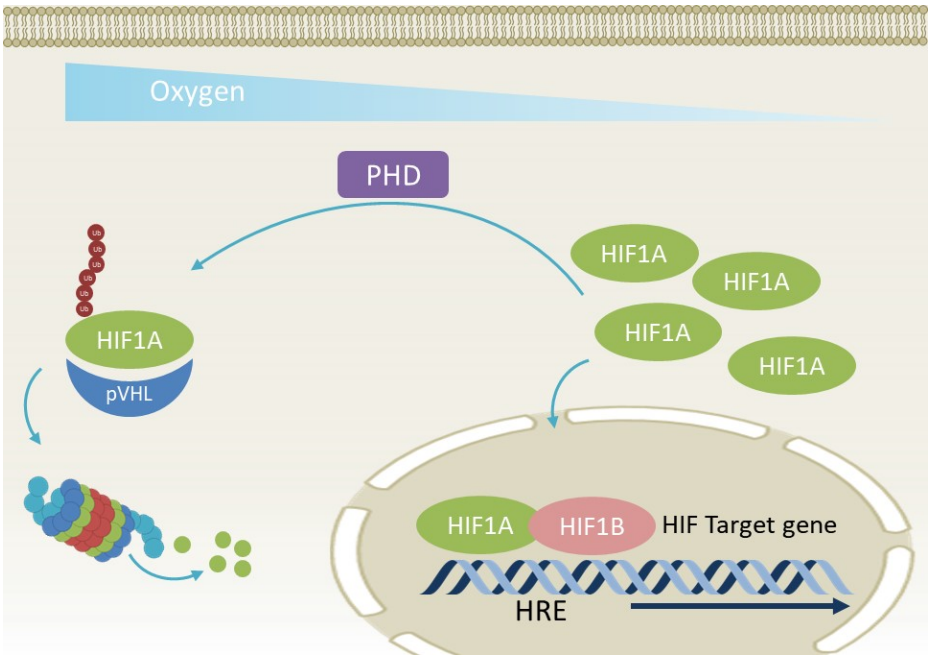

Figure 1.15: **HIFs mediate the genetic response to hypoxia.** In the presence of oxygen, the hydroxylation of HIF1A by prolyl-4-hydroxylases (PHD) signals the von Hippel–Lindau tumour suppressor protein (pVHL) and recruits an E3 ubiquitin ligase for ubiquitination and degradation via the proteasome. In hypoxia, the PHD-hydroxylation of HIF1A is inhibited, resulting in the accumulation of HIF1A, which then translocates to the nucleus, dimerises with HIF1B and binds to the hypoxia-response element (HRE) region to initiate the transcription of HIF target genes (Jing et al. 2019; Semenza 2010) that are involved in cancer cell proliferation, apoptosis and migration.

1.2 Statins have diabetogenic activity

1.2.1 Inhibition of the mevalonate pathway impairs β-cell function and promotes insulin resistance

All therapeutic drugs must have benefits that outweigh the risks. In the case of statins, one of the main risks is the increased incidence of new-onset type 2 diabetes (Betteridge and Carmena 2016; Coleman et al. 2008). In 2012, the FDA published a safety update that required potential increases in glycosylated haemoglobin and fasting serum glucose levels to be included in statin product labels (FDA 2012). The mechanisms behind this diabetogenic activity are not fully understood, yet it is a valid concern as this has been shown to be dose-dependent (Preiss et al. 2011) and correlated with patients

that are already at risk for metabolic syndrome (Waters et al. 2013).

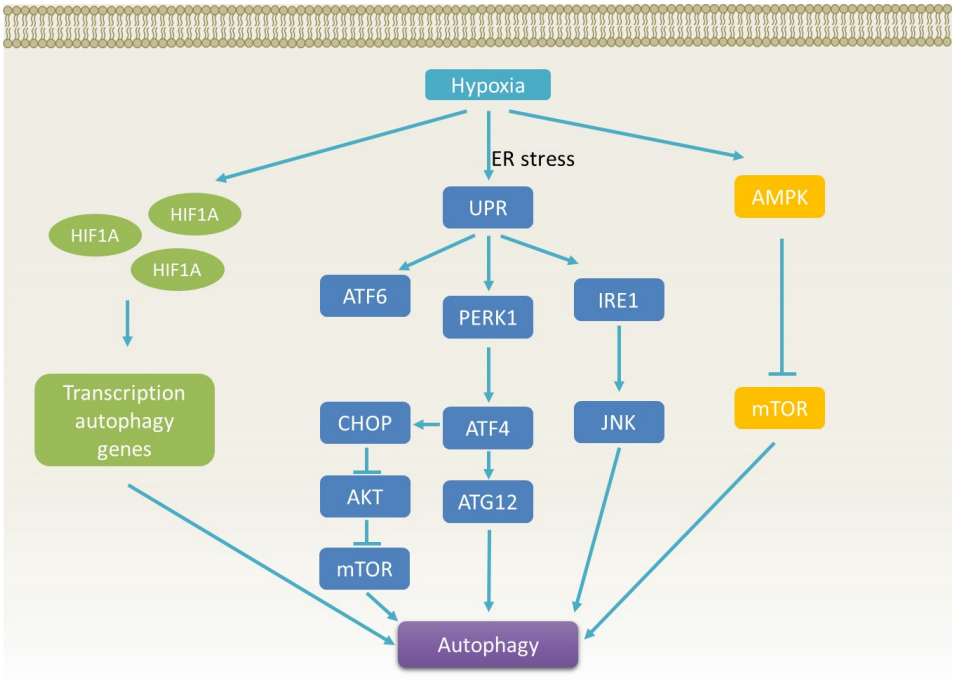

Figure 1.16: **Mechanisms of hypoxia-mediated autophagy.** Hypoxia induces three main pathways that converge on autophagy that likely confers tumour survival through the elimination of toxic metabolites. Hypoxic induction of HIF1A promotes the transcription of autophagic genes. Hypoxia induces ER stress thereby activating the UPR that induces autophagy through the activation of PERK1 and IRE1 pathways. Autophagy is also induced through the activation of AMPK and subsequent inhibition of the mTOR pathway.

There are generally two mechanisms that have thus far been elucidated for the diabetogenic activity of statins. The first mechanism would be disrupted abundance and localisation of insulin receptors due to statins impacting the sites in the membrane where insulin receptors localise, which leads to impaired translocation of the glucose transporter GLUT4 as well as insulin resistance in skeletal and adipose tissue. The second mechanism would be mediated by the inhibition of the glucose transporter GLUT2 and depolarisation of the membrane that impairs the pancreatic β-cell function (Betteridge and Carmena 2016).

More specifically, statins inhibit the insulin receptor substrate 1 (IRS-1) through activation of the NLRP3 inflammasome (Henriksbo et al. 2014), resulting in increased insulin resistance (Figure 1.17). Similarly, inhibited isoprenylation of proteins by the Rab and Rho complexes may impair the translocation of GLUT4. As explained before, statins suppress the PI3K/AKT pathway by activating PTEN (Wang et al. 2016). Statins also inhibit p85 and p110, mediators of the PI3K/AKT pathway (Betteridge and Carmena 2016).

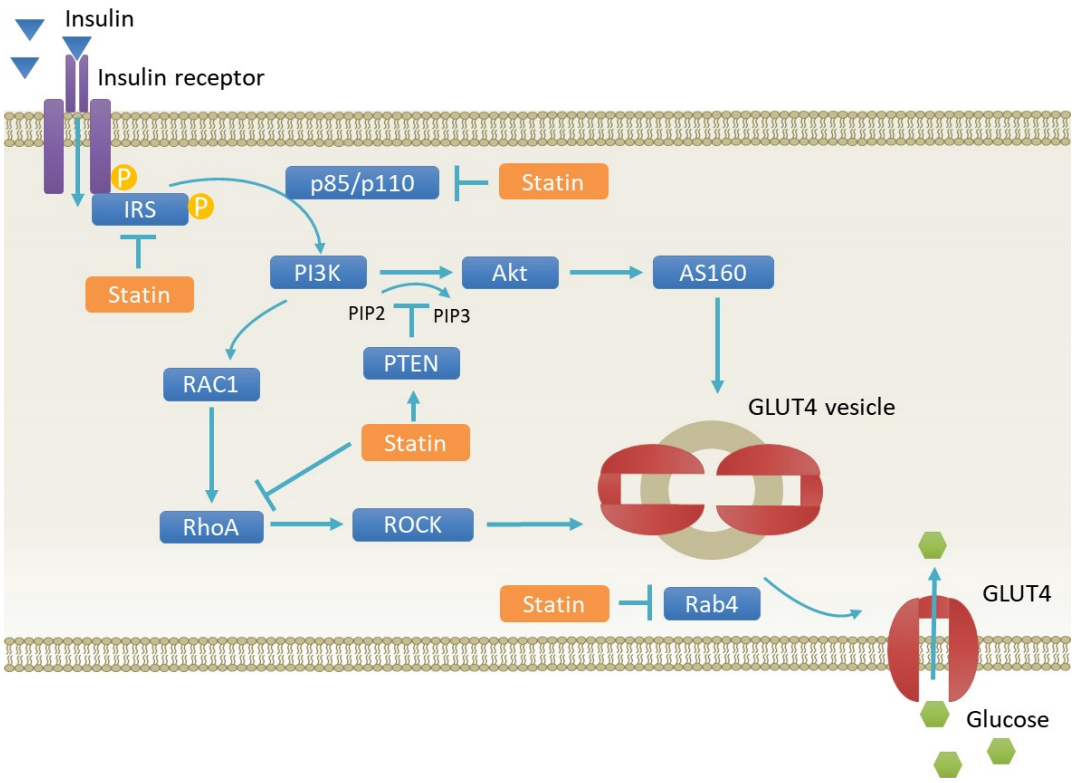

Figure 1.17: **Mechanisms of insulin resistance in skeletal muscle and adipose tissue.** Statin-mediated insulin resistance in skeletal and adipose cells is largely due to inhibition of the isoprenylation of Rab and Rho GTPases that translocate the glucose transporter GLUT4 and also due to inhibition of PI3K/AKT pathway upstream of GLUT4 translocation to the cellular membrane.

β-cell function impairment and apoptosis are caused by deregulated membrane depolarisation and calcium influx, which in turn inhibits insulin secretion. In normal conditions, glucose enters the cell through GLUT2 to undergo glycolysis, the TCA cycle and oxidative phosphorylation for production of ATP (Figure 1.18). The increased ATP/ADP ratio in the β-cells leads to the closure of K^+ channels, the accumulation of K^+, the depolarisation of the membrane opening Ca^{2+} channels, and an overall increase in Ca^{2+} that triggers insulin secretion (Betteridge and Carmena 2016).

Similarly, statins inhibit the synthesis of GLUT2, resulting in decreased glucose uptake (Zhou et al. 2014). In addition to statins inhibiting membrane depolarisation and calcium influx, statins inhibit the synthesis of ubiquinone and subsequently oxidative phosphorylation capacity in β-cells (Betteridge and Carmena 2016; Larsen et al. 2013). Furthermore, because statins inhibit isoprenylation of small GTPases required for exocytosis of insulin granules (Metz et al. 1993), this has also been proposed as another mechanism for the impairment of β-cells (Betteridge and Carmena 2016).

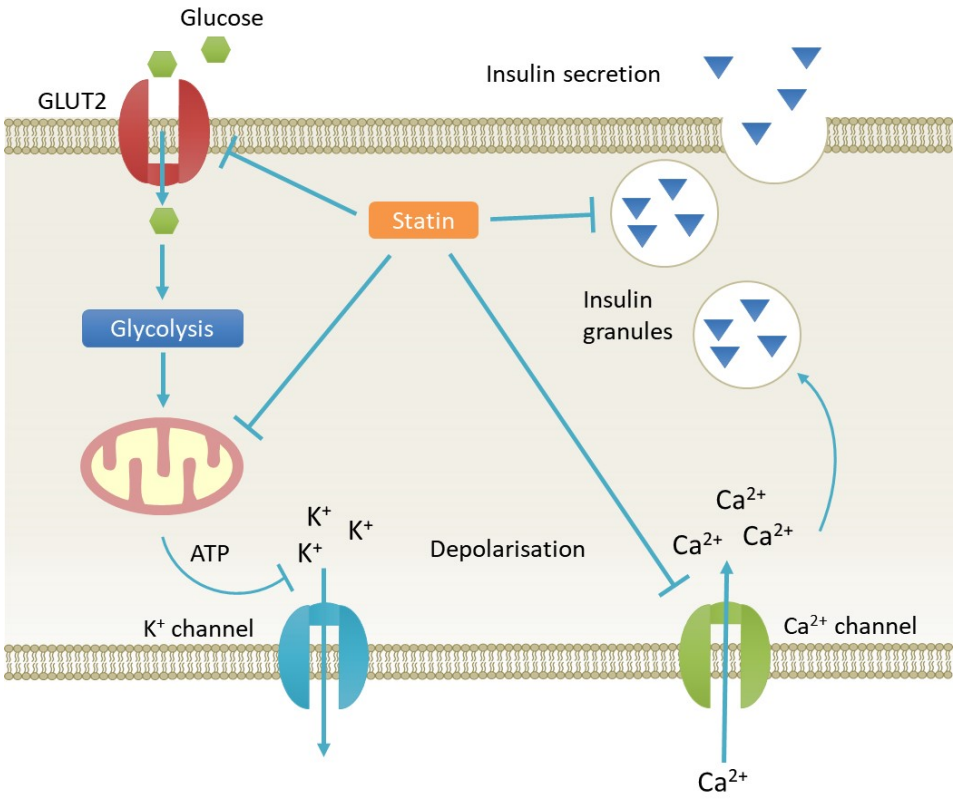

Figure 1.18: **Mechanisms of β-cells impairment by statins.** Statins impair β-cells through inhibiting the synthesis of the glucose transporter GLUT2, inhibiting the synthesis of ubiquinone decreasing the mitochondrial respiration capacity, disrupting membrane depolarisation, and inhibiting calcium influx and the exocytosis of insulin.

1.2.2 Lipotoxicity may have a role in statin-induced insulin resistance

In summary, the reasons thus far known that contribute to the diabetogenic activity of statins are either insulin resistance or β-cell impairment followed by apoptosis. Interestingly, both insulin resistance and β-cell dysfunction impairment have been linked previously to lipotoxicity. Roger Unger coined the term lipotoxicity in 1994, while studying free fatty acid dysregulation in the pathogenesis of obesity and type 2 diabetes in rats. When the cell is no longer capable of storing excess lipids in lipid droplets, this causes circulating fatty acids to accumulate in non-adipose tissue and become toxic (Lee et al. 1994; Unger 1995). Long-chain non-esterified fatty acids can also be stored in the form of triacylglycerides and thus accumulation of intermediates such as diacylglycerides and ceramides can also become toxic (Engin 2017). Fatty acids are oxidised in the mitochondria and insufficient oxidation that leads to increased lipid content has been linked to insulin resistance (Hegarty et al. 2003; Kelley and Simoneau 1994).

The use of statins has been linked to large lipid droplets in non-adipose tissue in humans (Phillips

2002) and shown to inhibit the lipid droplet-associated protein PLIN5 (Langhi et al. 2014). Some studies, however, have shown no effect of statins on the oxidation of fatty acids (Chung et al. 2008; Head et al. 1993), whereas others have shown lipid oxidation impairment (Fisher et al. 2007; Limprasertkul et al. 2012). Thus the molecular mechanisms behind this statin-induced lipotoxicity and overall statin-induced diabetes are only partially understood. Statin-induced insulin resistance has been linked to lipotoxicity via low levels of diacylglycerol acyltransferase (DGAT) and consequent reduced synthesis of triacylglycerols in skeletal muscle (Larsen et al. 2018). Because the benefit-risk balance of statin use favours their life-saving history as it is to date one of the most prescribed drugs in the world, there is a need to understand the molecular mechanisms behind their diabetogenic activity to identify better statins or candidate combination therapies that counteract this effect and increase their safety.

1.3 The yeast *Saccharomyces cerevisiae* is an established model for the study of cancer, diabetes and cholesterol metabolism

The yeast *Saccharomyces cerevisiae* (*S. cerevisiae*) is an established model organism to investigate eukaryotic metabolism (Botstein et al. 1997). Since its genome was sequenced in 1996 (Goffeau et al. 1996), it has shown high conservation with humans not only in sequence but also in biological function; this was cleanly illustrated with humanisation of yeast (*i.e.*, expression of human genes in yeast) where only 20% amino acid identity was required for human genes to complement the deletion of orthologous yeast genes (Kachroo et al. 2015). The mevalonate pathway is no exception and early studies showed that human HMGCR restored the viability of yeast lacking its two paralogue genes, *HMG1* and *HMG2* (Basson et al. 1988) and in fact the elucidation of many steps of the mevalonate pathway was originally elucidated in yeast (Bloch 1965; Hampton and Rine 1994). Therefore, yeast has demonstrated over the years to be a powerful tool for the study of cancer cell biology, diabetes and cholesterol metabolism (Busby et al. 2019; Ferreira et al. 2019; Hartwell et al. 1997; Kohlwein 2010; Munkacsi et al. 2011; Simon 2001).

Since 2001, three Nobel prizes in Physiology or Medicine have been awarded for discoveries of yeast research that determined mechanisms fundamental to the development of cancer and diabetes (Hohmann 2016). The first was awarded to Leland Hartwell, Paul Nurse and Tim Hunt for discovering genes involved in the cell cycle (Culotti and Hartwell 1971; Hartwell 1971a; Hartwell 1971b). James Rothman, Randy Scheckman and Thomas Sudhof received the Nobel Prize in 2013 for elucidating

mechanisms involved in the secretion of proteins (Novick and Schekman 1979; Novick et al. 1980; Schekman et al. 1983). The most recent Nobel prize of this sort was awarded in 2016 to Yoshinori Ohsumi for his discoveries of mechanisms required for autophagy (Nakatogawa et al. 2009; Ohsumi 2014; Tsukada and Ohsumi 1993).

In the case of diabetes, there are two established yeast models for the study of the metabolic syndrome and lipotoxicity. Double mutants lacking triacylglycerol lipase genes *TGL3* and *TGL4* are unable to degrade triacylglycerols and exert an 'obese' phenotype with oversized lipid droplets, the storage units of neutral lipids (Kurat et al. 2006). In contrast, double mutants lacking diacylglycerol acyltransferase genes *DGA1* and *LRO1* are unable to synthesise triacylglycerides and thus exert an 'anorexic' phenotype sensitive to fatty acid insult with only zero to one undersized lipid droplet per yeast cell (Kohlwein 2010; Petschnigg et al. 2009).

Elucidating the molecular mechanisms behind cancer and diabetes has been fundamental over the years to develop therapeutics. Patients, however, respond differently to every treatment and there is a need to develop more personalised and directed therapies at the individual level (Pearson 2016; Sawyers 2004). The genome of *S. cerevisiae* comprises 12,000 kilobases and nearly 6,200 potential protein encoding genes (Goffeau et al. 1996) in contrast to the 3 billion base pairs and about 20,000 genes in the human genome. This makes it a more manageable model to elucidate genetic interactions and molecular mechanisms. A number of high-throughput approaches are used to identify drug mechanisms by means of gene deletion mutant libraries. The next few sections will explain these approaches.

1.4 Genetic interaction networks reveal molecular mechanisms of drugs

Epistasis as defined in 1908 refers to the action of one gene upon another (Phillips 1998). Simultaneous mutation of genes and their phenotypes shed light on their interactions. When the mutation of two genes causes lethality but their individual mutation does not, the genetic interaction is defined as 'synthetic lethal' (Dobzhansky 1946) or 'synthetic sick' when the interaction causes a fitness defect that is not lethal (Figure 1.19A). Collectively, these are called 'negative genetic interactions'. Drugs can also mimic mutations in genes by binding and inhibiting their protein products. In such case, when the loss of function comes from the mutation of one gene and the inhibition of a second one with a drug, the synthetic lethality of the strain reveals a 'chemical genetic interaction' (Figure

1.19B) (Costanzo et al. 2019). Phenotypes can also depend on environmental conditions, that is, can be conditional for instance on ambient versus hypoxic conditions (Zitomer et al. 1997), and in this case, the interaction is 'conditional genetic' or 'conditional chemical genetic' (Figure 1.19C-D). Genetic interactions are also influenced by individual yeast genetic background (Busby et al. 2019; Galardini et al. 2019), a subject that is not yet well studied in higher eukaryotes owing to a lack of genome-wide deletion mutant libraries of cells and the difficulty creating double or triple mutants. CRISPR/Cas9 technologies are bound to change that in the next decade. As in yeast, synthetic lethality in human cells will also depend on genetic background and environmental stresses, which will both be useful for the development of anticancer therapeutics (Kaelin 2005; Li et al. 2020).

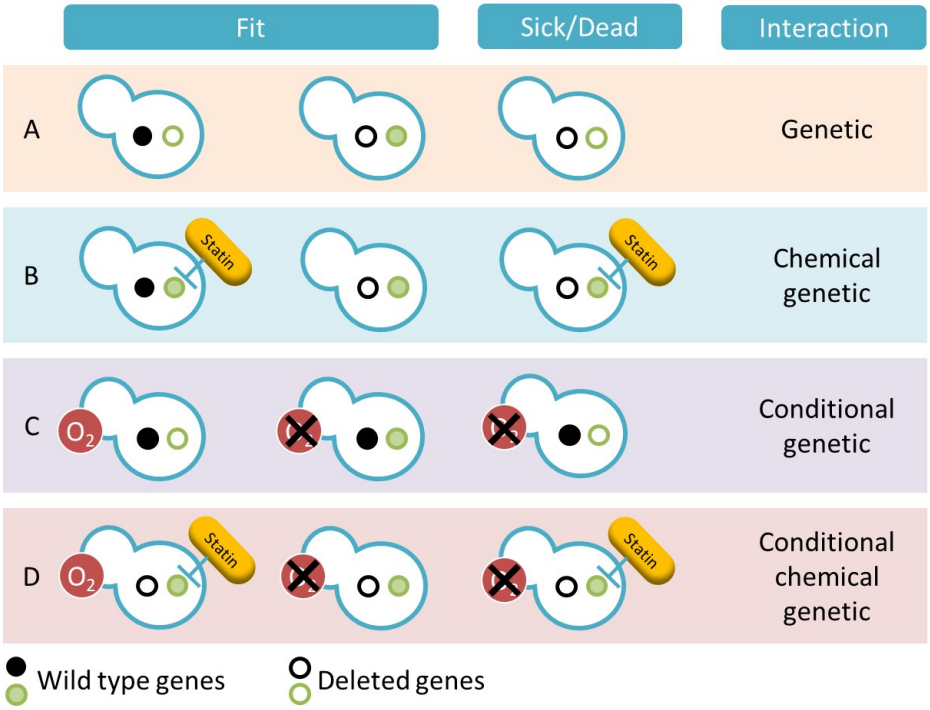

Figure 1.19: **Genetic interactions can be purely genetic, chemical genetic or conditional.** (A) Genetic interaction refers to a situation where two single deletion mutants are fit (*e.g.*, same growth phenotype as the non-mutated wild type strain) but the mutation of both in the same individual (double mutation) renders the strain sick or dead. (B) A chemical genetic interaction is defined by a sick or death phenotype that only occurs upon combination of a single deletion and a gene being inhibited by a drug mimicking a second mutation. (C and D) Conditional genetic interactions refer to sick/dead phenotypes that can only be seen upon exposure to an environmental condition (*e.g.*, hypoxia).

Whether purely genetic, chemical genetic or conditional, genetic interactions reveal compensatory metabolic pathways or functionally related genes within a metabolic pathway (Boone et al. 2007). To illustrate, when a pair of genes share a functional relationship, mutation of both genes will result in a loss of function phenotype (*e.g.*, decreased fitness), whether they act in the same (within-pathway) (Boone et al. 2007; Forsburg 2001; Guarente 1993) or in different metabolic pathways (between-pathway)

(Boone et al. 2007; Guarente 1993; Kelley and Ideker 2005; Pan et al. 2006) that compensate each other (Figure 1.20).

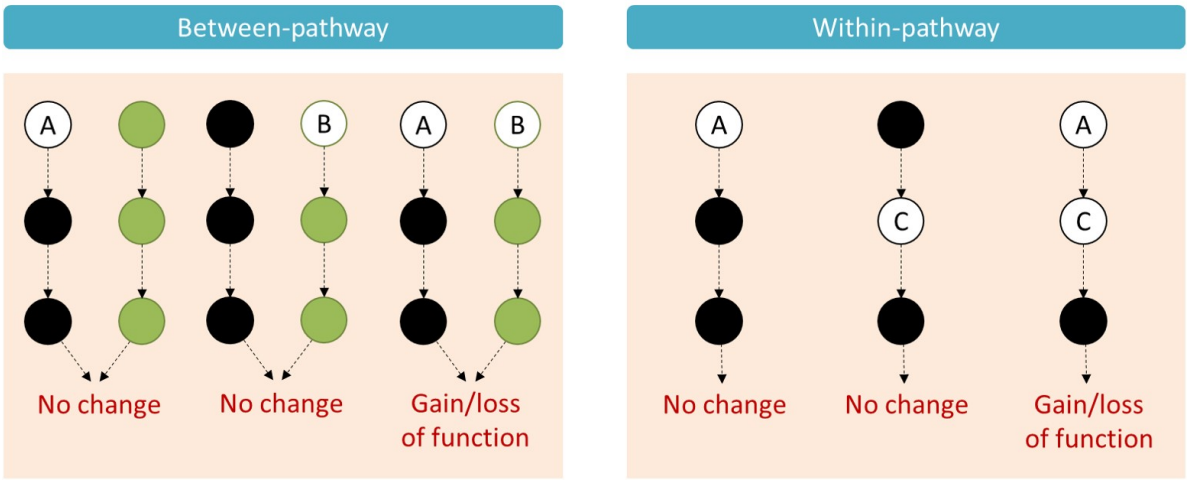

Figure 1.20: **Synthetic lethal interactions or phenotypic suppressions reveal between pathway and within pathway functional relationships.** Between-pathway interactions (left panel) refer to two genes that share a functional relationship but that belong to different but compensatory pathways. Within-pathway interactions (right panel) refer to genes within the same metabolic pathway that when deleted exert a loss-of-function phenotype, generally because they act in close proximity to each other (*e.g.*, subunits of the same complex).

While synthetic sick/lethal interactions reveal direct functional relationships and complementary functions or pathways, 'positive genetic interactions' reveal more general regulatory pathways often related to cell cycle, protein turnover and mRNA regulation unless the suppression is very strong, in which case they reveal strong functional connections (*e.g.*, rescuing the toxicity associated with another gene deleted in a deletion pair) (Costanzo et al. 2016; Costanzo et al. 2019; Costanzo et al. 2021). Most synthetic/lethal interactions are either between-pathway or within-pathway interactions (Costanzo et al. 2019).

1.4.1 The role of epistasis in drug response

Diseases such as cancer and diabetes may be probed for epistasis where the interacting genes are therapeutic targets (Li et al. 2020). In cancer, for instance, one of the well- established treatments based on synthetic lethality targets the impaired function of the genes BRCA1 and BRCA2, which makes them more sensitive to Poly (ADP-ribose) polymerase (PARP) inhibitors compared to cells with normal BRCA1/2 function (Bryant et al. 2005; Farmer et al. 2005). This led to the development of PARP inhibitors as anticancer therapeutics in persons with mutations in BRCA1 or BRCA2 (Dey et al. 2017; Gogola et al. 2018; Heeke et al. 2020; Litton et al. 2018). Other examples include the mutants of the tumour suppressor p53 with mTOR (Cordani et al. 2016), KRAS with SLC25A22 (Wong et al. 2016)

and many others (Li et al. 2020).

In the case of diabetes, pharmacogenetic studies have distinguished genetic variants as therapeutic drug targets to treat diabetes (Mannino et al. 2019). For example, gene variants of genes involved in the response to metformin, sulfonylureas/glinides, thiazolidinediones, and DPP-4 inhibitors/GLP-1 receptor agonists (Pollastro et al. 2015).

1.4.2 Synthetic Genetic Array (SGA) analysis

Synthetic Genetic Array (SGA) analysis is an experimental assay used to determine synthetic sick or synthetic lethal genetic interactions. It was developed by Tong and colleagues in 2001 for the systematic construction of double deletion mutants in yeast in the S288C genetic background (Tong et al. 2001). A major tool to construct these interactions on a high-throughput basis is a deletion mutant array (DMA), a genome-wide library of 4,800 haploid non-essential gene deletion mutants (Busby et al. 2019; Giaever et al. 2002; Winzeler et al. 1999). This DMA is then crossed with a particular query deletion strain in an SGA analysis to generate a new library of double deletion mutants. The first DMA of *S. cerevisiae* was built in S288C genetic background by Winzeler in 1999 by means of a PCR-mediated strategy in which every ORF was replaced with a 'deletion cassette' containing a resistance marker that confers resistance to kanamycin (*kanR*). More recently in 2019, my laboratory generated DMA libraries in three more genetic backgrounds (Y55, UWOPS87-2421 (hereby UWOPS87) and YPS606) via systematic backcrossing of the Y55, UWOPS87 and YPS606 strains with the S288C DMA library (Busby et al. 2019).

With high-throughput colony replication robots (most often the Singer RoToR robot), the SGA analysis can be conducted in any genetic background given the DMA and query strain have the appropriate selection markers. The first step of the SGA analysis involves mating the query strain with the DMA. As haploids, yeast have two mating types of two non-homologous alleles, *MAT*α and *MATa* (Haber 2012) and when they mate, they yield diploid progeny. This is used in the SGA analysis to mate a *MAT*α query gene deletion strain that also contains a reporter gene deletion of the *CAN1* gene (an arginine permease) that has been replaced by a *HIS3* gene but that can only be expressed in *MATa* (Figure 1.21A). Upon mating, the diploid progeny contains both wild type and deletion markers (Figure 1.21B). With nutrient deprivation, diploids are induced to sporulate and tetrad spores (meiotic products) contain all possible combinations of mating types and wild type/deletion genotypes (Figure 1.21C). To ensure germination of *MATa* progeny only, the spores are transferred to synthetic medium lacking histidine, thus enforcing the selection of *can1*Δ*::MFA1pr-HIS3* strains with every possibility

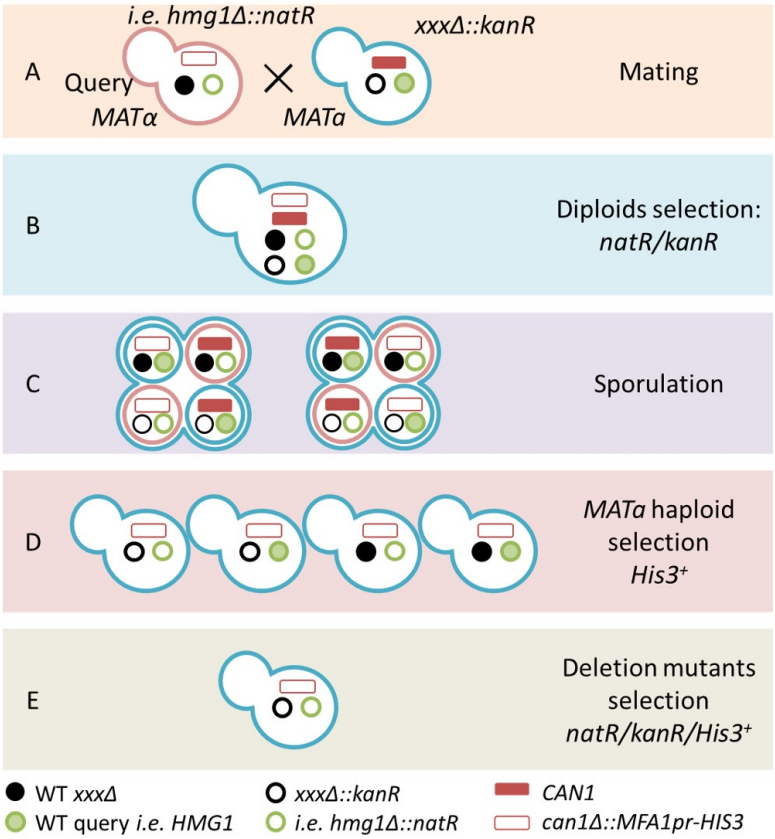

Figure 1.21: **Synthetic Genetic Array (SGA) Analysis.** The SGA analysis consists of mainly 5 steps. (A) The query strain *MAT*α with a gene deletion (*e.g.*, *hmg1*Δ) linked to a selectable marker, such as the nourseothricin-resistance marker *natMX* that confers resistance to the antibiotic nourseothricin and an *MFA1pr-HIS3* reporter that confers auxotrophy to histidine is crossed to the *MATa* DMA, each having a gene deletion that has been replaced by a kanamycin-resistance marker (*kanMX*). (B) The diploids are then selected on medium containing nourseothricin and kanamycin and (C) sporulation is induced in low nutrient media. (D) The *MATa* haploid progeny are then selected in media lacking histidine because these cells express the *MFA1pr-HIS3* reporter specifically followed by (E) growth on media containing nourseothricin and kanamycin to select for the double deletion mutants.

for the other genes that are to be deleted (Figure 1.21D). The *MATa* double deletion mutants are finally selected with the appropriate antibiotic markers (Figure 1.21D). To explore complex genetic interactions, trigenic interactions have also been explored (Costanzo et al. 2021; Kuzmin et al. 2018) whereby the starting query strain is a double deletion rather than a single deletion.

Growth of the double or triple deletion libraries created with SGA analysis can then be quantified via colony size measurements as a proxy for fitness, and then compared to parental libraries (*e.g.*, single mutant libraries in the case of a single mutant query). These data will identify fitness defects that will retrieve information about genetic interactions. These measurements comparing treated and untreated colonies (*i.e.*, drug-treated vs vehicle control, hypoxia vs aerobic) can also identify chemical genetic interactions and conditional genetic interactions (Figure 1.19).

1.4.3 Genetic interaction networks (GINs) assembly

Once genetic interactions have been identified for purely genetic, chemical genetic or conditional interactions, online tools can be used to assemble interaction networks and conduct network topology analyses to identify the genes and pathways critical to the network (phenotype). The genotype-to-phenotype connection should be studied in a whole-genome context to achieve an unbiased result through the analysis of interaction networks (Costanzo et al. 2019; Costanzo et al. 2021). In such networks, each node represents a gene and the interactions linking the nodes are are represented as edges. Large-scale studies have identified about 500,000 synthetic sick/lethal and 350,000 suppressor genetic interactions in yeast in the S288C background, which have been integrated in a global network (Costanzo et al. 2010; Costanzo et al. 2016). This comprehensive yeast network is accessible in many public databases along with networks for other organisms, albeit the other organisms are not as comprehensively constructed.

High-throughput screening derived networks are inherently noisy. One approach to increase the robustness of this type of analysis is using multi-layer networks that integrate various kinds of data (*e.g.*, genetic interactions, protein-protein interactions, co-expression) (Boccaletti et al. 2014; Wang et al. 2017) (Figure 1.22). Integration of different sources of interactions compose what is known as a multidimensional array or tensor (Kolda and Bader 2009). Such approaches are distinguished from aggregating techniques that increase the number of matrix features (*e.g.*, rows and columns representing individuals and genes), which though useful in some circumstances, inherently increase noise.

As an example, a list of synthetic lethal interactions can be linked through known gene-gene interactions or protein-protein interactions (Figure 1.22). Each network represents a dimension of the tensor or a layer of the multi-layer network. The two layers can then be integrated in one aggregated, multi-layer network that can then be used as the basis for network topology analysis.

1.4.4 Topological centrality of GINs

When genetic interactions are expanded, often to several hundred nodes as explained in the previous section, the network becomes so complex that it is hard to identify meaningful information. Network topology centrality analyses identify hub and bottleneck genes that often correlate with gene essentiality and biological relevance (Boccaletti et al. 2014; Yu et al. 2007). Three of the most common centrality measurements in a network are the degree, closeness and betweenness centralities based

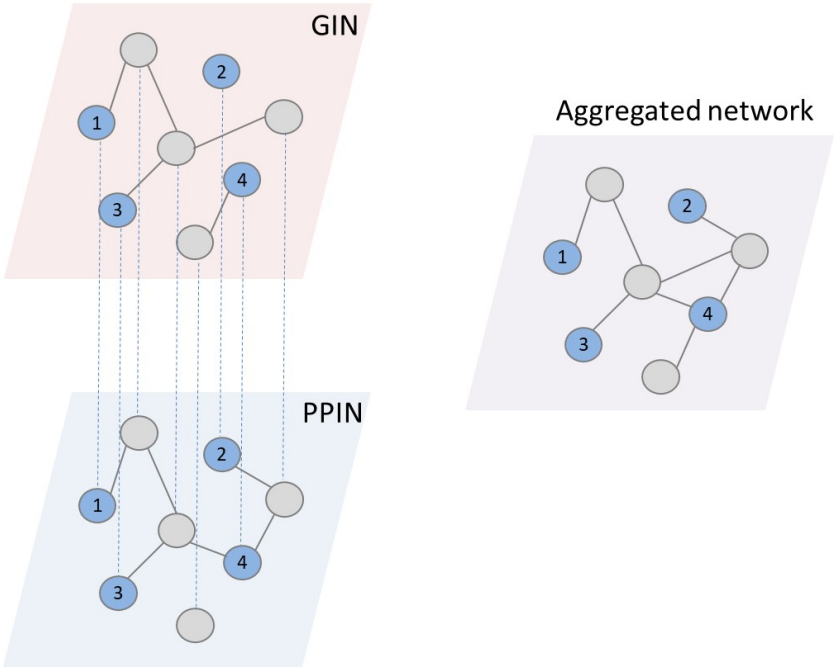

Figure 1.22: **Multi-layer networks are integrated in an aggregated network.** Multi-layer network analysis integrates two or more layers of interaction networks. To illustrate, nodes 2 and 4 in the diagram are isolated from the main network in the genetic (gene-gene) interaction network (GIN) and then integrated with known connections from the protein-protein interaction network (PPIN), which generates an aggregated network with enhanced connectivity.

on modularity of clusters or communities. Degree (Dong and Horvath 2007) refers to the number of edges linked to each node. In Figure 1.23, for instance, the degree of the green node is 1 given it is connected to only one node, whereas the yellow node has a degree of 10 as 10 edges connect it with 10 other nodes. In this case, the yellow node is also considered a hub gene due to its high connectivity. Closeness centrality (Newman 2005) corresponds to the average shortest path length of one node to every other node and thus a high closeness centrality means that the node is 'close' to other nodes, whereas a closeness centrality of 0 will mean the node is isolated from every other node.

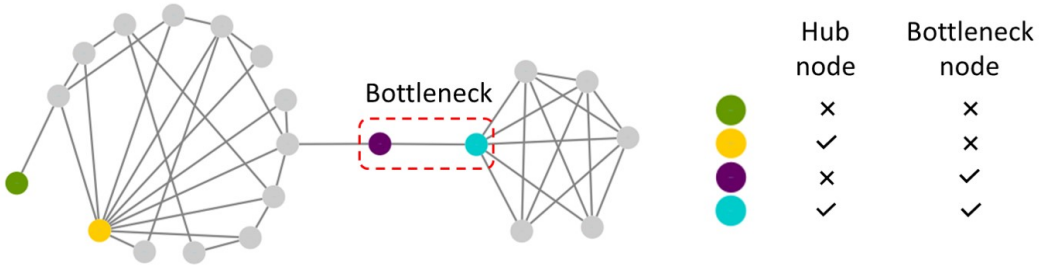

Figure 1.23: **Centrality metrics identify hub and bottleneck genes.** This diagram depicts the definition of hubs and bottlenecks that can be identified in a network topology centrality analysis. Low connectivity of a node, which generally correlates with low biological importance is depicted in green. The yellow and blue nodes are defined as hubs due to their high connectivity, however, the blue node is likely more biologically relevant as it forms a bottleneck, alongside the purple non-hub node, that connects two network clusters.

In the context of biological (*e.g.*, gene-gene, protein-protein, multi-layer) networks, betweenness centrality is perhaps the most meaningful because it pinpoints bottleneck genes that are required for the integrity of the network that represents a phenotype (Dunn et al. 2005; Freeman 1977; Girvan and Newman 2002; Yoon et al. 2006); for instance, being a bridge between two community modules (Figure 1.23). Betweenness centrality refers to the probability of passing through a node when using the shortest path length between two nodes and it is computed with a highly efficient algorithm (Brandes 2001). The betweenness centrality of a node thus correlates with the importance of a node to hold a network together.

Top centrality genes can also form the basis for gene set enrichment analysis (Subramanian et al. 2005) of, for instance, drugs and genes involved in the mechanism of these drugs (Yoo et al. 2015). Drugs and compounds have an effect on the regulation of several genes, not only its main target. Such data has been annotated and compiled in databases under the name of 'drug signatures' (Culhane et al. 2010; Yoo et al. 2015). One such a database is DSigDB (Yoo et al. 2015) that is accessible through online tools such as Enrichr (Chen et al. 2013; Kuleshov et al. 2016; Xie et al. 2021). Finding drug enrichment for highly ranked centrality genes in a network helps to identify drugs and compounds for drug repurposing.

1.4.5 Community analysis of GINs

Similar to centrality metrics, community analysis helps to identify meaningful information in complex networks. Community analysis clusters the network based on topology to statistically distinguish functional subnetworks termed communities or modules (Figure 1.24). The general idea behind it is that groups of genes that are more densely interconnected are clustered together and this density is lower than the density of the connections linking the cluster to other clusters. Upon clustering, a number of iterations are run to remove nodes from a cluster and evaluate the effect of placing it in another cluster. If such change creates modules of more similar sizes, then this modularity will be chosen. The iterations are run in all nodes until finding the most optimal clusters. Community/module determination can be accomplished using various algorithms such as the Louvain algorithm (Blondel et al. 2008) or the InfoMap algorithm (Rosvall and Bergstrom 2008). Infomap is the algorithm used in this thesis and it is largely based on random walks in the network. If a random walk was performed starting from a given node, the probability that the next step takes place within a highly connected cluster is much higher than the probability of walking to a different cluster. This way, the longer the random walk stays within a group of nodes, the more likely they are to be considered as part of the

same cluster. Infomap has comparatively been more accurate and efficient than many other algorithms (Lancichinetti and Fortunato 2009).

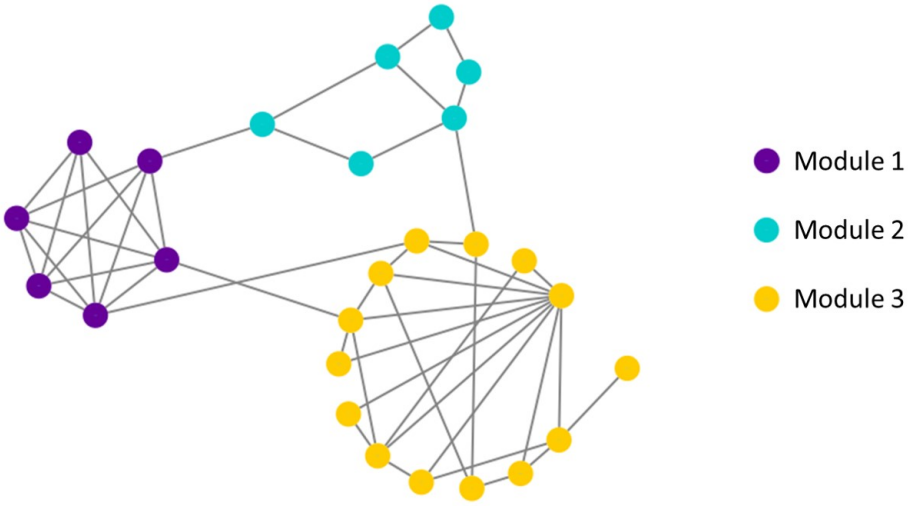

Figure 1.24: **Community analysis partitions networks based on modularity.** The diagram depicts a network partitioned in three modules or communities through community analysis. Each group of coloured nodes represents a module. To illustrate, if a random walk was performed from a yellow node, the probability that the random walk stays within the yellow module is higher than that of moving to the blue or purple communities.

Community modules tend to implicate function. Once the network has been clustered in modules, each module can then be analysed individually to identify cellular processes or metabolic pathways that are overrepresented using databases such as Gene Ontology or the Kyoto Encyclopedia of Genes and Genomes (KEGG) pathway database (Kanehisa and Goto 2000).

1.5 Aims and hypothesis

The aim of this thesis is to determine whether genetic interaction networks can unravel complex phenotypes, and if so, whether these networks can be used to elucidate the complex molecular mechanisms behind the anticancer and diabetogenic activity of atorvastatin. Atorvastatin was selected as it is the most prescribed of all statins worldwide and also a statin that has been well-investigated for anticancer and diabetogenic activity in preclinical and clinical trials. I hypothesised that the investigation of genetic interaction networks will further our understanding of genotype-to-phenotype mechanisms behind the anticancer (chapters 2 and 4) and diabetogenic (chapter 3) activity of statins. Specifically, my aims and accomplishments were the following:

Aim 1 (Chapter 2): To elucidate atorvastatin-specific epistasis with genes in the mevalonate pathway. Here I derived purely genetic and chemical genetic interactions from genome-wide double deletion libraries in three yeast backgrounds (S288C, UWOPS87, Y55). The GINs are derived from two query genes in the mevalonate pathway, namely, *HMG1*, the target of statins that is the rate-limiting step in the mevalonate pathway, and *BTS1*, a critical gene in the mevalonate pathway that mediates the branching of ergosterol synthesis towards the synthesis of isoprenoids that are relevant for cancer biology. Interestingly, knocking-down GGPS1 (the *BTS1* human orthologue), enhances the anticancer activity of statins in human cells (Pandyra et al. 2015). I thus screened the genome-wide double deletion *hmg1*Δ *xxx*Δ and *bts1*Δ *xxx*Δ libraries with and without atorvastatin. Key interactors and pathways were identified via hypersensitive mutations, multi-layer topology centrality metrics and functional enrichment that may be targeted to enhance the anticancer activity of statins. I also identified drugs and compounds that have been associated to these candidate targets that may enhance the anticancer activity of statins.

Aim 2 (Chapter 3): To elucidate atorvastatin-specific epistasis with genes outside the mevalonate pathway. Here I derived two sets of GINs from genome-wide triple deletion libraries in three yeast genetic backgrounds, each lacking genes involved in lipid metabolism. The first set of mutants was in the background of the yeast model of obesity (diabetic dyslipidaemia) characterised by high levels of triacylglycerides (fat). The second set of mutants was in the background of the yeast model of anorexia (lipoatrophic diabetes) characterised by the inability to synthesise and store triacylglycerides (fat). As a proxy to these conditions, I used a *tgl3*Δ *tgl4*Δ query gene to generate obese triple mutants *tgl3*Δ *tgl4*Δ *xxx*Δ lacking the ability to degrade triacylglycerides. The second set of triple mutants used a *dga1*Δ *lro1*Δ query gene to generate anorexic triple mutants *dga1*Δ

lro1△ *xxx*△ lacking the ability to synthesise and store triacylglycerides. I screened the *dga1*△ *lro1*△ *xxx*△ and *tgl3*△ *tgl4*△ *xxx*△ libraries with and without atorvastatin and similarly to Aim 1, identified key interactors and pathways via hypersensitive mutations, multi-layer topology centrality metrics and functional enrichment, that in this case, may be targeted to decrease the diabetogenic activity of statins. I also identified drugs and compounds associated with these candidate targets that may reduce the diabetogenic activity of statins.

Aim 3 (Chapter 4): To investigate conditional GINs and atorvastatin-specific epistasis as a proxy for hypoxic tumour conditions. Here I investigated the effect of hypoxia on atorvastatin sensitivity in genome-wide single deletion strains *xxx*△ in three genetic backgrounds. The aim was to identify genes that were hypersensitive in hypoxia but not in ambient oxygen conditions. In addition, since *bts1*△ strains in S288C genetic background are synthetic lethal in hypoxia, I sought to identify suppressors of lethality in S288C. As in chapters 2 and 3, I identified candidate interactors and pathways that may be targeted, but in this case, to either suppress or overexpress to enhance the anticancer activity of statins. I also identified drugs and compounds that have been associated to these candidate targets that may enhance the anticancer activity of statins in hypoxic tumours.

Chapter 2

Atorvastatin-specific epistasis with genes in the mevalonate pathway: *HMG1* and *BTS1*

2.1 Introduction

Since their discovery more than 40 years ago, statins have saved millions of lives by preventing accumulation of cholesterol and thus cardiovascular disease (Endo et al. 1976b). Through competitive inhibition of the rate-limiting enzyme in the mevalonate pathway 3-hydroxy-3-methyl-glutaryl-coenzyme A reductase (HMGCR) (Endo et al. 1976a, Goldstein and Brown 1973), statins inhibit the synthesis of downstream products in the mevalonate pathway that include cholesterol and other physiologically important cellular products such as dolichol, ubiquinone, steroid hormones and isoprenoids (Figure 2.1). In recent years, the mevalonate pathway has drawn attention as a target for anticancer therapeutics (Juarez and Fruman 2021) given its upregulation in promoting tumour progression (Göbel et al. 2020) and more broadly that genes in this pathway are essential in different types of cancer cells (Hart et al. 2015). Indeed, a myriad of *in vitro* and *in vivo* studies as well as clinical trials have made evident the pleiotropic potential of statins as anticancer therapeutics in different types of cancers (Ahmadi et al. 2020). Thus, it is apparent that statins inhibit proliferation, metastasis and induce apoptosis of tumour cells but the molecular mechanisms behind this are only partially understood.

The first and perhaps most obvious mechanism is the inhibition of HMGCR and its cholesterol product, which also serves as a precursor for steroid hormones that are drivers of hormone-dependent cancers (*e.g.*, breast and prostate cancer) (Ko and Balk 2004), and for oxysterols, which have a role in modulating the response to anticancer therapeutics (Kloudova-Spalenkova et al. 2021). However, this cholesterol-centric mechanism largely does not explain the anticancer activity of statins (Mullen et al.

2016).

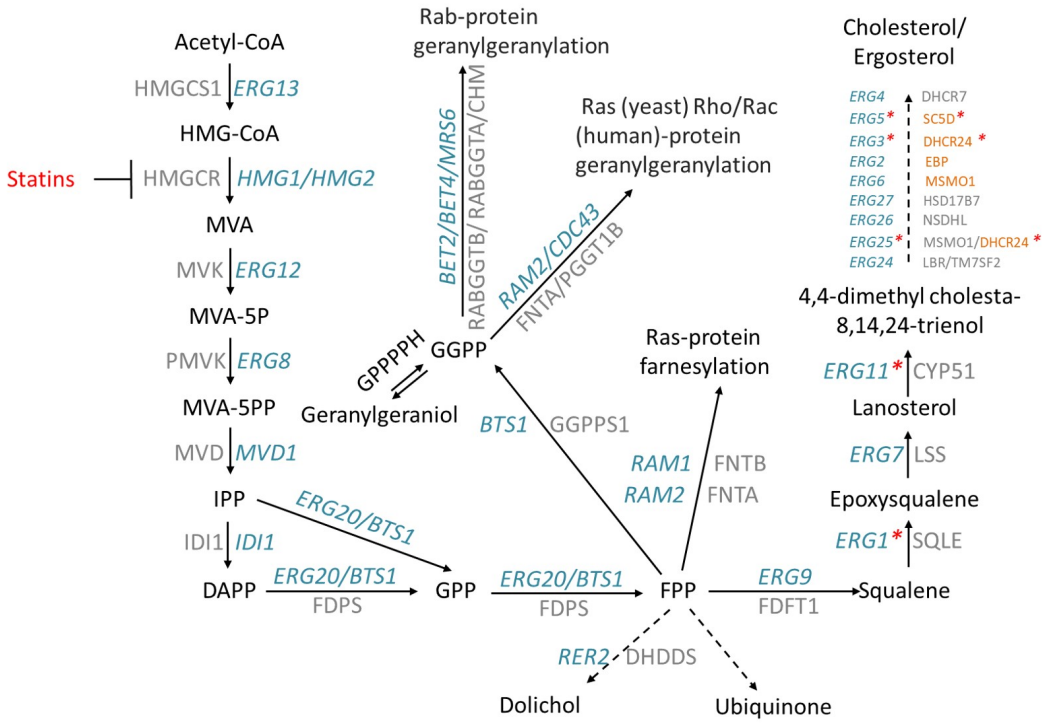

Figure 2.1: **Statins inhibit the synthesis of HMGCR and downstream products in the mevalonate pathway.** Statins are competitive inhibitors of HMGCR encoded by *HMG1* and *HMG2* in yeast and HMGCR in humans. A critical step in the mevalonate pathway is mediated by the enzyme geranylgeranyl diphosphate synthase (encoded by *BTS1* in yeast and GGPPS1 in humans), where the main ergosterol/cholesterol-synthesis pathway branches off to synthesise other fundamental cellular components for isoprenylation of small GTPases. Genes in blue are yeast genes and genes in grey are their human orthologues. Red asterisks in yeast genes indicate oxygen-dependent steps of the pathway. Human genes in orange at the end of the cholesterol pathway are less conserved with yeast and do not correspond to the yeast gene to the left.

Mechanistic studies have also focused on the decisive branching of the mevalonate pathway, mediated by the enzyme geranylgeranyl diphosphate synthase (GGPPS1 in humans, *BTS1* in yeast) (Figure 2.1). From this branch, at least two cellular processes that are essential for survival of cancer cells occur. Isoprenylation of small GTPases, mainly from the Ras and Rho families, are necessary for tumourigenesis and targeted via statin-induced apoptosis (Wong et al. 2007). Inhibition of this branch also results in accumulation of farnesyl diphosphate (FPP), a key precursor for the synthesis of dolichol involved in cell signalling, metastasis and other biological processes fundamental to cancer development (Pinho and Reis 2015) as well as the synthesis of ubiquinone that supports mitochondrial function and has an essential role in cancers that depend on oxidative phosphorylation (Maiuri and Kroemer 2015). However, there is still a need to gain more insight in the mechanistic activity of statins against cancer, particularly since half the multiple myeloma tumours of different genetic background were sensitive to statins, to develop targeted therapies based on genetic vulnerability of cancers.

One strategy to determine mechanisms and develop targeted therapies is through the exploration of synthetic sick/lethal interactions (Hopkins 2008; Parameswaran et al. 2019). Coined by Theodore Dobzhansky (Dobzhansky 1946), the term 'synthetic lethality' refers to cases when the mutation of two genes causes lethality (or sickness in the case of synthetic sick interactions) but their individual mutation does not. If the genetic vulnerability of cancer cells to a small molecule inhibitor is known, it is possible to use this vulnerability to identify a second mutation that would be toxic for the cancer cell but not the healthy cell. For instance, breast cancer caused by mutations in BRCA1 or BRCA2 can be treated with an inhibitor of the interacting Poly(ADP-ribose) polymerase (PARP) (Farmer et al. 2005). Since genetic interactions have not been comprehensively determined for statin anticancer activity, a genetic model organism was used here, Baker's yeast (*S. cerevisiae*) that has been extensively used to elucidate drug mechanism of action (Giaever et al. 1999; Hillenmeyer et al. 2008; Lee et al. 2014; Parsons et al. 2004; Parsons et al. 2006). The target and downstream effects of statins are conserved in the yeast *S. cerevisiae*, and in addition this model organism is a well-established model for the study of cancer cell biology and cholesterol metabolism across various genetic backgrounds (Busby et al. 2019; Gardner et al. 2001; Hampton and Rine 1994; Hartwell et al. 1997; Munkacsi et al. 2011; Simon 2001).

In this chapter, I aimed to elucidate the mevalonate pathway-specific genetic interactions integral to statin bioactivity. Using SGA methodology (Tong et al. 2001), I generated 25,800 double deletion yeast strains, each lacking a gene in the statin pathway and a second gene in the yeast genome of statin-susceptible and statin-resistant genetic backgrounds since anticancer and cholesterol-lowering activities of statins vary among individuals (Ahangari et al. 2020; Guan et al. 2019; Mullen et al. 2016). The genes within the mevalonate pathway investigated were *HMG1*, the predominantly active target of atorvastatin under aerobic conditions (about 80% of the activity compared to its paralogue *HMG2* (Basson et al. 1986), and *BTS1*, the mediator of the off-branch pathway from the main ergosterol synthesis pathway to isoprenylation of GTPases. The double deletion mutants were treated with atorvastatin and hypersensitive mutants were compiled into multi-layered networks. Topology centrality metrics and functional enrichment in chemical genetic interaction networks were used to identify key genes and cellular processes regulating statin activity, which by definition are candidate targets to use in combination with statins to enhance its anticancer activity.

2.2 Experimental Procedures

The overall flow of experimental and computational methods is depicted in Figure 2.2.

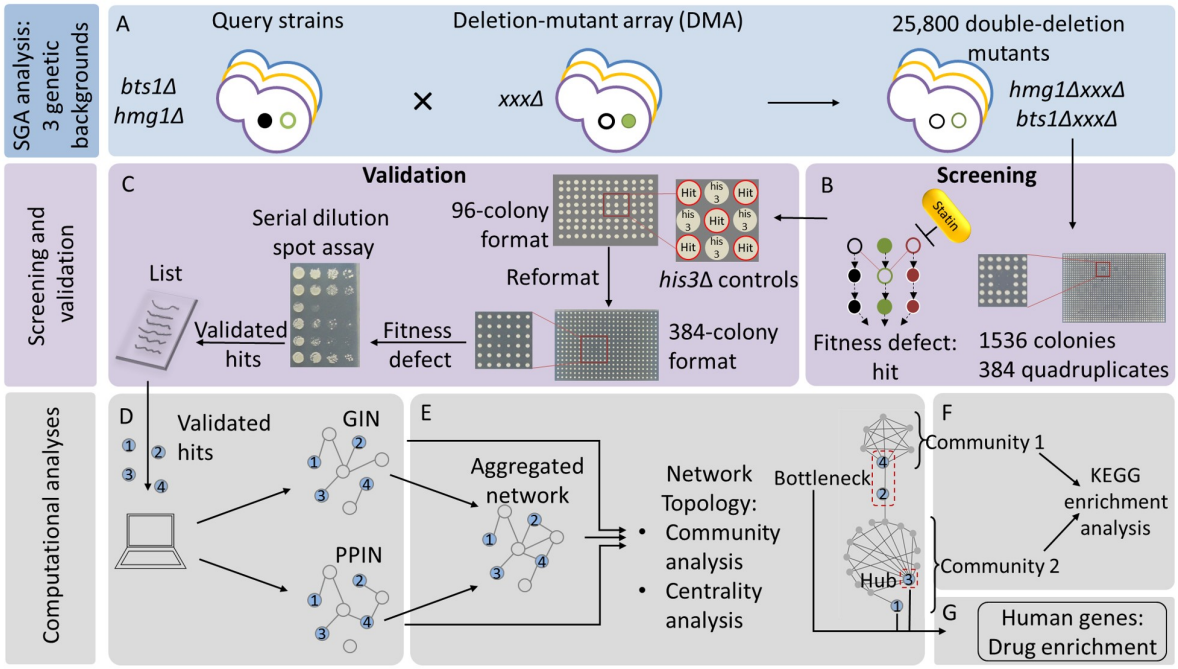

Figure 2.2: **Flow diagram for the methods used to identify interactions, pathways and drugs to enhance the anticancer activity of atorvastatin.** Single deletion mutant query strains were constructed (A) (deletion mutant genes depicted as empty circles) as models to investigate the anticancer activity of atorvastatin (*hmg1*Δ and *bts1*Δ) in three yeast genetic backgrounds (S288C, UWOPS87 and Y55 indicated here as purple, yellow and blue), and mated against DMAs of the same genetic backgrounds to generate 25,800 double deletion mutants in 1536-colony format (384 quadruplicate colonies per agar plate). These mutants were treated with atorvastatin (B) and screened to identify fitness defects that would reveal epistatic interactions (hits) as measured by decreased colony size. Hits were then validated in two steps (C). First, hits were formatted in 96-colony format plates with each hit surrounded by *his3*Δ strains for growth control. These plates were then reformatted to 384-colony format (96 quadruplicate colonies) and screened again with atorvastatin. Colonies that showed fitness defects were selected for the second step, which consisted of serial dilution spot assays. Hits that showed growth inhibition in the latter were considered as validated interactions and used as input to create genetic (GIN) and protein-protein (PPIN) interaction networks (D). GINs and PPINs were aggregated in one network (E) per genetic background and subjected to network topology analyses. The network centrality metrics pinpointed bottleneck and hub genes of high biological relevance. The communities of genes identified through network modularity (F) were analysed through a KEGG enrichment analysis to distinguish key metabolic pathways. Human orthologues of the key yeast genes were used in a search for drug enrichment (G) to identify potential combination therapies to enhance the anticancer activity of atorvastatin.

2.2.1 Yeast strains

The *S. cerevisiae* strains used in this study are described in Table 2.1. Stocks were stored at -80°C in 15% glycerol. Strains that contained the URA3_CEN plasmid were grown on agar with 1 mg/mL of 5-Fluoroorotic Acid (5-FOA, Kaixuan Chemical Co) to select for uracil auxotrophs before construction

of the query strains.

Background	Genotype	Description	Reference
Y7092 (S288C)	*Matα can1::STE2pr-Sp_his5 lyp1Δ his3Δ1 leu2Δ0 ura3Δ0 met15Δ0*	Query construction starting strain	Tong and Boone 2006
Y55	*Matα ho::HPH ura3Δ0 his3Δ0 [URA3_CEN]*	Query construction starting strain	Busby et al. 2019
UWOPS87	*Matα ho::HPH ura3Δ0 his3Δ0 [URA3_CEN]*	Query construction starting strain	Busby et al. 2019
Y7092 (S288C)	*Matα can1::STE2pr-Sp_his5 lyp1Δ his3Δ1 leu2Δ0 ura3Δ0 met15Δ0 hmg1::NatR*	*hmg1Δ* query strain	This study
Y55	*Matα ho::HPH ura3Δ0 his3Δ0 hmg1::NatR*	*hmg1Δ* query strain	This study
UWOPS87	*Matα ho::HPH ura3Δ0 his3Δ0 hmg1::NatR*	*hmg1Δ* query strain	This study
Y7092 (S288C)	*Matα can1::STE2pr-Sp_his5 lyp1Δ his3Δ1 leu2Δ0 ura3Δ0 met15Δ0 bts1::NatR*	*bts1Δ* query strain	This study
Y55	*Matα ho::HPH ura3Δ0 his3Δ0 bts1::NatR*	*bts1Δ* query strain	This study
UWOPS87	*Matα ho::HPH ura3Δ0 his3Δ0 bts1::NatR*	*bts1Δ* query strain	This study
Y7092 (S288C)	*MATa his3Δ1 leu2Δ0 met15Δ0 ura3Δ0 xxx::KanR*	Yeast deletion collection (DMA)	Tong and Boone 2006
Y55	*Mata can1::STE2pr-Sp_his5 lyp1Δ his3Δ1 ura3Δ0 xxx::KanR*	Yeast deletion collection (DMA)	Busby et al. 2019
UWOPS87	*Mata can1::STE2pr-Sp_his5 lyp1Δ his3Δ1 ura3Δ0 xxx::KanR*	Yeast deletion collection (DMA)	Busby et al. 2019
Y7092 (S288C)	*Mata can1::STE2pr-Sp_his5 lyp1Δ his3Δ1 leu2Δ0 ura3Δ0 met15Δ0 hmg1::NatR xxx::KanR*	*hmg1Δ xxxΔ* SGA	This study
Y55	*Mata can1::STE2pr-Sp_his5 lyp1Δ his3Δ1 ura3Δ0 ho::HPH hmg1::NatR xxx::KanR*	*hmg1Δ xxxΔ* SGA	This study
UWOPS87	*Mata can1::STE2pr-Sp_his5 lyp1Δ his3Δ1 ura3Δ0 ho::HPH hmg1::NatR xxx::KanR*	*hmg1Δ xxxΔ* SGA	This study
Y7092 (S288C)	*Mata can1::STE2pr-Sp_his5 lyp1Δ his3Δ1 leu2Δ0 ura3Δ0 met15Δ0 bts1::NatR xxx::KanR*	*bts1Δ xxxΔ* SGA	This study
Y55	*Mata can1::STE2pr-Sp_his5 lyp1Δ his3Δ1 ura3Δ0 ho::HPH bts1::NatR xxx::KanR*	*bts1Δ xxxΔ* SGA	This study
UWOPS87	*Mata can1::STE2pr-Sp_his5 lyp1Δ his3Δ1 ura3Δ0 ho::HPH bts1::NatR xxx::KanR*	*bts1Δ xxxΔ* SGA	This study

Table 2.1: **Strains used in this study.**

2.2.2 Plasmids

The plasmids used for this study were conserved in *Escherichia coli* (DH5α) and stored at -80°C (Table 2.2).

Plasmid	Description	Reference
p4339	MX4-natR switcher cassette	Tong et al. 2001
pAG60	*URA3* from *Candida albicans* for uracil prototrophy	Goldstein and McCusker 1999

Table 2.2: **Plasmids used in this study.**

2.2.3 Media and Solutions

The media and solutions used to culture *S. cerevisiae* and *E. coli* strains were prepared as described below and autoclaved at 121°C for 15 minutes unless otherwise stated. Agar was left to cool to approximately 60°C before adding glucose or drugs/antibiotics. All agar and liquid culture media recipes are for a final volume of 1 L in ddH_2O.

Amino acid mixes for specific media

Synthetic Complete (SC) amino acid mix (all Formedium): 3 g adenine, 2 g uracil, 2 g inositol, 0.2 g para-aminobenzoic acid, 2 g alanine, 2 g arginine, 2 g asparagine, 2 g aspartic acid, 2 g cysteine, 2 g glutamic acid, 2 g glutamine, 2 g glycine, 2 g histidine, 2 g isoleucine, 10 g leucine, 2 g lysine, 2 g methionine, 2 g phenylalanine, 2 g proline, 2 g serine, 2 g threonine, 2 g tryptophan, 2 g tyrosine, 2 g valine.

Synthetic Drop-out (SD) amino acid mix: Same as SC minus one or more amino acids.

Sporulation (SPO) amino acid mix: 2 g uracil, 2 g histidine, 10 g leucine, 2 g lysine.

Media

Sporulation (SPO) agar: 10 g potassium acetate (Sigma-Aldrich), 1 g yeast extract (Formedium), 0.5 g glucose (Sigma-Aldrich), 0.1 g SPO mix, 20 g agar (Formedium), 250 μL 200 mg/mL G418.

LB agar + Ampicillin: 5 g yeast extract, 10 g tryptone, 5 g sodium chloride, 20 g agar, 50 mL 40% glucose, 1 mL 100 mg/mL ampicillin.

LB liquid + Ampicillin: Same as LB agar without the addition of agar.

SC or SD agar: 1.7 g yeast nitrogen base (Formedium), 1 g monosodium glutamate (MSG), 2 g SC or SD amino acid mix in 450 mL ddH_2O, stirred and sonicated until completely dissolved. In a separate bottle, 20 g agar in 500 mL ddH_2O. After autoclaving, agar was poured into the mix bottle and 50 mL 40% glucose was added.

SC or SD liquid: Same as agar but without the addition of agar, all contents in one bottle with 950 mL ddH_2O.

YPD agar: 10 g yeast extract, 20 g peptone (Formedium), 0.120 g adenine, 20 g agar and 50 mL 40% glucose.

YPD liquid: Same as YPD agar without the addition of agar.

Antibiotics and supplements stocks

All antibiotics and supplements stocks were filter sterilised with 22 μM pore filters (Jet Biofil).

ClonNAT 100 mg/mL: 3 g nourseothricin sulfate (Werner BioAgents) in the amount which is enough for (abbreviated *q.s.* for the latin term *quantum satis*) 30 mL ddH_2O.

G418 200 mg/mL: 6 g geneticin sulfate (Carbosynth) in *q.s.* 30 mL ddH_2O.

Canavanine 50 mg/mL: 1.5 g L-canavanine sulfate (Carbosynth) in *q.s.* 30 mL ddH_2O.

S-aminoethyl-L-cysteine hydrochloride (thyalisine) 50 mg/mL: 1.5 g thyalisine (Carbosynth) in *q.s.* 30 mL ddH_2O.

Hygromycin 300 mg/mL: 3 g hygromycin B (Life Technologies) in *q.s.* 10 mL ddH_2O.

Ampicillin 100 mg/mL: 1 g ampicillin (Sigma-Aldrich) in *q.s.* 10 mL ddH_2O.

Atorvastatin 25 mM: 0.578 g atorvastatin calcium (Sigma-Aldrich) in *q.s.* 20 mL DMSO. Aliquots were stored at -80°C.

2.2.4 Synthetic Genetic Array (SGA) analysis

SGA analysis was conducted in quadruplicate as previously described (Busby et al. 2019; Tong et al. 2001) in three genetic backgrounds (S288C, UWOPS87 and Y55) with newly constructed query deletion strains in which *HMG1* and *BTS1* was replaced with NATMX antibiotic resistance gene via PCR-mediated disruption using specific primers (Table 2.3) and cycle conditions (Tables 2.4 and 2.5). PCR products were then transformed into a *MATα* SGA starter strain via homologous transformation as previously described (Gietz and Schiestl 2007) and integration into the genome was confirmed by PCR as previously described (Tong and Boone 2006). An overnight culture of the query strain was replicated on YPD+NAT agar in 384-colony format and then reformatted to 1536-colony format. The query *Matα*

Primer	Sequence	Description
hmg1Δ forward	ATAGTGTATCATTGTCTAATTGTTGATACAAAGTAGATA AATACATAAAACAAGCACATGGAGGCCCAGAATACCCT	5' *HMG1* loci KO with clonNAT resistance cassette
hmg1Δ reverse	ACATGGTGCTGTTGTGCTTCTTTTTCAAGAGAATACCAAT GACGTATGACTAAGTCAGTATAGAGCGACCAGCATTCAC	3' *HMG1* loci KO with clonNAT resistance cassette
bts1Δ forward	TTCAAAGAAGCTACTAATAGAAAGAGAACAAAGCGTTTA CGAGTCTGGAAAATCAACATGGAGGCCCAGAATACCCT	5' *BTS1* loci KO with clonNAT resistance cassette
bts1Δ reverse	GAGAAGGCTTTATTTCTGACTATCTTCCTCCACTAATTT GATTGATCAATTTATTCAGTATAGCGACCAGCATTCAC	3' *BTS1* loci KO with clonNAT resistance cassette
hmg1Δ confirmation forward (A)	AGTCTCTACGCCCGCTCG	5' *HMG1* loci KO confirmation A
hmg1Δ confirmation reverse (D)	CGCATGACTCAAGAGAAGC	3' *HMG1* loci KO confirmation D
bts1Δ confirmation forward (A)	AGTCTCTACGCCCGCTCG	5' *BTS1* loci KO confirmation A
bts1Δ confirmation reverse (D)	GGAGTTTCAGAAATCGTGG	3' *BTS1* loci KO confirmation D
NAT confirmation reverse (B)	TACGAGATGACCACGAAGC	3' clonNAT resistance loci confirmation B
NAT confirmation forward (C)	TGGAACCGCCGGCTGACC	5' clonNAT resistance loci confirmation C

Table 2.3: **PCR primers used for NATMX cassette construction and confirmation of its integration.**

plates were mated with the 14 plates of the *MATa* deletion mutant array of the corresponding genetic background for 1 day at room temperature on YPD agar. The resulting diploids were selected on YPD+NAT/G418 via growth at 30°C overnight and then sporulated on SPO agar for 7-10 days. Then haploids were selected via two rounds of growth at 30°C overnight on SD -histidine/arginine/lysine (HRK) + canavanine (CAN)/thialysine (THIA), followed by selection for double deletion mutants via two rounds of growth at 30°C overnight on SD-HRK+CAN/THIA/G418/NAT agar.

2.2.5 Genome-wide growth analysis

The selected double deletion mutant libraries (*hmg1*△ *xxx*△ and *bts1*△ *xxx*△) were pinned on SC agar, incubated at 30°C overnight, and used as an inoculum source to pin on SC agar with and without

Component	Volume (µL)
ddH2O	17.625
10X Buffer	2.5
dNTPs	2
DMSO	1.25
Deletion primer Fwd	0.5
Deletion primer Rev	0.5
Taq	0.125
Template (plasmid)	0.5

Table 2.4: **PCR mix used for the construction of NATMX cassettes.**

PCR phase	Temperature (°C)	Time	# cycles
Initial denaturation	95	5 min	1
Denaturation	94	40 s	36
Annealing	58	1 min	36
Extension	68	2 min	36
Final extension	72	5 min	1

Table 2.5: **PCR conditions used for the construction of NATMX cassettes.**

IC_{30} concentrations of atorvastatin that were determined for each genetic background. These plates were incubated at 30°for 12 and 24 h, time points when the colonies were imaged using a digital camera (Canon). The colony sizes were quantified and scored through SGAtools (Wagih et al. 2013) where z-scores were used to compare growth with and without atorvastatin (zero indicates no difference between the control and treatment, negative scores indicate reduced fitness with atorvastatin, and positive scores indicate increased fitness with atorvastatin). All SGA scores were visualised in violin plots generated in R and based on their point of inflection, the cut-offs were selected to identify strains for experimental validation in 384-colony format and serial dilution spot assay.

2.2.6 Validation of negative genetic interactions in 384-colony format

The validation of negative genetic interactions was performed in a two-step process. First, 96-colony format plates were arrayed containing no more than 29 hits each with *his3*Δ control border strains and also *his3*Δ control strains surrounding each candidate to ensure the colony sizes were not biased. Each plate also included a wild type strain. The hits for S288C, Y55 and UWOPS87 *hmg1*Δ *xxx*Δ or *bts1*Δ *xxx*Δ that did not overlap with the single deletions *xxx*Δ were arrayed as described. Control single deletions were also arrayed to confirm that negative interactions pertained to double deletions only. The arrayed plates were screened with the same IC_{30} concentrations of

atorvastatin used in the 1536-colony format. Plates were incubated at 30°C for 24 h, imaged using a digital camera, growth was quantified using SGAtools (Wagih et al. 2013) as described above for the 1536-colony format, and hypersensitive strains were then selected for an additional experimental validation step through serial dilution spot assays.

2.2.7 Validation of negative genetic interactions in serial dilution spot assay

Overnight cultures were prepared in 96-well plates and four 1:10 serial dilutions were spotted using a manual pinning tool on SC agar with and without an IC_{30} concentration of atorvastatin. Plates were incubated at 30°C for 48 h, imaged using a digital camera, and evaluated visually for atorvastatin-specific growth defects. A cut-off for growth defect was determined as one spot less of atorvastatin-treated versus non-treated strains and of the double deletion compared to the single deletions (query gene deletion and *xxx*Δ). Those hits that validated in spot assays were then submitted to another round of spot assays this time including the three genetic backgrounds.

2.2.8 Single-layer network analyses

Validated genetic interactions that enhanced the hypersensitivity to atorvastatin were examined in the context of gene-gene and protein-protein interaction networks. The list of validated genes was augmented with gene-gene interactions using GeneMania (Warde-Farley et al. 2010) using all available studies with a maximum number 110 interacting genes. Using NetworkAnalyst (Xia et al. 2015; Zhou et al. 2019), the list of validated genes was augmented with protein-protein interactions using the STRING database (Szklarczyk et al. 2015) that includes text-mining, genomic information, co-expression and orthology with the additional requirement for experimental evidence with a confidence score cut-off of 900. The resulting protein-protein interaction network was a first-order network representing the input nodes with their direct interactors, which was then augmented into a second-order network to include nodes that connected the input genes as well as nodes that were interactors, but that only included the minimum number of nodes necessary to maintain connectivity of the network (minimum network). The gene-gene interaction networks (GINs) and the protein-protein interaction networks (PPINs) were then integrated into a single multi-layer network using TimeNexus (Pierrelée et al. 2021) in Cytoscape (Shannon et al. 2003).

2.2.9 Topology centrality analysis

The single-layer and multi-layer networks were analysed for various measurements of network centrality using the NetworkAnalyzer for undirected networks application in Cytoscape (Boccaletti et al. 2014). Three centrality measurements were calculated: (1) Degree centrality, which computes the number of edges linked to each node so that a node with degree 5 has 5 edges associated, that is, it is linked to 5 other nodes (Dong and Horvath 2007); (2) closeness centrality, which corresponds to the average shortest path length of one node to every other node computed by the Newman method (Newman 2005), where 0 means an isolated node and 1 is the highest centrality and connectivity; and (3) betweenness centrality, which is the probability of passing through a node when using the shortest path length between two nodes and is computed with the highly precise algorithm developed by Brandes (Brandes 2001) to distinguish nodes critical to maintain a network. The three measurements of centrality were visualised as 3D plots using R (Soetaert 2019).

2.2.10 Community analysis

Functional modules (communities) in the single-layer and multi-layer networks were determined using the InfoMap algorithm (Rosvall and Bergstrom 2008) in NetworkAnalyst (Xia et al. 2015). Statistical significance for each module was evaluated for their clustering significance or network connectivity as computed by a Wilcoxon rank-sum test ($P < 0.05$).

2.2.11 Pathway enrichment analysis

Modules were investigated for their function via metabolic pathway enrichment analysis using the Kyoto Encyclopedia of Genes and Genomes (KEGG) pathway database (Kanehisa and Goto 2000) implemented in Enrichr (Chen et al. 2013; Kuleshov et al. 2016). Pathway enrichment was statistically evaluated using an adjusted *P*-value with the Benjamini-Hochberg method for correction (Benjamini and Hochberg 1995), a z-score reflecting the deviation of a Fisher's exact test from an expected rank, and a combined score that is the product of the natural logarithm of the *P*-value multiplied by the z-score. Fold-enrichment and *P*-value (<0.05) for statistically significant pathways in each module were visualised in bubble plots using R (Wickham 2016).

2.2.12 Gene set enrichment for drug signatures

Human orthologues of genes that interact with *HMG1*/*BTS1* query strains as well as highly ranked centrality genes were determined using Yeastmine in the Saccharomyces Genome Database (Cherry et al. 2012) and examined for significant enrichment ($P < 0.05$) in the Drug Signature Database (Yoo et al. 2015) implemented in Enrichr (Chen et al. 2013; Kuleshov et al. 2016; Xie et al. 2021).

2.3 Results

2.3.1 Atorvastatin sensitivity varies in three genetic backgrounds and is enhanced with BTS1-deficiency

To construct the query strains that were used to investigate chemical genetic interactions with genes in the mevalonate pathway, the *HMG1* or *BTS1* gene was replaced in three yeast genetic backgrounds with NATMX4 through PCR-directed mutagenesis and homologous recombination. The deletion strains *hmg1*Δ and *bts1*Δ were then treated with atorvastatin to characterise the toxicity of the drug in these deletion strains (Figure 2.3). Synthetic sick and synthetic lethal fitness defects were expected in *hmg1*Δ and *bts1*Δ upon treatment with atorvastatin because *HMG1* is the target of atorvastatin and *BTS1* is downstream in the same pathway. Since S288C is known to be statin-sensitive while UWOPS87 and Y55 are statin-resistant (Busby et al. 2019), I expected fitness defects that correspond to those phenotypes. Surprisingly, all three genetic backgrounds showed the same sensitivity when *HMG1* was deleted (*i.e.*, synthetic sick at 5 μM, synthetic lethal at 50 μM), revealing all backgrounds are equally reliant on this gene to cope with atorvastatin treatment. However, the fitness defect differs across backgrounds when *BTS1* is deleted. The interaction is synthetic lethal in 1 μM of atorvastatin in S288C, while the same concentration of atorvastatin exerts only a mild fitness defect in UWOPS87 and Y55. Synthetic lethality was observed with 5 μM of atorvastatin treatment in these two genetic backgrounds. Hence, it seems that *HMG1* and perhaps early steps in the pathway mediate the increased resistance of UWOPS87 and Y55 to atorvastatin. The downstream *BTS1*-mediated branch of the mevalonate pathway may be distinct from statin resistance, possibly as a means to alleviate atorvastatin-induced UPR that is more pronounced in S288C than in the resistant strains (Busby et al. 2019).

2.3.2 Genome-wide analysis of hmg1Δ and bts1Δ synthetic sick/lethal interactions shows the genes buffering statin sensitivity in three genetic backgrounds

Via the generation and quantification of growth of double deletion mutant libraries, SGA analyses reveal gene-gene interactions integral to drug mechanism of action (Busby et al. 2019; Boone et al. 2007). To investigate atorvastatin-specific epistasis in the mevalonate pathway, genome-wide double deletion libraries for the statin-susceptible (S288C) and the two statin-resistant strains (UWOPS87 and Y55) were constructed by integrating *hmg1*Δ and *bts1*Δ into single deletion libraries in three genetic

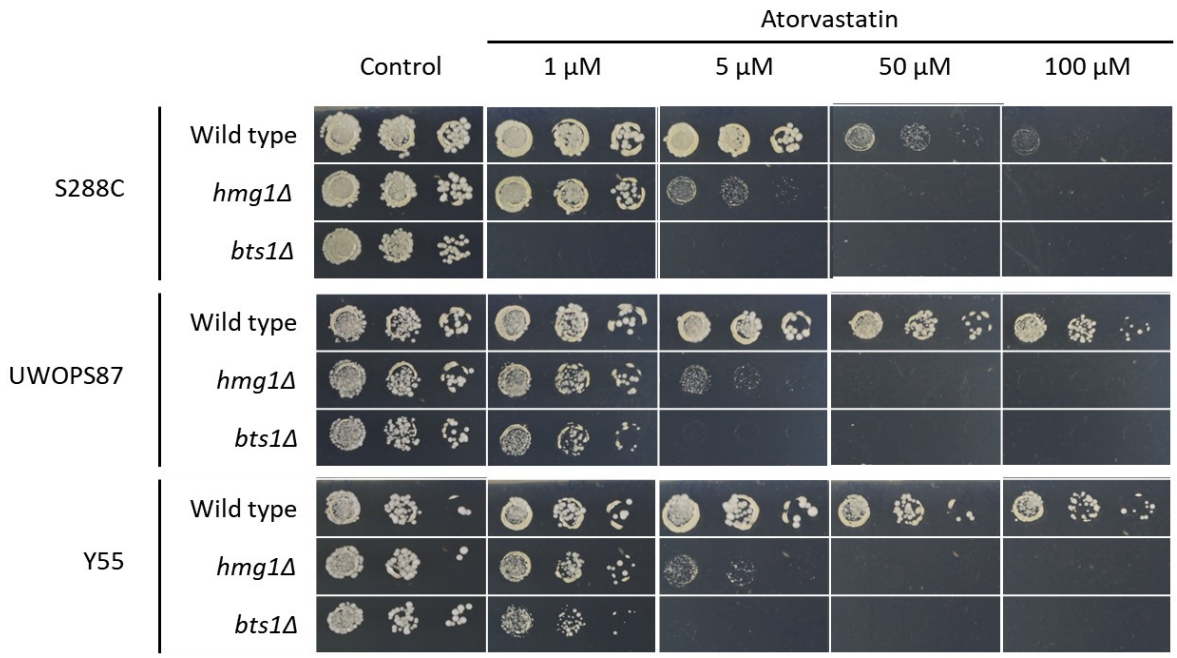

Figure 2.3: **Atorvastatin sensitivity confers similar synthetic sickness/lethality in *HMG1*-deleted strains and varies in *BTS1*-deleted strains in three genetic backgrounds.** Haploid cells deficient of *HMG1* or *BTS1* and their wild types in three genetic backgrounds were pinned on increasing concentrations of atorvastatin in serial dilution and incubated for 2 days at 30°C.

backgrounds (Busby et al. 2019; Winzeler et al. 1999) using SGA technology (Tong et al. 2001). To assist the understanding of this and the following sections, the flow diagram of methods is repeated in Figure 2.4 (refer to panels A and B for this section).

In order to detect growth defects due to synthetic sick/lethal interactions, IC_{30} concentrations of atorvastatin were determined for *hmg1*Δ *xxx*Δ, *bts1*Δ *xxx*Δ and *xxx*Δ libraries (Figure 2.5) upon trials with several concentrations ranging from 0.2 to 64 μM for *hmg1*Δ *xxx*Δ, 0.01 to 64 μM for *bts1*Δ *xxx*Δ and 10 to 320 μM for *xxx*Δ. All *hmg1*Δ *xxx*Δ double deletions were then screened at 0.8 μM atorvastatin, *bts1*Δ *xxx*Δ double deletions in S288C were screened at 0.05 μM and 0.5 μM was used to screen *bts1*Δ *xxx*Δ double deletions in Y55 and UWOPS87. Single deletion *xxx*Δ controls were screened with 9 μM for S288C, 10 μM for UWOPS87 and 35 μM for Y55. All strains were screened in quadruplicate at the IC_{30} concentrations, which provided a 70% window to detect additional growth reduction due to synthetic sick/lethal interactions.

The chemical genetic profiles of atorvastatin-treated strains were significantly different between the single and double deletions based on the distribution of scored colony sizes where negative scores represent fitness defects (synthetic sick/lethal interactions) and positive values relate to increased fitness (suppressors) (Figure 2.6). As expected, the distribution of scored colony sizes in the single deletions were similar between the two resistant backgrounds UWOPS87 and Y55, but differed

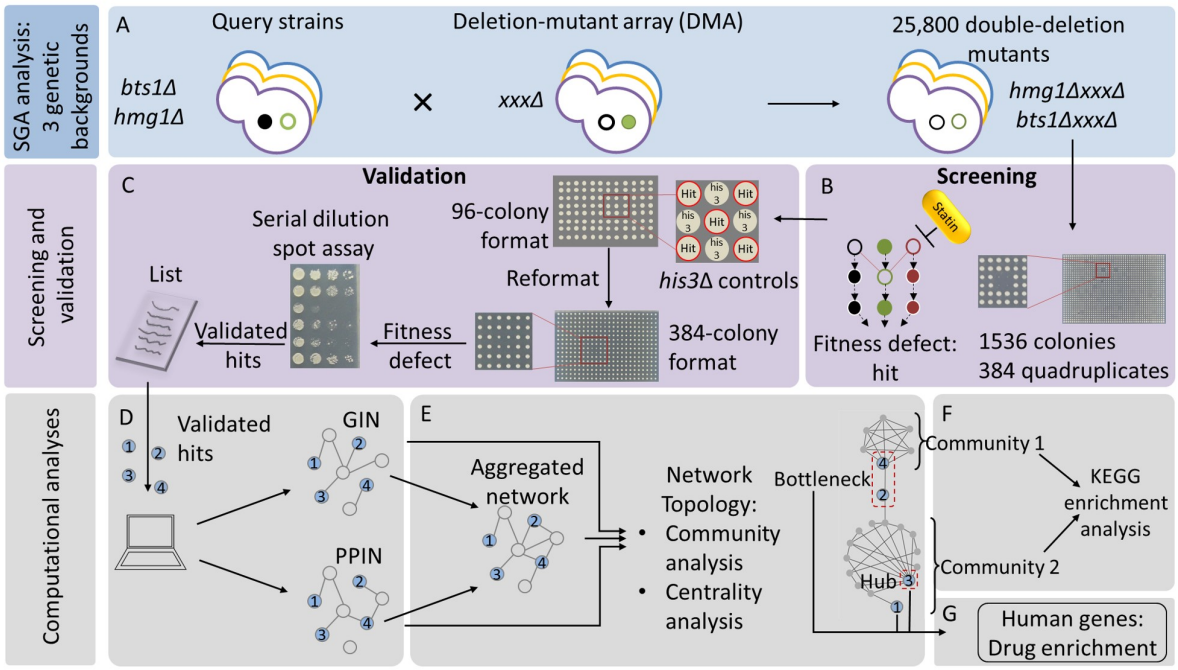

Figure 2.4: **Flow diagram for the methods used to identify interactions, pathways and drugs to enhance the anticancer activity of atorvastatin.**

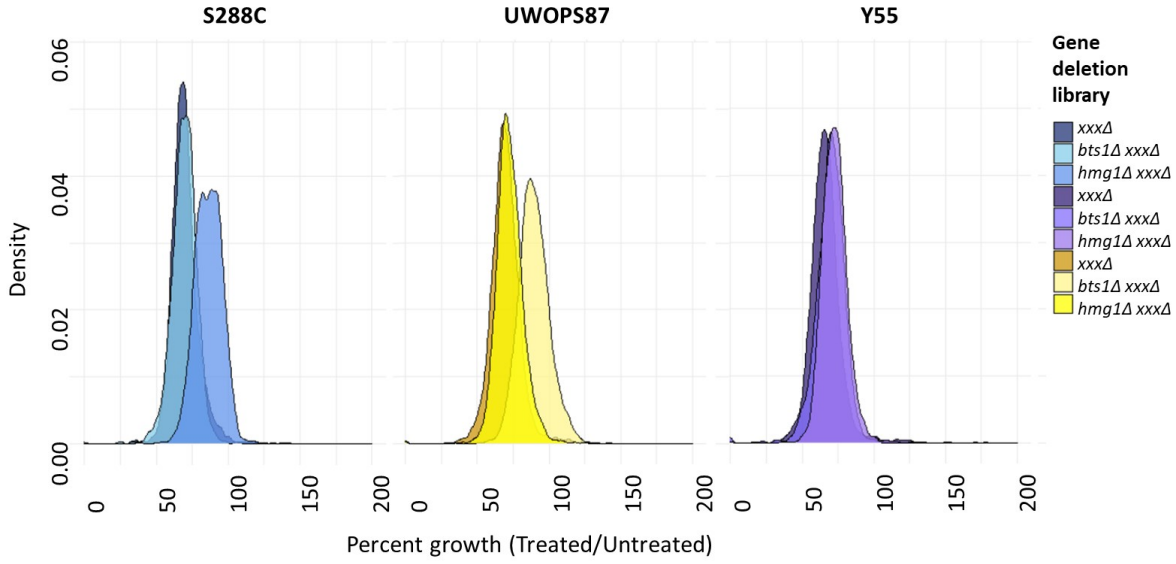

Figure 2.5: **Atorvastatin concentration for maximum overlap at 30% of growth inhibition between the single and double deletions.** DMA-derived *xxx*Δ and SGA-derived *bts1*Δ *xxx*Δ and *hmg1*Δ *xxx*Δ libraries were screened in IC_{30} concentrations of atorvastatin. Density plots represent distribution of percent growth where higher density (y-axis) indicates more gene deletions having the corresponding percent growth in the x-axis.

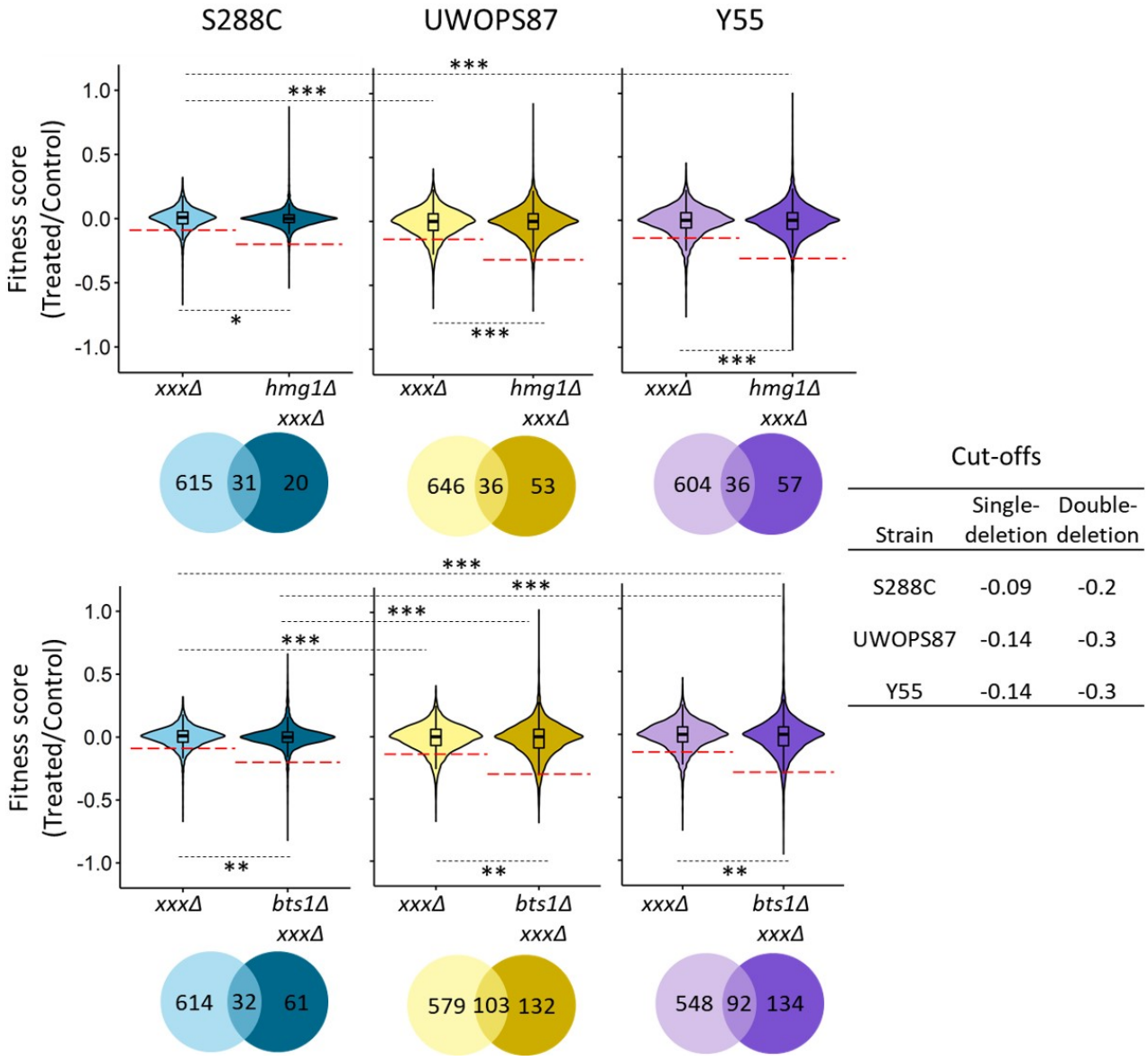

Figure 2.6: **The strength of synthetic sick/lethal interactions does not differ significantly in *hmg1*Δ *xxx*Δ strains in three genetic backgrounds but it differs between the statin-susceptible S288C *bts1*Δ *xxx*Δ and the statin-resistant UWOPS87 and Y55.** Violin plot distributions of average fitness of 12,900 strains as measured by colony sizes (n = 4) of *xxx*Δ and *hmg1*Δ *xxx*Δ (upper panel) as well as *xxx*Δ and *bts1*Δ *xxx*Δ (lower panel) where positive scores represent increased fitness and negative scores represent decreased fitness. The red dashed lines indicate the score cut-off values selected for validation in independent assays for double deletions that did not overlap with the *xxx*Δ single deletions. Venn diagrams visualise the overlap in the number of genes below the cut-off lines. Statistical differences were evaluated with a Student's *t*-test (*, $P < 0.05$; **, $P < 0.01$; ***, $P < 0.001$).

between the statin-susceptible strain S288C and the two statin-resistant backgrounds. Regarding the *hmg1*△ and *bts1*△ single deletion phenotypes in response to atorvastatin, the distribution of scored colony sizes did not differ among the three genetic backgrounds when *HMG1* was deleted, but it did differ between S288C and the resistant genetic backgrounds when *BTS1* was deleted.

High-throughput screening experiments tend to suffer from noisy data and thus it was necessary to validate the hypersensitive interactions identified in 1536-colony format. To aid validation, I established a cut-off for the scored colonies (pixel-based colony size scored values assigned in SGAtools via Gitter (Wagih and Parts 2014)) of 3 standard deviations below the median for *hmg1*△ strains and of 2.5 standard deviations below the median for *bts1*△ strains. That way, genes with scores below -0.2 for S288C and below -0.3 for UWOPS87 and Y55 were considered hits for validation. Notably, given my specific interest in epistatic interaction effects unique to the double deletions, hits that were sensitive in single and double deletion mutants were excluded from further analysis. For instance, the 31 interactions below the score cut-offs that overlapped between the *hmg1*△ *xxx*△ double deletions and the *xxx*△ single deletions in S288C (Figure 2.6) were excluded from further analysis.

2.3.3 Validation of atorvastatin-specific genetic interactions with HMG1 in three genetic backgrounds

Using the cut-off criteria in the SGA analysis, I selected to validate atorvastatin-specific growth defects in 20, 53, and 57 *hmg1*△ *xxx*△ strains for S288C, UWOPS87 and Y55, respectively. To complement the high-throughput growth assay in 1536-colony, growth of candidate *hmg1*△ *xxx*△ strains was monitored in an independent assay where strains were grown individually as serial spot dilutions on agar (Figure 2.4C).

First, chemical genetic interactions conserved across the three genetic backgrounds provide insight into atorvastatin bioactivity in all individuals. Four chemical genetic interactions with *HMG1* were apparent in the spot dilution assay (Figure 2.7; Table 2.6). Deletion of *DBP7* in *HMG1*-deleted strains showed growth in only one spot in contrast to *DBP7* or *HMG1* deletion alone. The double deletion *hmg1*△ *rim15*△ deemed S288C almost inviable and completely inviable in atorvastatin treatment, whereas the double deletion did not exert decreased fitness for UWOPS87 and Y55 but treatment with atorvastatin showed high toxicity. *TRM7* deletion itself deemed UWOPS87 increased susceptibility to atorvastatin but this was exacerbated in the *hmg1*△ *trm7*△ double deletion, which also turned S288C and Y55 hypersensitive to atorvastatin treatment. *VPS51* deletion did not increase sensitivity to atorvastatin treatment on its own but the double deletion was highly toxic, especially for S288C and

UWOPS87.

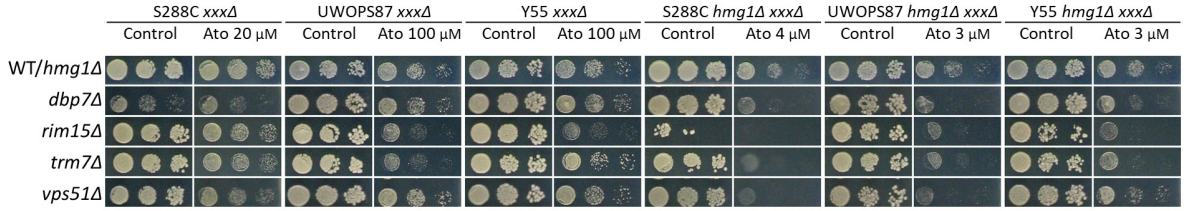

Figure 2.7: **Four *hmg1*Δ *xxx*Δ double deletions were hypersensitive to atorvastatin treatment in three genetic backgrounds.** Haploid cells derived from SGA analyses and DMA libraries were pinned on SC with or without supplementation of atorvastatin in serial dilution and incubated for 2 days at 30°C. Shown here are deletions of genes that enhanced sensitivity to atorvastatin treatment. WT/*hmg1*Δ panel refers to either the non-mutated wild types (WT) for the *xxx*Δ strain panels or the *hmg1*Δ single deletions for the *hmg1*Δ *xxx*Δ double deletion strain panels.

DBP7 and *TRM7* each function in the process of translation; specifically *DBP7* is an RNA helicase of the DEAD-box family involved in ribosomal biogenesis and *TRM7* is a ribose methyltransferase that methylates the tRNA-Phe, tRNA-Trp, and tRNA-Leu at positions C32 and N34 of the tRNA anticodon loop. The other two validated hits do not seem to have obvious connections. *RIM15* is a protein kinase involved in cell proliferation in response to nutrients, while *VPS51* is a component of the Golgi-associated retrograde protein required for the recycling of proteins from endosomes to the late Golgi. All four yeast genes are conserved in humans, either at the gene level for *DBP7*, *TRM7* and *RIM15*, or alternatively at the complex level for *VPS51* (Table 2.6). These results indicate that specific mechanisms in translation, kinase activity and the retrograde pathway are buffering atorvastatin bioactivity.

ORF	Gene	Name	Description	Human orthologue(s)
YKR024C	*DBP7*	Dead Box Protein	RNA helicase of the DEAD-box family involved in ribosomal biogenesis	DDX41, DDX46
YFL033C	*RIM15*	Regulator of IME2	Protein kinase involved in cell proliferation in response to nutrients	MAST1, MAST2, MAST3, MAST4, MASTL
YBR061C	*TRM7*	Transfer RNA Methyltransferase	Ribose methyltransferase that methylates the tRNA-Phe, -Trp, and -Leu at the anticodon loop	FTSJ1
YKR020W	*VPS51*	Vacuolar Protein Sorting	Required for the recycling of proteins from endosomes to the late Golgi	GARP complex

Table 2.6: **List of atorvastatin *hmg1*Δ *xxx*Δ strains that overlap in three genetic backgrounds.** Description was obtained from SGD (Cherry et al. 2012). Human orthologues were obtained from YeastMine (Balakrishnan et al. 2012).

Because genetic interactions mediating the drug response to atorvastatin are known to be unique to individuals (Busby et al. 2019), I expected to detect epistatic interactions that were unique to each genetic background. Indeed, two chemical genetic interactions (*LEM3* and *SLG1*) were unique to S288C, seven chemical genetic interactions (*COX5A*, *CSG2*, *EOS1*, *HST1*, *KEX2*, *TPM1* and *TSR3*) were unique to UWOPS87, and four chemical genetic interactions (*ADH4*, *BTS1*, *CCP1* and *YAK1*) were unique to Y55 (Figure 2.8; Table 2.7).

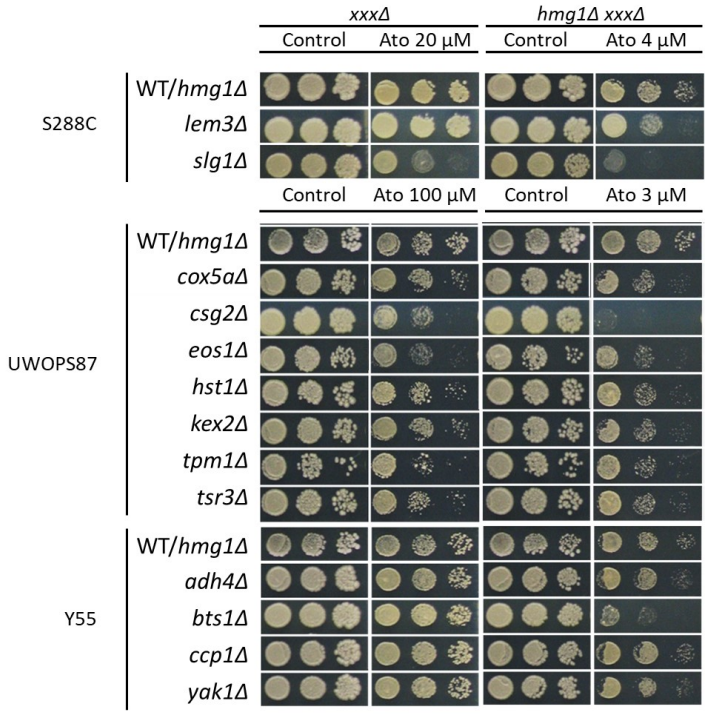

Figure 2.8: **Some epistatic interactions depend on the genetic background.** Haploid cells derived from SGA analyses and DMA libraries were pinned on SC with or without supplementation of atorvastatin in serial dilution and incubated for 2 days at 30°C. WT/*hmg1*Δ refers to either the non-mutated wild type (WT) for the *xxx*Δ strain panels or the *hmg1*Δ single deletions for the *hmg1*Δ *xxx*Δ double deletion strain panels.

Genetic background	Validated hypersensitive interactions
S288C	*LEM3, SLG1,* ***DBP7, RIM15, TRM7, VPS51***
UWOPS87	*COX5A, CSG2, EOS1, HST1, KEX2, TPM1, TSR3,* ***DBP7, RIM15, TRM7, VPS51***
Y55	*ADH4, BTS1, CCP1, YAK1,* ***DBP7, RIM15, TRM7, VPS51***

Table 2.7: **List of validated *hmg1*Δ *xxx*Δ double deletion strains in each of three yeast genetic backgrounds.** Interactions overlapping in three genetic backgrounds are shown in bold.

Interestingly, some of the genes that did not overlap between genetic backgrounds have similar functions to other hits in different genetic backgrounds, indicating that the genetic interactions are not conserved but the cellular coping mechanisms might be conserved (Table 2.8). For example,

SLG1 in S288C and *TPM1* in UWOPS87 have roles in organisation and stabilisation of actin cables, emphasising the relevance of actin in the response to atorvastatin. Similarly, *COX5A* in UWOPS87 has a role in electron transport chain, similarly to *CCP1* in Y55. Ion homeostasis seems to also play an important role in the response to atorvastatin since *CSG2* and *KEX2* in UWOPS87 regulate calcium and *ADH4* in Y55 regulate zinc homeostasis. As noted previously for other hits, most of the non-overlapping genes are conserved in humans which underlines their relevance for the eukaryotic cellular function and not only for yeast (Table 2.8), pointing to concise experiments with human cells that could be done in the future.

Background	ORF	Gene	Name	Description	Human orthologue(s)
S288C	YNL323W	*LEM3*	Ligand Effect Modulator	Membrane protein of the plasma membrane and ER; involved in translocation of phospholipids and alkylphosphocholine drugs across the plasma membrane	TMEM30A, TMEM30B, TMEM30C
	YOR008C	*SLG1*	Synthetic Lethal with Gap	Sensor-transducer of the stressactivated PKC1-MPK1 kinase pathway; involved in organization of the actin cytoskeleton	MUC15
UWOPS87	YNL052W	*COX5A*	Cytochrome c OXidase	Subunit Va of cytochrome c oxidase, the terminal member of the mitochondrial inner membrane electron transport chain	COX4I1, COX4I2
	YBR036C	*CSG2*	Calcium Sensitive Growth	ER membrane protein with a role in mannosylation of inositolphosphorylceramide required for growth at high calcium concentrations	None
	YNL080C	*EOS1*	ER-localized and Oxidants Sensitive	Protein involved in N-glycosylation; deletion mutation confers sensitivity to oxidative stress	None
	YOL068C	*HST1*	Homolog of SIR Two	NAD(+)-dependent histone deacetylase; involved in meiotic repression and telomere maintenance	SIRT1, SIRT4, SIRT5
	YNL238W	*KEX2*	Killer EXpression defective	Kexin, a calcium-dependent serine protease with a role in the secretory pathway	FURIN, PCSK6, PCSK5, PCSK4, PCSK1, PCSK2, PCSK7
	YNL079C	*TPM1*	TroPoMyosin	Major isoform of tropomyosin, which stabilizes actin cables and filaments	TPM1, TPM2, TPM3, TPM4
	YOR006C	*TSR3*	Twenty S rRNA accumulation	Protein required for 20S pre-rRNA processing	TSR3
Y55	YGL256W	*ADH4*	Alcohol DeHydrogenase	Alcohol32 dehydrogenase that has induced transcription upon zinc deficiency	ADHFE1
	YPL069C	*BTS1*	Bet Two Suppressor	Geranylgeranyl diphosphate synthase (GGPPS); suppressor of bet2 mutation that causes defective vesicular traffic	GGPS1
	YKR066C	*CCP1*	Cytochrome c Peroxidase	Mitochondrial cytochrome-c peroxidase involved in the response to oxidative stress	None
	YJL141C	*YAK1*	Yet Another Kinase	Serine-threonine protein kinase sensitive to glucose that phosphorylates Crf1p in response to nutrient deprivation inhibiting transcription of ribosomal genes	HIPK3, HIPK4, DYRK1A, HIPK1, HIPK2, DYRK3, PRPF4B, DYRK1B

Table 2.8: **Human orthologues of genes interacting with *HMG1* that are not conserved in all three genetic backgrounds.** Description was obtained from SGD (Cherry et al. 2012). Human orthologues were obtained from YeastMine (Balakrishnan et al. 2012)

2.3.4 Validation of atorvastatin-specific genetic interactions with BTS1 in three genetic backgrounds

Using the cut-off criteria in the high-throughput screen, I selected to validate atorvastatin-specific growth defects in 61, 132, and 134 *bts1*Δ *xxx*Δ strains for S288C, UWOPS87 and Y55, respectively. To complement the high-throughput growth assay in 1536-colony, growth of candidate *bts1*Δ *xxx*Δ strains was monitored in an independent assay where strains were grown individually as serial spot dilutions on agar (Figure 2.4C).

First, chemical genetic interactions conserved across the three genetic backgrounds provide insight into atorvastatin bioactivity in all individuals. Three chemical genetic interactions with *HMG1*, namely *ARL1*, *SYN8* and *UBX3*, were apparent in the spot dilution assay (Figure 2.9). Deletion of *UBX3* by itself did not increase sensitivity to atorvastatin in S288C and had some degree of effect on UWOPS87 and Y55 (one less spot), but the double deletion with *BTS1* clearly enhanced sensitivity to atorvastatin compared to the single deletions (*bts1*Δ and *ubx3*Δ) and to the non-treated control. *SYN8* deletion slightly enhanced sensitivity to atorvastatin in UWOPS87 (one less spot) but not for S288C and Y55, whereas the double deletion *bts1*Δ *syn8*Δ enhanced sensitivity in S288C and more so in UWOPS87 and Y55. Similarly, deletion of *ARL1* enhanced sensitivity to atorvastatin in UWOPS87 and Y55 (one less spot) but not for S288C, while the double deletion with *BTS1* resulted in lethality for UWOPS87 and Y55 and enhanced toxicity for S288C. *UBX3* and *SYN8* have roles in the secretory pathway and *ARL1* has a role in autophagy (Table 2.9).

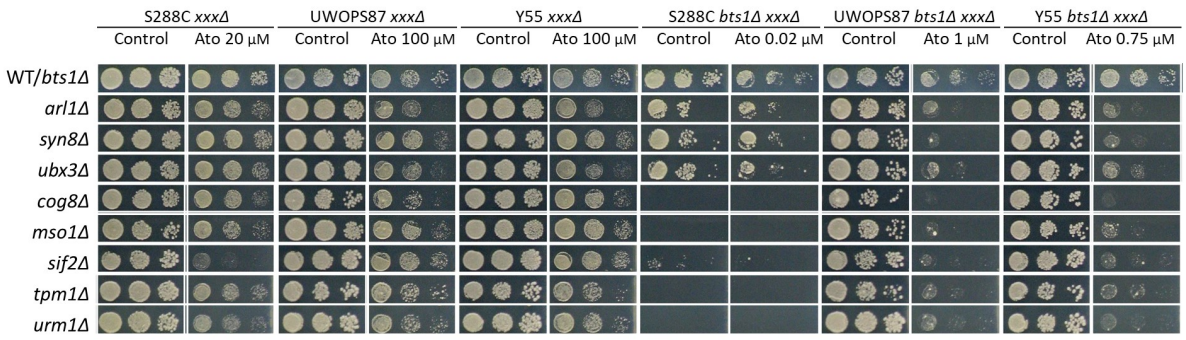

Figure 2.9: **Eight *bts1*Δ *xxx*Δ double deletions were hypersensitive to atorvastatin treatment in at least two resistant genetic backgrounds.** Haploid cells derived from SGA analyses and DMA libraries were pinned on SC with or without supplementation of atorvastatin in serial dilution and incubated for 2 days at 30°C. WT/*bts1*Δ refers to either the non-mutated wild type for the *xxx*Δ strain panels or the *bts1*Δ single deletion for the *bts1*Δ *xxx*Δ double deletion strain panels.

ORF	Gene	Name	Description	Human orthologue(s)
YBR164C	*ARL1*	ADP-Ribosylation factor-Like	Soluble GTPase of the Ras superfamily that regulates potassium influx and a role in starvation-induced autophagy	ARL8A, ARL1, ARL15, ARL8B, ARL6
YAL014C	*SYN8*	SYNtaxin	Endosomal SNARE related to mammalian syntaxin 8	STX6, STX8, STX10
YDL091C	*UBX3*	UBiquitin regulatory X	Vesicle component required for efficient clathrin-mediated endocytosis that interacts with CDC48	FAF1, UBXN10, FAF2, UBXN8
YML071C	*COG8*	Conserved Oligomeric Golgi complex	Component of the oligomeric Golgi complex that mediates fusion of transport vesicles to Golgi compartments	COG8
YNR049C	*MSO1*	Multicopy suppressor of Sec1	Lipid-interacting protein in SNARE complex assembly machinery with a role in late secretion	None
YBR103W	*SIF2*	Sir4p-Interacting Factor	Subunit of Set3C histone deacetylase complex that antagonizes telomeric silencing	WDR17, TBL1X, TBL1XR1, THOC3, TBL1Y
YNL079C	*TPM1*	TroPoMyosin	Major isoform of tropomyosin, which stabilises actin cables and filaments	TPM1, TPM2, TPM3, TPM4
YIL008W	*URM1*	Ubiquitin Related Modifier	Ubiquitin-like protein involved in thiolation of cytoplasmic tRNAs that also has roles in oxidative stress response	URM1

Table 2.9: **List of atorvastatin *bts1*△ *xxx*△ strains that overlap in two genetic backgrounds.** Description was obtained from SGD (Cherry et al. 2012). Human orthologues were obtained from YeastMine (Balakrishnan et al. 2012). The horizontal line between genes delimits validated strains in three (top) and two (bottom) genetic backgrounds

Additionally, five atorvastatin-specific genetic interactions (*COG8*, *MSO1*, *SIF2*, *TPM1* and *URM1*) were synthetic sick with *BTS1* in the statin-resistant UWOPS87 and Y55 backgrounds, while these interactions were synthetic lethal independent of atorvastatin in the statin-sensitive S288C background (Figure 2.9). These genes are involved in epigenetic functions, vesicular transport, actin and oxidative stress (Table 2.9).

The involvement of vesicular transport became apparent. *UBX3*, for instance, is required for clathrin-mediated endocytosis, a process that is closely linked to actin cables and filaments, for which *TPM1* is a mediator. *COG8* mediates the fusion of transport vesicles to Golgi, while *SYN8* and *MSO1* are involved in SNARE interactions. A role for oxidative stress and starvation processes also showed relevance with *URM1* having a role in oxidative stress response and *ARL1* having a role in starvation-induced autophagy.

Consistent with my observation that chemical genetic interactions with *HMG1* included interactions that were unique to each genetic background (Figure 2.8), here I also detected chemical genetic interactions with *BTS1* that were unique to each genetic background (Figure 2.10; Table 2.10). Four chemical genetic interactions (*BRE5*, *IMH1*, *VPS21* and *YOR1*) were unique to S288C, seven chemical genetic interactions (*ELF1*, *INO4*, *MVP1*, *RTR1*, *SKY1*, *VPS8* and *YRM1*) were unique to UWOPS87,

and four chemical genetic interactions (*ASN2*, *NCS6*, *RIC1* and *UBA4*) were unique to Y55 (Figure 2.10). These genes are mainly involved in the secretory pathway, drug transport and urmylation (Table 2.11).

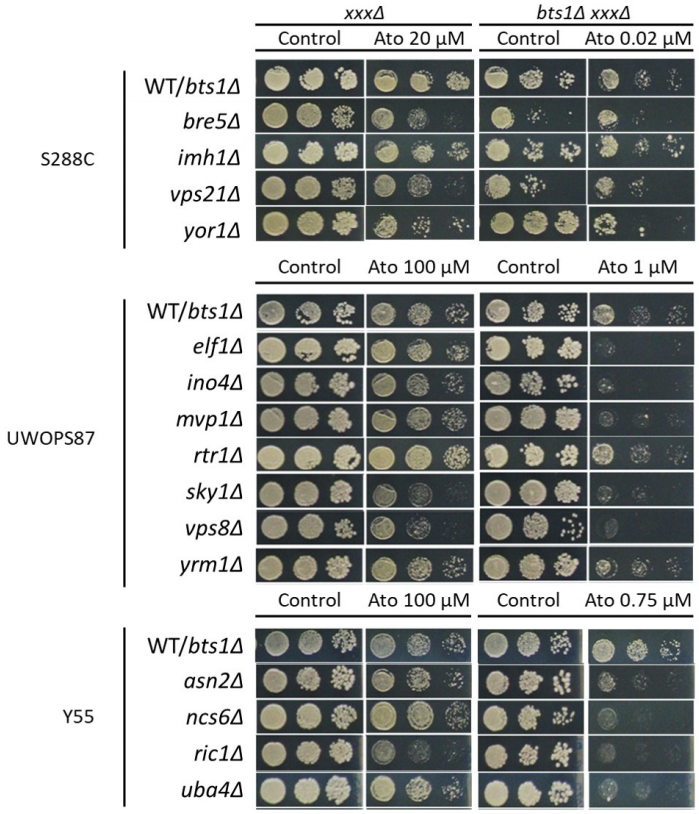

Figure 2.10: **Some epistatic interactions depend on the genetic background.** Haploid cells derived from SGA analyses and DMA libraries were pinned on SC with or without supplementation of atorvastatin in serial dilution and incubated for 2 days at 30°C. WT/*bts1*Δ refers to either the non-mutated wild type (WT) for the *xxx*Δ strain panels or the *bts1*Δ single deletion for the *bts1*Δ *xxx*Δ double deletion strain panels

Genetic Background	Validated hypersensitive interactions
S288C	*BRE5, VPS21, IMH1, YOR1,* ***ARL1***, ***SYN8***, ***UBX3***
UWOPS87	*ELF1, INO4, MVP1, RTR1, SKY1, VPS8, YRM1,* ***ARL1***, ***SYN8***, ***UBX3***, ***COG8***, ***MSO1***, ***SIF2***, ***TPM1***, ***URM1***
Y55	*ASN2, NCS6, RIC1, UBA4,* ***ARL1***, ***SYN8***, ***UBX3***, ***COG8***, ***MSO1***, ***SIF2***, ***TPM1***, ***URM1***

Table 2.10: **List of validated *bts1*Δ *xxx*Δ double deletion strains in each of three yeast genetic backgrounds.** Interactions overlapping in two or three genetic backgrounds are shown in bold.

The functions and human orthologues of the genes that did not overlap between genetic backgrounds are annotated in Table 2.11. Generally, these functions include vesicular transport and ion homeostasis. Similar to observations made above with the *HMG1* query, many *BTS1* interactions have similar functions to chemical genetic interactions that were conserved across genetic backgrounds. For

Background	ORF	Gene	Name	Description	Human orthologue(s)
S288C	YNR051C	*BRE5*	BREfeldin A sensitivity	Ubiquitin protease cofactor; forms deubiquitination complex with UBP3 and deubiquitinate COPII and COPI vesicle coat constituents, SEC23 and SEC27	G3BP1, G3BP2
	YLR309C	*IMH1*	Integrins and Myosins significant Homology	Protein involved in vesicular transport between an endosome and the Golgi	None
	YOR089C	*VPS21*	Vacuolar Protein Sorting	Endosomal Rab family GTPase required for endosomal localization of the CORVET complex and has a role in autophagy and ionic stress tolerance; geranylgeranylation required for membrane association	RAB31, RAB24, RAB20, RAB22A, RAB5A, RAB5B, RAB5C, RAB17
	YGR281W	*YOR1*	Yeast Oligomycin Resistance	Plasma membrane ATP-binding cassette (ABC) transporter of drugs	ABCC5, ABCC9, ABCC4, CFTR, ABCC2, ABCC6, ABCC1, ABCC8, ABCC11, ABCC3, ABCC10, ABCC12
UWOPS87	YKL160W	*ELF1*	ELongation Factor	Transcription elongation factor with a role in chromatin structure	ELOF1
	YOL108C	*INO4*	INOsitol requiring	Transcription factor involved in phospholipid synthesis	TFEC, MITF, TFE3, USF1, USF2, TFEB
	YMR004W	*MVP1*	Multi-copy suppressor of vps1	Protein required for sorting proteins to the vacuole	SNX18, SNX32, SNX33, SNX5, SNX8, SNX10, SNX11, SNX12, SNX30, SNX7, SNX9, SNX6, SNX1, SNX2, SNX3
	YER139C	*RTR1*	Regulator of TRanscription	Protein phosphatase that dephosphorylates T1 and S5 of RNA polymerase II largest subunit	RPAP2
	YMR216C	*SKY1*	SRPK1-like Kinase in Yeast	SR protein kinase (SRPK) involved in mRNA 3' splice site recognition with PRP8 and CDC40 and has a role in cation uptake and homeostasis	SRPK1, SRPK2, SRPK3
	YAL002W	*VPS8*	Vacuolar Protein Sorting	Component of the CORVET complex involved in endosomal vesicle tethering that interacts with VPS21	VPS8, VPS41
	YOR172W	*YRM1*	Yeast Reveromycin resistance Modulator	Zinc finger transcription factor involved in multidrug resistance	None
Y55	YGR124W	*ASN2*	ASparagiNe requiring	Asparagine synthetase; catalyzes the synthesis of L-asparagine from L-aspartate	ASNS
	YGL211W	*NCS6*	Needs Cla4 to Survive	Protein required for uridine thiolation of Gln, Lys, and Glu tRNAs with a role in urmylation	CTU1
	YLR039C	*RIC1*	RIbosome Control	Protein involved in retrograde transport to the cis-Golgi network involved in transcription of rRNA and ribosomal genes	RIC1
	YHR111W	*UBA4*	UBiquitin-Activating	E1-like protein that activates URM1 before urmylation	MOCS3, UBA5

Table 2.11: **List of validated *bts1*△ *xxx*△ double deletion strains in two resistant yeast genetic backgrounds.** Description was obtained from SGD (Cherry et al. 2012). Human orthologues were obtained from YeastMine (Balakrishnan et al. 2012).

example, genes involved in vesicular transport are represented in the three genetic backgrounds via *VPS21* and *IMH1* in S288C, *VPS8* and *MVP1* in UWOPS87 and *RIC1* in Y55. Drug transporters were also identified in both S288C (*YOR1*) and UWOPS87 (*YRM1*). Further, *URM1*, is a ubiquitin-like protein involved in thiolation of cytoplasmic tRNAs (Table 2.11), and two other genes in the same pathway, *NCS6* and *UBA4* were atorvastatin-sensitive in Y55, synthetic lethal in S288C, and not epistatic in UWOPS87. As for the conservation of the genes that did not overlap between backgrounds, most of these genes (12 out of 14) are conserved in humans. Together, these results emphasise the importance of these genes and their associated functions in yeast and potentially also in humans.

2.3.5 Construction of genetic and protein-protein interaction networks

The results thus far reveal specific genes, and in some cases shared processes, interacting with atorvastatin via *HMG1* and *BTS1*. To further understand the functional basis of these chemical genetic interactions that enhanced atorvastatin sensitivity, the genetic (GINs) and protein-protein interactions (PPINs) of these genes (the 17 and 23 genes that were validated to be interactive with *HMG1* and *BTS1*, respectively (Tables 2.7 and 2.10)), were identified and visualised within networks specific to each type of interaction and each genetic background (Figures 2.4D, 2.11-2.12). The numbers of nodes and edges for the *HMG1* GINs were 117 nodes/1478 edges for S288C, 112 nodes/702 edges for UWOPS87 and 109 nodes/732 edges for Y55 relative to 6, 11 and 8 input genes, respectively (Table 2.7, Figure 2.11). For the *BTS1* query, it was 109 nodes/1873 edges for S288C, 116/1901 edges for UWOPS87 and 113 nodes/1834 edges for Y55 relative to 7, 15 and 12 input genes, respectively (Table 2.10, Figure 2.12). The numbers of nodes and edges for the *HMG1* PPINs were 203 nodes/950 edges for S288C, 372 nodes/1858 edges for UWOPS87 and 186 nodes/835 edges for Y55 relative to the same 6, 11 and 8 input genes, respectively. The numbers of nodes and edges for the *BTS1* PPINs were 139 nodes/388 edges for S288C, 370 nodes/1944 edges for UWOPS87 and 233 nodes/1018 edges for Y55 relative to the same 7, 15 and 12 input genes, respectively.

2.3.6 Network topology centrality analyses identify genes critical to atorvastatin sensitivity in GINs and PPINs

The more central a gene is to a network, the more biological relevance (importance) it has to the phenotype (Yu et al. 2007). Three centrality measurements were thus calculated from the GINs and PPINs (Figure 2.4E). The centralities were betweenness centrality (shortest path length between two

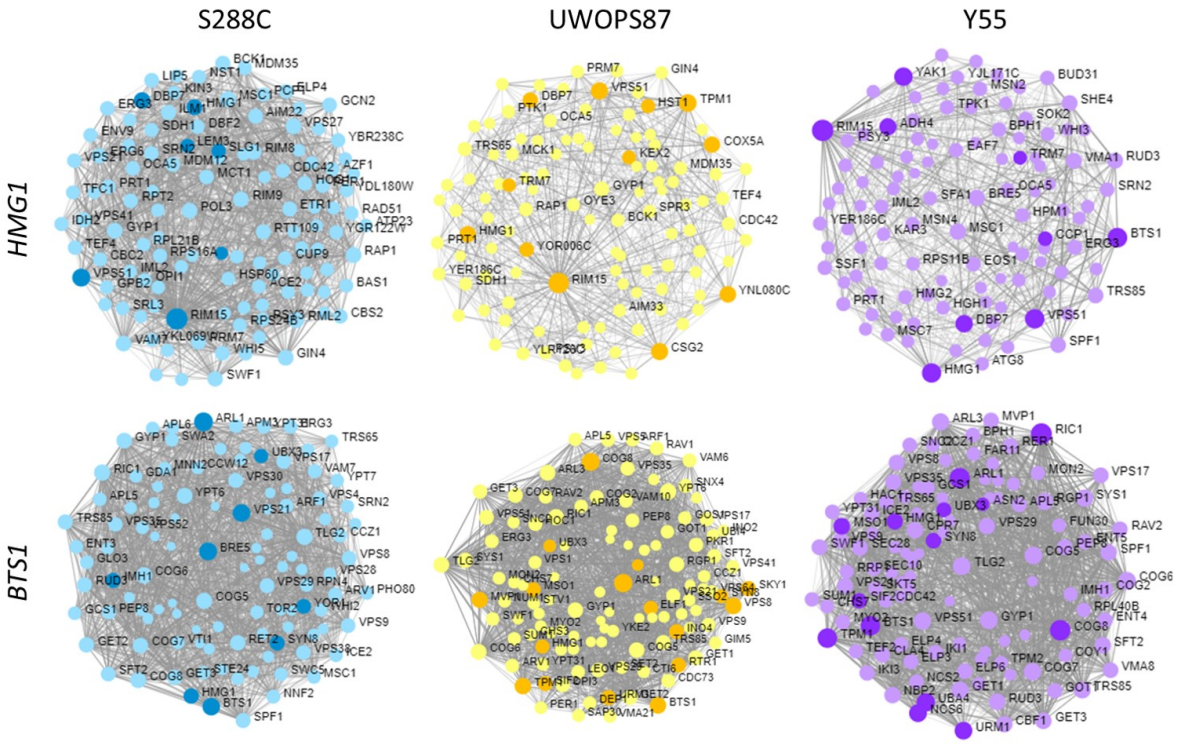

Figure 2.11: **Genetic interaction networks connecting validated hits hypersensitive to atorvastatin.** Genetic interactions networks for the *HMG1* query (upper panel) and *BTS1* query (lower panel) were constructed using GeneMania and visualised using NetworkAnalyst. Darker nodes in each network are the input genes.

nodes) (Brandes 2001), closeness centrality (shortest path length between one and all other nodes) (Newman 2005), and degree centrality (number of neighbours) (Dong and Horvath 2007). 3D scatter plots were used to visually aid in the identification of nodes distinct for each centrality (Figure 2.13). All genes were plotted with one exception; *UBI4*, a protein tag for the selective degradation of hundreds of proteins, was excluded because it bunched all the other nodes to one corner of the plot obscuring the relevance of other genes due to its highly interacting nature.

With this proviso, *RIM15*, was ranked consistently high in the three genetic backgrounds for genetic interactions in the *HMG1* query, a result that reflects the atorvastatin hypersensitivity of *hmg1*Δ *rim15*Δ (Figure 2.7). Betweenness, closeness and degree centrality metrics were 0.08, 0.8 and 74, respectively for S288C, 0.1, 0.63 and 50 for UWOPS87 and 0.08, 0.6 and 41 for Y55. Similarly, *CDC28* ranked consistently high in three genetic backgrounds for protein-protein interactions in the *HMG1* query. Betweenness, closeness and degree centrality metrics were 0.06, 0.5 and 31, respectively for S288C, 0.05, 0.4 and 53 for UWOPS87 and 0.09, 0.5 and 37 for Y55. *RIM15* has a role in cell proliferation in response to nutrients and *CDC28* is a master regulator of mitotic and meiotic cell cycles. Noteworthy, *RIM15* is a protein kinase and *CDC28* is the catalytic subunit of a cyclin-dependent kinase. The involvement of kinases in statin responses points to fundamental effects of statins on aspects of

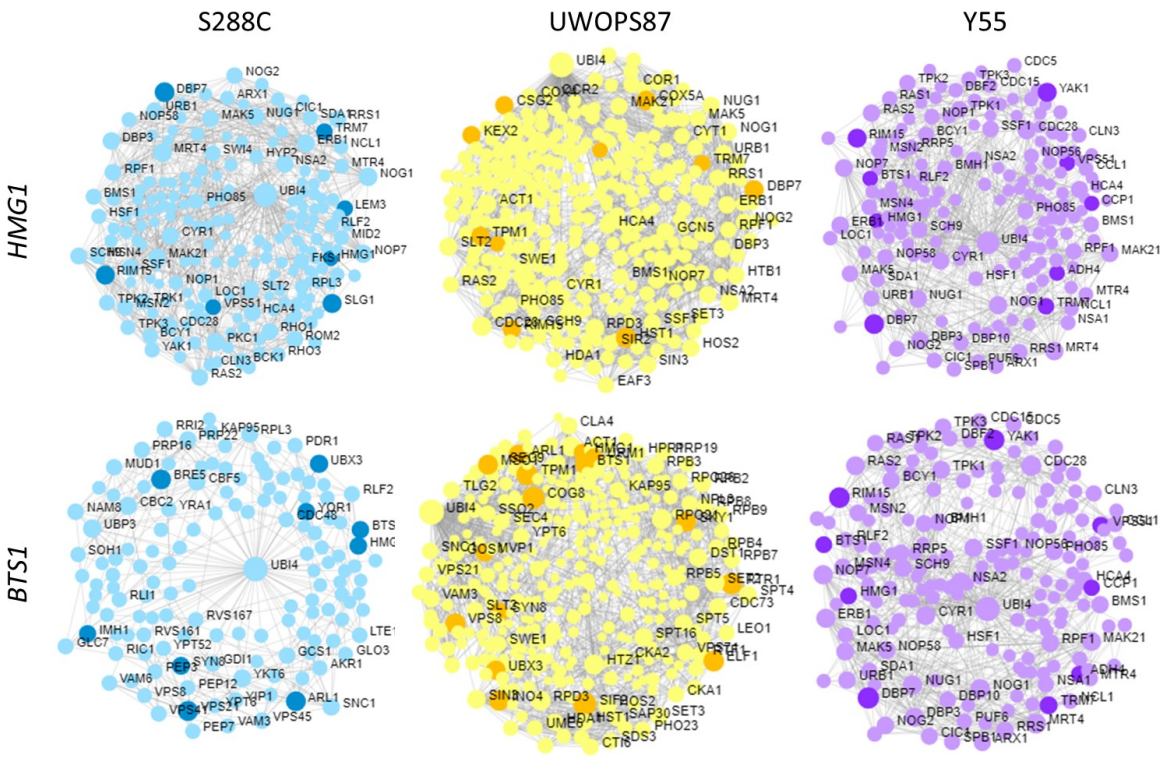

Figure 2.12: **Protein-protein interaction networks connecting validated hits hypersensitive to atorvastatin.** Protein-protein interaction networks for the *HMG1* query (upper panel) and *BTS1* query (lower panel) were constructed using STRING and visualised using NetworkAnalyst. Darker nodes in each network are the input genes.

metabolism other than cholesterol metabolism.

Also regarding the *HMG1* interactions, top central genes in GINs included *WHI5* (betweenness (bet) = 0.03, closeness (close) = 0.6, degree (deg) = 25), *RAP1* (bet = 0.02, close = 0.6, deg = 44) and *POL3* (bet = 0.02, close 0.6, deg = 44) in S288C; *GYP1* (bet = 0.07, close = 0.6, deg = 37), *TPM1* (bet = 0.05, close = 0.6, deg = 31) and *HMG1* (bet = 0.05, close = 0.5, deg = 23) in UWOPS87, and *BTS1* (bet = 0.08, close = 0.6, deg = 37), *YAK1* (bet = 0.05, close = 0.6, deg = 31) and *HMG1* (bet = 0.05, close = 0.6, deg = 31) in Y55. Top central genes in PPINs included *PKC1* (bet = 0.04, close = 0.4, deg = 31), *CYR1* (bet = 0.04, close = 0.5, deg = 27) and *RAS2* (bet = 0.4, close 0.5, deg = 23) in S288C; *ACT1* (bet = 0.07, close = 0.5, deg = 53), *HTB1* (bet = 0.04, close = 0.4, deg = 34) and *RPD3* (bet = 0.04, close = 0.4, deg = 50) in UWOPS87, and *CYR1* (bet = 0.05, close = 0.5, deg = 28), *RAS2* (bet = 0.05, close = 0.5, deg = 27) and *ADH1* (bet = 0.04, close = 0.4, deg = 9) in Y55.

As for the GINs representing the *BTS1* query, two genetic interactions with high centrality overlapped in the three genetic backgrounds, *ARL1* and *BTS1* itself (Figure 2.13). Betweenness, closeness and degree centrality metrics for *ARL1* were 0.03, 0.7 and 71, respectively for S288C, 0.02, 0.7 and 66 for UWOPS87 and 0.03, 0.7 and 64 for Y55, whereas for *BTS1* were 0.04, 0.7 and 61

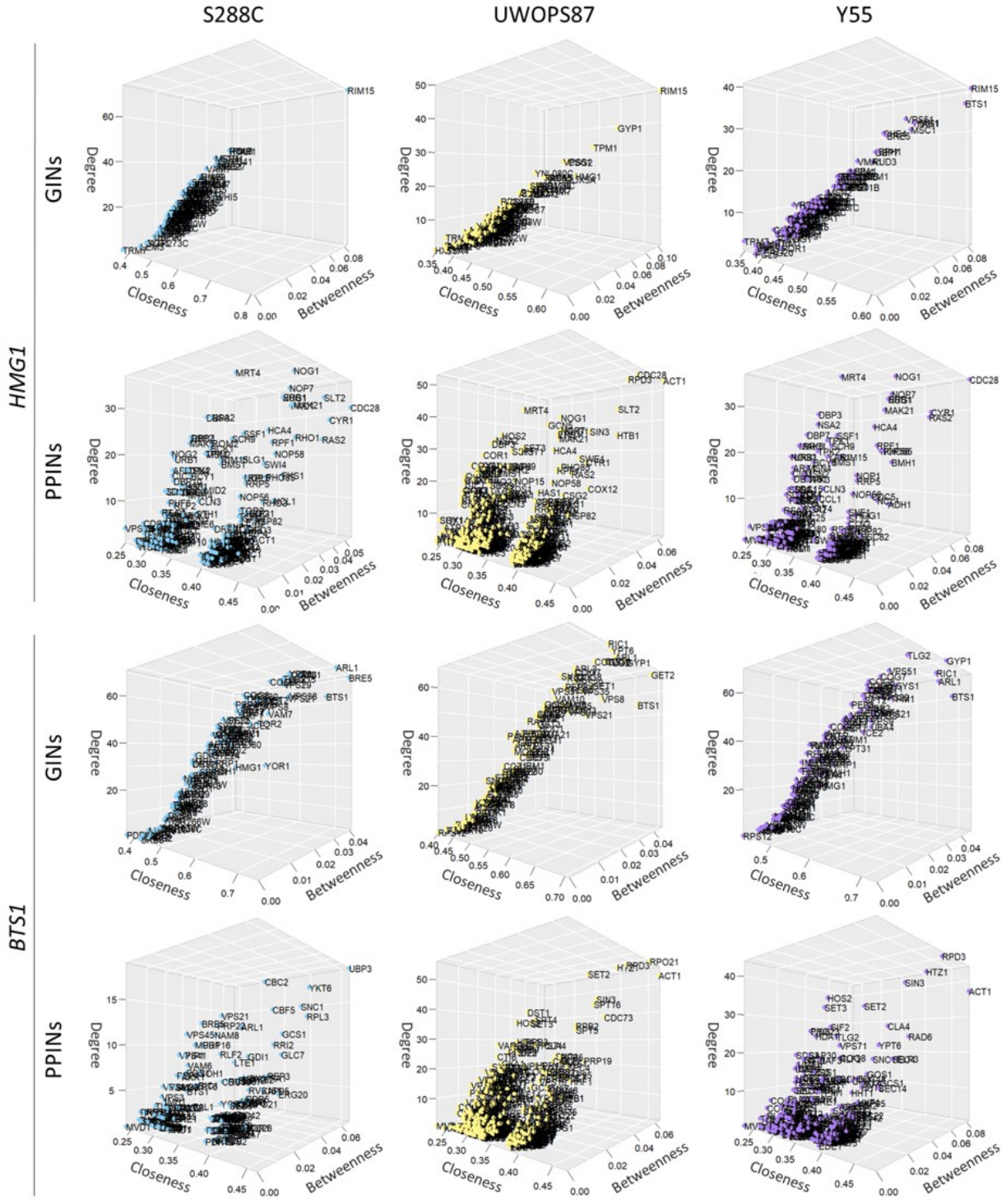

Figure 2.13: **Network topology centrality analyses of GINs and PPINs identify key *HMG1*/*BTS1* interactors for atorvastatin sensitivity.** Centrality measurements (degree, closeness and betweenness) were calculated for each gene and visualised in a 3D plot.

for S288C, 0.05, 0.6 and 55 for UWOPS87 and 0.05, 0.7 and 61 for Y55. *ARL1* is a GTPase that regulates membrane traffic with a central role in autophagy (Abudugupur et al. 2002; Rosenwald et al. 2002). The double deletion of *ARL1* and *BTS1* (*arl1*Δ *bts1*Δ) is synthetic sick (Costanzo et al. 2016), suggesting this interaction is functional within my GINs.

Unlike centralities in the GINs, there was no obvious bottleneck/hub gene in the PPINs overlapping in the three genetic backgrounds for *BTS1*. Interestingly, the histone deacetylase *RPD3* and the actin component *ACT1* were highly central for UWOPS87 (bet = 0.07, close = 0.5, deg = 53 for *ACT1* and bet = 0.04, close = 0.5, deg = 53 for *RPD3*) and Y55 (bet = 0.08, close = 0.5, deg = 37 for *ACT1* and bet = 0.06, close = 0.5, deg = 44 for *RPD3*) but not for S288C (bet = 0.00, close = 0.4, deg = 4 for *ACT1* and *RPD3* was not present in the network). Instead, *UBP3* appeared to be a bottleneck and hub gene for S288C (bet = 0.07, close = 0.5, deg = 19). A similar situation can be seen in the GINs for the *GYP1* and *RIC1* that were central to UWOPS87 (bet = 0.03, close = 0.7, deg = 66 for *GYP1* and bet = 0.01, close = 0.7, deg = 68 for *RIC1*) and Y55 (bet = 0.03, close = 0.7, deg = 70 for *GYP1* and bet = 0.03, close = 0.7, deg = 66 for *RIC1*), while *BRE5* was more central to S288C (bet = 0.04, close = 0.7, deg = 70 for *BRE5* as opposed to bet = 0.01, close = 0.7, deg = 61 for *GYP1* and bet = 0.02, close = 0.7, deg = 65 for *RIC1*). These results suggest that processes involved in the secretory pathway might buffer the increased resistance to atorvastatin for UWOPS87 and Y55 given that *ACT1* (actin) has a role in endocytosis, *GYP1* is an activator of GTPases involved in vesicle-mediated transport, and *RIC1* is a protein involved in retrograde transport. Another possible buffer for this might be autophagy as *RPD3* is a histone deacetylase that among other processes, regulates autophagy.

Other top central genes in GINs included *YOR1* (bet = 0.03, close = 0.6, deg = 30), *VPS38* (bet = 0.02, close = 0.7, deg = 58) and *VPS21* (bet = 0.02, close 0.7, deg = 57) in S288C; *GET2* (bet = 0.04, close = 0.7, deg = 66), *VPS8* (bet = 0.02, close = 0.6, deg = 54) and *VPS21* (bet = 0.02, close = 0.6, deg = 48) in UWOPS87, and *VPS21* (bet = 0.02, close = 0.6, deg = 50), *TPM1* (bet = 0.02, close = 0.7, deg = 55) and *UBA4* (bet = 0.02, close = 0.6, deg = 45) in Y55. Top central genes in PPINs also included *RPL3* (bet = 0.04, close = 0.4, deg = 13), *YKT6* (bet = 0.04, close = 0.4, deg = 16) and *SNC1* (bet = 0.4, close 0.4, deg = 14) in S288C; *RPO21* (bet = 0.05, close = 0.5, deg = 56), *HTZ1* (bet = 0.05, close = 0.4, deg = 54) and *RPD3* (bet = 0.04, close = 0.5, deg = 53) in UWOPS87, and *HTZ1* (bet = 0.06, close = 0.4, deg = 41), *CLA4* (bet = 0.05, close = 0.4, deg = 27) and *YPT6* (bet = 0.04, close = 0.4, deg = 22) in Y55.

2.3.7 *Community analysis identifies functional modules in GINs and PPINs for three genetic backgrounds*

To gain more insight into the structural organisation of the GINs and PPINs in order to identify metabolic pathways mediating atorvastatin sensitivity, community analysis was conducted to partition the networks to functional subnetworks (modules) that are more interconnected compared to random (Blondel et al. 2008) (Figure 2.4F). For all GINs across all backgrounds and all query genes, modules were not detected possibly due to the high connectivity throughout the network that may have deemed the network as a whole community. For the PPINs, 3-8 significantly clustered ($P < 0.05$) modules were detected in each network. Pathway enrichment analysis for each module was then conducted, which revealed significant enrichment ($P < 0.05$) for a range of metabolic pathways and in most cases these pathways did not overlap in all three genetic backgrounds (Figure 2.14), suggesting that individual genetic backgrounds use different pathways to mount their response to atorvastatin treatment.

The enrichment revealed, however, that all three genetic backgrounds seem to be reliant on a few pathways in response to atorvastatin treatment (Figure 2.14). The longevity regulation pathway and its tightly linked processes of SNARE-mediated vesicular transport, autophagy and mitophagy overlapped in three genetic backgrounds for both *HMG1* and *BTS1* queries. Cell cycle pathways, meiosis, oxidative phosphorylation, ribosome biogenesis, and RNA transport and degradation also overlapped in the three genetic backgrounds for the *HMG1* interactions (Fig. 2.14), whereas endocytosis and phagosome pathways, overlapped in all three genetic backgrounds for the *BTS1* interactions. Together, these results reveal the critical pathways for atorvastatin sensitivity in various genetic backgrounds in the presence or absence of *HMG1*/*BTS1* mutations in the mevalonate pathway.

2.3.8 *Multi-layer network analysis enhances connectivity of networks*

Most network centrality analyses are performed in single-layer networks as I did in the previous sections, that is, connections between nodes based on one type of functional relationship. Recently, the use of multi-layer networks expanded the usefulness of centrality analyses through the generation of aggregated networks that come from two or more layers of interactions of different types of data (Wang et al. 2017). Similar to a single-layer network, albeit just more complex, aggregated networks are basically n-dimensional matrices or tensors that can be investigated using mathematical methodologies. In my case, the first layer was derived from the GINs, the second layer derived from the PPINs, and the aggregated network was derived from both the GINs and PPINs (Figure 2.4E).

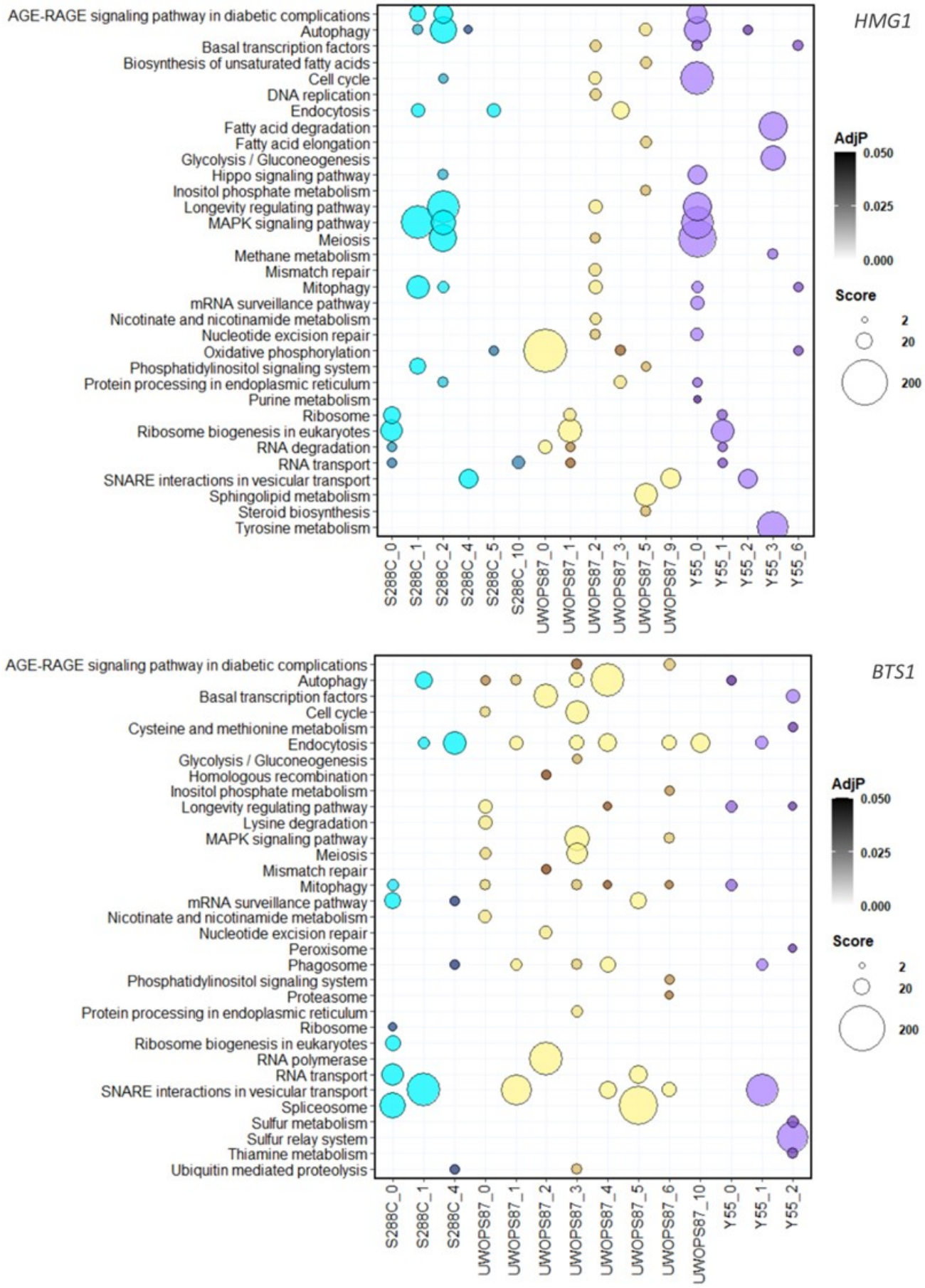

Figure 2.14: (Caption next page.)

Figure 2.14: **Metabolic pathway enrichment of modules in protein-protein interaction networks for atorvastatin sensitivity.** Bubble plots showing enrichment for each of the modules (named for their genetic background) identified through community analysis for *HMG1* (top panel) and *BTS1* (bottom panel) interactions. The size of the bubbles is relative to the enrichment score for each pathway, while the intensity of the colours is relative to the adjusted *P*-value. The x axis labels show the genetic background followed by the number of modules. Numbers missing in the sequence are modules without significantly enriched pathways.

Few gene nodes were common to both GINs and PPINs, which include the input genes (Figure 2.15-2.16). Most nodes and hence most interactions, however, were not shared between GINs and PPINs. The aggregated network for S288C comprised 288 nodes and 2118 edges, as opposed to the GIN (98 nodes, 1171 edges) and PPIN (203 nodes, 950 edges) alone. For UWOPS87, the aggregated network had 464 nodes and 2556 edges (GIN = 112 nodes, 703 edges; PPIN = 372 nodes, 1858 edges), while Y55 had 265 nodes and 1525 edges (GIN = 109 nodes, 733 edges; PPIN = 186 nodes, 835 edges).

Similarly for the *BTS1* networks, few genes were shared between the GINs and PINs and most genes were unique to each individual network. The aggregated network for S288C comprised 224 nodes and 2239 edges, as opposed to GIN (109 nodes, 1874 edges) and PPIN (139 nodes, 388 edges) alone. For UWOPS87, the aggregated network had 428 nodes and 3743 edges (GIN = 117 nodes, 1902 edges; PPIN = 370 nodes, 1944 edges), while Y55 had 300 nodes and 2767 edges (GIN = 114 nodes, 1835 edges; PPIN = 233 nodes, 1018 edges).

2.3.9 Network topology centrality analyses identify bottleneck genes in aggregated networks

To compare the functional insight of an aggregated network relative to the single-layer GINs and PPINs, three measurements of centrality (degree, closeness and betweenness) were obtained for every gene in each aggregated network (Figure 2.17). Firstly for the *HMG1* interactions, as with the single-layer networks, *UBI4* was excluded from the 3D plots because it obscured the relevance of other genes. Consistent with the network centrality measurements derived from single-layer GINs for the query *HMG1*, *RIM15* ranked the highest in all three genetic backgrounds, indicating this gene is as central to the atorvastatin response as the atorvastatin target *HMG1* (*i.e.*, *RIM15* was more highly ranked for betweenness than *HMG1*). Similarly, *CDC28* which was ranked high in the PPINs, was also ranked high in the aggregated networks in all three genetic backgrounds. As points of distinction, the putative ATP-dependent RNA helicase *DBP7* as well as *HMG1* itself were highly ranked in the

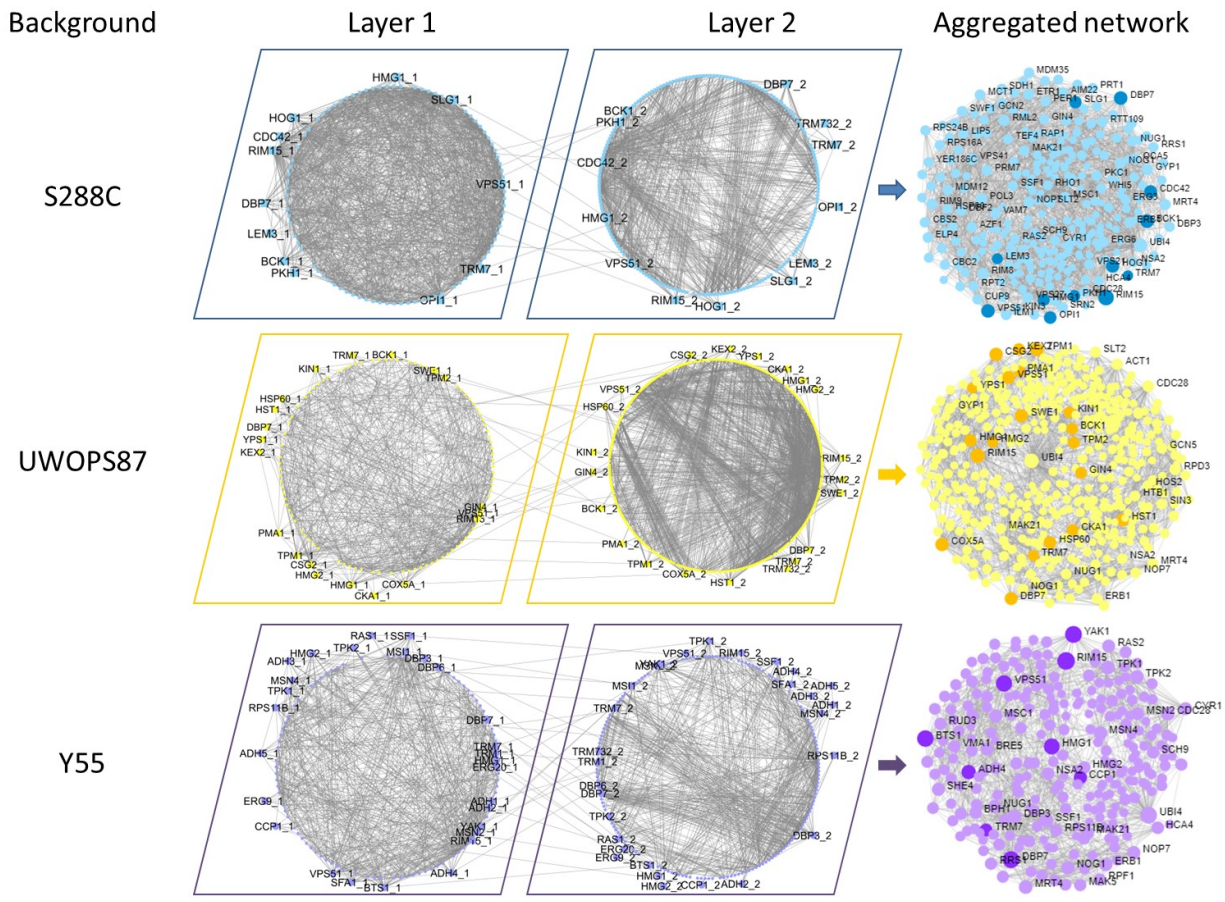

Figure 2.15: **Multi-layer networks derived from atorvastatin-sensitive *hmg1*△ *xxx*△ interactions.** GINs (Layer 1), PPINs (Layer 2) and the edges between them were integrated in an aggregated network using TimeNexus. Edges between layers connect overlapping nodes in the two layers and the genes linking these edges are shown in the periphery of circular networks. Darker nodes in aggregated networks are validated hits.

multi-layer aggregated network but were not detected in the single-layer PPINs. In the case of the aggregated *BTS1* network, *BRE5* integral to deubiquitination was distinct in S288C and the trans-Golgi component *TLG2* was distinct in UWOPS87 and Y55. Given the above, aggregated networks not only seemed to pinpoint the most relevant genes that stood out in the single-layer GINs and PPINs, but it also identified additional interactions of high topological relevance.

3D scatter plots were used to visually aid in the identification of nodes that stand out from the rest by visualising the three centrality measurements at the same time (Figure 2.17). As before, *UBI4* was excluded from the 3D plots because it obscured the relevance of other genes (as in Section 2.3.6). Correspondingly with the network centrality measurements derived from genetic interactions for the query *HMG1*, *RIM15* ranked the highest in all three genetic backgrounds (bet = 0.12 (2^{nd} overall), close = 0.49 (4^{th} overall), deg = 93 (2^{nd} overall) in S288C, bet = 0.07 (2^{nd} overall), close = 0.42 (15^{st} overall), deg = 66 (2^{nd} overall) in UWOPS87, bet = 0.09 (2^{nd} overall), close = 0.48 (3^{rd} overall), deg

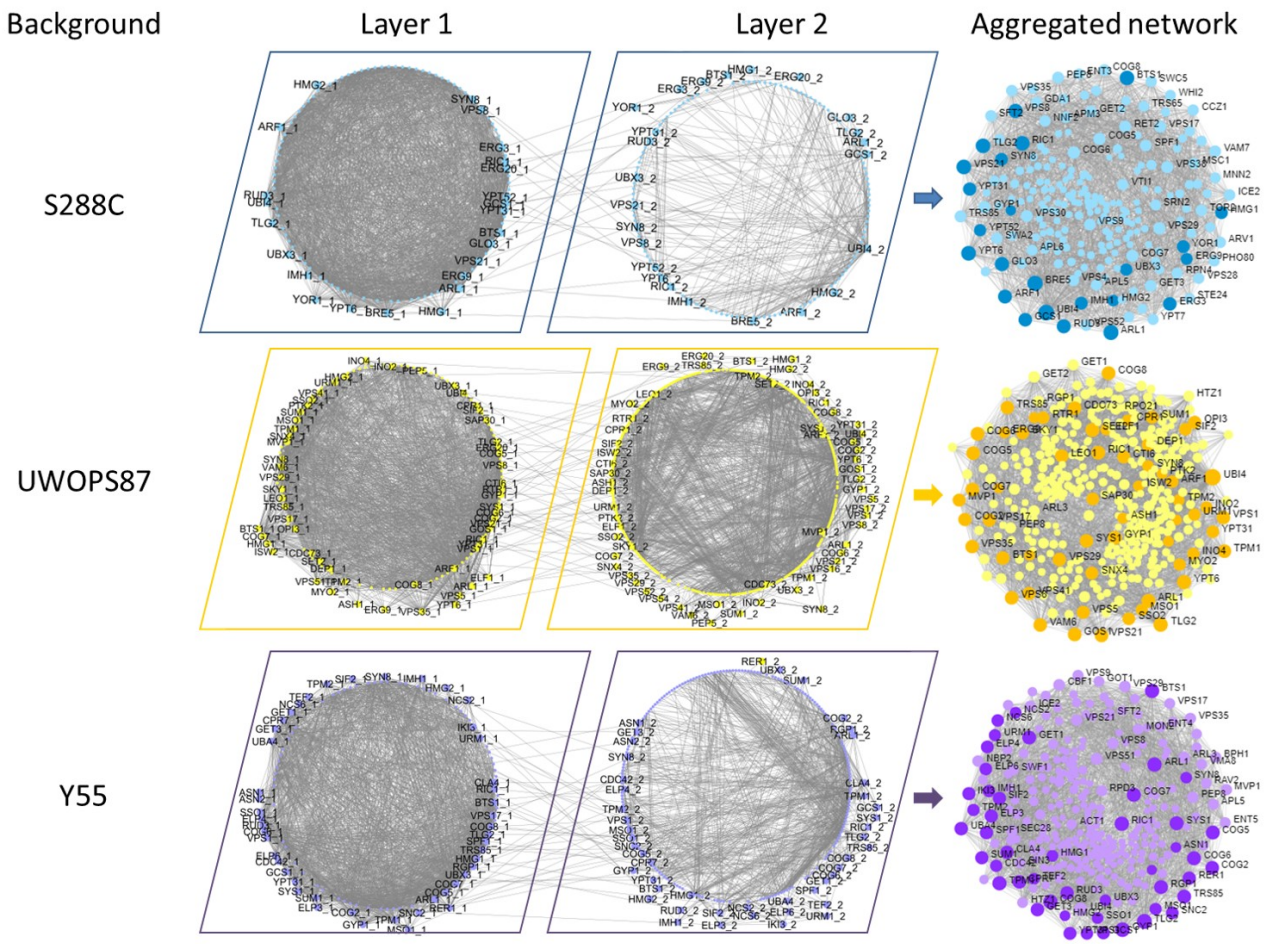

Figure 2.16: **Multi-layer networks derived from atorvastatin-sensitive *bts1*Δ *xxx*Δ interactions.** GINs (Layer 1), PPINs (Layer 2) and the edges between them were integrated in an aggregated network using TimeNexus. Edges between layers connect overlapping nodes in the two layers and the genes linking these edges are shown in the periphery of circular networks. Darker nodes in aggregated networks are validated hits.

= 55 in Y55 (2nd overall)), and similarly, *CDC28*, which ranked high in the networks based on protein interactions, also ranked high in the aggregated networks in three genetic backgrounds (bet = 0.03 (7th overall), close = 0.47 (7th overall), deg = 31 (25th overall) in S288C, bet = 0.04 (8th overall), close = 0.44 (4th overall), deg = 53 (3th overall) in UWOPS87, bet = 0.05 (7th overall), close = 0.46 (8th overall), deg = 37 in Y55 (7th overall)). Surprisingly, one gene that was not picked up in the PPINs is *DBP7*, which in the aggregated networks was ranked in the top ten highest betweenness centralities (bet = 0.11 (3rd overall), close = 0.45 (10th overall), deg = 44 (4th overall) in S288C, bet = 0.04 (6th overall), close = 0.40 (44th overall), deg = 36 (14th overall) in UWOPS87, bet = 0.06 (4th overall), close = 0.45 (12th overall), deg = 45 in Y55 (3rd overall)) (Figure 2.18). Though *DBP7*, a putative ATP-dependent RNA helicase, does not code for a kinase-related activity as *RIM15* and *CDC28* do, negative interactions of it have been reported with genes involved in kinase activity. Given the above, aggregated networks not only seemed to pinpoint the most relevant genes that stood out in the individual analyses of each

of the layers, genetic and protein interaction networks, but it also seemed to identify other interactions of high relevance that analyses of non-aggregated networks did not show (*e.g.*, *DBP7*).

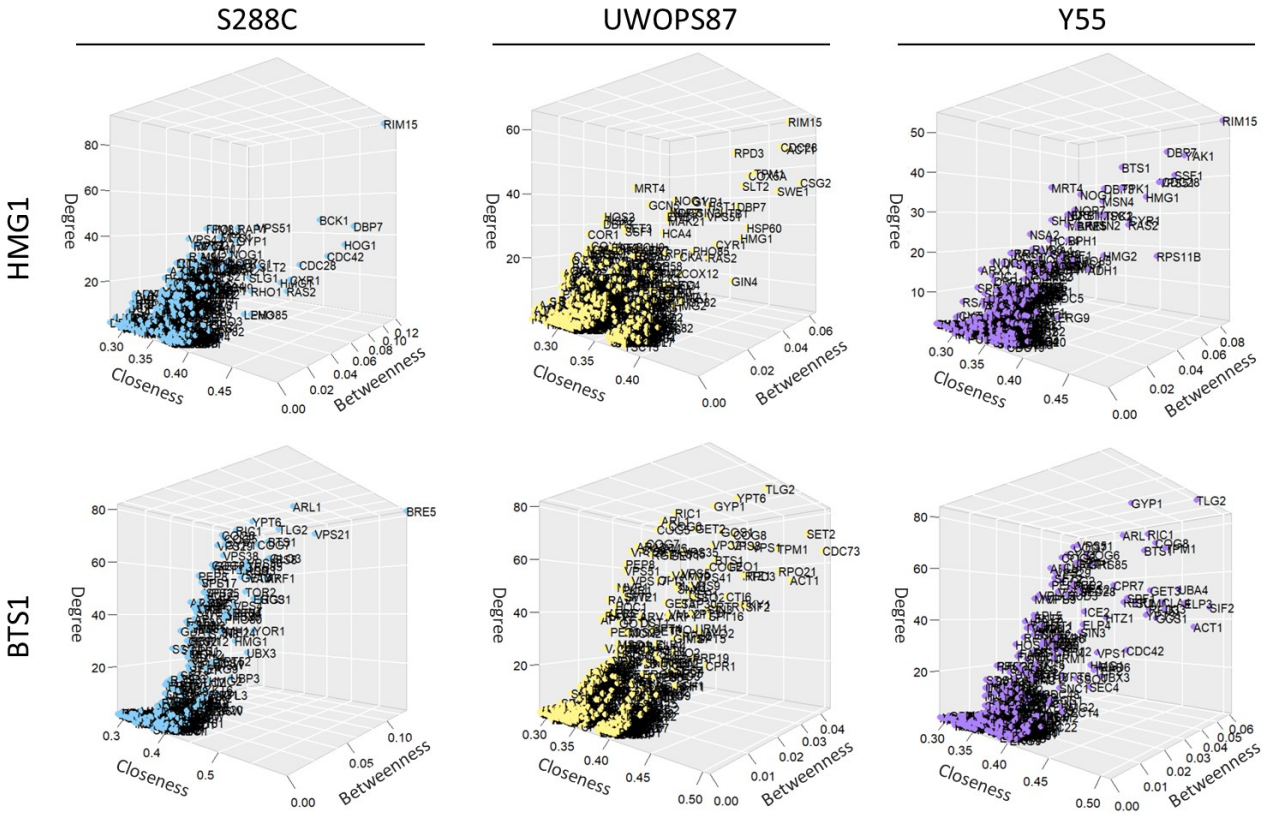

Figure 2.17: **Network topology centrality analyses of aggregated networks identify key *HMG1*/*BTS1* interactors for atorvastatin sensitivity.** Centrality measurements (degree, closeness and betweenness) were calculated for each gene and visualised in a 3D plot.

To identify which of the top central genes may be bottlenecks and which ones are central due to their closeness or higher connectivity, I generated individual networks for the top ten betweenness, closeness and degree centralities (Figures 2.18-2.19). In this context, betweenness centrality is the most meaningful because it points to bottlenecks required for the integrity of networks (Brandes 2001; Freeman 1977; Girvan and Newman 2002; Yu et al. 2007), as opposed to closeness centrality that measures how 'close' is one node to others (*e.g.*, having zero centrality means a node isolated from every other node) (Newman 2005) and degree that simply points to the number of neighbours of a given node (Dong and Horvath 2007). Nodes with high betweenness or bottlenecks often correlate with gene essentiality and biological relevance and are bridges that connect community modules (Yu et al. 2007). This way, I identified *RIM15*, *HMG1* (bet = 0.03 (9th overall), close = 0.45 (11th overall), deg = 24 (54th overall) in S288C, bet = 0.03 (11th overall), close = 0.43 (9th overall), deg = 27 (32nd overall) in UWOPS87, bet = 0.04 (9th overall), close = 0.46 (6th overall), deg = 33 in Y55 (12th overall)), *CDC28*

and *DBP7* as bottlenecks for *HMG1* interactors that enhance sensitivity to atorvastatin overlapping in three genetic backgrounds (Figure 2.18), but no bottleneck overlapped in three genetic backgrounds for the *BTS1* interactors (Figure 2.19). Instead, most bottlenecks overlapped in UWOPS87 and Y55 only, whereas most bottlenecks identified in S288C were unique to this genetic background. *TLG2*, however, seems to be a highly relevant gene that might participate in off-target effects of atorvastatin when the function of *BTS1* is inhibited since it had high betweenness, closeness and degree (bet = 0.02 (12^{th} overall), close = 0.55 (3^{rd} overall), deg = 65 (7^{th} overall) in S288C, bet = 0.02 (10^{th} overall), close = 0.49 (5^{th} overall), deg = 82 (2^{nd} overall) in UWOPS87, bet = 0.04 (5^{th} overall), close = 0.50 (3^{rd} overall), deg = 84 in Y55 (2^{nd} overall)) (Figure 2.19).

2.3.10 Community analysis identifies functional modules in aggregated networks for three genetic backgrounds

To gain more insight into the structural organisation of the aggregated networks and how they compared to those of the single-layer PPINs (GINs could not be partitioned, see Section 2.3.7), the aggregated networks were partitioned through community analysis (Figure 2.4F). For the aggregated networks, 3-6 modules were detected in each network with significant enrichment for metabolic pathways ($P < 0.05$), and in most cases, pathways enriched in these modules did not overlap in all three genetic backgrounds (Figure 2.20). However, the longevity regulation pathway and its tightly linked processes autophagy and mitophagy that were identified in the single layer analysis were found correspondingly enriched in the aggregated multi-layer analysis for *HMG1* and *BTS1* queries. Similarly, all other pathways enriched for the *BTS1* query (*i.e.*, endocytosis, phagosome and SNARE interactions in vesicular transport in the single-layer analysis) were enriched in the multi-layer analysis. For the *HMG1* query, other than oxidative phosphorylation and SNARE interactions in vesicular transport, all other metabolic pathways that were enriched in the *HMG1* single-layer analysis were enriched in the aggregated networks overlapping in three genetic backgrounds (*i.e.*, cell cycle, meiosis, ribosome biogenesis and RNA transport and degradation).

As expected, metabolic pathways were enriched in the single-layer analysis but not in the multi-layer analysis, and vice versa (Figure 2.21). Most pathways that did not overlap in the single-layer and multi-layer analyses were not highly enriched, that is, the score of enrichment was low. For instance, the maximum score of non-overlapping enrichment was 45 in the single-layer and 24 in the aggregated network for *HMG1* compared to the maximum overall scores of 181 and 179, respectively. Correspondingly, the maximum score of non-overlapping enrichment was 9 in single-layer and 39

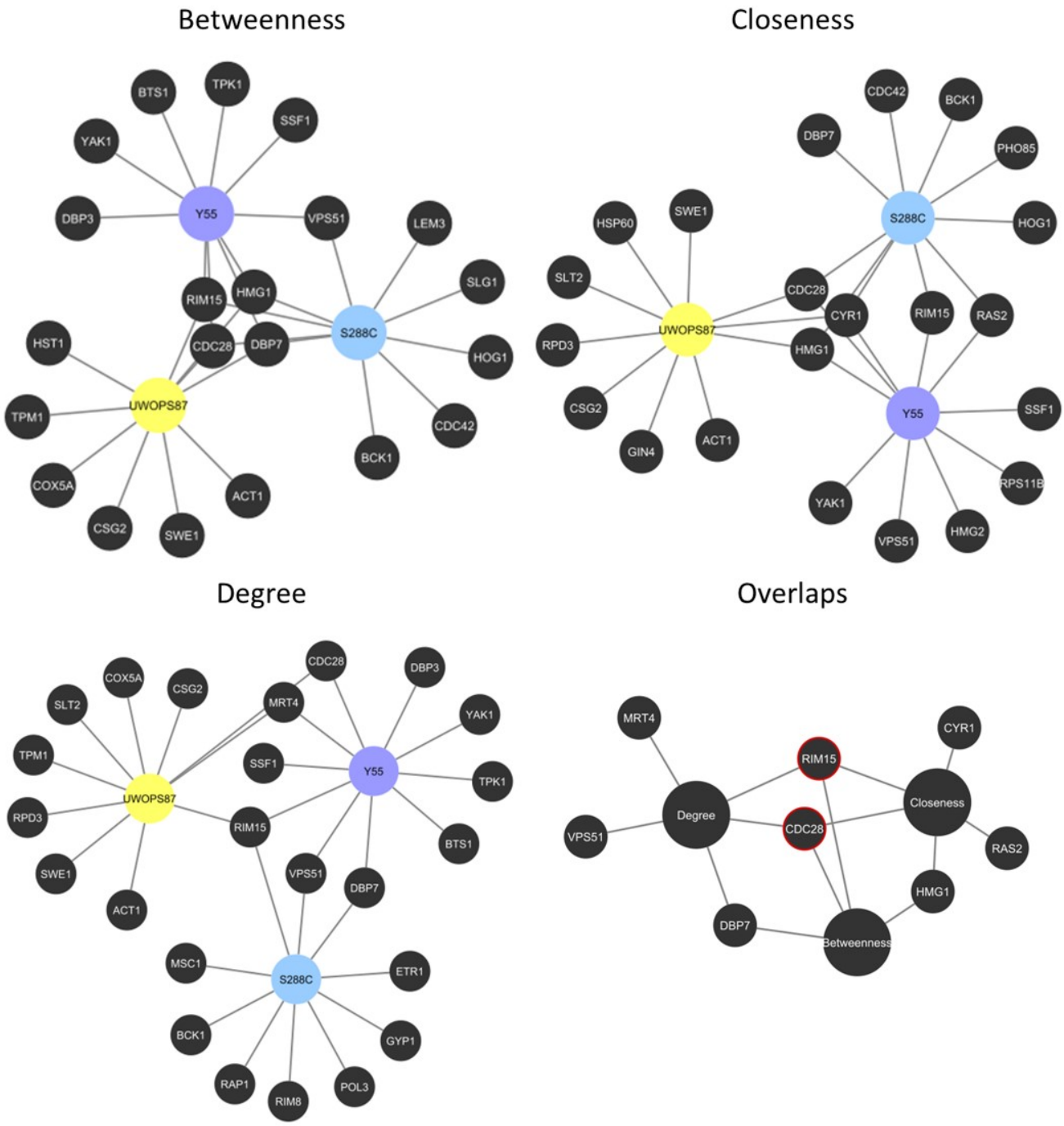

Figure 2.18: **Network centrality of genes behind hypersensitivity to atorvastatin for *HMG1* interactors overlap in three genetic backgrounds.** Genes that ranked in the top ten centrality measurements were found to confirm phenotypic findings. Centrality measurements (betweeness, closeness and degree) were calculated in NetworkAnalyzer app in Cytoscape (Boccaletti et al. 2014) and networks were built in Cytoscape. The red outline points to highly central hub/bottleneck genes.

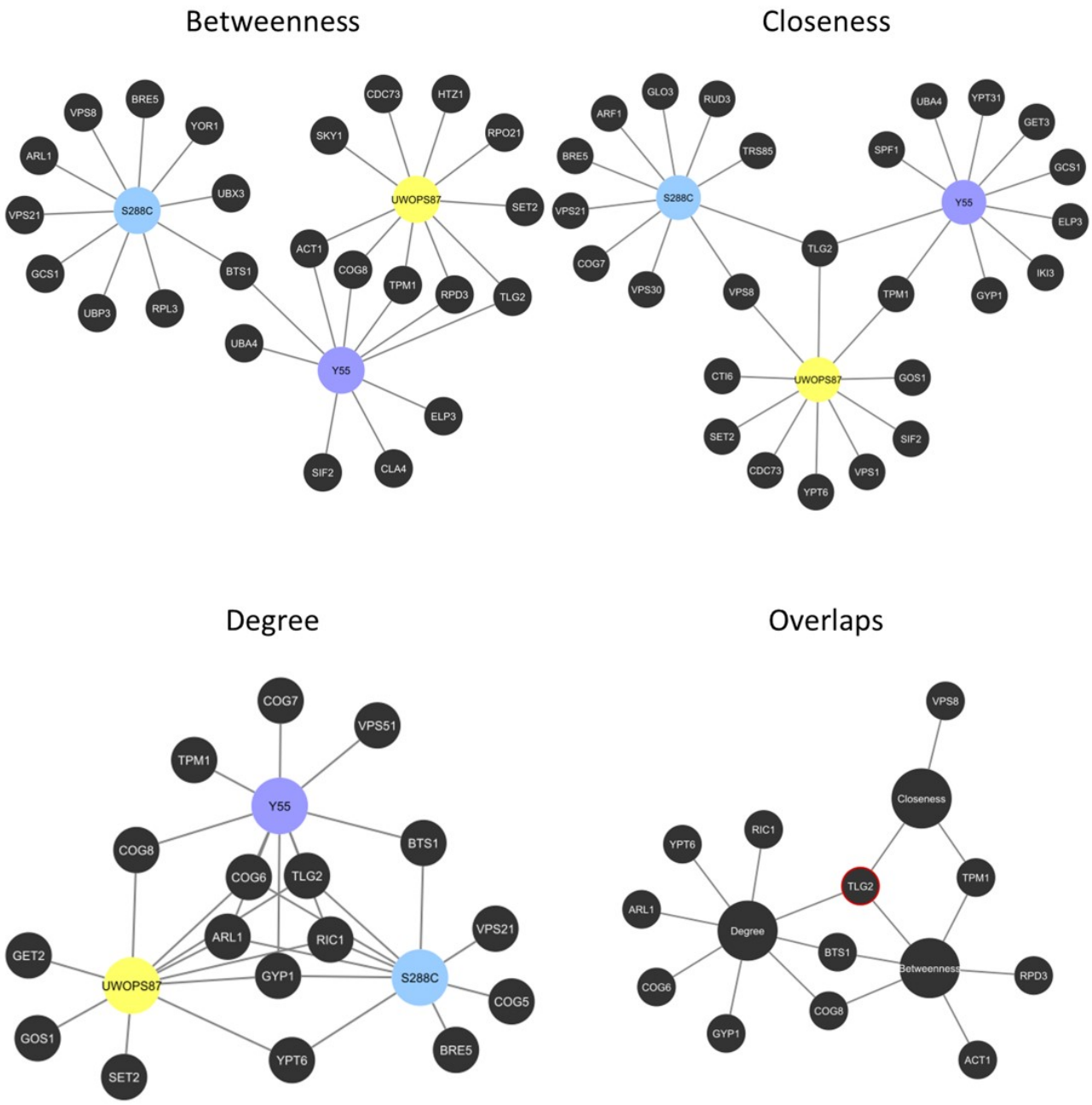

Figure 2.19: **Network centrality of genes behind hypersensitivity to atorvastatin for *BTS1* interactors overlap in three genetic backgrounds.** Genes that ranked in the top ten centrality measurements were found to confirm phenotypic findings. Centrality measurements (betweeness, closeness and degree) were calculated in NetworkAnalyzer app in Cytoscape (Boccaletti et al. 2014) and networks were built in Cytoscape. The red outline points to highly central hub/bottleneck genes.

in the aggregated network for *BST1* compared to the maximum overall scores of 144 and 138, respectively. One important metabolic pathway, SNARE interactions in vesicular transport, was enriched for the *HMG1* single-layer analysis but not in the multi-layer analysis, suggesting this pathway may be more important in one or the other single-layer analysis. Glycerolipid and glycerophospholipid metabolism pathways were not observed in single-layer analyses, but were enriched in the aggregated network in Y55 only when *HMG1* was deleted and in UWOPS87 and S288C only when *BTS1* was deleted, suggesting the involvement of lipid droplet metabolism in the response to atorvastatin. Since the multi-layer analysis showed enrichment for terpenoid backbone synthesis that is regulated by the mevalonate pathway, there is proof-of-concept to prioritise the results obtained with the multi-layer analysis. Thus, the single-layer and multi-layer network analyses showed different pathway enrichments, which indicate that both need to be taken into consideration.

2.3.11 Humanised enrichment analysis identifies candidate drugs to improve anticancer activity of statins

Combination therapies increase efficacy of repurposed drugs (Sun et al. 2016). Synergy with statins has been previously examined (Agrawal et al. 2019; Jouve et al. 2019; Kim et al. 2014; Kim et al. 2019), but not in the context of building off genes identified in unbiased genome-wide analyses. Therefore, I identified the human orthologues of key hub/bottleneck genes identified in my yeast genomic analyses across three genetic backgrounds (Table 2.12) and integrated these genes in an enrichment analysis in the gene set analysis database Drug Signature Database (Yoo et al. 2015), which detects over-representation of drugs and compounds with their 'signature genes' integral to their bioactivity (Figure 2.4G). A total of 1749 drugs and compounds were identified of which 205 had adjusted *P* values lower than 0.05. Of these, the maximum and minimum odd ratios were 86 and 2, respectively. I then selected a cut-off for the top 20 drugs and compounds based on the lowest adjusted *P* values since these represent the highest enrichment.

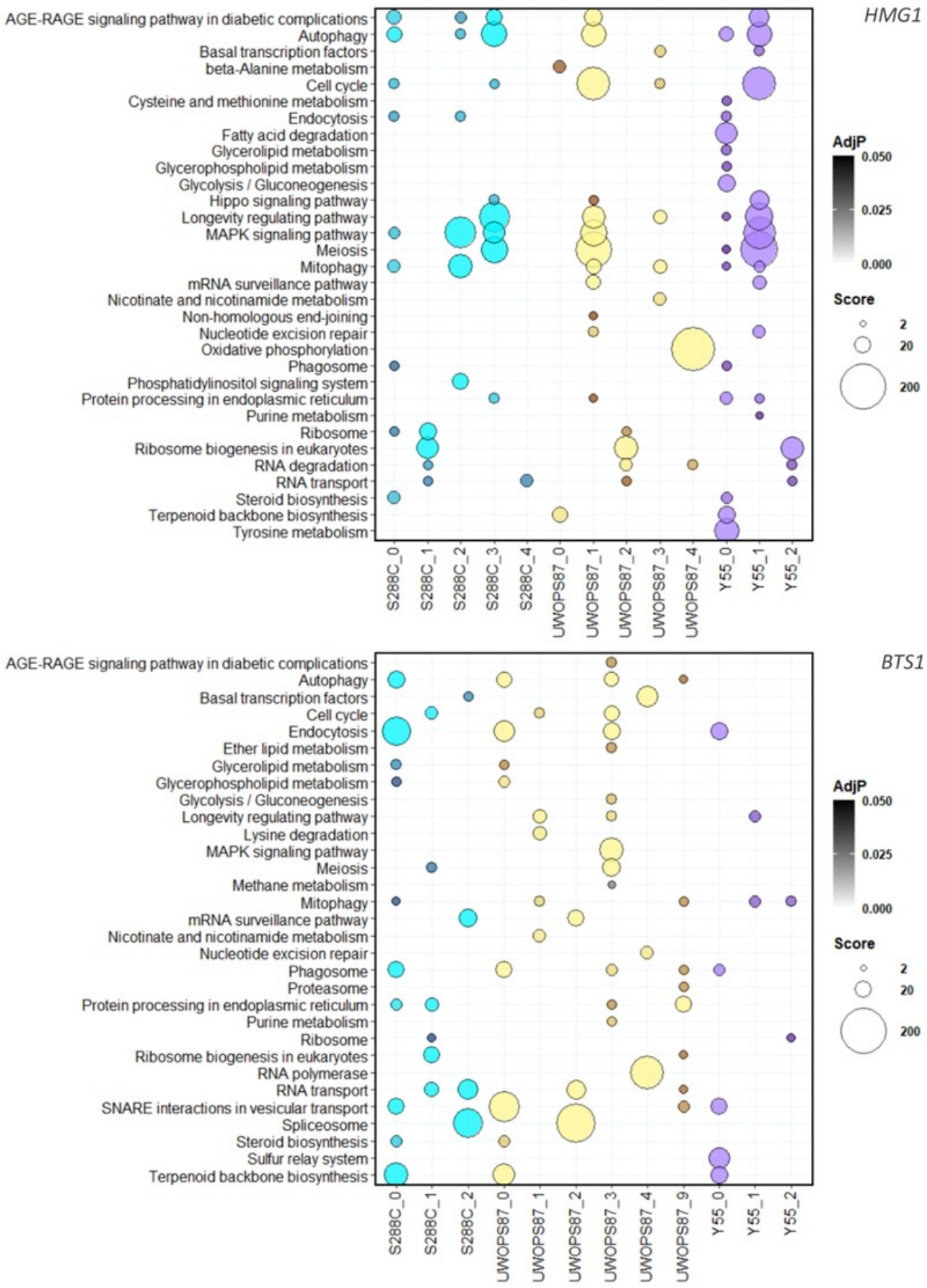

Figure 2.20: (Caption next page.)

Figure 2.20: **Metabolic pathway enrichment of modules in aggregated networks for atorvastatin sensitivity.** Bubble plots showing enrichment for each of the modules (named for their genetic background) identified through community analysis for *HMG1* (top panel) and *BTS1* (bottom panel) interactions. The size of the bubbles is relative to the enrichment score for each pathway, while the intensity of the colours is relative to the adjusted *P* value. The x axis labels show the genetic background followed by the number of modules. Numbers missing in the sequence are modules without significantly enriched pathways.

To compare the chemical genetic profiles of the top-ranked drugs/compounds, the odds ratio values for the top 20 drugs/compounds and their signature genes were visualised in a bubble plot (Figure 2.22). The 32 signature genes represented seven major processes. Four drugs/compounds (docetaxel, probenecid, verlukast, hesperetin) were correlated with ABC transporter genes involved in numerous functions including drug efflux and that provoke failure of chemotherapeutics (El-Awady et al. 2016).

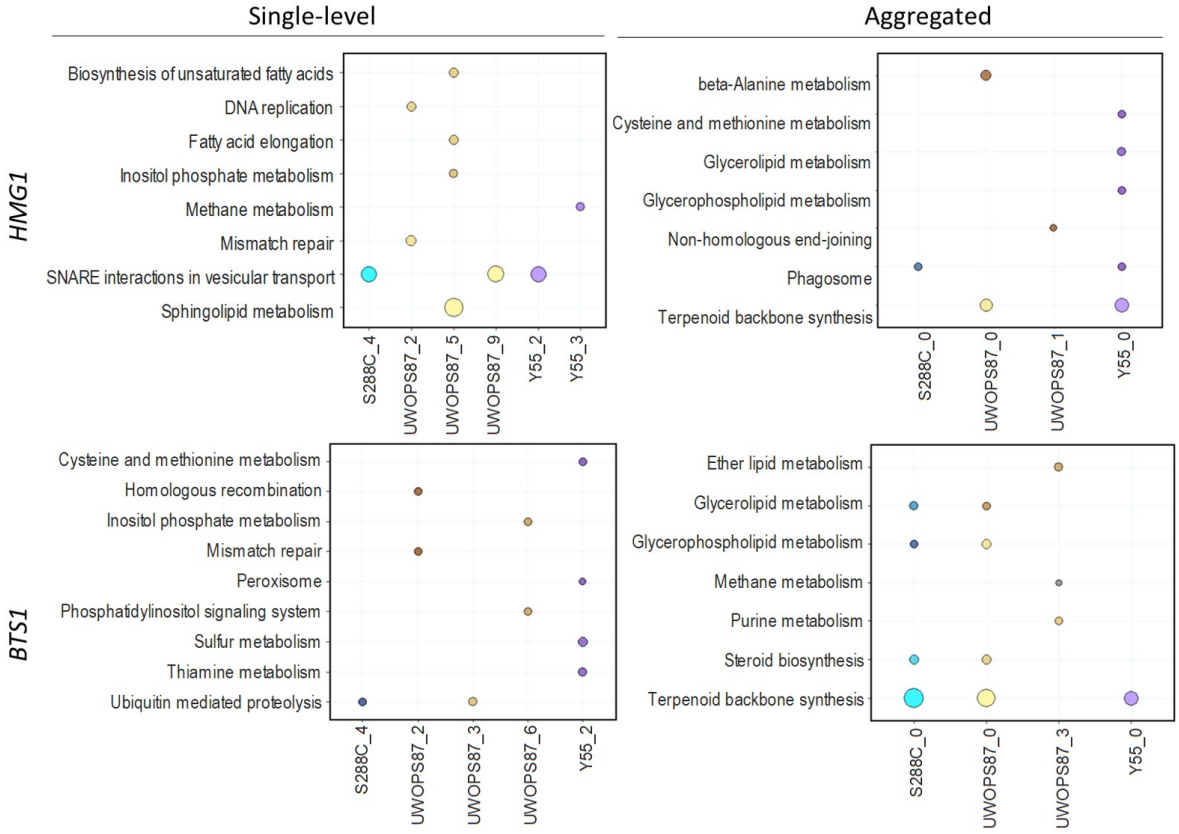

Figure 2.21: **Metabolic pathway enrichment of modules that did not overlap in single-layer and multi-layer network community analysis.** Bubble plots showing enrichment for each of the modules (named for their genetic background) identified through community analysis for *HMG1* (top panel) and *BTS1* (bottom panel) interactions that were unique to either single-layer (left panel) or multi-layer (right panel) analyses. The size of the bubbles is relative to the enrichment score for each pathway, while the intensity of the colours is relative to the adjusted *P* value. The x axis labels show the genetic background followed by the number of modules. Numbers missing in the sequence are modules without significantly enriched pathways.

Yeast query	Yeast interactor	Human orthologue	Yeast query	Yeast interactor	Human orthologue	Yeast query	Yeast interactor	Human orthologue	Yeast query	Yeast interactor	Human orthologue
HMG1/BTS1	*DBP7*	DDX41	*HMG1*	*YAK1*	HIPK2	*BTS1*	*INO4*	MITF	*BTS1*	*SKY1*	SRPK3
HMG1/BTS1	*DBP7*	DDX46	*HMG1*	*YAK1*	HIPK3	*BTS1*	*INO4*	TFE3	*BTS1*	*SYN8*	STX10
HMG1/BTS1	*RIM15*	MAST1	*HMG1*	*YAK1*	HIPK4	*BTS1*	*INO4*	TFEB	*BTS1*	*SYN8*	STX6
HMG1/BTS1	*RIM15*	MAST2	*HMG1*	*YAK1*	PRPF4B	*BTS1*	*INO4*	TFEC	*BTS1*	*SYN8*	STX8
HMG1/BTS1	*RIM15*	MAST3	*BTS1*	*ACT1*	ACTA1	*BTS1*	*INO4*	USF1	*BTS1*	*TLG2*	STX16
HMG1/BTS1	*RIM15*	MAST4	*BTS1*	*ACT1*	ACTA2	*BTS1*	*INO4*	USF2	*BTS1*	*TLG2*	STX16-NPEPL1
HMG1/BTS1	*RIM15*	MASTL	*BTS1*	*ACT1*	ACTB	*BTS1*	*MVP1*	SNX1	*BTS1*	*UBA4*	MOCS3
HMG1/BTS1	*TPM1*	TPM1	*BTS1*	*ACT1*	ACTBL2	*BTS1*	*MVP1*	SNX10	*BTS1*	*UBA4*	UBA5
HMG1/BTS1	*TPM1*	TPM2	*BTS1*	*ACT1*	ACTC1	*BTS1*	*MVP1*	SNX11	*BTS1*	*UBX3*	FAF1
HMG1/BTS1	*TPM1*	TPM3	*BTS1*	*ACT1*	ACTG1	*BTS1*	*MVP1*	SNX12	*BTS1*	*UBX3*	FAF2
HMG1/BTS1	*TPM1*	TPM4	*BTS1*	*ACT1*	ACTG2	*BTS1*	*MVP1*	SNX18	*BTS1*	*UBX3*	UBXN10
HMG1	*ADH4*	ADHFE1	*BTS1*	*ACT1*	ACTL8	*BTS1*	*MVP1*	SNX2	*BTS1*	*UBX3*	UBXN8
HMG1	*BTS1*	GGPS1	*BTS1*	*ACT1*	ACTR1A	*BTS1*	*MVP1*	SNX3	*BTS1*	*URM1*	URM1
HMG1	*COX5A*	COX4I1	*BTS1*	*ACT1*	ACTR1B	*BTS1*	*MVP1*	SNX30	*BTS1*	*VPS21*	RAB17
HMG1	*COX5A*	COX4I2	*BTS1*	*ACT1*	ACTRT1	*BTS1*	*MVP1*	SNX32	*BTS1*	*VPS21*	RAB20
HMG1	*HST1*	SIRT1	*BTS1*	*ACT1*	ACTRT2	*BTS1*	*MVP1*	SNX33	*BTS1*	*VPS21*	RAB22A
HMG1	*HST1*	SIRT4	*BTS1*	*ACT1*	ACTRT3	*BTS1*	*MVP1*	SNX5	*BTS1*	*VPS21*	RAB24
HMG1	*HST1*	SIRT5	*BTS1*	*ACT1*	POTEE	*BTS1*	*MVP1*	SNX6	*BTS1*	*VPS21*	RAB31
HMG1	*KEX2*	FURIN	*BTS1*	*ACT1*	POTEKP	*BTS1*	*MVP1*	SNX7	*BTS1*	*VPS21*	RAB5A
HMG1	*KEX2*	PCSK1	*BTS1*	*ARL1*	ARL1	*BTS1*	*MVP1*	SNX8	*BTS1*	*VPS21*	RAB5B
HMG1	*KEX2*	PCSK2	*BTS1*	*ARL1*	ARL15	*BTS1*	*MVP1*	SNX9	*BTS1*	*VPS21*	RAB5C
HMG1	*KEX2*	PCSK4	*BTS1*	*ARL1*	ARL6	*BTS1*	*NCS6*	CTU1	*BTS1*	*VPS8*	VPS41
HMG1	*KEX2*	PCSK5	*BTS1*	*ARL1*	ARL8A	*BTS1*	*RIC1*	RIC1	*BTS1*	*VPS8*	VPS8
HMG1	*KEX2*	PCSK6	*BTS1*	*ARL1*	ARL8B	*BTS1*	*RPD3*	HDAC1	*BTS1*	*YOR1*	ABCC1
HMG1	*KEX2*	PCSK7	*BTS1*	*ASN2*	ASNS	*BTS1*	*RPD3*	HDAC2	*BTS1*	*YOR1*	ABCC10
HMG1	*LEM3*	TMEM30A	*BTS1*	*BRE5*	G3BP1	*BTS1*	*RPD3*	HDAC3	*BTS1*	*YOR1*	ABCC11
HMG1	*LEM3*	TMEM30B	*BTS1*	*BRE5*	G3BP2	*BTS1*	*RPD3*	HDAC8	*BTS1*	*YOR1*	ABCC12
HMG1	*LEM3*	TMEM30C	*BTS1*	*CDC28*	CDK1	*BTS1*	*RTR1*	RPAP2	*BTS1*	*YOR1*	ABCC2
HMG1	*SLG1*	MUC15	*BTS1*	*CDC28*	CDK2	*BTS1*	*SIF2*	TBL1X	*BTS1*	*YOR1*	ABCC3
HMG1	*TRM7*	FTSJ1	*BTS1*	*CDC28*	CDK3	*BTS1*	*SIF2*	TBL1XR1	*BTS1*	*YOR1*	ABCC4
HMG1	*TSR3*	TSR3	*BTS1*	*CDC28*	CDK4	*BTS1*	*SIF2*	TBL1Y	*BTS1*	*YOR1*	ABCC5
HMG1	*YAK1*	DYRK1A	*BTS1*	*CDC28*	CDK6	*BTS1*	*SIF2*	THOC3	*BTS1*	*YOR1*	ABCC6
HMG1	*YAK1*	DYRK1B	*BTS1*	*COG8*	COG8	*BTS1*	*SIF2*	WDR17	*BTS1*	*YOR1*	ABCC8
HMG1	*YAK1*	DYRK3	*BTS1*	*ELF1*	ELOF1	*BTS1*	*SKY1*	SRPK1	*BTS1*	*YOR1*	ABCC9
HMG1	*YAK1*	HIPK1	*BTS1*	*HMG1*	HMGCR	*BTS1*	*SKY1*	SRPK2	*BTS1*	*YOR1*	CFTR

Table 2.12: **Human orthologues of top validated hits and centralities used as input for enrichment analysis in Drug Signature Database.** Human orthologues were obtained from YeastMine (Balakrishnan et al. 2012). *HMG1*/*BTS1* refers to genes identified in both queries. Yeast interactor column comprises all validated hits, bottlenecks in *HMG1* query overlapping in three genetic backgrounds and bottlenecks in *BTS1* query overlapping in two genetic backgrounds.

Fifteen drugs/compounds (GW779439X, dinaclinib, docetaxel, lestaurtinib, KW-2449, RO-31-8220, palbociclib, AZD5438, CGP74514A, sunitinib, JNK-9L, staurosporine, PKR inhibitor, hesperetin and AS-59957) were correlated with kinase activity contributed by cyclin-dependent kinase (CDK) genes, dual-specificity tyrosine-regulated kinase (DYRK) genes and MAP kinase (HPK) genes involved in cell cycle. Four drugs/compounds (lestaurtinib, palbociclib, sunitinib, staurosporine) were correlated with the MAST1 gene involved in survival signalling pathways that confers cell resistance to the chemotherapeutic cisplatin (Jin et al. 2018). Four drugs/compounds (lestaurtinib, KW2449, sunitinib, staurosporine) were correlated with the PRPF4B gene, an essential gene for triple-negative breast cancer metastasis (Koedoot et al. 2019). Lastly, eight drugs/compounds (lestaurtinib, KW-2449, RO-31-8220, AZD5438, GW5074, sunitinib, staurosporine, A-674563) were correlated with serine/arginine-rich protein-specific kinase (SRPK) genes involved in activation of various signalling pathways that mediate cytotoxic effects of genotoxic agents including cisplatin (Sigala et al. 2021).

The pyrazolopyridazine GW779439X ranked the highest of all drugs and compounds (*P* = 2.42E-09; odds ratio = 86), which was mainly due to hubs/bottlenecks in cyclin-dependent kinase genes (CDK genes) identified with the *HMG1* query.

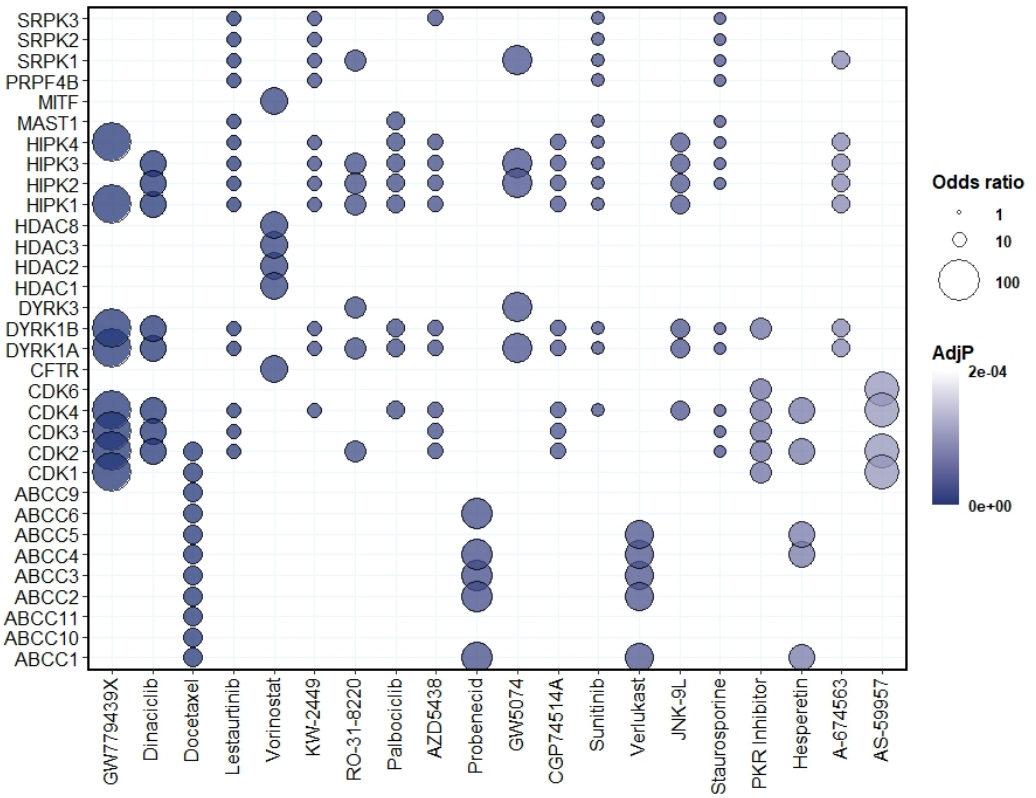

Figure 2.22: **Human orthologues of yeast interactions reveal drugs/compounds to test for synergy with atorvastatin.** Human orthologues of validated genes and bottleneck genes were processed via an enrichment analysis for signature genes in the Drug Signature Database. Bubble plot representing the human orthologues (y-axis) that were enriched for drugs/compounds (x-axis). The colour of each bubble is determined by the adjusted *P*-value and the size of bubble reflects a score computed by running the Fisher exact test for random gene sets to determine the deviation from the expected rank, where bigger bubbles represent greater enrichment.

Overall, the majority of the top 20 drugs/compounds detected here for potential synergy with atorvastatin have exhibited anticancer activity and only two have been investigated for such synergy (Table 2.13). These drugs with established anticancer activity include dinaciclib, docetaxel, lestaurtinib, vorinostat, palbociclib, and sunitinib. Interestingly, one of the top results is docetaxel, a well-established chemotherapeutic for the treatment of breast cancer that was previously investigated for synergy with lovastatin, albeit the trial was terminated for lack of funding (NCT00584012). Another noteworthy candidate combination therapy is probenecid, which is a drug that inhibits renal excretion and would thus increase the half-life of statin drugs. Clinical trial NCT03307252 evaluated the pharmacokinetics of probenecid with a number of drugs including rosuvastatin, but this trial did not evaluate the anticancer activity of the statin. In addition to drugs/compounds with established anticancer activity, I also propose

combination therapies with GW779439X with antibiotic properties, verlukast with bronchodilator properties and hesperetin with a wide variety of properties including cholesterol-lowering, antioxidant, anti-inflammatory and anticancer properties.

Drug/ compound	Description	Approved	Intended/ approved use	Clinical trial(s)	Clinical trial(s) with statin
GW779439X	Pyrazolopyridazine with antibiotic synergistic properties	No	Antibiotic	No	No
Dinaciclib	UPR inhibitor via CDK1 and 5	No	Cancer	Yes	No
Docetaxel	Chemotherapeutic for breast cancer	Yes	Cancer	Yes	Yes
Lestaurtinib	Tyorine kinase inhibitor	Yes	Cancer	Yes	No
Vorinostat	Used to treat cutaneous T-cell lymphoma	Yes	Cancer	Yes	No
KW-2449	Multikinase inhibitor	No	Cancer	Yes	No
RO-31-8220	Protein kinase C inhibitor	No	Various	No	No
Palbociclib	Ibrance, inhibitor of the cyclin-dependent kinases CDK4 and 6	Yes	Cancer	Yes	No
AZD5438	Oral inhibitor of cyclin-dependent kinases 1, 2, and 9	No	Cancer	Yes	No
Probenecid	Probalan, increases uric acid excretion and inhibits drug renal excretion	Yes	Prevention of gout	Yes	Yes
GW5074	cRaf1 kinase inhibitor	No	Cancer, neurodegenerative disorders	Yes	No
CGP74514A	CDK1 inhibitor	No	Cancer	No	No
Sunitinib	Sutent, multi-targeted receptor tyrosine kinase (RTK) inhibitor	Yes	Cancer	Yes	No
Verlukast	selective inhibitor of leukotriene	No	Bronchodilator	No	No
JNK-9L	c-jun-N-terminal kinase (JNK) inhibitor	No	Cancer	No	No
Staurosporine	Protein kinases inhibitor	No	Cancer	Yes	No
PKR Inhibitor	C16, inhibitor of RNA-dependent protein kinase (PKR)	No	Cancer	No	No
Hesperetin	Cholesterol lowering flavanoid found in citrus juices	No	Lowering cholesterol, cancer, antioxidant, anti-inflammatory, vasoprotective	Yes	No
A-674563	AKT1 inhibitor that also suppresses CDK2 activity	No	Cancer	No	No
AS-59957	1H-Pyrrole-2,5-dione, 3,4-diphenyl	No	Various	No	No

Table 2.13: **Most of the top 20 drugs that share signature genes with atorvastatin identified have anticancer activity but have not been investigated for synergy with statins.**

2.4 Discussion

2.4.1 Summary

Mapping genetic interactions is intended to simplify the understanding of complex genetic interactions (Busby et al. 2019; Leeuwen et al. 2017; Tong et al. 2004; Tutuncuoglu and Krogan 2019). With the network topological centrality and community algorithms used here, clear pathways of GO cellular processes emerged in the case of the *HMG1* or *BTS1* for interactions involved in autophagy, ageing, endocytosis, actin and UPR pathways. In the following discussion I make a distinction of grouping of genes by network topological centrality analysis as 'clusters' and community groupings as 'modules'.

Specifically, *RIM15* was identified a key statin modulator in positively regulating autophagy, a validated hit in atorvastatin-treated *HMG1* query and a high betweenness gene (bottleneck) in three genetic backgrounds. I identified *TPM1* gene mediating actin, endocytosis and autophagy, a validated hit in *BTS1* query and bottleneck gene for UWOPS87 and Y55 treated with atorvastatin and a synthetic lethal genetic interactions with S288C. *CDC28* was found as another bottleneck gene with the *HMG1* query in the aggregated networks of the three genetic backgrounds though not picked up in the screenings, that is an activator of UPR. I also identified potential anticancer combination therapies with atorvastatin with approved chemotherapeutic drugs (*e.g.*, lestaurtinib, sunitinib) and approved non-anticancer drugs (*e.g.*, probenecid) but also relatively understudied compounds (*e.g.*, GW779439X, verlukast, hesperetin).

2.4.2 Yeast as a model to study anticancer activity of statins

In this chapter, I used yeast models with two genetic probes into the mevalonate pathway and the study of the anticancer activity of atorvastatin in three genetic backgrounds. Insights into the complexity of the response to statins influenced by genetic and protein interactions have been demonstrated by others (Busby et al. 2019; Chakrabarty et al. 2020; Kamal et al. 2018; Kanugula et al. 2014; Loregger et al. 2017; Pandyra et al. 2015) and this thesis extends our understanding in by the following.

Firstly, investigations of causality and mechanism of action in human cells typically require randomised clinical trials, Mendelian randomisation approaches for observational data, or genetic manipulation of mammalian cell lines that are limited by high cost, complicated procedures and lack the ability to screen gene deletions of the whole genome for drug hypersensitivity in one high-throughput

step. Here I used yeast screening systems that do not suffer from these drawbacks because causality can be directly established by simple experimentation using genome-wide haploid deletion libraries that allowed unbiased high-throughput screening for genes and drugs that interact with atorvastatin.

Secondly, in most high-throughput yeast gene deletion studies, genetic interactions have been centralised in a single genetic background, the well-characterised S288C yeast strain (Winzeler et al. 1999). Individual genetic background is known to affect genetic interactions (Busby et al. 2019; Deutschbauer and Davis 2005; Galardini et al. 2019), and a generalised picture of drug mechanism requires more studies in more genetic backgrounds. Here I investigated genetic interactions in S288C and two additional genetic backgrounds, UWOPS87 and Y55.

Thirdly, high-throughput chemical genetic interaction studies are mostly based on high-throughput data that has not been independently validated, thus data can be noisy and difficult to interpret. Here I validated the atorvastatin-specific genetic interactions that I identified in high-throughput screens, which enhanced the reliability of the results and data analysis.

2.4.3 Genetic interactions point to the role of autophagy in atorvastatin anticancer activity

RIM15 was distinguished as a top bottleneck gene in centrality analyses (based on high betweenness scores) that overlapped in all three genetic backgrounds. Bottlenecks are of high relevance because they tend to connect functional clusters of genes (Brandes 2001; Yu et al. 2007). When I enhanced the network by looking for interactors with *RIM15* (of pathlength 2) about 75% of the genes that were found to interact with *RIM15* belonged to a single community module in all the genetic backgrounds that was enriched for meiosis, longevity and autophagy. In S288C that was module 3 (Figure 2.20) and module 1 for both UWOPS87 and Y55. Community modules are held to be functional (Chen and Yuan 2006; Rahiminejad et al. 2019) and that these genes tended to appear in topology clusters also, a point worthy of note.

Characteristically for bottleneck genes, when removed, the network collapses. This result was experimentally validated via synthetic lethal interactions in S288C and synthetic sick interactions in UWOPS87 and Y55. In the haploinsufficiency profiling (HIP) chemogenomic platform (Lee et al. 2014), *RIM15* was reported as a non-significant interactor with atorvastatin, cerivastatin, lovastatin and fluvastatin. There are also no reports of its interaction with *HMG1* or *HMG2* in the *Saccharomyces* genome database (SGD) (Cherry et al. 2012). A negative chemical genetic interaction of *RIM15* with atorvastatin has been reported for UWOPS87 and Y55 and a negative genetic interaction of *HMG1*

with *RIM15* (Busby et al. 2019), however, not strong enough to stand out from this analysis and a screen for the *HMG1* query double deletions with atorvastatin was not performed.

In the community analyses, *RIM15* belonged to the community module enriched for meiosis, longevity and autophagy. This is consistent with the role for *RIM15* in ribophagy, that is, the autophagy of ribosomes (Li et al. 2021). Autophagy is a known and partially characterised pathway for the anticancer activity of statins. Statins are known to activate autophagy through the suppression of PI3K/Akt/mTOR and activation of AMPK (Okubo et al. 2020; Wang et al. 2016; Yang et al. 2010). None of these mechanisms point to a role for the human orthologues of *RIM15* (MASTL, MAST1, MAST2, MAST3, MAST4) in the statin-induced autophagy or any other statin-related activity, and none of such human orthologues have been linked to statin activity before. The human orthologues of *RIM15*, however, are not involved in ribophagy but rather ribophagy is orchestrated by NUFIP1 and ZNHIT3. Whether NUFIP1 and ZNHIT3-mediated ribophagy or whether the MAST orthologues of *RIM15* are behind the anticancer role of atorvastatin is a research direction worth of exploration. Interestingly, ZNHIT3 has been found upregulated in statin users who developed type 2 diabetes but this was not linked to autophagy (Leitzmann et al. 2005).

MAST1 has been defined as a main driver of the resistance to the chemotherapeutic cisplatin in humans (Jin et al. 2018) and induction of autophagy has also shown a role in cisplatin in ovarian cancer (Wang and Wu 2014). Though the mechanism by which MAST1 mediates resistance to cisplatin is through the HSP90-mediated protection from proteasomal degradation (Pan et al. 2019) a role for autophagy cannot be ruled out. MAST4, for instance, has shown to have an unknown role in autophagy (Bennetzen et al. 2012). *RIM15* is also a downstream protein kinase of *SCH9*, which is required for TORC1-mediated regulation of ribosome biogenesis, and both *RIM15* and *SCH9* are involved in the induction of ribophagy (Waliullah et al. 2017).

2.4.4 Genetic interactions point to the role of chronological lifespan in atorvastatin anticancer activity

In addition to autophagy, that is already an established mechanism of statin bioactivity (King et al. 2016; Parikh et al. 2010; Toepfer et al. 2011), my growth phenotypes as well as network analyses distinguish a role for *RIM15* in atorvastatin-specific aspects of chronological lifespan, the lifespan of non-dividing cells. Consistently, *RIM15* has been linked with chronological lifespan independent of any drug treatment (Cao et al. 2016; Wei et al. 2008; Zhang and Cao 2017). More specifically, starvation activates yeast AMPK, one of the conserved metabolic pathways involved in the anticancer activity of

statins (Yang et al. 2010), via integration with Rim15, Yak1 and Mck1 to induce stress resistance and metabolic reprogramming that leads to lifespan extension (Zhang and Cao 2017). Additionally, *RIM15* is required for increased lifespan in yeast due to deficiency of Ras2, Tor1, and Sch9 (Wei et al. 2008). It is thus possible that inhibition of Ras2 prenylation by atorvastatin may also have an anti-ageing effect via *RIM15* but how this affects cancer cells is unclear. The connection between yeast *RIM15* and cancer has been previously reported where *RIM15* yeast deletion mutants were unable to adapt to calorie-restricted conditions by entering post-mitotic state, a state that was compared by the authors to cancer cell physiology (Bisschops et al. 2014). The link of chronological lifespan with the anticancer activity of atorvastatin, however, is interesting given that ageing is considered one of the main risk factors for cancer development, which is linked to biological changes that come with biological age such as DNA damage and cellular senescence (Berben et al. 2021). Since statins have increased lifespan of the model organism *Caenorhabditis elegans* (Jahn et al. 2020) and decreased mortality independent of cholesterol in humans aged 78-90 years old (Jacobs et al. 2013), it is plausible that statins increase lifespan in general, particularly since these worm and human studies were not specific to ageing of non-dividing cells.

More evidence on the potential link between the anticancer activity of statins and its anti-ageing properties comes from the human orthologue of *HST1*, which was one of the genes that was experimentally demonstrated to be synthetic sick with *HMG1* in UWOPS87 and was also one of the genes belonging to the community modules that were enriched for the longevity regulating pathway mediated by the sirtuin (SIRT) genes. Sirtuins are a family of protein deacetylases that regulate ageing and longevity (Imai and Guarente 2016; Longo and Kennedy 2006). Humans have seven sirtuins, most of which have an involvement in cancer (Chalkiadaki and Guarente 2015). SIRT1 is a known target of the drug resveratrol, which also prolongs lifespan via autophagy in worms and human cells (Morselli et al. 2010) and atorvastatin reduced the expression of SIRT1 (Kilic et al. 2015). As there is no evidence regarding the impact of HST1/SIRT genes on the anticancer activity of statins, this will be interesting research for future studies as it is plausible that these genes have been overlooked to date.

2.4.5 Genetic interactions point to the role of actin-mediated endocytosis in atorvastatin anticancer activity

The previous section showed us that autophagy and ageing are involved in statin mechanisms but my studies allow us to go further than that. I also identified *TPM1*, an actin cable stabiliser with a role in endocytosis, to be essential for *BTS1*-deleted strains in S288C genetic background. This

deletion became essential for UWOPS87 and Y55 only upon treatment with atorvastatin, which would be consistent with these two genetic backgrounds being more tolerant to UPR (Busby et al. 2019) where it was proposed that an insufficiency in UPR caused cells to resort to endocytosis with atorvastatin treatment.

Network science illustrates that cellular pathways are functionally redundant. My results for *RIM15* and its interactors reiterate this phenomenon for a dual role in actin and endocytosis. *CDC28*, one of the top centralities in the *HMG1* genetic interaction networks, has shown a positive (suppressing) interaction with *RIM15* (Juanes et al. 2013; Talarek et al. 2017). In a study investigating the molecular chaperone function in yeast genetic interaction networks, *CDC28* and *RIM15* were clustered together in a cochaperone module that was overrepresented for 'actin and morphogenesis' (Rizzolo et al. 2017). The fact that these genes appeared in this study points to a role as cochaperone interactors in atorvastatin bioactivity. Although *CDC28* did not belong to a statistically significant community module in my study, 86% of the genes that interacted with *CDC28* in Y55 and UWOPS87 belonged to the community module corresponding to meiosis, cell cycle and MAPK signalling, suggesting that networks are functionally redundant for these processes as well as actin/endocytosis.

Relatedly in human cells, human orthologues of *RIM15* code for microtubule serine/threonine kinases and cytoskeleton components, such as actin and the intermediate filament that have shown to be part of the statin response (Denoyelle et al. 2003). Statins are also known to down-regulate *CDC28* human orthologues such as CDK1 that was part of the mechanism for the anticancer activity of atorvastatin in esophageal squamous cell carcinoma (ESCC) cells because it was down-regulated after atorvastatin treatment (Yuan et al. 2019). Simvastatin induced G1 arrest and inhibited cell growth of colorectal cancer cell lines by a mechanism that included down-regulating CDK4/cyclin D1 and CDK2/cyclin E1 (Chen et al. 2018). Simvastatin and lovastatin suppressed expression of CDK1, CDK2, CDK3, CDK4 and CDK6 in prostate cancer cells with reduced cell viability due to induced apoptosis and cell cycle arrest (Hoque et al. 2008). Although not investigated in these studies, it is possible that reduced cell proliferation was partly due to cytoskeletal (*e.g.*, actin) instability.

F-actin is a modulator of clathrin-mediated endocytosis (Loebrich 2014) and a known component involved in the anticancer activity of statins, *e.g.*, via the inhibition of prenylation of RhoA GTPases (see Figure 1.14 in Chapter 1). This leads to inhibition of the F-actin dependent transcriptional regulators YAP and TAZ (Zanconato et al. 2016). These in turn mediate tumour initiation, growth, metastasis and chemoresistance (Cordenonsi et al. 2011; Panciera et al. 2016; Zanconato et al. 2016). Given F-actin mediated endocytosis is also the mechanism by which low density lipoprotein (LDL) are

internalised for the delivery of exogenous cholesterol (Goldstein et al. 1982), it is thus possible that destabilisation of the cytoskeleton and consequent inhibition of endocytic cargo (*e.g.*, LDL cholesterol) molecules endocytosis might be another mechanism for the anticancer activity of atorvastatin. This would be in agreement with the finding that atorvastatin upregulated LDL receptor while preserving cholesterol levels in tumours (Feldt et al. 2020). From my perspective, aberrant endocytosis may impede internalisation of cholesterol regardless of the upregulation of LDL receptor. Since simvastatin has also inhibited uptake inhibition of extracellular vesicles due to clathrin-independent endocytosis (Costa Verdera et al. 2017), it is possible that clathrin-dependent and clathrin-independent endocytosis are both altered by statins. Though actin is also fundamental for the endocytic pathway in yeast, yeast do not uptake ergosterol (the cholesterol equivalent) from the extracellular medium in aerobic conditions (Trocha and Sprinson 1976), suggesting that other cargo molecules may be part of the anticancer mechanisms of atorvastatin.

In addition, *TPM1*, a major isoform of tropomyosin that binds and stabilises actin cables (Liu and Bretscher 1989), was essential in S288C *BTS1*-deleted strains (Figure 2.9) (Liu and Bretscher 1989). This extreme case of inhibited prenylation of Ras GTPases also points to exacerbation of cytoskeleton instability given that tropomyosin, like Ras GTPases, regulate the polarity of the actin cytoskeleton and thus polarised growth (Ho and Bretscher 2001). *TPM1* is not a known mechanism for statins in yeast but its human orthologue has been pointed as a potential tumour suppressor with it being downregulated in cancer cells (Pan et al. 2017; Tang et al. 2018; Wang et al. 2019a). Inhibition of *TPM1* in combination with atorvastatin therapy is thus a potential therapy to explore in future studies.

2.4.6 Genetic interactions point to the role of UPR in atorvastatin anticancer role

One more pathway that I found was enrichment for the unfolded protein response (or more broadly, protein and processing in ER) in statin-treated cells. This is not surprising given that ER stress is a known mechanism of the anticancer activity of statins (Yang et al. 2010) and UPR is part of the global ER stress response. My contribution, however, points to UPR being the link among the cellular pathways identified here (Figure 2.23).

Given that UPR is tightly linked to autophagy (Senft and Ronai 2015; Yan et al. 2015), actin-mediated endocytosis (Mattiazzi Usaj et al. 2020) and ageing pathways (Estébanez et al. 2018; Taylor 2016), it is plausible that all of them have a role in the anticancer activity of atorvastatin via induction of UPR. Atorvastatin, for instance, may indirectly inhibit endocytosis and induce UPR via inhibition of actin for the following reasons (1) atorvastatin and simvastatin have shown inhibition and

remodelling of the actin cytoskeleton (Boerma et al. 2008; Chubinskiy-Nadezhdin et al. 2017) and Ras GTPases inhibited by statins also regulate the polarity of the actin cytoskeleton (Ho and Bretscher 2001); (2) actin is necessary for endocytosis (Mooren et al. 2012); and (3) UPR is induced in yeast mutants deficient of actin-mediated steps in endocytosis (Mattiazzi Usaj et al. 2020).

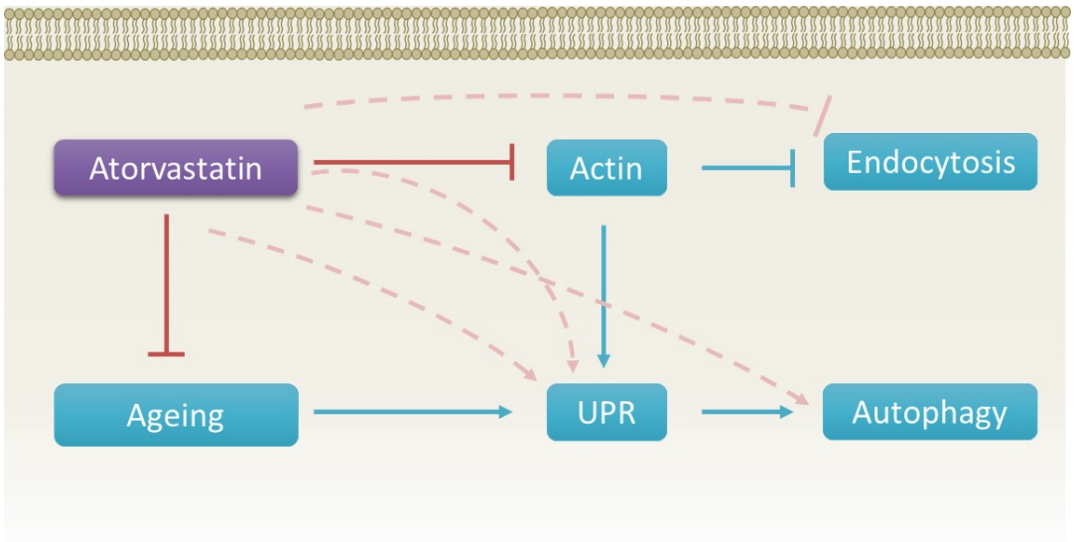

Figure 2.23: **Proposed integration of mechanisms identified in this chapter.** Atorvastatin inhibits components of the actin cytoskeleton, which in turn inhibits actin-mediated endocytosis and induces UPR. Atorvastatin inhibits ageing pathways, which also results in the dual induction of UPR and autophagy. Hence, atorvastatin is an indirect inhibitor of endocytosis and indirect activator of UPR and autophagy. Red blunt head arrows point to pathways inhibited by atorvastatin. Blue arrows and blue blunt head arrow point to pathways that are inhibited or induced, respectively. Hashed pink arrows and hashed blunt head arrow point to inhibition or induction, respectively, of pathways via indirect mechanisms of atorvastatin.

Statins have also been shown to increase lifespan and hence ameliorate ageing (Boccardi et al. 2013; Jacobs et al. 2013; Jahn et al. 2020). Statins were associated with higher telomerase activity, lower telomere erosion and hence reduced ageing in persons 30-86 years old (Boccardi et al. 2013), whereas in another study statin treatment was associated with decreased mortality in persons 85-90 years old (Jacobs et al. 2013). This seems to be the case across species since *C. elegans* has also showed extended lifespan due to statin-mediated mevalonate depletion and JNK1-mediated activation of DAF-16/hFOXO3a, a transcription factor in ageing and longevity (Sun et al. 2017; Jahn et al. 2020). Ageing in turn decreases the resistance to stress and weakens the UPR (Taylor 2016; Minakshi et al. 2017), thus atorvastatin may indirectly induce UPR via increased lifespan.

UPR is a transcriptional activator of components of the autophagy pathway (Deegan et al. 2013). Thus, UPR induction through the pathways mentioned above would consequently induce autophagy. In other words, statins are indirect activators of autophagy through UPR. Atorvastatin has indeed induced autophagy in prostate cancer cells, which was associated with enhanced expression of LC3

through inhibition of geranylgeranyl biosynthesis (Toepfer et al. 2011). Simvastatin also sensitised glioblastoma cells to temozolomide treatment via autophagic flux inhibition regulated by IRE1 and PERK, signalling arms of UPR (Dastghaib et al. 2020). The benefits of statin-mediated autophagy induction as anticancer therapeutic, however, need more research because autophagy itself is a double-edged protective mechanism against cell death (*i.e.*, too much or too little can be damaging). In fact, inhibition of autophagy with bafilomycin A1 enhanced anticancer activity of atorvastatin in hepatocellular and colorectal carcinoma cells (Yang et al. 2010).

2.4.7 Conclusion

Taken together, I have demonstrated the utility of using chemical genetics and network analyses to elucidate specific interactors and metabolic pathways that may be behind the anticancer activity of atorvastatin. Known pathways in the literature, such as UPR and autophagy, give us confidence that other pathways identified in this chapter such as chronological lifespan and actin-mediated endocytosis are more than findings by chance. Given that *RIM15* also stands out as a key interactor that plays a role in more than one of the aforementioned pathways, this and other interactors identified in this chapter (*e.g.*, *CDC28* in yeast and its CDK human orthologues) should be further explored in mammalian cell lines and animal models.

Chapter 3

Atorvastatin-specific epistasis with genes outside the mevalonate pathway: DGAT and TGL genes in triacylglycerol metabolism

3.1 Introduction

Discovered by Akira Endo in the 1970s, statins were shown to decrease unhealthy levels of LDL cholesterol in clinical trials (Tobert et al. 1982a; Tobert et al. 1982b) and were approved for commercial use 40 years ago. Simvastatin reduced mortality in patients with cardiovascular disease by 30% (Scandinavian Simvastatin Survival Study Group 1994). However, statin use also shows undesirable side-effects in some patients, for example, new onset diabetes mellitus in ~10% of cases (Betteridge and Carmena 2016; Coleman et al. 2008), causing the US Federal Drug Administration (FDA) to publish an advisory on diabetes markers like glycosylated haemoglobin and fasting serum glucose levels (FDA 2012). Statin-induced diabetes is dose-dependent (Preiss et al. 2011) and more frequent in patients with metabolic syndrome (Waters et al. 2013). Statin-induced insulin resistance has been linked to lipotoxicity (Lee et al. 1994) due to low levels of diacylglycerol acyltransferase (DGAT) and consequently reduced synthesis of triacylglycerols (triacylglycerides) in skeletal muscle (Larsen et al. 2018).

The molecular mechanisms behind statin-induced lipotoxicity and overall statin-induced diabetes are only partially understood. The most direct mechanism is decreased activity of 3-hydroxy-3-methyl-glutaryl-coenzyme A reductase (HMGCR) (Figure 3.1), because reduction in activity caused by single nucleotide polymorphisms (SNPs) in this gene show a similar increased

incidence of diabetes (Swerdlow et al. 2015). Such a mechanism could include down-stream disruption of membrane sites at which insulin receptors localise as a result of decreased cholesterol levels. Indirect effects of statins in the mevalonate pathway could also be involved, such as (i) impaired translocation of the glucose transporter GLUT4 to the cellular membrane caused by the inhibited isoprenylation of Rab and Rho GTPases as well as ubiquinone (Ganesan and Ito 2013; Takaguri et al. 2008); and (ii) impaired pancreatic β-cells function through the inhibition of glucose-induced insulin secretion, decreased expression of GLUT2, and increased cellular influx of calcium (Zhou et al. 2014). It is thus critical to understand the direct and indirect mechanisms mediating the diabetogenic activity of statins.

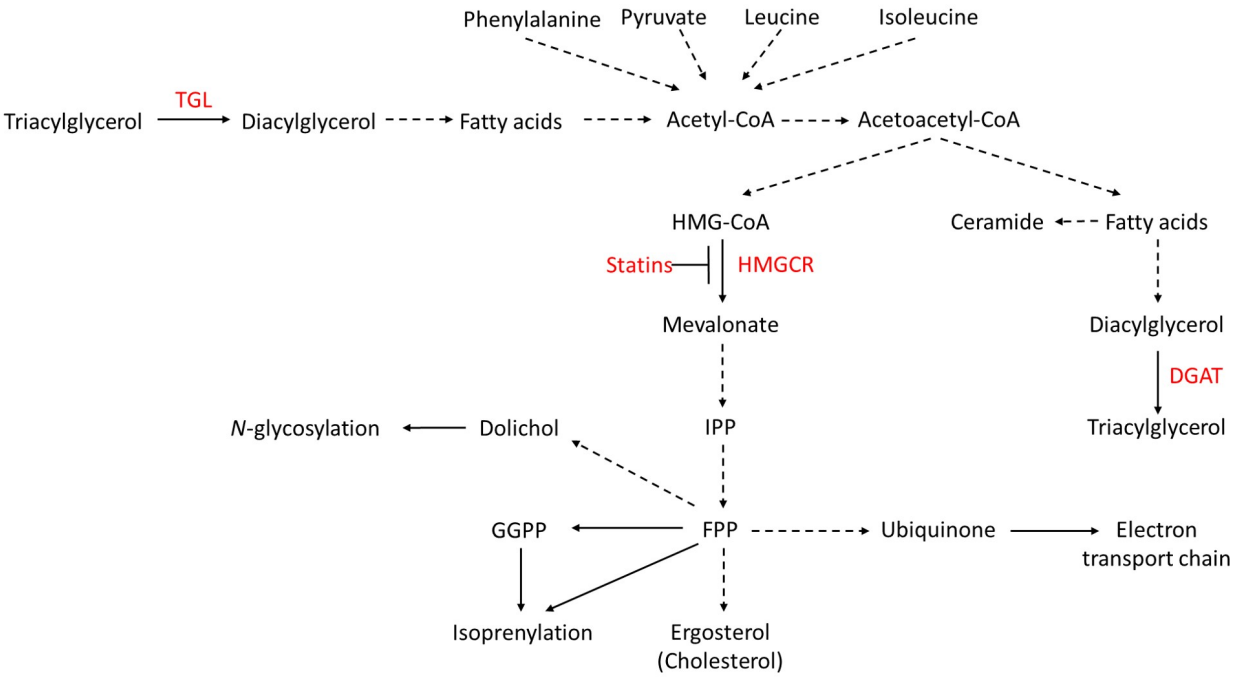

Figure 3.1: **Fatty acid and cholesterol metabolism are linked by acetoacetyl-CoA.** Statins are competitive inhibitors of HMGCR, the rate-limiting step in the mevalonate pathway. The mevalonate pathway is linked to the fatty acid metabolic pathways. While triacylglycerides, diacylglycerols and fatty acids are precursors of acetyl-CoA in the catabolic pathway, acetoacetyl-CoA is the precursor for the synthesis of fatty acids, diacylglycerols and triacylglycerides in the anabolic pathway as well as being upstream of HMG-CoA in the mevalonate pathway. The interplay between the mevalonate pathway and fatty acid synthesis is thus mediated by acetoacetyl-CoA.

Given the subset (~10%) of cases of statin treatments being associated with the onset of diabetes, it is plausible that there are gene-gene or perhaps gene-drug combinations that explain these cases and/or the cases without this association. Combination and targeted therapies may be explored genetically by means of drug-induced synthetic lethality (Dobzhansky 1946; Hopkins 2008; Parameswaran et al. 2019). At its simplest, mutation of one gene can be compatible with

cellular viability but when a second mutation (or drug) causes lethality or sickness (fitness defect), this epistatic interaction reveals a functional relationship between the two genes or pathways (Costanzo et al. 2019; Mackay and Moore 2014). Thus, seeking epistatic interactions genome-wide between diabetes-related genes and statins should identify interactions in diabetogenic pathways and pinpoint candidate interactions to suppress this risk.

Here I used established yeast models with conserved targets and downstream effects of statins that have been developed for the study of metabolic syndrome and lipotoxicity (Kohlwein 2010; Kurat et al. 2006; Petschnigg et al. 2009). These mutants differ in their levels of lipid droplets, fat-storage organelles within cells. Double mutants lacking triacylglycerol lipase genes *TGL3* and *TGL4* are unable to degrade triacylglycerides, providing an 'obese' model displaying 4-6 oversized lipid droplets per cell (Kurat et al. 2006). There is a corresponding 'anorexic' model namely the double mutants lacking DGAT genes *DGA1* and *LRO1*; this strain is unable to synthesise triacylglycerides and hence accumulates diacylglycerol and fatty acids that become toxic with only one small lipid droplet per cell (Kohlwein 2010; Petschnigg et al. 2009).

Diabetogenic activity of statins is more apparent in patients with pre-existent conditions such as metabolic syndrome and there is evidence that one of the contributing factors to statin-induced glucose intolerance is lipotoxicity, yet the molecular mechanisms are not fully understood. In this chapter, I used the established yeast models for metabolic syndrome (*tgl3*Δ*tgl4*Δ) and lipodystrophy (*dga1*Δ *lro1*Δ) as query strains in SGA analyses to generate 25,800 triple deletion strains (*dga1*Δ *lro1*Δ *xxx*Δ or *tgl3*Δ *tgl4*Δ *xxx*Δ) in statin-susceptible (S288C) and statin-resistant genetic backgrounds (UWOPS87, Y55). Building off experimentally validated statin-hypersensitive mutants, analyses of genetic interaction networks including topology centrality, pathway enrichment and drug enrichment were used to identify key genes and cellular processes regulating statin activity in the metabolic syndrome and lipodystrophy in multi-layer networks. This chapter expands our knowledge on specific genes and pathways that potentially mediate the diabetogenic activity of atorvastatin and proposes candidate combination therapies to counteract such activity.

3.2 Experimental Procedures

The methods used in this chapter are similar to those in Chapter 2 (Figure 3.2). The main differences lie with the query strains constructed here that were specific to the obese and anorexic yeast models and that network topology analyses were limited to multi-layered aggregated networks rather than single-layer networks.

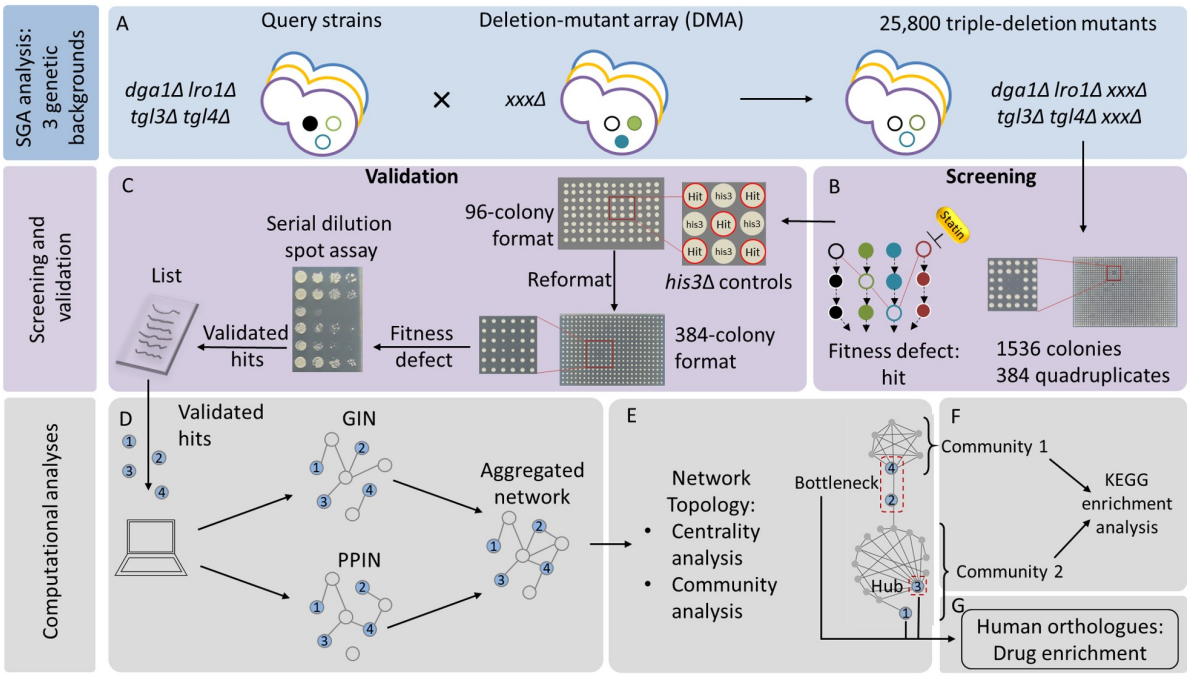

Figure 3.2: **Flow diagram for the methods used to identify interactions, pathways and drugs to reduce the diabetogenic activity of atorvastatin.** Double deletion mutant query strains were constructed (A) (deletion mutant genes depicted as empty circles) as models to investigate the diabetogenic activity of atorvastatin (*dga1*Δ *lro1*Δ and *tgl3*Δ *tgl4*Δ) in three yeast genetic backgrounds (S288C, UWOPS87 and Y55 indicated here as purple, yellow and blue), and mated against DMAs of the same genetic backgrounds to generate 25,800 triple deletion mutants in 1536-colony format (384 quadruplicate colonies per agar plate). These mutants were treated with atorvastatin (B) and screened to identify fitness defects that would reveal epistatic interactions (hits) as measured by decreased colony size. Hits were then validated in two steps (C). First, hits were formatted in 96-colony format plates with each hit surrounded by *his3*Δ strains for growth control. These plates were then reformatted to 384-colony format (96 quadruplicate colonies) and screened again with atorvastatin. Colonies that showed fitness defects were selected for the second step, which consisted of serial dilution spot assays. Hits that showed growth inhibition in the latter were considered as validated interactions and used as input to create genetic (GIN) and protein-protein (PPIN) interaction networks (D). GINs and PPINs were aggregated in one network (E) per genetic background and subjected to network topology analyses. The network centrality metrics pinpointed bottleneck and hub genes of high biological relevance. The communities of genes identified through network modularity (F) were analysed through a KEGG enrichment analysis to distinguish key metabolic pathways. Human orthologues of the key yeast genes were used in a search for drug enrichment (G) to identify potential combination therapies to inhibit the diabetogenic activity of atorvastatin.

3.2.1 Yeast strains

The *S. cerevisiae* strains used in this study are described in Table 3.1. Stocks were stored at 80°C in 15% glycerol. Strains that contained the URA3_CEN plasmid were grown on agar with 1 mg/mL of 5-Fluoroorotic Acid (5-FOA, Kaixuan Chemical Co) to select for uracil auxotrophs before construction of the query strains.

Background	Genotype	Description	Reference
Y7092 (S288C)	*Matα can1::STE2pr-Sp_his5 lyp1Δ his3Δ1 leu2Δ0 ura3Δ0 met15Δ0*	Query construction starting strain	Tong & Boone 2006
Y55	*Matα ho::HPH ura3Δ0 his3Δ0 [URA3_CEN]*	Query construction starting strain	Busby 2019
UWOPS87	*Matα ho::HPH ura3Δ0 his3Δ0 [URA3_CEN]*	Query construction starting strain	Busby 2019
Y7092 (S288C)	*Matα can1::STE2pr-Sp_his5 lyp1Δ his3Δ1 leu2Δ0 ura3Δ0 met15Δ0 dga1::NatR lro1::LEU2*	*dga1Δ lro1Δ* query strain	Joblin-Mills 2020
Y55	*Matα ho::HPH ura3Δ0 his3Δ0 dga1::NatR lro1::URA3*	*dga1Δ lro1Δ* query strain	This study
UWOPS87	*Matα ho::HPH ura3Δ0 his3Δ0 dga1::NatR lro1::URA3*	*dga1Δ lro1Δ* query strain	This study
Y7092 (S288C)	*Matα can1::STE2pr-Sp_his5 lyp1Δ his3Δ1 leu2Δ0 ura3Δ0 met15Δ0 tgl3::NatR tgl4::LEU2*	*tgl3Δ tgl4Δ* query strain	This study
Y55	*Matα ho::HPH ura3Δ0 his3Δ0 tgl3::NatR tgl4::URA3*	*tgl3Δ tgl4Δ* query strain	This study
UWOPS87	*Matα ho::HPH ura3Δ0 his3Δ0 tgl3::NatR tgl4::URA3*	*tgl3Δ tgl4Δ* query strain	This study
Y7092 (S288C)	*MATa his3Δ1 leu2Δ0 met15Δ0 ura3Δ0 xxx::KanR*	Yeast deletion collection (DMA)	Tong & Boone 2006
Y55	*Mata can1::STE2pr-Sp_his5 lyp1Δ his3Δ1 ura3Δ0 xxx::KanR*	Yeast deletion collection (DMA)	Busby 2019
UWOPS87	*Mata can1::STE2pr-Sp_his5 lyp1Δ his3Δ1 ura3Δ0 xxx::KanR*	Yeast deletion collection (DMA)	Busby 2019
Y7092 (S288C)	*Mata can1::STE2pr-Sp_his5 lyp1Δ his3Δ1 leu2Δ0 ura3Δ0 met15Δ0 dga1::NatR lro1::LEU2 xxx::KanR*	*dga1Δ lro1Δ xxxΔ* SGA	This study
Y55	*Mata can1::STE2pr-Sp_his5 lyp1Δ his3Δ1 ura3Δ0 ho::HPH dga1::NatR lro1::URA3 xxx::KanR*	*dga1Δ lro1Δ xxxΔ* SGA	This study
UWOPS87	*Mata can1::STE2pr-Sp_his5 lyp1Δ his3Δ1 ura3Δ0 ho::HPH dga1::NatR lro1::URA3 xxx::KanR*	*dga1Δ lro1Δ xxxΔ* SGA	This study
Y7092 (S288C)	*Mata can1::STE2pr-Sp_his5 lyp1Δ his3Δ1 leu2Δ0 ura3Δ0 met15Δ0 tgl3::NatR tgl4::LEU2 xxx::KanR*	*tgl3Δ tgl4Δ xxxΔ* SGA	This study
Y55	*Mata can1::STE2pr-Sp_his5 lyp1Δ his3Δ1 ura3Δ0 ho::HPH tgl3::NatR tgl4::URA3 xxx::KanR*	*tgl3Δ tgl4Δ xxxΔ* SGA	This study
UWOPS87	*Mata can1::STE2pr-Sp_his5 lyp1Δ his3Δ1 ura3Δ0 ho::HPH tgl3::NatR tgl4::URA3 xxx::KanR*	*tgl3Δ tgl4Δ xxxΔ* SGA	This study

Table 3.1: **Strains used in this study.**

3.2.2 Plasmids

The plasmids used in this study were conserved in *E. coli* (DH5α) stored at 80°C (Table 3.2).

Plasmid	Description	Reference
p4339	MX4-natR switcher cassette	Tong et al. 2001
pAG60	*URA3* from *C. albicans* for uracil prototrophy	Goldstein and McCusker 1999
puG73	*LEU2* from *Kluyveromyces lactis*	Zhang et al. 1992

Table 3.2: **Plasmids used in this study.**

3.2.3 Media and Solutions

The media and solutions used for the analyses described in this chapter were the same described in Chapter 2 (Section 2.2.3).

3.2.4 Synthetic Genetic Array (SGA) analysis

Query strains were constructed using PCR disruption and homologous recombination as previously described in Chapter 2 (Section 2.2.4). Briefly, selection markers were amplified using primers (Tables 3.3) from plasmids (Table 3.2) and transformed into strains representing different genetic backgrounds. The plasmid pUG73 was used to replace *TGL4* with *LEU2* in S288C, whereas the plasmid pAG60 was used to replace *TGL4* and *LRO1* with *URA3* in UWOPS87 and Y55 due to differences in the strains' genetic markers (Table 3.1). The amplified cassettes were then transformed and selected on SD-Ura + NAT or SD-Leu + NAT as appropriate. For UWOPS87 and Y55 strains, the agar was also supplemented with 300 µg/mL hygromycin (HPH) to prevent the selection of transformants that may have cassettes inserted in the highly homologous *ho::HPH* region. The *dga1::NAT lro1::LEU2* double deletion in S288C was a kind gift from Aidan Joblin-Mills. PCR primers (Table 3.4) and conditions (Section 2.2.4) were then used to confirm the genotypes.

SGA analysis with the MATα *dga1*Δ *lro1*Δ and the *tgl3*Δ *tgl4*Δ double deletion strains in three genetic backgrounds (S288C, UWOPS87 and Y55) was performed using the standard protocols (Tong et al. 2001) and as described in Section 2.2.4 with the additional modification to allow for starting with a double deletion query to generate triple deletion strains. In this case, the final two selection steps were for triple deletion strains on SD-His/Arg/Lys/Leu+CAN/THIA/G418/NAT or SD-His/Arg/Lys/Ura+CAN/THIA/G418/NAT.

Primer	Sequence	Description
lro1Δ forward	ACAAAAGGTTCTCTACCAACGAATTCGGCGAC AATCGAGTAAAAACAGCTGAAGCTTCGTACGC	5' *LRO1* loci KO with leucine or uracil auxotrophic cassettes
lro1Δ reverse	TTCTTTTCGCTCTTTGAAATAATACACGGATGGATAG TGAGTCAATGTCGGTCATAGGCCACTAGTGGATCTG	3' *LRO1* loci KO with leucine or uracil auxotrophic cassettes
tgl4Δ forward	TAATTATTGAAGGGAGTACAGGTATATGTAAT AAAAGTCTGAATGCAGCTGAAGCTTCGTACGC	5' *TGL4* loci KO with leucine or uracil auxotrophic cassettes
tgl4Δ reverse	AAAAAGAATATCTAGAGGATATATAAGCAAG CCCGTGTTTTCTTAAGGCCACTAGTGGATCTG	3' *TGL4* loci KO with leucine or uracil auxotrophic cassettes
dga1Δ forward	TACATATACATAAGGAAACGCAGAGGCATACAGTTT GAACAGTCACATAACATGGAGGCCCAGAATACCCT	5' *DGA1* loci KO with clonNAT resistance cassette
dga1Δ reverse	AAAATCCTTATTTATTCTAACATATTTTGTGTTTTCC AATGAATTCATTACAGTATAGCGACCAGCATTCAC	3' *DGA1* loci KO with clonNAT resistance cassette
tgl3Δ forward	AATCATCTATTCATATATCACATCTTTGAGTTGCC GTTAAGCATGACATGGAGGCCCAGAATACCCT	5' *TGL3* loci KO with clonNAT resistance cassette
tgl3Δ reverse	CTATCAATAAAAAAAATAAGACAGAAAAAAGTG GAAACGATACTACAGTATAGCGACCAGCATTCAC	3' *TGL3* loci KO with clonNAT resistance cassette

Table 3.3: **PCR primers used for NATMX cassette construction.**

Primer	Sequence	Description
lro1Δ confirmation forward (A)	TCCTTTAAATAGCCCTTCGC	5' *LRO1* loci KO confirmation A
lro1Δ confirmation reverse (D)	CTCCGCAGCCTACTTAGAAA	3' *LRO1* loci KO confirmation D
tgl4Δ confirmation forward (A)	ATTGAAAATTTCGAAAGAAATAGGG	5' *TGL4* loci KO confirmation A
tgl4Δ confirmation reverse (D)	TGTCCATTATTACTATTTGGCATGA	3' *TGL4* loci KO confirmation D
dga1Δ confirmation forward (A)	CCAGTACTTCCACCGCATTT	5' *DGA1* loci KO confirmation A
dga1Δ confirmation reverse (D)	GCTTTGCCTGGTAAGCTATG	3' *DGA1* loci KO confirmation D
tgl3Δ confirmation forward (A)	TCTTGGTTCTTTTCCATACTTTGAC	5' *TGL3* loci KO confirmation A
tgl3Δ confirmation reverse (D)	ATTTGAACTTGAATCCTCTGAAGAC	3' *TGL3* loci KO confirmation D
LEU2 confirmation reverse (B)	AGTTATCCTTGGATTTGG	3' leucine auxotrophic cassette confirmation B
LEU2 confirmation forward (C)	ATCTCATGGATGATATCC	5' leucine auxotrophic cassette confirmation C
URA3 confirmation reverse (B)	AATTCAACGCGTCTGTGAGG	3' uracil auxotrophic cassette confirmation B
URA3 confirmation forward (C)	GACACCTGGAGTTGGATT	5' uracil auxotrophic cassette confirmation C
NAT confirmation reverse (B)	TACGAGATGACCACGAAGC	3' clonNAT resistance loci confirmation B
NAT confirmation forward (C)	TGGAACCGCCGGCTGACC	5' clonNAT resistance loci confirmation C

Table 3.4: **PCR primers used to confirm NATMX cassette integration.**

3.2.5 Genome-wide growth analysis

The selected MATa *dga1*△ *lro1*△ *xxx*△ and the *tgl3*△ *tgl4*△ *xxx*△ triple deletion strains were grown in quadruplicate in 1536-colony format in the presence and absence of atorvastatin as described in Chapter 2 (Section 2.2.5). The plates were imaged after 12 and 24 h of incubation at 30˚C and processed through SGAtools (Wagih et al. 2013) to quantify the average colony size for each strain in treated compared to untreated media.

3.2.6 Validation of hypersensitive strains

The validation of sensitive strains was performed as previously described (Sections 2.2.6-2.2.7). Briefly, 96-colony format plates were arrayed containing no more than 29 triple deletion strains and the double deletion query strain (*dga1*△ *lro1*△ or *tgl3*△ *tgl4*△) each with *his3*△ control strains at the border and also surrounding each hit. The arrayed plates were screened in the presence and absence of atorvastatin. Hypersensitive strains (with a percent growth of about 20% lower than that of the double deletion *dga1*△ *lro1*△ and about 30% for *tgl3*△ *tgl4*△) were then selected for an additional independent validation via analysis of growth of ten-fold serially diluted cells on agar.

3.2.7 Computational analyses

To identify robust functional associations for the chemical genetic interactions that enhanced the hypersensitivity to atorvastatin, aggregated networks from two layers of interaction networks (GINs and PPINs) were generated and analysed for topology, centrality, communities (modules), pathway enrichment and drug signature enrichment. All of these analyses were described in detail in chapter 2 (Sections 2.2.8-2.2.12).

3.3 Results

3.3.1 Atorvastatin sensitivity is enhanced in DGAT but not in TGL strains

To construct the query strains that were used to investigate interactions with genes involved in lipotoxicity and metabolic syndrome, the *DGA1*, *LRO1*, *TGL3* and *TGL4* genes were replaced in three yeast genetic backgrounds with NATMX4, *LEU2* or *URA3* through PCR-directed mutagenesis and homologous recombination. The deletion strains *dga1*△ *lro1*△ (DGAT) and *tgl3*△ *tgl4*△ (TGL) were then treated with atorvastatin to characterise the toxicity of the drug in these deletion strains (Figure 3.3). Fitness defects were expected in both DGAT and TGL double deletion strains upon treatment with atorvastatin because atorvastatin treatment would impair the metabolism of sterols in these strains with already impaired triacylglyceride metabolism. The expected phenotypes were not the same, however, for DGAT and TGL strains, due to the abundance of lipid droplets, the storage units for triacylglycerides and steryl esters, in each of these strains (Kohlwein 2010; Kohlwein et al. 2013). Given the low number of lipid droplets in DGAT strains (usually from 0 to 1 per cell) and the abnormally large lipid droplets of TGL strains, I expected that atorvastatin would inhibit ergosterol synthesis and exacerbate the fitness defect of the DGAT strains compared to wild type, because the cells would not have enough storage of steryl esters to compensate for the lack of ergosterol. In the case of TGL, I expected minor changes in cell growth because TGL strains would have more storage capacity for steryl esters to compensate for the decreased synthesis of ergosterol. Indeed I observed decreased fitness of DGAT strains in the three genetic backgrounds and the fitness of TGL strains seemed to remain unchanged compared to wild type (Figure 3.3), implying that lipid droplets compensated for the reduced synthesis of ergosterol.

Notably, one phenotype I did not expect was that of the S288C strain. Double deletions in S288C were expected to be more sensitive to atorvastatin treatment than UWOPS87 and Y55 because the S288C wild type strain is naturally sensitive to atorvastatin whereas the UWOPS87 and Y55 wild types are naturally resistant to atorvastatin (Busby et al. 2019). While this was still the case for TGL strains, DGAT S288C strains were more resistant to atorvastatin than Y55 and UWOPS87, the latter being the most sensitive of all three. I conclude that UWOPS87 and Y55 may be more reliant on this pathway to cope with the stress of atorvastatin, but the molecular mechanism behind this increased resistance remains unknown.

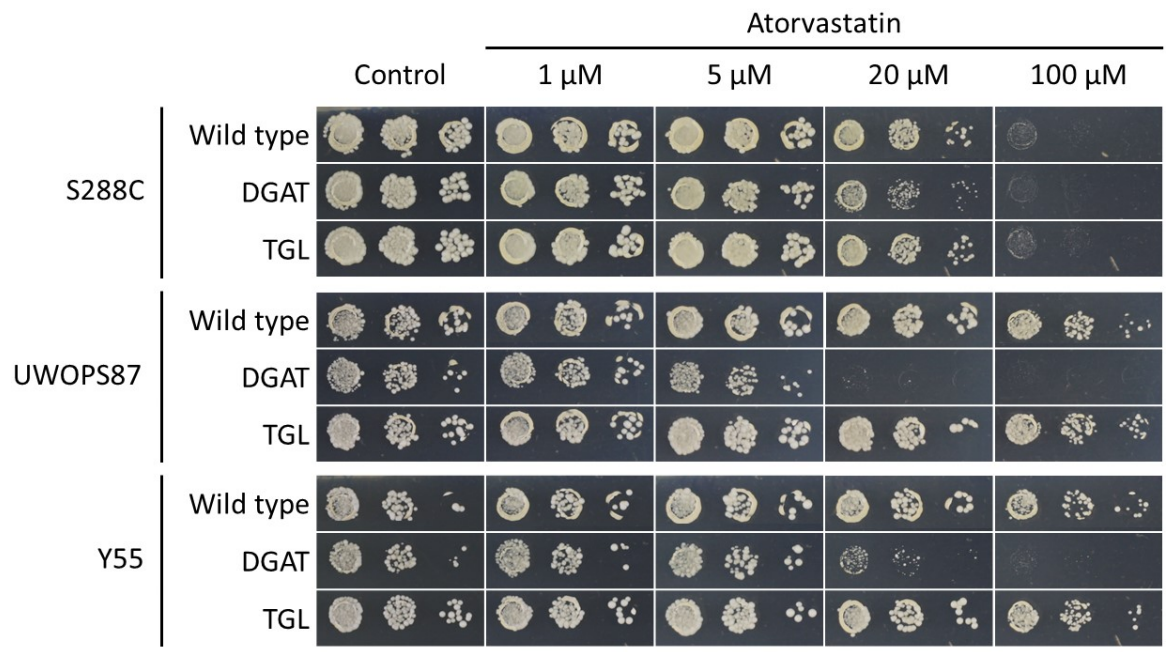

Figure 3.3: **Atorvastatin sensitivity is increased in DGAT strains compared to TGL strains.** Haploid cells deficient of DGAT (*dga1*Δ *lro1*Δ) or TGL (*tgl3*Δ *tgl4*Δ) in three genetic backgrounds (S288C, UWOPS87 and Y55) were pinned on increasing concentrations of atorvastatin in serial dilution and incubated for 2 days at 30°C.

3.3.2 Genome-wide analysis of DGAT and TGL synthetic sick/lethal interactions identifies genes buffering statin sensitivity in three genetic backgrounds

Via the generation and quantification of growth of triple deletion mutant libraries, SGA analyses reveal gene-gene interactions integral to drug mechanism of action (Kuzmin et al. 2018). To investigate atorvastatin-specific epistasis in the lipotoxic DGAT and metabolic syndrome TGL yeast models, genome-wide triple deletion libraries for the statin-susceptible (S288C) and the two statin-resistant strains (UWOPS87 and Y55) were constructed by integrating *dga1*Δ *lro1*Δ and *tgl3*Δ *tgl4*Δ into single deletion libraries in three genetic backgrounds using SGA technology (Figure 3.2A-B).

In order to detect growth defects due to synthetic sick/lethal interactions, IC_{30} concentrations of atorvastatin were determined for *dga1*Δ *lro1*Δ *xxx*Δ and *tgl3*Δ *tgl4*Δ *xxx*Δ libraries (Figure 3.4) upon trials with several concentrations ranging from 0.1 to 128 μM. All *dga1*Δ *lro1*Δ *xxx*Δ triple deletions were then screened at 9 μM atorvastatin for S288C, 10 μM for UWOPS87 and 35 μM for Y55; *tgl3*Δ *tgl4*Δ *xxx*Δ triple deletions were screened at 8 μM for S288C, 20 μM for UWOPS87 and 10 μM for Y55. Single deletion *xxx*Δ controls were screened as described in Chapter 2 (9 μM for S288C, 10 μM for UWOPS87 and 35 μM for Y55). All strains were screened in quadruplicate at the IC_{30} concentrations, which provided a 70% window to detect additional growth reduction due to

synthetic sick/lethal interactions.

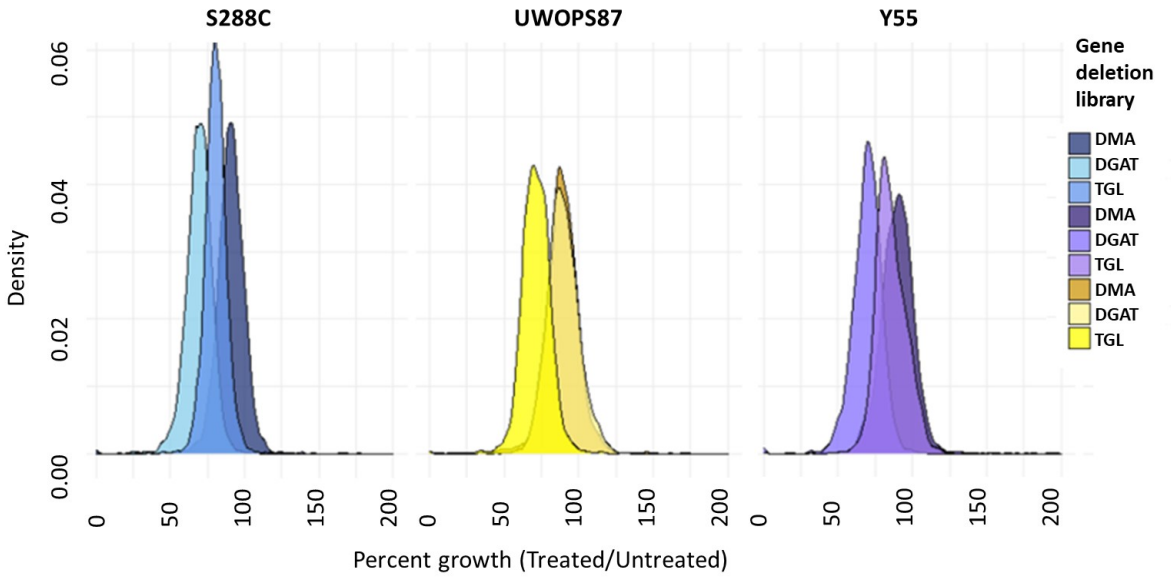

Figure 3.4: **Atorvastatin concentration for maximum overlap at 30% of growth inhibition between the single and triple deletions.** Growth of *xxx*Δ, DGAT (*dga1*Δ *lro1*Δ *xxx*Δ) and TGL (*tgl3*Δ *tgl4*Δ *xxx*Δ) libraries were screened in IC_{30} concentrations of atorvastatin. Density plots represent distribution of percent growth where higher density (y-axis) indicates more gene deletions having the corresponding percent growth in the x-axis.

The chemical genetic profiles of atorvastatin-treated strains were significantly different between the single and triple deletions based on the distribution of scored colony sizes where negative scores represent fitness defects (synthetic sick/lethal interactions) and positive values relate to increased fitness (suppressors) (Figure 3.5). The distribution of scored colony sizes differed among the three genetic backgrounds in DGAT strains (Figure 3.5 top panel), while in TGL strains it differed between S288C and Y55 and also between UWOPS87 and Y55 but not between S288C and UWOPS87 (Figure 3.5 bottom panel).

As discussed previously, high-throughput screening experiments tend to suffer from noisy data (*e.g.*, false positives) and thus it was necessary to validate the hypersensitive interactions identified in 1536-colony format. To aid validation I established a cut-off for the scored colonies (pixel-based colony size scored values assigned in SGAtools via Gitter (Wagih and Parts 2014)) of three standard deviations below the median. That way, genes with scores below -0.3 were considered hits for validation. Given my specific interest in epistatic interactions unique to the triple deletions, hits that were sensitive in single and triple deletion mutants were excluded from further analysis. For instance, the 13 interactions below the score cut-offs that overlapped between the DGAT triple deletions and the *xxx*Δ single deletions in S288C (Figure 3.5) were excluded from further analysis.

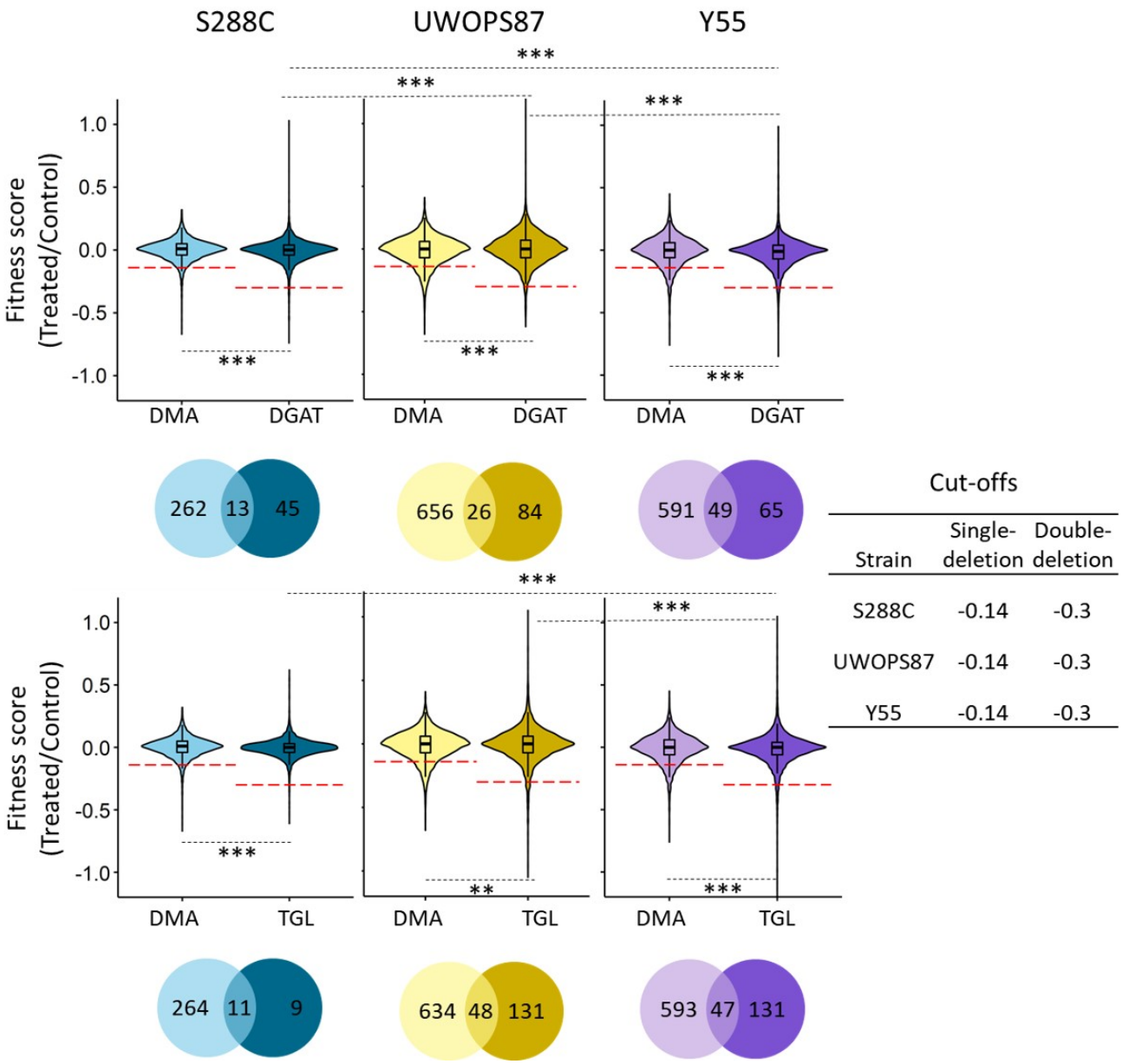

Figure 3.5: **The strength of synthetic sick/lethal interactions differs significantly in DGAT and TGL strains in three genetic backgrounds.** Violin plot distributions of average fitness of 12,900 strains as measured by colony sizes (n = 4) of *xxx*Δ and *dga1*Δ *lro1*Δ *xxx*Δ (upper panel) as well as *xxx*Δ and *tgl3*Δ *tgl4*Δ *xxx*Δ (lower panel) where positive scores represent increased fitness and negative scores represent decreased fitness. The red dashed lines indicate the score cut-off values selected for validation in independent assays for triple deletions that did not overlap with the *xxx*Δ single deletions. Venn diagrams visualise the overlap in the number of genes below the cut-off lines. Statistical differences were evaluated with a Student's *t*-test (*, $P < 0.05$; **, $P < 0.01$; ***, $P < 0.001$).

3.3.3 *Validation of atorvastatin-specific genetic interactions with DGAT strains in three genetic backgrounds*

Using the cut-off criteria in the SGA analysis, I selected to validate atorvastatin-specific growth defects in 45, 84 and 65 DGAT strains for S288C, UWOPS87 and Y55, respectively. To complement the high-throughput growth assay in 1536-colony format, growth of candidate DGAT strains was monitored in an independent assay where strains were grown individually as serial spot dilutions on agar (Figure 3.2C). Chemical genetic interactions conserved across the three genetic backgrounds provide insight into atorvastatin bioactivity in all individuals. One chemical genetic interaction with DGAT was apparent in the spot dilution assay (Figure 3.6). Atorvastatin treatment of the triple deletion *dga1*Δ *lro1*Δ *gyp1*Δ was synthetic lethal in S288C and synthetic sick in UWOPS87 and Y55. These growth defects were not observed in the single deletion *gyp1*Δ nor the double deletion queries *dga1*Δ *lro1*Δ in any genetic background. The conserved gene *GYP1* has a dual function as an activator of Ypt1 involved in the ER-to-Golgi step of the secretory pathway and the unfolded protein response (UPR), and also as an interactor of Atg8 involved in autophagy (Table 3.5). These results suggest that ER-to-Golgi vesicle transport, UPR and autophagy might be buffers of lipotoxicity upon treatment with atorvastatin.

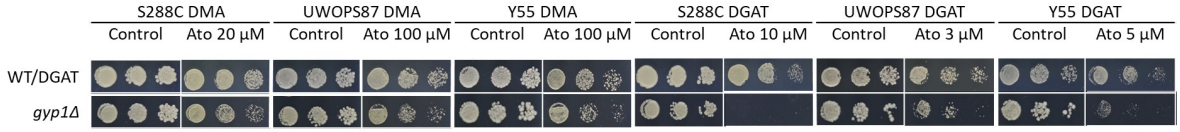

Figure 3.6: **The triple deletion *dga1*Δ *lro1*Δ *gyp1*Δ was hypersensitive to atorvastatin in three genetic backgrounds.** Haploid cells derived from SGA analyses and DMA libraries were pinned on SC with or without atorvastatin (Ato) in serial dilution and incubated for 2 days at 30°C. WT/DGAT refers to either the non-mutated wild types for the *xxx*Δ strain panels or the *dga1*Δ *lro1*Δ double deletion for the *dga1*Δ *lro1*Δ *xxx*Δ strain panels

ORF	Gene	Name	Description	Human orthologue(s)
YOR070C	*GYP1*	GTPase-activating protein for YPt1p	Cis-golgi GTPase-activating protein for Rabs involved in vesicle docking and fusion; interacts with autophagosome component Atg8p	TBC1D22A, TBC1D22B

Table 3.5: **The validated hit that overlapped in three genetic backgrounds, *GYP1*, is a conserved GTPase-activating protein.** Description was obtained from SGD (Cherry et al. 2012). Human orthologues were obtained from YeastMine (Balakrishnan et al. 2012).

Because chemical genetic interactions mediating the drug response to atorvastatin are known to be unique to individuals (Busby et al. 2019), I expected to detect epistatic interactions that were unique to each genetic background. Indeed, three chemical genetic interactions (*COG8, RUD3 and VPS72*)

were unique to S288C, four chemical genetic interactions (*ERV25, MCP2, TMA7 and YLR279W*) were unique to UWOPS87, and four chemical genetic interactions (*COQ10, MDM38, SHE4 and SHR5*) were unique to Y55 (Figure 3.7; Table 3.6), emphasising the genetic complexity of drug response.

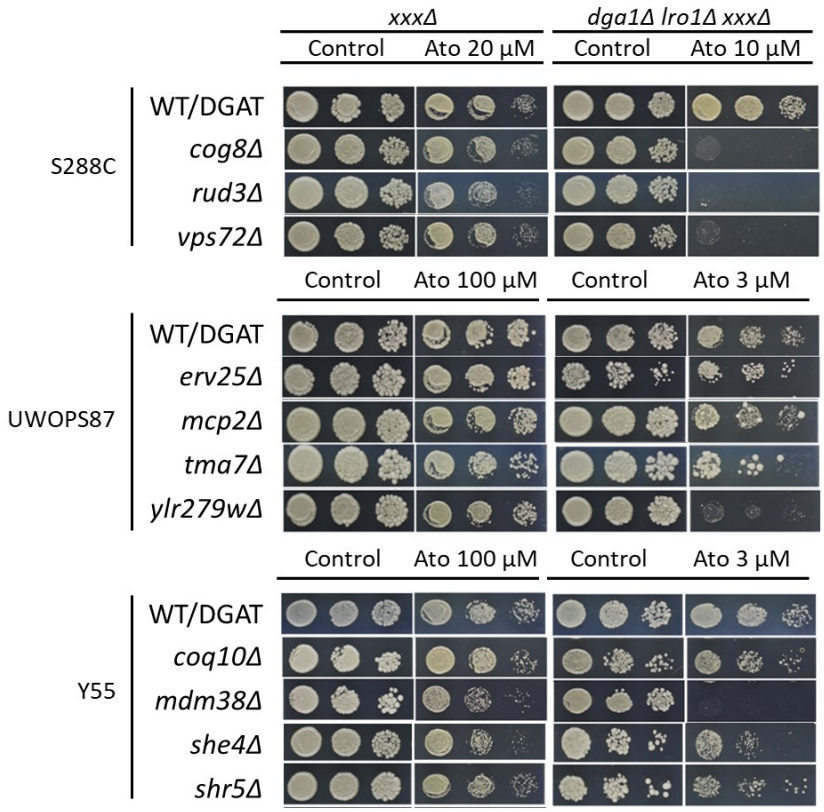

Figure 3.7: **Epistatic DGAT interactions depend on the genetic background.** Haploid cells derived from SGA analyses and DMA libraries were pinned on SC with or without atorvastatin (Ato) in serial dilution and incubated for 2 days at 30°C. WT/DGAT refers to either the non-mutated wild types for the *xxx*Δ strain panels or the *dga1*Δ *lro1*Δ double deletion for the *dga1*Δ *lro1*Δ *xxx*Δ strain panels.

Genetic background	Validated hypersensitive interactions
S288C	*COG8, RUD3, VPS72,* ***GYP1***
UWOPS87	*ERV25, MCP2, TMA7, YLR279W,* ***GYP1***
Y55	*COQ10, MDM38, SHE4, SHR5,* ***GYP1***

Table 3.6: **List of validated *dga1*Δ *lro1*Δ *xxx*Δ triple deletion strains in each of three yeast genetic backgrounds.** Interaction overlapping in three genetic backgrounds is shown in bold.

Consistently with my findings from the previous chapter, there were chemical genetic interactions that did not overlap between genetic backgrounds, but nonetheless have similar functions, indicating that the chemical genetic interactions are not conserved but the cellular coping mechanisms are conserved (Table 3.7). For instance, both *COG8* and *RUD3* (epistatic in S288C) and *ERV25* (epistatic in UWOPS87) participate in Golgi vesicle transport. Additionally *MCP2* (epistatic in UWOPS87) is

Background	ORF	Gene	Name	Description	Human orthologue(s)
S288C	YML071C	*COG8*	Conserved Oligomeric Golgi complex	Component of the oligomeric Golgi complex that mediates fusion of transport vesicles to Golgi compartments	COG8
	YOR216C	*RUD3*	Relieves Uso1-1 transport Defect	Golgi matrix protein involved in the structural organization of the cis-Golgi; interacts genetically with *COG3* and *USO1*	TRIP11
	YDR485C	*VPS72*	Vacuolar Protein Sorting	Htz1p-binding component of the SWR1 complex; required for vacuolar protein sorting	VPS72
UWOP87	YML012W	*ERV25*	ER Vesicle	Member of the p24 family involved in ER to Golgi transport; role in misfolded protein quality control	TMED10
	YLR253W	*MCP2*	Mdm10 Complementing Protein	Mitochondrial protein of unknown function involved in lipid homeostasis; interacts genetically with *MDM10*, and other members of the ERMES complex	ADCK1, ADCK5
	YLR262C-A	*TMA7*	Translation Machinery Associated	Protein of unknown that associates with ribosomes; protein abundance increases in response to DNA replication stress	TMA7
	YLR279W	YLR279W	Dubious open reading frame	Dubious open reading frame; unlikely to encode a functional protein, based on available experimental and comparative sequence data	None
Y55	YOL008W	*COQ10*	COenzyme Q	Coenzyme Q (ubiquinone) binding protein; functions in the delivery of Q6 to its proper location for electron transport during respiration	COQ10A, COQ10AB
	YOL027C	*MDM38*	Mitochondrial Distribution and Morphology	Membrane-associated mitochondrial ribosome receptor; involved in the insertion of newly synthesized proteins into the mitochondrial inner membrane; role in protein export and K+/H+ exchange	LETM1, LETM2
	YOR035C	*SHE4*	Swi5p-dependent HO Expression	Protein containing a UCS domain; binds to myosin motor domains to regulate myosin function; involved in endocytosis, polarization of the actin cytoskeleton	STIP1
	YOL110W	*SHR5*	Suppressor of Hyperactive Ras	Palmitoyltransferase subunit; this complex adds a palmitoyl lipid moiety to Ras2p (and Ras1p) required for Ras2p membrane localization	GOLGA7, GOLGA7B

Table 3.7: **Human orthologues of genes interacting with *DGA1* and *LRO1* that are not conserved in all three genetic backgrounds.** Description was obtained from SGD (Cherry et al. 2012). Human orthologues were obtained from YeastMine (Balakrishnan et al. 2012).

an interactor of *MDM10*, while the latter and *MDM38* (epistatic in Y55) participate in mitophagy. The aforementioned genes are conserved in humans (Table 3.7), pointing to concise experiments that could be done in the future in human cells.

3.3.4 Validation of atorvastatin-specific genetic interactions with TGL strains in three genetic backgrounds

Using the cut-off criteria in the high-throughput screen, I selected to validate atorvastatin-specific growth defects in 9, 131, and 131 *tgl3*△ *tgl4*△ *xxx*△ strains for S288C, UWOPS87 and Y55, respectively. To complement the high-throughput growth assay in 1536-colony format, growth of candidate TGL strains was monitored in an independent assay where strains were grown individually as serial spot dilutions on agar (Figure 3.2C). Validation of TGL strains revealed that most TGL triple deletions showed the same phenotype as the single *xxx*△ deletions upon treatment with the same concentration of atorvastatin. Only *yor1*△ in S288C showed a clear atorvastatin-specific epistatic interaction with the TGL strain that was distinct from the single deletion (Figure 3.8). *YOR1* is an ATP-binding cassette (ABC) transporter of drugs (Table 3.8). The *tgl3*△ *tgl4*△ *yor1*△ strain was similar to the *yor1*△ single deletion in Y55. Interestingly, deletion of *YOR1* seemed to rescue lethality of the TGL strain in UWOPS87, implying a distinct role for this gene in UWOPS87. For S288C and Y55, *YOR1* buffers atorvastatin toxicity in the TGL strain, which is not surprising given that it mediates drug efflux. For UWOPS87, however, deletion of *YOR1* prevents atorvastatin toxicity in the TGL strain, emphasising that chemical genetic interactions depend on genetic background.

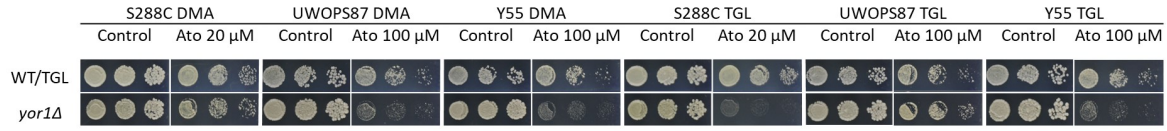

Figure 3.8: **The triple deletion *tgl3*△ *tgl4*△ *yor1*△ was hypersensitive to atorvastatin treatment in S288C and Y55 but not in UWOPS87.** Haploid cells derived from SGA analyses and DMA libraries were pinned on SC with or without atorvastatin (Ato) in serial dilution and incubated for 2 days at 30°C.

ORF	Gene	Name	Description	Human Orthologue(s)
YGR281W	*YOR1*	Yeast Oligomycin Resistance	Plasma membrane ATP-binding cassette (ABC) transporter; multidrug transporter mediates export of many organic anions	CFTR, ABCC4

Table 3.8: **The only validated epistatic interaction in S288C was *YOR1*, a conserved ABC transporter.** Description was obtained from SGD (Cherry et al. 2012). Human orthologues were obtained from YeastMine (Balakrishnan et al. 2012).

3.3.5 *Multi-layer network analysis enhances connectivity of networks*

Similar to a single-layer network, albeit just more complex, aggregated networks are basically n-dimensional matrices or tensors that can be investigated using mathematical methodologies. As explained in Chapter 2, the first layer was derived from the GINs, the second layer derived from the PPINs, and the aggregated network was derived from both the GINs and PPINs (Figures 3.2D and 3.9). These networks were created only for the validated DGAT interactions (Table 3.6) since not enough TGL strains validated to perform further analyses. Most nodes and hence most interactions were not shared between GINs and PPINs (Figure 3.9). The aggregated network for S288C comprised 244 nodes and 2767 edges (interactions), as opposed to the GIN (107 nodes, 1961 edges) and PPIN (182 nodes, 920 edges) alone. For UWOPS87, the aggregated network had 220 nodes and 989 edges (GIN = 108 nodes, 574 edges; PPIN = 124 nodes, 439 edges), while Y55 had 214 nodes and 1067 edges (GIN = 108 nodes, 795 edges; PPIN = 124 nodes, 357 edges).

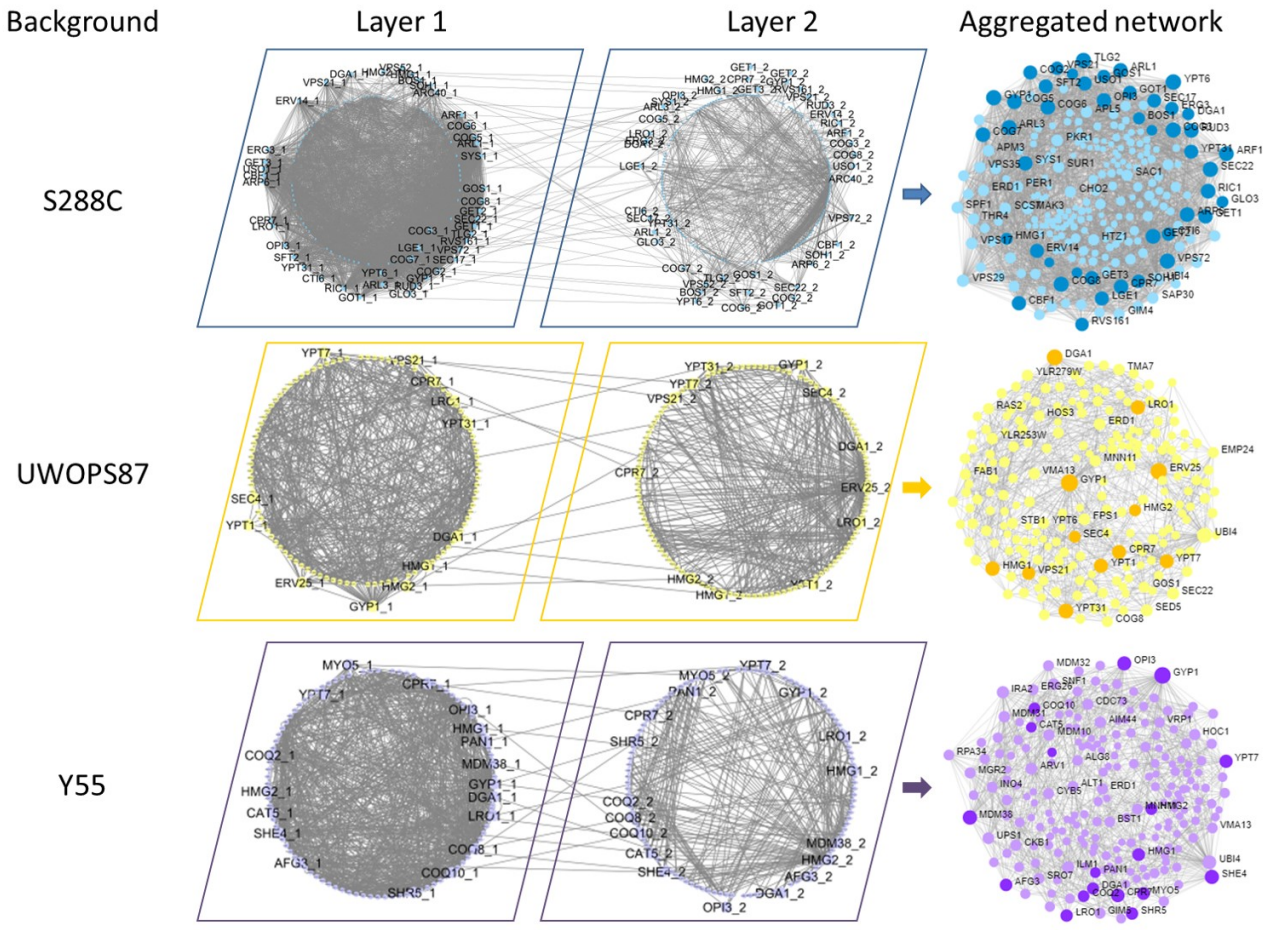

Figure 3.9: **Multi-layer networks derived from atorvastatin-sensitive *dga1*△ *lro1*△ *xxx*△ interactions.** GINs (Layer 1), PPINs (Layer 2) and the edges between them were integrated in an aggregated network using TimeNexus. Edges between layers connect overlapping nodes in the two layers and the genes linking these edges are shown in the periphery of circular networks. Darker nodes in aggregated networks are validated hits.

3.3.6 Network centrality analyses identify potential bottleneck genes buffering DGAT-specific atorvastatin toxicity

To obtain functional insight into the aggregated networks, three measurements of centrality (degree (deg), closeness (close) and betweenness (bet)) were obtained for every gene in each aggregated network (Figures 3.2E and 3.10). Relative to the centrality values for *UBI4* (bet = 0.15, close = 0.54, deg = 64 in S288C, bet = 0.22, close = 0.52, deg = 58 in UWOPS87, bet = 0.24, close = 0.50, deg = 61 in Y55), there were other genes with more highly ranked centrality values; thus *UBI4* was not excluded from the 3D plots as it was in Chapter 2. Remarkably, *GYP1*, the only chemical genetic interaction that was validated across three genetic backgrounds (Figure 3.6), was a top-ranked gene across all genetic backgrounds and all centrality analyses (bet = 0.05 (4th overall), close = 0.53 (11th overall), deg = 77 (2nd overall) in S288C, bet = 0.22 (2nd overall), close = 0.53 (1st overall), deg = 58 (1st overall) in UWOPS87, bet = 0.28 (1st overall), close = 0.53 (1st overall), deg = 72 in Y55 (1st overall)) (Figure 3.10). These results emphasise the importance of *GYP1* to buffer atorvastatin-induced lipotoxicity.

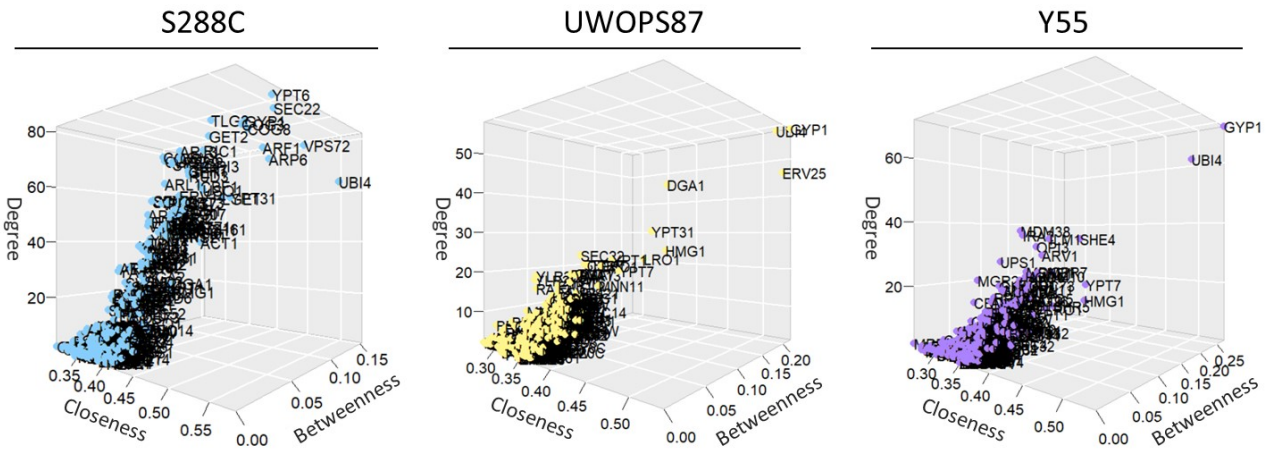

Figure 3.10: **Network topology centrality analyses of aggregated networks identify key DGAT interactors for atorvastatin sensitivity.** Centrality measurements (degree, closeness and betweenness) were calculated for each gene and visualised in a 3D plot.

Betweenness centrality is arguably the most meaningful measurement of centrality because it distinguishes bottleneck genes required for the integrity of networks (Brandes 2001; Freeman 1977; Girvan and Newman 2002; Yu et al. 2007). To identify the bottleneck genes, I generated individual networks for the genes ranked in the top ten betweenness, closeness and degree centralities (Figure 3.11).

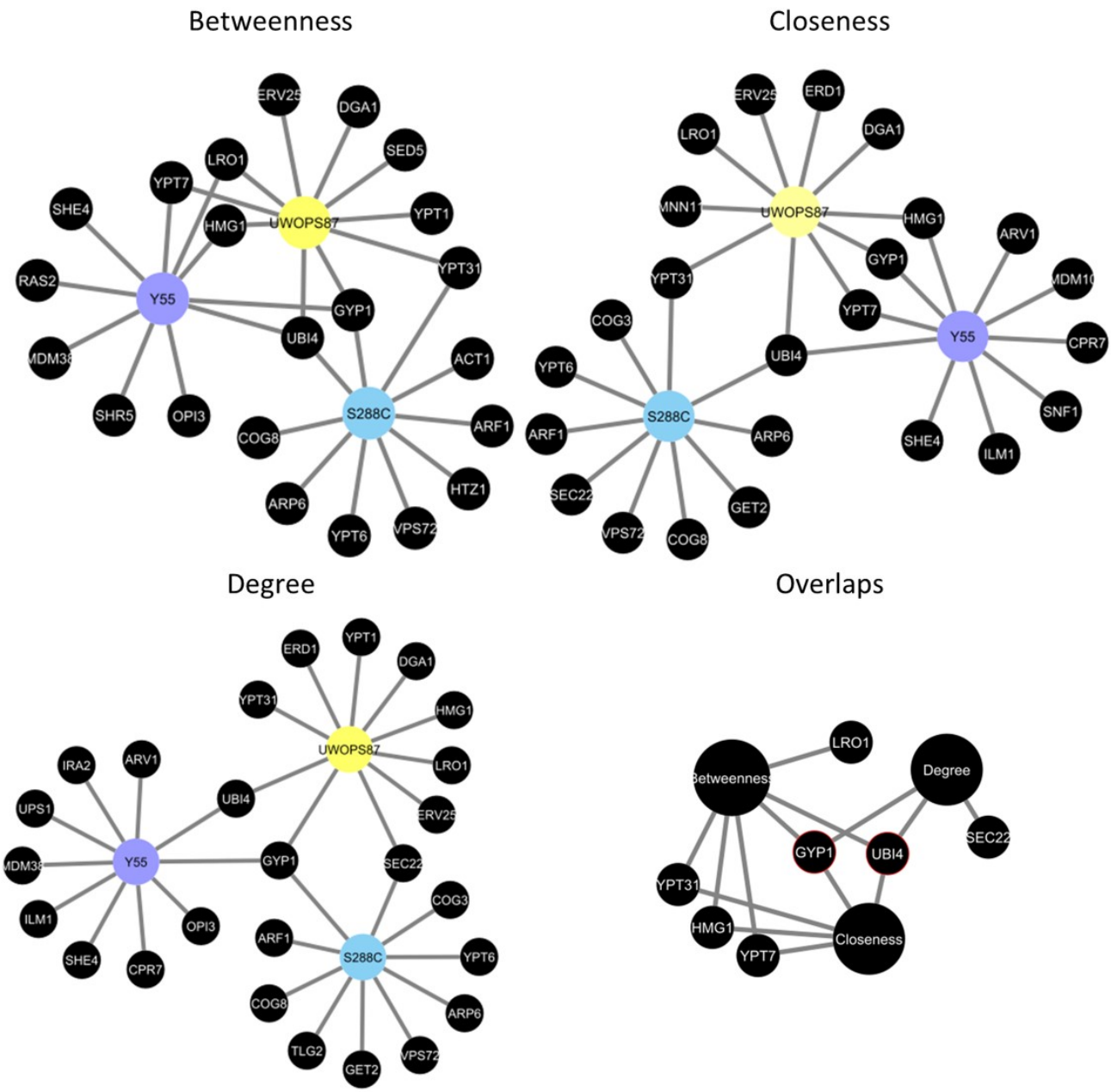

Figure 3.11: **Network centrality of genes behind hypersensitivity to atorvastatin for DGAT interactors overlap in three genetic backgrounds.** Genes that ranked in the top ten centrality measurements were found to confirm phenotypic findings. Centrality measurements (betweeness, closeness and degree) were calculated in NetworkAnalyzer app in Cytoscape (Boccaletti et al. 2014) and networks were built in Cytoscape. The red outline points to highly central hub/bottleneck genes.

GYP1 and *UBI4* are bottlenecks and hub genes in three genetic backgrounds. The target of statins *HMG1* (bet = 0.02, close = 0.47, deg = 25 in S288C, bet = 0.07, close = 0.48, deg = 26 in UWOPS87, bet = 0.05, close = 0.48, deg = 20 in Y55), one of the two query gene deletions *LRO1* (bet = 0.01, close = 0.44, deg = 15 in S288C, bet = 0.06, close = 0.46, deg = 24 in UWOPS87, bet = 0.04, close = 0.44, deg = 17 in Y55) and the *GYP1* closely related gene *YPT7* (bet = 0.00, close = 0.42, deg = 10 in S288C, bet = 0.03, close = 0.46, deg = 22 in UWOPS87, bet = 0.05, close = 0.48, deg = 24 in

Y55) were high betweenness genes overlapping in UWOPS87 and Y55. The *GYP1* closely related gene *YPT31* (bet = 0.03, close = 0.53, deg = 53 in S288C, bet = 0.05, close = 0.48, deg = 30 in UWOPS87, bet = 0.01, close = 0.43, deg = 12 in Y55) was a high betweenness gene overlapping in S288C and UWOPS87. To determine whether top network central genes were distinct to the DGAT strains, I compared the overlaps panel of DGAT against those of *HMG1* (the target of statins) retrieved from Chapter 2 confirming that the top overlapping centralities were distinct for each of these queries (Figure 3.12).

These results indicate that targeting *GYP1* is a means to inhibit the diabetogenic effect of atorvastatin, although it would likely cause other cellular disturbances that might become too toxic for the cells. Inhibition of less central genes that interact with *GYP1* could be a 'tunable' and less toxic intervention. For instance, the R-SNARE protein *SEC22* (bet = 0.03, close = 0.58, deg = 76 in S288C, bet = 0.02, close = 0.41, deg = 25 in UWOPS87, no data for Y55 as this gene was not required for network connectivity) or the Rab GTPases *YPT7* and *YPT31* mentioned above are candidate targets to indirectly modify *GYP1* since they all act in the secretory pathway (Figure 3.13).

3.3.7 Community analysis identifies functional modules in aggregated networks for three genetic backgrounds

To gain more insight into the structural organisation of the aggregated networks, the networks were partitioned through community analysis (Figure 3.2F). In this analysis, 3-5 communities (modules) were detected in each network with significant enrichment ($P < 0.05$) for metabolic pathways, and in most cases, pathways enriched in these modules did not overlap in all three genetic backgrounds (Figure 3.14). However, in good agreement with the experimentally validated fitness defect of *dga1*Δ *lro1*Δ *gyp1*Δ and network centrality analyses that distinguished *GYP1* (bet = 0.05 (4^{th} overall), close = 0.53 (11^{th} overall), deg = 77 (2^{nd} overall) in S288C, bet = 0.22 (2^{nd} overall), close = 0.53 (1^{st} overall), deg = 58 (1^{st} overall) in UWOPS87, bet = 0.28 (1^{st} overall), close = 0.53 (1^{st} overall), deg = 72 in Y55 (1^{st} overall)), UPR (found as the KEGG category named 'Protein processing in endoplasmic reticulum') and autophagy pathways that include *GYP1* were enriched, overlapping in three genetic backgrounds. Furthermore, endocytosis, phagosome and SNARE interactions in vesicular transport identified in the previous section also showed enrichment in the community analysis in three genetic backgrounds, thus providing additional support for the involvement of the secretory pathway proposed in Figure 3.13. It is noteworthy that these are specific pathways (*i.e.*, not generic such as transport), thus pointing to their increased significance.

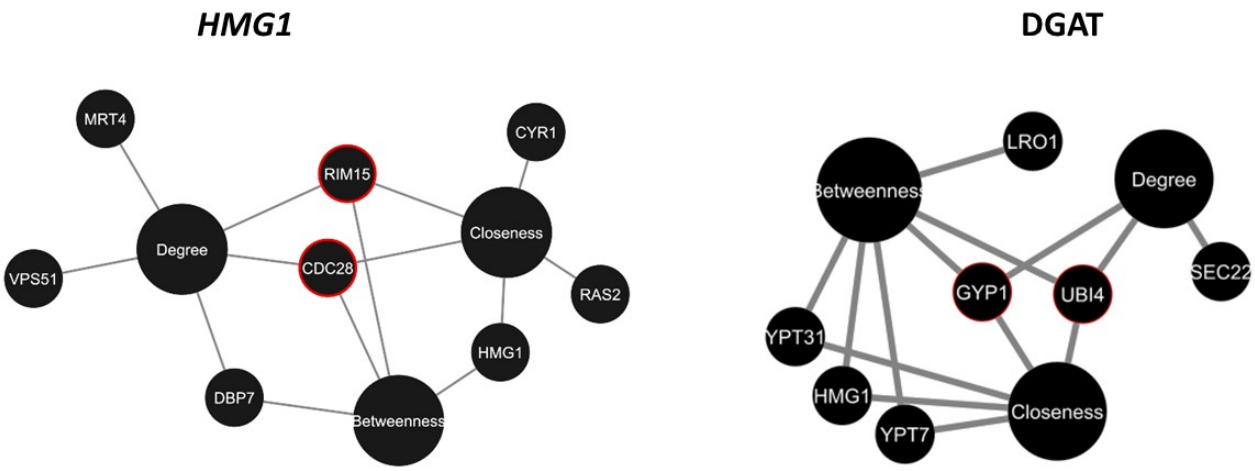

Figure 3.12: **Network central genes mediating hypersensitivity to atorvastatin for DGAT and the atorvastatin target *HMG1* are distinct.** Genes that ranked in the top ten centrality measurements and overlapped in three genetic backgrounds are shown for *HMG1* (left panel) vs DGAT (right panel). Centrality measurements (betweeness, closeness and degree) were calculated in NetworkAnalyzer app in Cytoscape (Boccaletti et al. 2014) and networks were built in Cytoscape. The red outline points to highly central hub/bottleneck genes.

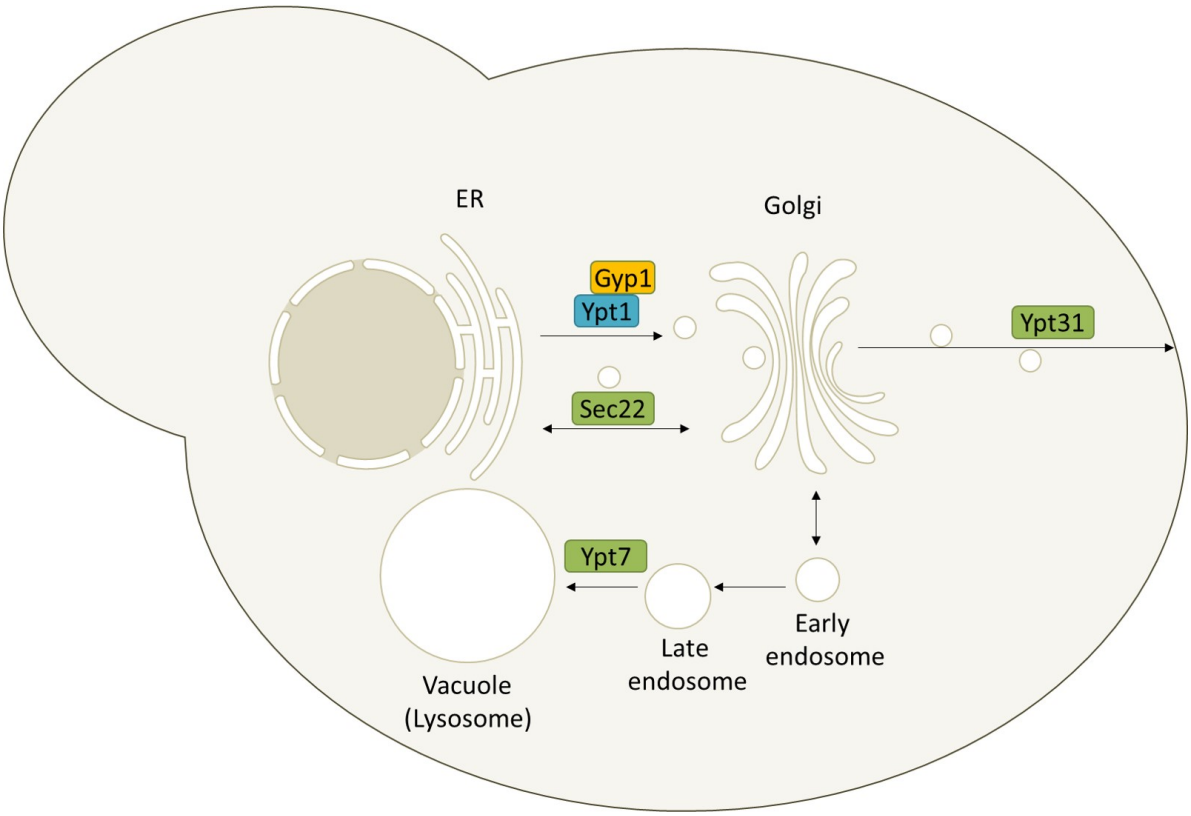

Figure 3.13: **Targeting genes in the secretory pathway other than *GYP1* may decrease the atorvastatin-induced toxicity in lipodystrophic DGAT cells.** The Gyp1 protein activates Ypt1 involved in the ER-to-Golgi step of the secretory pathway. Other proteins coded by genes identified through centrality analyses in this study (*YPT31*, *SEC22* and *YPT7*) participate in other steps of this pathway and are thus candidate targets to decrease atorvastatin-induced toxicity in lipodystrophic DGAT cells.

Two metabolic pathways that were not identified in the previous sections were the glycerophospholipid metabolism pathway and the terpenoid backbone synthesis pathway (or yeast mevalonate pathway), the former serving as proof of concept for DGAT strains and the latter serving as a proof of concept for atorvastatin. The glycerophospholipid metabolism pathway was represented by different genes in different backgrounds (*GPT2, TGL5, SPO14, PCT1, OPI3* and *CHO2* for S288C; *GPT2, DGK1* and *PGC1* for UWOPS87; and *GPT2, SPO14, PCT1, OPI3, GEP4* and *CRD1* for Y55). Only *OPI3* was a top central gene and that was for Y55 only. The rest of these genes were not ranked in the top ten central nodes nor were validated genes, emphasising the utility of this type of analysis as it may uncover otherwise ignored metabolic pathways.

As expected, there were some categories that were unique to one or two but not all genetic backgrounds (Figure 3.14), highlighting the uniqueness of genetic interactions mediating the response to atorvastatin. The signalling pathway known as AGE-RAGE signalling pathway in diabetes, which has a role in the activation of numerous other signalling pathways (including MAPK signalling pathways that were also enriched for UWOPS87), was enriched in UWOPS87 and Y55 but not in S288C. Some of the signalling pathways activated via this pathway have links to diabetic complications via a role in cell proliferation and apoptosis. This fits well with the enrichment of *N*-glycan biosynthesis for UWOPS87 and Y55, implicating glycation pathways as potential contributors for the increased DGAT-specific sensitivity to atorvastatin of these strains compared to S288C (Figure 3.3). Furthermore, two metabolic pathways were unique to S288C; these were basal transcription factors represented by *TAF14* and *SPT15* and inositol phosphate metabolism pathways represented by *FAB1* and *SAC1*. These results implicate these genes and their associated pathways as potential mediators of the increased resistance of S288C DGAT strain to atorvastatin compared to UWOPS87 and Y55 (Figure 3.3).

Regarding the DGAT UWOPS87 genetic background most sensitive to atorvastatin, there were distinct enrichments for glycerolpid metabolism (represented by genes *YJU3*, *LRO1*, *DGA1* and *PAH1*) and glycosylphosphatidylinositol (GPI)-anchor biosynthesis (represented by genes *LAS21*, *BTS1*, *GPI10* and *MCD4*). These specific enrichments to UWOPS87 indicate that the GPI-anchor, a glycolipid structure that anchors proteins to the cell surface, is perhaps crucial to cope with the atorvastatin-induced lipotoxicity in this genetic background.

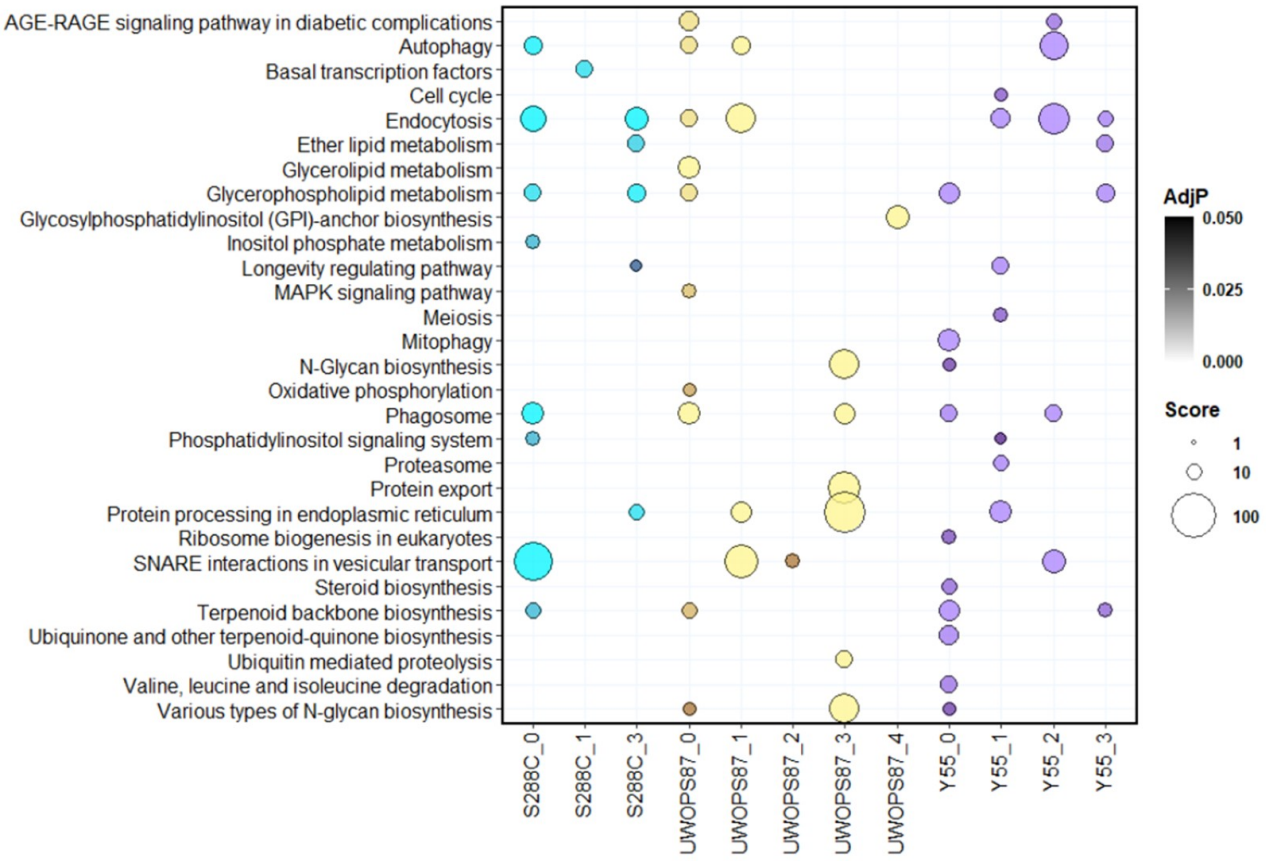

Figure 3.14: **Metabolic pathway enrichment of modules in aggregated networks for atorvastatin sensitivity.** Bubble plots showing enrichment for each of the modules (named for their genetic background) identified through community analysis for DGAT interactions. The size of the bubbles is relative to the enrichment score for each pathway, while the intensity of the colours is relative to the adjusted *P* value. The x axis labels show the genetic background followed by the number of modules. Numbers missing in the sequence are modules without significantly enriched pathways.

3.3.8 Humanised enrichment analysis identifies drugs that may decrease the diabetogenic activity of statins

Combination therapies increase efficacy of repurposed drugs (Sun et al. 2016). Therefore, I identified the human orthologues of experimentally validated genes as well as key centrality genes identified in my yeast genomic analyses (Table 3.9) and evaluated these genes for enrichment in the Drug Signature Database (Yoo et al. 2015) (Figure 3.2G). A total of 583 drugs/compounds were identified, of which 41 were statistically significant ($P < 0.05$) with odds ratios ranging from 2-39. To compare the chemical genetic profiles of the top-ranked drugs/compounds, the odds ratio values for the top 20 drugs/compounds and their signature genes were visualised in a bubble plot (Figure 3.15). The 20 drugs/compounds identified were generally correlated with genes involved in the secretory pathway, mainly Rab GTPases and other genes involved in vesicular transport. Four drugs were correlated

with the biosynthesis of ubiquinone (chlorzoxazone, cimetidinde, glibenclamide and digoxin). Nine drugs/compounds (metronidazole, minoxidil, chlorzoxazone, cadmium sulfate, AC1L1FUW, hydrogen peroxide, glibenclamide, geldanamycin and pioglitazone) were correlated with lipid metabolism genes (ADCK1, HMGCR, DGAT2 and LCAT). Notably, DGAT2 is the orthologue of the *DGA1* query and LCAT is the orthologue of the *LRO1* query, while *HMGCR* is the orthologue of *HMG1* that was identified as a key centrality gene in the yeast DGAT network.

Yeast gene	**Human orthologue**	**Yeast gene**	**Human orthologue**	**Yeast gene**	**Human orthologue**
COG8	COG8	*MCP2*	ADCK5	*YPT31*	RAB2B
COQ10	COQ10A	*MDM38*	LETM1	*YPT31*	RAB30
COQ10	COQ10B	*MDM38*	LETM2	*YPT31*	RAB39A
DGA1	AWAT1	*RUD3*	TRIP11	*YPT31*	RAB39B
DGA1	AWAT2	*SEC22*	SEC22A	*YPT31*	RAB43
DGA1	DGAT2	*SEC22*	SEC22B	*YPT31*	RAB4A
DGA1	DGAT2L6	*SEC22*	SEC22C	*YPT31*	RAB4B
DGA1	DGAT2L7P	*SHE4*	STIP1	*YPT31*	RAB4B-EGLN2
DGA1	MOGAT1	*SHR5*	GOLGA7	*YPT7*	RAB29
DGA1	MOGAT2	*SHR5*	GOLGA7B	*YPT7*	RAB32
DGA1	MOGAT3	*TMA7*	TMA7	*YPT7*	RAB38
ERV25	TMED10	*VPS72*	VPS72	*YPT7*	RAB7A
GYP1	TBC1D21	*YPT31*	RAB11A	*YPT7*	RAB7B
GYP1	TBC1D22A	*YPT31*	RAB11B	*YPT7*	RAB9B
GYP1	TBC1D22B	*YPT31*	RAB14	*YPT7*	RABL2A
HMG1	HMGCR	*YPT31*	RAB19	*YPT7*	RABL2B
LRO1	LCAT	*YPT31*	RAB25		
MCP2	ADCK1	*YPT31*	RAB2A		

Table 3.9: **Human orthologues of validated interactors and key network centrality genes used as input for enrichment analysis in Drug Signature Database.** Human orthologues were obtained from YeastMine (Balakrishnan et al. 2012). Yeast gene column comprises all validated hits, main bottleneck genes and query genes.

Two of the top 20 drugs/compounds retrieved from this search (glibenclamide and pioglitazone) are approved and established drugs for the treatment of diabetes (Figure 3.15; Table 3.10). I considered these a proof of concept that the yeast model and analyses performed in this study revealed candidate combination therapies to lessen the diabetogenic effect of atorvastatin. A combination therapy of atorvastatin and pioglitazone, has in fact been trialled (NCT00770575) to improve the outcome of atorvastatin in treating patients with elevated risk for cardiovascular disease, indicating the combination might be a safe and effective combinatorial treatment to potentiate their efficacy while reducing health risks.

The drug metronidazole ranked the highest of all drugs and compounds, which was correlated with several genes involved in the secretory pathway and lipid homeostasis (Figure 3.15). Metronidazole

is an approved drug used as an antibiotic and antiparasitic (Table 3.10), and although it has been trialled to treat periodontitis in diabetic patients there are no other clinical trials relevant to the context described in this chapter nor have any antidiabetic effects been reported for this drug. However, other interesting drugs/compounds found in this search, bafilomycin and niclosamide that are antibiotic and anthelmintic, respectively, have been reported for the potential to improve insulin secretion and treat diabetes. Interestingly, both bafilomycin and niclosamide are reported to have anticancer activity, which makes them strong candidates for combination therapies with atorvastatin to test in cell models of cancer and diabetes to evaluate enhancing its anticancer activity while reducing its diabetogenic effect.

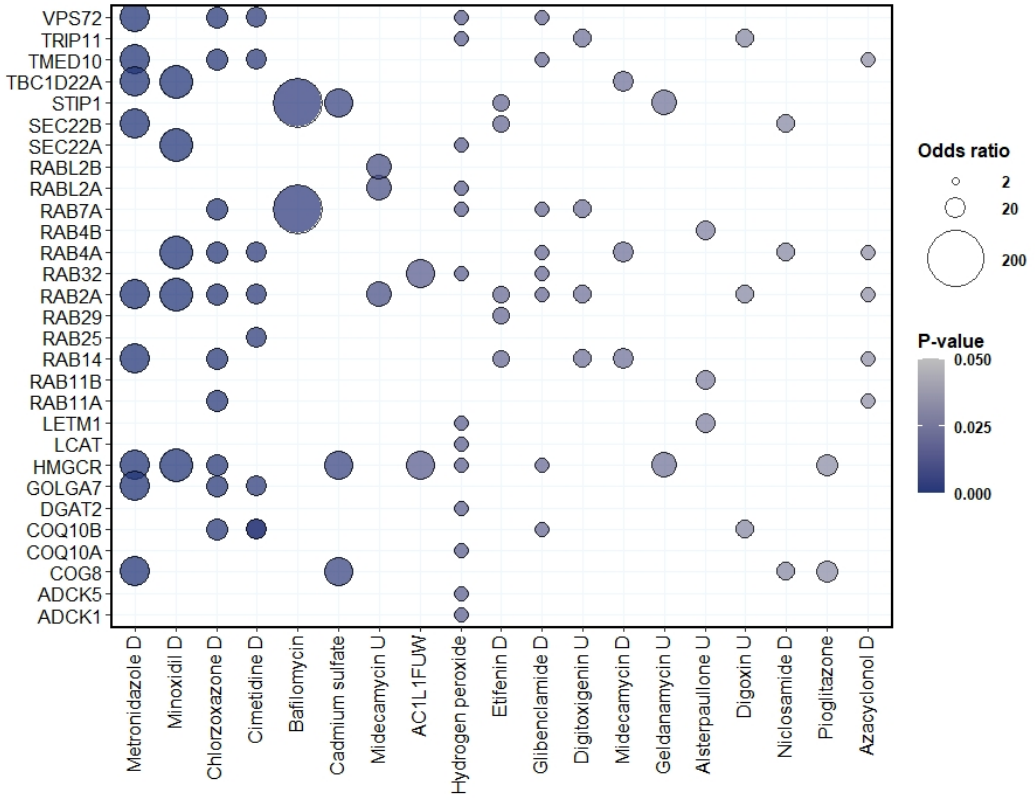

Figure 3.15: **Human orthologues of hits/bottleneck yeast genes reveal drugs/compounds to test for synergy with atorvastatin.** Human orthologues of validated genes and genes identified through centrality analyses were processed via an enrichment analysis for signature genes in the Drug Signature Database. Bubble plot representing the human orthologues (y-axis) that were enriched for drugs/compounds (x-axis). The colour of each bubble is determined by the *P*-value and the size of bubble reflects the odds ratio, where bigger bubbles represent greater enrichment.

Drug/compound	Description	Approved	Intended use	Diabetes-related clinical trials relevant to this study	Statin-related clinical trials relevant to this study
Metronidazole	Synthetic nitroimidazole	Yes	Antibiotic, antiparasitic	No	No
Minoxidil	Vasodilator	Yes	Hair growth stimulation and hypertension	No	No
Chlorzoxazone	Sedative and centrally-acting muscle relaxant	Yes	Painful muscle spasm	No	No
2,3-diformyloxy-propyl formate	IUPAC name for Triglyceride	NA	NA	NA	NA
Cimetidine	Histamine H(2)-receptor antagonist and P450 inhibitor	Yes	Acid-peptic disease and heartburn and has anticancer properties	No	No
Bafilomycin	A family of toxic macrolide antibiotics, inhibitors V-ATPase	No	Antibiotics, potential improved insulin secretion and antiancer activity	No	No
Cadmium sulfate	Inorganic compound, toxic and carcinogen	NA	NA	NA	NA
Midecamycin	Naturally occurring macrolide	No	Antibiotics	No	No
AC1L1FUW	7-[3-(4-fluorophenyl)-1-propan-2-ylindol-2-yl]-3,5-dihydroxyhept-6-enoic acid	No	NA	NA	NA
Glibenclamide	Sulfonamide urea derivative with antihyperglycemic activity	Yes	Diabetes	No	No
Etifenin	Diagnostic radiopharmaceutical for the liver function assessment	No	Diagnostic	No	No
Digitoxigenin	A 3beta-hydroxy steroid and a 14beta-hydroxy steroid	No	Anticancer neoadjuvant Clinical trial	No	No
Geldanamycin	Benzoquinone , inhibits HSP90 promoting proteasomal degradation of oncogenic signaling proteins	No	Antineoplastic antibiotic	No	No
Alsterpaullone	Kinase inhibitor	No	Antineoplastic agent, apoptosis inducer and anti-HIV-1 agent	No	No
Digoxin	Cardiac glycoside, inhibits the sodium potassium ATP pump	Yes	Heart conditions, potential for anticancer	No	No
Niclosamide	Induces degradation of the androgen receptor variant V7 through the proteasome-mediated pathway	Yes	Antihelmintic, potential antineoplasic activity and potential improved diabetes	Yes	No
Pioglitazone	Activates peroxisome PPAR-gamma, modulates the transcription of insulin-responsive genes	Yes	Antidiabetic and potential antineoplastic activity	NA	Yes
Azacyclonol	Ataractive, diminished hallucinations	No	Psychiatric disorders	No	No
Hydrogen peroxide	Oxidizing agent	Yes	Disinfectant, antiviral and anti-bacterial activities	No	No

Table 3.10: **Some of the top 20 drugs that share signature genes with atorvastatin have antidiabetic activity but have not been investigated for synergy with statins.** Description and intended uses were obtained from PubChem (Kim et al. 2021), and clinical trials were identified at https://clinicaltrials.gov/.

3.4 Discussion

3.4.1 Summary

Mapping genetic interactions is intended to simplify the understanding of complex genetic interactions (Busby et al. 2019; Leeuwen et al. 2017; Tong et al. 2004; Tutuncuoglu and Krogan 2019). With the network topological centrality and community algorithms used here, clear pathways of GO cellular processes emerged and in the case of DGAT-deficiency, genes involved in the ER-to-Golgi vesicle transport, UPR and autophagy pathways were deemed to be important to atorvastatin activity. Here, I have used yeast models with two genetic probes (the *dga1*△ *lro1*△ and *tgl3*△ *tgl4*△ query strains) for the study of the contribution of lipodystrophy and metabolic syndrome to the diabetogenic activity of atorvastatin in three genetic backgrounds. This dissertation extends previous insights into the complexity of the response to atorvastatin and the influence of genetic background (Busby et al. 2019; Chakrabarty et al. 2020; Galardini et al. 2019; Kamal et al. 2018; Kanugula et al. 2014; Loregger et al. 2017; Pandyra et al. 2015). Consistently with my findings from the previous chapter, some of the chemical genetic interactions that did not overlap between genetic backgrounds have similar functions to other chemical genetic interactions in different genetic backgrounds, indicating that the chemical genetic interactions are not conserved but the cellular coping mechanisms are conserved.

Specifically, *GYP1* was identified as a key modulator in buffering atorvastatin-induced toxicity via this being a highly ranked betweenness (bottleneck) gene in network centrality analysis and *dga1*△ *lro1*△ *gyp1*△ exhibiting a significant growth defect in all three genetic backgrounds. I identified other genes closely related to *GYP1*; these may also serve as modulators to buffer atorvastatin toxicity (*YPT7*, *YPT31* and *SEC22*) that were less central to the interaction networks than *GYP1* and may thus represent less intrusive statin-modifying candidates. I also identified potential combination therapies with approved antidiabetic drugs (glibenclamide, pioglitazone) as well as other approved and non-approved drugs that have the potential to exert antidiabetic activity (niclosamide, bafilomycin). Eleven chemical genetic interactions were found to enhance hypersensitivity to atorvastatin in DGAT-deficient strains but that were unique to S288C (*COG8, RUD3, VPS72*), UWOPS87 (*ERV25, MCP2, TMA7, YLR279W*) and Y55 (*COQ10, MDM38, SHE4, SHR5*) genetic backgrounds. In the case of TGL-deficient strains, I did not identify chemical genetic interactions that were unique to the triple deletion *tgl3*△ *tgl4*△ *xxx*△, but rather hypersensitive strains to atorvastatin were as hypersensitive as *xxx*△ single deletions, indicating redundancy of compensatory pathways.

In this chapter I have affirmed the central theme of this dissertation, namely that the genetic underpinnings of complex phenotypes can be unravelled by assembly of genetic interaction networks and analysis of their properties. Thus, topological centrality analyses and community analyses identify new potential interactors behind the diabetogenic activity of atorvastatin. Taken together, both centrality and community analyses complemented each other's findings. While centrality analyses reveal specific interactors and bottleneck genes, community analysis reveals relevant metabolic pathways to target.

3.4.2 Molecular insight into lipotoxicity as a mechanism for atorvastatin-induced insulin resistance

The synthesis of cholesterol and fatty acids is interconnected through acetoacetyl CoA (Figure 3.1). It is thus possible that inhibition of HMGCR with atorvastatin resulted in accumulation of this precursor, which would have in turn increased the synthesis of fatty acids. I thus believe that atorvastatin exacerbated lipotoxicity in the DGAT yeast model through the increased accumulation of fatty acids, diacylglycerol and other intermediates, such as ceramides. It is indeed known that statins increase fatty acid synthesis that lead to defective insulin signalling (Kain et al. 2015; Williams et al. 1992), and interestingly, simvastatin has shown to induce insulin resistance linked to decreased capacity of DGAT1 and DGAT2 and with it inhibiting the synthesis of triacylglycerides and accumulating lipotoxic intermediates, such as fatty acids and diacylglycerol in humans (Larsen et al. 2018). It remains unclear, however, whether the molecular mechanisms by which statins induce diabetes via lipotoxicity are applicable to all statins.

Genes involved in the ER-to-Golgi pathway (*GYP1*, *ERV25*, *COG8*, *RUD3*) were identified in this chapter as mediators of survival in DGAT strains. This cellular process is linked to lipotoxicity and may thus be part of the molecular mechanism of atorvastatin-induced lipotoxicity. Lipotoxic accumulation of ceramides, for instance, has been found to be alleviated by an ER-to-Golgi tether that prevents their accumulation in yeast (Liu et al. 2017). Although this type of transport was non-vesicular and the genes I identified here are mediators of vesicular transport, about 80% of the transport of ceramides is mediated by vesicular traffic (Funato and Riezman 2001). Thus it is possible that this mechanism also serves to alleviate lipotoxicity, which would be supported by my results that deletion of genes mediating this pathway enhanced toxicity of atorvastatin.

Mitochondrial dysfunction is also linked to lipotoxicity and insulin resistance (da Silva Rosa et al. 2020; Schrauwen et al. 2010) and genes involved in mitochondrial functions were also identified in this chapter (*MCP2*, *MDM38*, *COQ10*). In mouse models, for instance, lipotoxicity disrupted mitochondrial

functions and/or mitophagy contributing to muscle insulin resistance (da Silva Rosa et al. 2020). As atorvastatin is also known to impair mitochondrial function through the inhibition of ubiquinone (Urbano et al. 2017), mitochondrial oxidative phosphorylation impairment may contribute to atorvastatin-induced lipotoxicity as this mechanism has also been linked to the lipotoxic accumulation of diacylglycerol and ceramides with insulin resistance (Möhlig et al. 2004; Samuel et al. 2010). Consistently, I found important mitochondrial genes buffer the toxicity of atorvastatin in the DGAT yeast strains. Specifically, this was the case for the DGAT-deficient strains in the statin-resistant UWOPS87 and Y55. It is thus possible that the mitochondrial genes that I found buffering atorvastatin toxicity might help to mitigate lipotoxicity, such as *MCP2* and *MDM38*, which would be supported by my finding of the ubiquinone-encoding *COQ10* in Y55. Interestingly, gene expression of CD36 decreased in the simvastatin-treated patients that showed lipotoxic accumulation of fatty acids and diacylglycerol (Larsen et al. 2018), which has a role in ubiquinone metabolism further supporting the involvement of ubiquinone in atorvastatin-induced lipotoxicity (Anderson et al. 2015).

3.4.3 Genetic interactions point to three roles of GYP1 in the lipotoxic diabetogenic activity of atorvastatin

GYP1 may be a target for the regulation of the diabetogenic activity of atorvastatin since *GYP1* was a highly betweenness gene, and high betweenness tends to correlate with bridges between network modules that despite their high relevance become suitable druggable targets as they show less essentiality than highly interconnected nodes, i.e., nodes of high degree. *GYP1* was associated with the UPR, vesicular transport, endocytosis and autophagy pathways in all three genetic backgrounds. These results indicate that genes involved in these processes can be considered buffers of lipotoxicity upon treatment with atorvastatin. More specifically, *GYP1* expression affects Ypt1, a central Rab-family GTPase involved in both protein transport and autophagy (Thomas et al. 2018).

Interestingly, nearly 90% of the genes and proteins identified in the aggregated network analysis that interact with *GYP1* in S288C belonged to the community module enriched for autophagy and SNARE interactions of vesicular transport. Similarly, about 67% of the genes and protein interacting with *GYP1* in UWOPS87 belonged to the community module enriched for autophagy. However, only 8% of the interactors with *GYP1* in Y55 belonged to the community module enriched for SNARE interactions in vesicular transport and autophagy. Most of the *GYP1* interactors in Y55 (about 70%) belonged to the community module for this genetic background that was not enriched for SNARE or autophagy, but rather this module was enriched for mitophagy. Taken together, my findings point to an involvement of

GYP1 in cellular homeostasis upon lipotoxic stress, a hypothesis that requires to be tested.

For the three genetic backgrounds only very few (for S288C and UWOPS87) or none (for Y55) of the interactors of *GYP1* belonged to the community module enriched for UPR. It is thus possible that, of all three metabolic pathways identified (vesicular traffic, UPR and autophagy), UPR is the least relevant for the activity of *GYP1* buffering atorvastatin-induced lipotoxicity. This is somewhat surprising given that ER stress is considered a key contributor to β-cells dysfunction and lipotoxicity is a known initiator of UPR in β-cells that leads to apoptosis (Biden et al. 2014; Han and Kaufman 2016). The secretory pathway is also known to directly regulate UPR (Tsvetanova 2013), where Ypt1, which is activated by *GYP1*, was found a key interactor.

3.4.4 Genetic interactions point to the role of GYP1-mediated ER-to-Golgi vesicle transport in the lipotoxic diabetogenic activity of atorvastatin

Montgomery et al. postulated that it is "highly likely that lipotoxicity-induced ER stress will affect COPII, ER exit sites, and classical protein secretion capacity" (Montgomery et al. 2019). My results add evidence to these predictions in that I found genes involved in the secretory pathway impacted by atorvastatin and DGAT-mediated accumulation of lipids and their intermediates. Specifically, I found *GYP1* as a top centrality gene that showed decreased fitness in atorvastatin-treated strains in three genetic backgrounds, and three other top centrality genes (*SEC22*, *YPT7* and *YPT31*) overlapping in two genetic backgrounds. This points to a role for these genes in buffering lipotoxicity possibly through their overexpression as a result of lipotoxic accumulation of intermediates. This is in line with findings in the literature that elevated levels of diacylglycerol through deletion of the diacylglycerol kinase *DGK1* enhanced vacuole fusion through increased activity of Ypt7 (Miner et al. 2017). Also, accumulation of ceramides due to the phosphatidylinositol:ceramide phosphoinositol transferase Aur1 repression, was buffered by genes in vesicular traffic from Golgi to vacuole, and Aur1 was identified a negative interactor of *GYP1*, and less strongly *YPT1* (Voynova et al. 2015). It is thus possible that atorvastatin- and DGAT-induced lipotoxicity enhanced the activity of the genes identified here (*GYP1*, *SEC22*, *YPT7* and *YPT31*) as a buffering mechanism. Furthermore, proteins secreted through this pathway are glycosylated in the ER and also in COPII-coated vesicles (Montgomery et al. 2019). It is possible that inhibition of glycosylation caused by atorvastatin also exacerbated the dysregulation of protein secretion under lipotoxic conditions. This fits well with the enrichment of *N*-glycan biosynthesis for two genetic backgrounds, UWOPS87 and Y55, and implicates glycation pathways as potential contributors for the increased toxicity of atorvastatin in these DGAT-deficient strains.

Similarly, the human orthologues of *GYP1*, TBC1D22A and TBC1D22B, are Rab GTPase activating proteins, in this case of RAB33B (Greninger et al. 2013). In humans, Rab GTPases also are regulators of trafficking and vesicle transport, notably the insulin-mediated uptake of glucose, and thus tighly linked to diabetes (Watson and Pessin 2006). Interestingly, although human RAB1A and RAB1B are more conserved with yeast Ypt1 (82% and 67% protein sequence similarity, respectively) than RAB33B (64% similarity) (Hu et al. 2017), RAB33B seems to share more similarity with Ypt1 in terms of the dual function of autophagy and membrane trafficking, though this may only be a result of RAB33B being more characterised than RAB1 GTPases. RAB33 has also been found to interact with TBC1D22A (Greninger et al. 2013), thus both RAB1 and RAB33 as well as TBC1D22 should be considered for further studies in human cell models as it is unclear what their contribution to the lipotoxic-mediated diabetogenic activity of atorvastatin might be. Human orthologues of other genes identified here have been associated with lipid droplet metabolism, such as YPT7A, orthologue of yeast *YPT7*, that associates with lipid droplets in adipocytes (Brasaemle et al. 2004) and RAB25, orthologue of *YPT31*, a regulator of lipid droplet autophagy in hepatic stellate cell activation (Zhang et al. 2017). However, their role as buffers of lipotoxicity or contribution to the diabetogenic activity of statins has not been explored.

Human orthologues of these genes have also shown links to insulin secretion and diabetes but their involvement in the prodiabetic activity of statins is unknown. SEC22B, for instance, a human orthologue of *SEC22*, has been found to physically interact with CTAGE5 in an interaction essential for the processing of the precursor of insulin and proinsulin in pancreatic β-cells by possibly regulating the release of proinsulin-containing COPII vesicles from ER to Golgi trafficking (Fan et al. 2017). RAB11A and RAB11B, human orthologues of *YPT31*, are mediators of GLUT4, the insulin-regulated glucose transporter in skeletal and adipose tissues (Kessler et al. 2000; Schwenk and Eckel 2007; Zeigerer et al. 2002) and RAB11A is a physical interactor of RAC1, a regulator of insulin secretion in pancreatic β-cells (Damacharla et al. 2019). Thus, their contribution as buffers of lipotoxicity or the diabetogenic activity of statins should be addressed in future studies.

3.4.5 Genetic interactions point to the role of GYP1-mediated autophagy in the lipotoxic diabetogenic activity of atorvastatin

The role of autophagy in the diabetogenic activity of statins has been previously studied (Qian et al. 2019; Wang et al. 2015) and my thesis extends these findings. I suggest *GYP1* could be a key mediator of autophagy under lipotoxic conditions. Gyp1 is a physical interactor of Atg8 that is integral

in selective autophagy (Mitter et al. 2019). Although the human orthologues of Gyp1 (TBC1D21, TBC1D22A and TBC1D21B) are not known to be interactors of GABARAP, the human orthologue of Atg8, other TBC1 domain family members (TBC1D2B, TBC1D5, TBC1D7, TBC1D25, TBC1D10A, TBC1D10B, TBC1D11, TBC1D1) have been reported as physical interactors and thus are regulators of autophagy (Popovic et al. 2012). These are candidate interactions to test in human cell models. Interestingly, TBC1D4 has been reported as having a role in increasing insulin sensitivity of skeletal muscle (Cartee 2015) and it is then possible that other TBC domain family members have a role in insulin resistance. None of them, however, have been reported as contributors to the diabetogenic activity of statins. Similarly, although autophagy is a known mechanism for the diabetogenic activity of statins (Wang et al. 2015) and lipotoxicity is known to impair autophagy (Choi et al. 2009; Jaishy and Abel 2016), these specific mechanisms have not been associated with GABARAP.

3.4.6 Potential combination therapies to decrease the diabetogenic activity of atorvastatin

Yeast bottleneck genes potentially involved in the diabetogenic activity of atorvastatin were matched with their human orthologs, and then used to find existing drugs to counteract this effect of atorvastatin. Different types of drugs resulting from this analysis target more than one of the genes that I identified and often times targeting a group of functionally related genes is a better approach than focusing on one sole target (Arrell and Terzic 2010). For instance, two of the top 20 drugs/compounds retrieved from this search (glibenclamide and pioglitazone) are approved and well established drugs for the treatment of diabetes (Figure 3.15; Table 3.10) that shared signature genes with atorvastatin, respectively. Glibenclamide, also known as glyburide, is a second-generation hypoglycemic sulfonylurea that reduces K^+ efflux and membrane depolarisation causing influx of Ca^{2+} that triggers insulin secretion (Luzi and Pozza 1997). Genes involved in protein secretion and lipid metabolism were the signature genes shared between atorvastatin and glibenclamide, and interestingly, 7 out of 8 (VPS72, TMED10, RAB7A, RAB4A, RAB2A, HMGCR and COQ10B) of these genes were shared with chlorzoxazone (Figure 3.15), a muscle pain reliever that has no association with diabetes and would thus be a novel candidate to test for a potential anti-diabetic activity.

Pioglitazone, the other well-established antidiabetic drug found in this analysis, is a thiazolidinedione agent that activates the nuclear PPAR-γ to increase transcription of various genes regulating glucose and lipid metabolism, such as GLUT1 and GLUT4 (Gillies and Dunn 2000). COG8 and HMGCR were the signature genes shared between atorvastatin and pioglitazone and these genes

were also shared with other two drugs/compounds, metronidazole and cadmium sulfate (Figure 3.15). Metronidazole is a drug for the treatment of bacterial and parasitic infections (Weir and Le 2021), which in itself has not shown antidiabetic activity but metronidazole-carboxylate derivatives have exerted antidiabetic activity (Patel et al. 2021; Salar et al. 2017) and have not been trialled in combination with statins. Cadmium sulfate would likely not be a suitable combination given its toxic and carcinogenic nature, which emphasises that drug signatures must be taken with caution since sharing drug signature genes does not necessarily point to a suitable combination therapy. Such is the case as well for minoxidil, an antihypertensive vasodilating agent that opens ATP-sensitive potassium channels, which has been repurposed for the stimulation of hair growth, since similarly to statins, minoxidil has elicited prodiabetic activity (Stein et al. 1997).

3.4.7 Genetic interactions point to the protective role of lipid droplets and triacylglyceride lipases against atorvastatin-induced toxicity

Until recently, genome-wide studies of genetic interactions had been limited to digenic interactions, that is, the interaction between two genes and their phenotypes (Boone et al. 2007; Costanzo et al. 2016). Kuzmin et al. showed that higher-order interactions, in this case trigenic (triple mutant analyses), showed associations of genes that participated in the same or connected diverse biological processes though phenotypes tended to be less pronounced than those found in digenic interactions (Kuzmin et al. 2018). Kuzmin also noted that trigenic interactions tend to amplify the phenotype of double deletions, that is, if a digenic interaction is epistatic, a third epistatic interaction would amplify the growth defect. It was not expected, however, that the phenotypes of triple deletions treated with atorvastatin (mimicking a fourth mutation) would be nearly identical to the phenotypes of the treated single deletion strains in the three genetic backgrounds studied. This emphasises that there must exist a high number of redundant and compensatory pathways for a triple deletion and a fourth mimicked mutation not to cause detectable alterations in my validations, unusual in such high-order genetic interactions and thus emphasising the complexity of the genotype to phenotype relationship (Costanzo et al. 2019; Kuzmin et al. 2018; Taylor and Ehrenreich 2015).

It is thus possible that the lack of identification of atorvastatin-linked trigenic interactions (quadrigenic), might be due to *tgl3*△ *tgl4*△ itself not being epistatic (see Figure 3.3), as opposed to *dga1*△ *lro1*△ that clearly shows a fitness defect compared to the wild type and the parental single deletions. Another possibility is the redundancy of triacylglyceride lipases. Yeast have five triacylglycerol lipases coded by *TGL3*, *TGL4*, *TGL5*, *AYR1* and *LDH1* (Athenstaedt and Daum 2003;

Athenstaedt and Daum 2005; Debelyy et al. 2011; Ploier et al. 2013). The latter three are less active in degrading triacylglycerides as they have dual functions. Given the importance of the degradation of triacylglycerides, which is an essential process for lipid and cellular homeostasis, it is possible that *TGL5*, *AYR1* and *LDH1* were upregulated to compensate for the lack of *tgl3*Δ and *tgl4*Δ. It is also possible that atorvastatin may have conferred some degree of protection; although it may have caused cellular stress through other mechanisms, it may also have limited the stress of inhibited degradation of triacylglycerides through inhibiting DGAT as I hypothesised in the previous sections, thus preventing more synthesis of triacylglycerides. Future studies should focus on other deletion combinations with the *TGL3*, *TGL5*, *AYR1* and *LDH1* but at this stage, there is no evidence in this thesis that accumulation of triacylglycerides and lipid droplets have any effect on the diabetogenic activity of atorvastatin. It is indeed known that lipid droplets protect cells from lipotoxicity (Olzmann and Carvalho 2019). Interestingly, *TGL5* has been suggested as a potential substrate of *CDC28* (Kurat et al. 2009), and I identified *CDC28* as a potential off-target mechanism of atorvastatin in Chapter 2. This may be an important point to consider for the design of future studies.

3.4.8 Conclusion

Taken together, I have demonstrated the utility of using chemical genetics and network analyses to elucidate specific interactors and metabolic pathways that may be behind the diabetogenic activity of atorvastatin. I have identified *GYP1* as a key modulator in buffering atorvastatin-induced lipotoxicity and insulin resistance. Specific cellular processes, such as ER-to-Golgi vesicle transport, UPR and autophagy pathways were also identified as buffers of atorvastatin-induced lipotoxicity. Combination therapies with established antidiabetic and other drugs with potential antidiabetic activity were proposed. It was also concluded that deletion combinations with more than two triacylglyceride lipases might be necessary to identify metabolic syndrome-related interactions behind the diabetogenic activity of statins.

Chapter 4

Investigating yeast conditional genetic interactions as a proxy for hypoxic tumour conditions

4.1 Introduction

Tumour hypoxia, the limited access of some tumours to oxygen due to aberrant vascularisation and rapid proliferation, has long been acknowledged as a mechanism of decreased sensitivity to anticancer treatments (*e.g.*, radiotherapy) and poor prognosis (Gray et al. 1953; Sørensen and Horsman 2020; Thomlinson and Gray 1955). Therefore, combination therapies that overcome hypoxia-induced resistance have been pursued but have yielded mixed results (*e.g.*, DiSilvestro et al. 2014; Panduro et al. 1983, NCT01440088). Strategies to overcome or alleviate hypoxia have been mainly based on oxygen delivery, hypoxia-activated prodrugs (compounds that are differentially activated in hypoxic tissue) (Zeman et al. 1986), and modulation of cellular metabolism to oxygenate the tissue. The latter includes modulators of the electron transport chain and oxygen consumption inhibitors (Diepart et al. 2012; Gallez et al. 2017; Graham and Unger 2018; Kelly et al. 2014) that overcome radiotherapy resistance through the inhibition of the oxidative phosphorylation pathway and through reduced oxygen consumption (Mudassar et al. 2020). The response to hypoxia in mammalian cells is known to include the hypoxia-inducible transcription factor HIF1A, which in aerobic conditions is degraded through the ubiquitin-proteasome system (Dengler et al. 2014; Majmundar et al. 2010; Pezzuto and Carico 2018). Under hypoxia, however, this system is inhibited and HIF1A accumulation upregulates the transcription of genes involved in cell proliferation, angiogenesis, apoptosis and migration.

The unfolded protein response (UPR) and autophagy are also oxygen-sensitive pathways that may mediate the response of tumour cells to hypoxia (Chipurupalli et al. 2019). Notably, anticancer activity of statins has been linked to HIF1A, UPR, and mTOR kinase signalling (Alupei et al. 2014; Chen et al. 2017; Dastghaib et al. 2020; Okubo et al. 2020). The cytotoxic activity of statins in melanoma, for instance, has been linked to inhibition of HIF1A (Alupei et al. 2014) and atorvastatin inhibits hypoxia-induced radiosensitivity in prostate cancer cells by inhibition of HIF1A expression (Chen et al. 2017). Further, simvastatin enhanced apoptosis induced by the therapeutic temozolomide in glioblastoma cells via UPR (Dastghaib et al. 2020). Statins also activate the AMPK pathway and thereby inhibit mTOR, thus combination of autophagy-inhibiting vorinostat and fluvastatin enhanced anticancer activity in renal cancer cells (Okubo et al. 2020). Statins are also indirect inhibitors of the electron transport chain via ubiquinone (Figure 4.1). The molecular mechanism of statin-increased sensitisation of cancer cells to anticancer therapeutics in hypoxia, however, has not been fully elucidated.

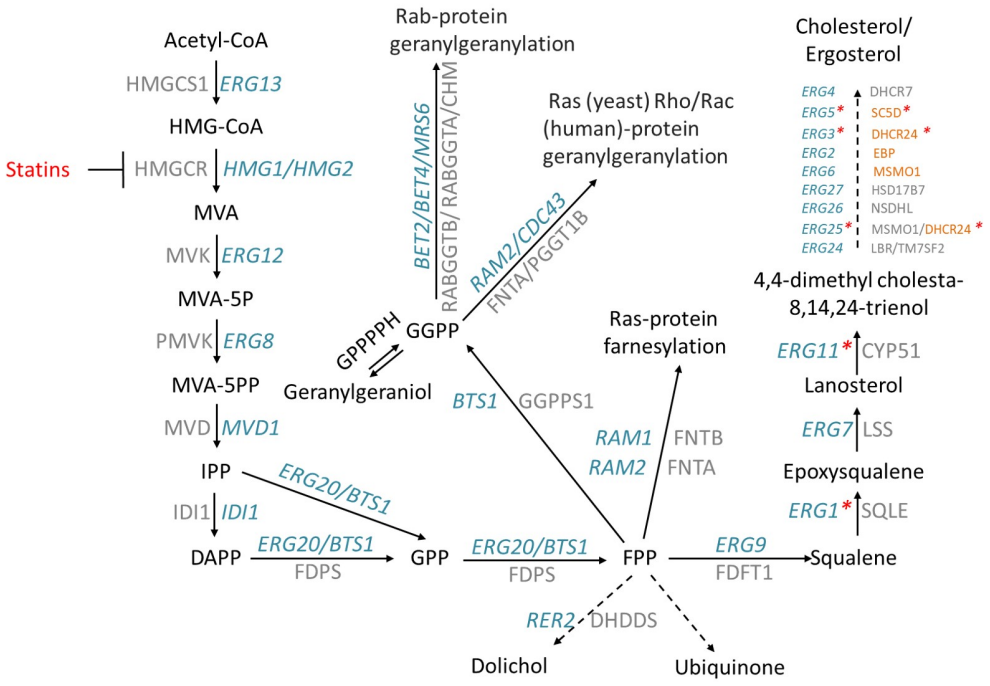

Figure 4.1: **Oxygen-dependent steps in the mevalonate pathway targeted by statins.** Statins are competitive inhibitors of HMGCR encoded by *HMG1*/*HMG2* in yeast and HMGCR in humans. A critical step in the mevalonate pathway is mediated by FPP, where the mevalonate pathway branches off to either the synthesis of cholesterol, isoprenes, dolichol or ubiquinone. Genes in blue are yeast genes and genes in grey are their human orthologues. Red asterisks indicate oxygen-dependent steps of the pathway. Human genes in orange at the end of the cholesterol pathway are less conserved with yeast and do not correspond to the yeast gene to the left.

The genetic model *S. cerevisiae* (yeast) is auxotrophic for sterols in anaerobiosis and is forced to uptake exogenous sterols from the medium, hence the term 'aerobic sterol exclusion' (Lorenz and

Parks 1987; Zavrel et al. 2013). Genetic screens have pointed to essentiality of genes in response to anaerobic and hypoxic growth (Giaever et al. 2002; Snoek and Steensma 2006; Reiner et al. 2006; Walker et al. 2014). A genome-wide screen of the diploid yeast deletion library (Giaever et al. 2002), for instance, identified 23 essential genes in anaerobiosis (Snoek and Steensma 2006), while in haploid mutant collections 37 genes were found essential for anaerobic growth where all but four participate in ergosterol uptake and processing (Reiner et al. 2006). Sterol auxotrophy has proven useful for identifying genetic modifiers of the yeast model of Niemann-Pick type C disease, a rare fatal disease with defective lysosomal accumulation of lipids (Munkacsi et al. 2011).

Studies of drugs/compound toxicity in yeast have shown differential response in aerobic and anaerobic conditions (Barakat et al. 2014; Serratore et al. 2018). Yeast genes involved in the response to pyocyanin and antifungal drug treatments, for instance, informed higher toxicity and the involvement of specific genes in anaerobic compared to aerobic conditions (Barakat et al. 2014; Serratore et al. 2018). Given the metabolic similarities between fermentative yeast and tumour cells (Diaz-Ruiz et al. 2009; Diaz-Ruiz et al. 2011), yeast models have been used to study the Warburg effect, the inhibited respiration and increased glycolysis of cancer cells (Bouchez et al. 2020; Santos and Hartman 2019). A yeast genome-wide study of the Warburg effect on doxorubicin treatment used fermentable/glycolytic compared to non-fermentable/respiratory media (Santos and Hartman 2019) and other studies have used heme mutants to induce fermentative metabolism (Bouchez et al. 2020). However, there is a need to develop methodologies with yeast models to investigate the resistance of hypoxic tumours to anticancer treatments.

In this chapter, I have developed a strategy that involves using experimental and computational analyses to elucidate genes specifically involved in inhibitory activity of *BTS1* and/or atorvastatin in cells grown hypoxically compared to cells grown in normal oxygenated conditions in three genetic backgrounds that are variably sensitive to atorvastatin. *BTS1*, the mediator of the off-branch pathway from the main ergosterol synthesis pathway to isoprenylation of GTPases (Figure 4.1), was specifically selected here since knockdown of the GGPPS1 mammalian orthologue enhanced anticancer activity of statins (Pandyra et al. 2015), yet the relevance to hypoxia has not been explored prior to this thesis. The human orthologues that relieve hypoxia should make hypoxic tumours more susceptible to chemo or radiotherapy. Conversely, overexpression of these genes might decrease proliferation of hypoxic tumours while having less toxicity in normal tissue. In either case, the genetic modifers of hypoxia identified in this chapter should be good candidates for further studies in human cell lines.

4.2 Experimental procedures

The overall flow of methods is depicted in Figure 4.2.

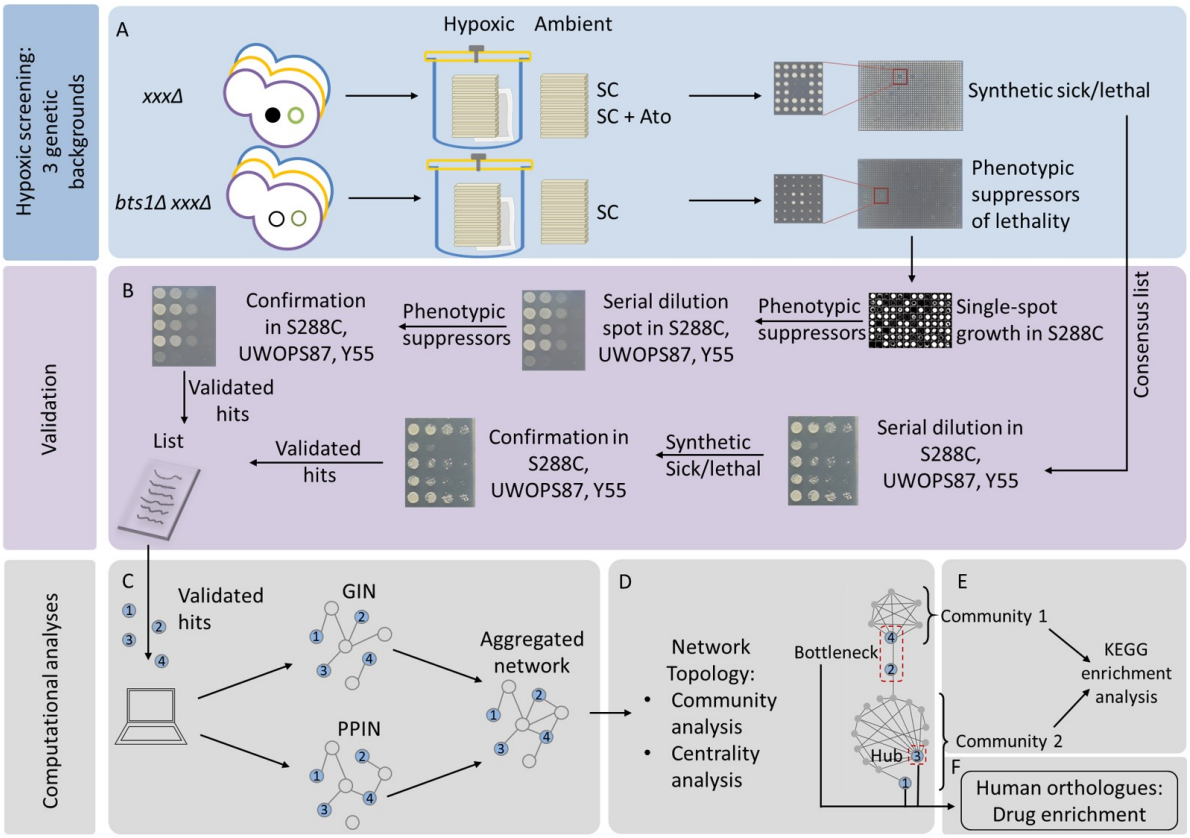

Figure 4.2: **Flow diagram for the methods used to identify hypoxia-specific interactions, pathways and drugs to enhance the anticancer activity of atorvastatin.** Single deletion and *BTS1* double deletion mutant query strains were screened in hypoxic chambers (A) (deletion mutant genes depicted as empty circles) as models to investigate the anticancer activity of atorvastatin in hypoxia in three yeast genetic backgrounds (S288C, UWOPS87 and Y55 indicated here as purple, yellow and blue). The 12,900 single deletion mutants were treated with atorvastatin in 1536-colony format (384 quadruplicate colonies per agar plate) and screened to identify fitness defects that would reveal epistatic interactions (hits) as measured by decreased colony size (top row). The <12,900 *bts1*Δ *xxx*Δ double deletion mutants were screened in 1536-colony format (384 quadruplicate colonies per agar plate) to identify suppressors of sickness/lethality that would reveal epistatic interactions (hits) as measured by increased colony size (bottom row). Hits were then validated in two steps (B). First, *xxx*Δ hits were grown in serial dilution spot assays and deletion strains that showed fitness defects in three genetic backgrounds were confirmed on a second round of serial dilution spot assays. Then, *bts1*Δ *xxx*Δ hits were arrayed in single-spots, where suppressors of lethality were confirmed in two rounds of serial dilution spot assays in three genetic backgrounds. Hits that showed the expected phenotypes (*i.e.*, growth inhibition for *xxx*Δ and sickness/lethality suppression for *bts1*Δ *xxx*Δ) were considered as validated interactions and used as input to create genetic (GIN) and protein-protein (PPIN) interaction networks (C). GINs and PPINs were aggregated in one network per genetic background and subjected to network topology analyses (D). The network centrality metrics pinpointed bottleneck and hub genes of high biological relevance. The communities of genes identified through network modularity (E) were analysed through a KEGG enrichment analysis to distinguish key metabolic pathways. Human orthologues of the key yeast genes were used in a search for drug enrichment (F) to identify potential combination therapies to enhance the anticancer activity of atorvastatin in hypoxic tumours.

4.2.1 Yeast strains and plasmids

The *S. cerevisiae* strains and plasmids used in this study are described in Chapter 2 (Sections 2.2.1-2.2.2).

4.2.2 Media and solutions

The media and solutions used to culture *S. cerevisiae* strains are described in Chapter 2 (Section 2.2.3), except for the ergosterol/Tween 80 mixture prepared as previously described (Longley et al. 1978).

Ergosterol/Tween 80 (2 mg/mL): 5 mL of Tween 80 (Sigma-Aldrich) was mixed with 5 mL of absolute ethanol (Fisher BioReagents) in a sterile conical tube followed by the addition of 0.02 g of ergosterol (Sigma-Aldrich) in darkness to prevent the degradation of light-sensitive ergosterol. The tube was wrapped in aluminium foil and left overnight in slow rotation at room temperature. For the addition to SC agar, 1 mL of the dissolved mixture was added for each 100 mL of SC agar (final concentration 0.02 mg/mL) before pouring plates. Plates were stored in darkness until use, with pinning and incubation also in darkness.

4.2.3 Hypoxic chambers

The BBL GasPak 150 large anaerobic chamber system (Becton Dickinson) was used for the hypoxic assays where each chamber contained three EZ Gas Generating Container Systems sachets that produced an anaerobic atmosphere within 2.5 h with less than 1% oxygen, and greater than or equal to 13% carbon dioxide within 24 h according to vendor's specifications.

4.2.4 Hypoxic genetic and chemical screenings

Yeast deletion libraries were screened in 1536-colony format (384 quadruplicate colonies) in SC agar media in ambient and hypoxic conditions with and without atorvastatin. The plates were incubated at 30°C for 48 h, imaged, and processed in SGAtools to score the average colony size (Wagih et al. 2013) in hypoxia compared to ambient conditions.

4.2.5 Validation of hits in serial dilution spot assay in hypoxic conditions

Strains that displayed enhanced or reduced synthetic sick/lethal phenotypes in hypoxia were selected for validation in serial dilution spot assays as explained in Chapter 2 (Section 2.2.7). Plates were incubated in hypoxic chambers and in ambient conditions for 72 h at 30°C.

4.2.6 Computational analyses

To identify robust functional associations for validated conditional genetic interactions, aggregated networks from two layers of interaction networks (GINs and PPINs) were generated and analysed for topology, centrality, communities (modules), metabolic pathway and drug signature enrichment. All of these analyses were described in detail in chapter 2 (Sections 2.2.8-2.2.12).

4.3 Results

4.3.1 Hypoxia sensitivity varies in three genetic backgrounds

To construct the query strains that were used to investigate GINs in hypoxia with *BTS1*, this gene was replaced in three yeast genetic backgrounds with NATMX4 through PCR-directed mutagenesis and homologous recombination in Chapter 2. Here *bts1*Δ strains were treated with atorvastatin in normal conditions as well as hypoxia (Figure 4.3). Hypoxia is demonstrated via two controls: 1) dramatically reduced growth of the wild type on control media lacking ergosterol/tween is evidence for hypoxia and distinct from no growth that would be evident of full anaerobiosis, since yeast are fully dependent on the uptake of ergosterol/tween in anaerobiosis (Lorenz and Parks 1987; Zavrel et al. 2013) and 2) inviability of *npt1*Δ, a strain that is established to be sensitive to hypoxia in the S288C genetic background (Panozzo et al. 2002). I thus included *npt1*Δ in S288C to indicate effective hypoxia and also included *npt1*Δ in Y55 and UWOPS87 for comparison. In S288C, *bts1*Δ was inviable in ambient conditions with atorvastatin and also inviable in all hypoxia conditions. In Y55 and UWOPS87, *bts1*Δ was indistinguishable from the wild type in normal conditions and exhibited similar growth (perhaps even improved growth) in all treatments in hypoxia. Similarly, *npt1*Δ was inviable in S288C in all hypoxia conditions but not in ambient conditions. Distinctly, UWOPS87 and Y55 *npt1*Δ strains were capable of growth in hypoxia, whereby Y55 exhibited slightly more inhibited growth than UWOPS87. These results reveal, for the first time, that genetic backgrounds are variably sensitive to hypoxia and more specifically reveal that genetic backgrounds variably rely on the *BTS1* branch of the mevalonate pathway and the salvage pathway of NAD^+ biosynthesis to cope with the stress of hypoxia.

4.3.2 Genome-wide analysis identifies candidate genes buffering statin sensitivity in hypoxia in three genetic backgrounds

Given the complexity of phenotypes and responses shown above, I decided to run the hypoxic screenings without ergosterol supplementation to remove one variable. Synthetic sick/lethal interactions of single deletions were thus investigated in atorvastatin treated and untreated agar in ambient and hypoxic conditions. To investigate atorvastatin-specific epistasis in hypoxia, genome-wide single deletion libraries for the statin-susceptible (S288C) and statin-resistant (UWOPS87 and Y55) backgrounds were screened with atorvastatin (Figure 4.2A). In order to detect growth defects due

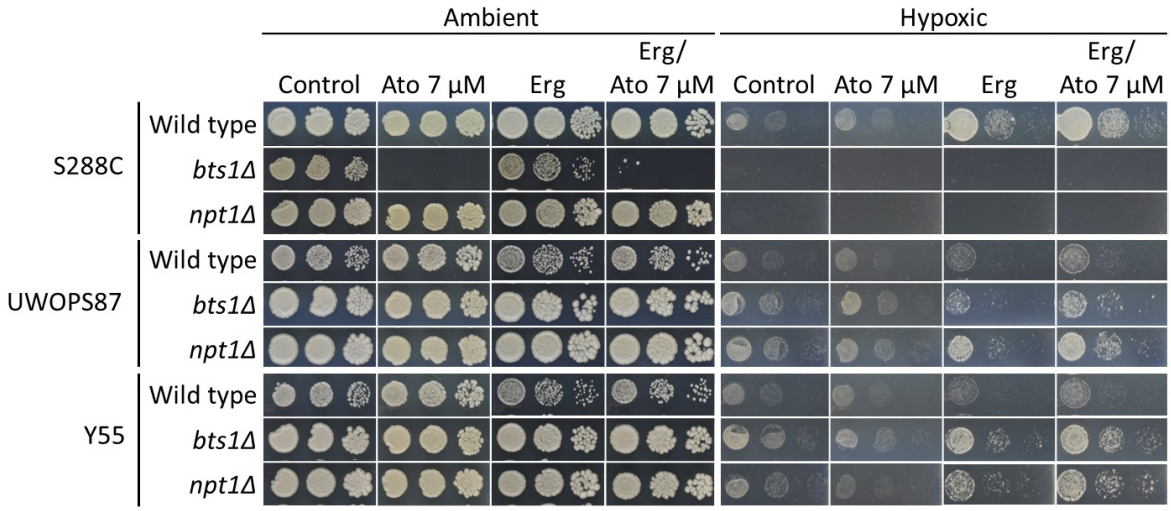

Figure 4.3: **Deletion of *BTS1* or *NPT1* confers hypoxia phenotypes that vary between genetic backgrounds.** Haploid cells in three genetic backgrounds were pinned on SC agar supplemented with atorvastatin (Ato, 7 μM), ergosterol (Erg, 0.02 mg/mL) or both in serial dilution and incubated for 3 days at 30°C.

to synthetic sick/lethal interactions, IC_{30} concentrations of atorvastatin were determined (Figure 4.4) upon trials with several concentrations ranging from 5 to 40 μM before selecting 7 μM, 20 μM and 30 μM to screen S288C, UWOPS87 and Y55, respectively, in ambient and hypoxic conditions. The same concentrations were used for both conditions because the aim was to identify interactions unique to hypoxia, which would be a proxy to treating healthy vs hypoxic cancer cells using the same concentration of atorvastatin. All deletion strains were screened in quadruplicate at the IC_{30} concentrations, which provided a 70% window to detect additional growth reduction due to synthetic sick/lethal interactions.

The chemical genetic profiles of atorvastatin-treated strains were significantly different between ambient and hypoxic conditions based on the distribution of average colony sizes where lower scores represent fitness defects (synthetic sick/lethal interactions) and higher values relate to increased fitness (suppressors) (Figure 4.5). Unlike previous chapters where the scored colony sizes were used to determine the interactions to be validated, in this case I decided to use average colony sizes of atorvastatin-treated strains. I reasoned this would increase the chances of finding interactions with atorvastatin that were unique to hypoxic conditions. Given that some steps in the mevalonate pathway are oxygen-dependent (Figure 4.1), the overall growth of colonies was more inhibited in hypoxia compared to ambient conditions (Figure 4.5). The distribution of average colony sizes (n = 4) significantly differed among the three genetic backgrounds in both ambient and hypoxic conditions

(Figure 4.5).

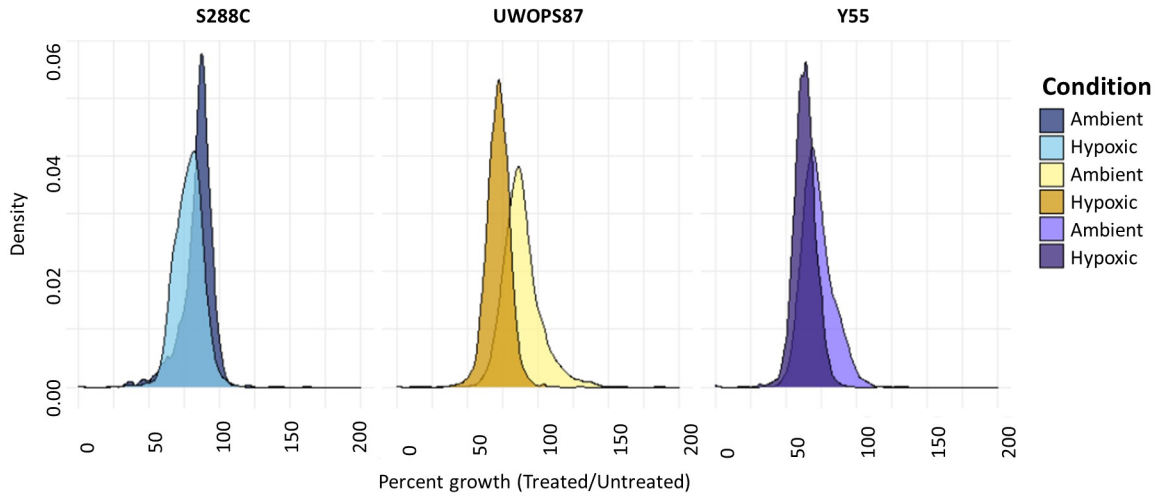

Figure 4.4: **Atorvastatin concentration for maximum overlap at 30% of growth inhibition between the ambient and hypoxic conditions.** The *xxx*Δ libraries were screened in IC_{30} concentrations of atorvastatin. Density plots represent distribution of percent growth where higher density (y-axis) indicates more gene deletions having the corresponding percent growth in the x-axis.

As discussed previously, high-throughput screening experiments tend to suffer from noisy data (*e.g.*, false positives) and thus it was necessary to validate the hypersensitive interactions identified in 1536-colony format. To aid validation, I established a cut-off for the average colony sizes of 2 standard deviations below the median for both ambient and hypoxic. That way, genes with average colony sizes below 547 (pixel-based colony size values assigned in SGAtools via Gitter (Wagih and Parts 2014)) were considered hits for validation in S288C, 458 for UWOPS87 and 367 for Y55. Given my specific interest in epistatic interaction effects unique to the hypoxic conditions, hits that were sensitive in ambient conditions were excluded from further analysis. For instance, the 47 interactions below the score cut-offs that overlapped between the ambient and hypoxia screens in S288C (Figure 4.5) were excluded from further analysis.

4.3.3 Validation of hypoxia-specific genetic interactions with atorvastatin strains in three genetic backgrounds

Using the cut-off criteria in the SGA analysis, I selected to validate hypoxia-specific growth defects in 130, 35 and 27 atorvastatin-treated strains for S288C, UWOPS87 and Y55, respectively. Conditional chemical genetic interactions conserved across the genetic backgrounds provide insight into atorvastatin bioactivity in all individuals. To complement the high-throughput growth assay in

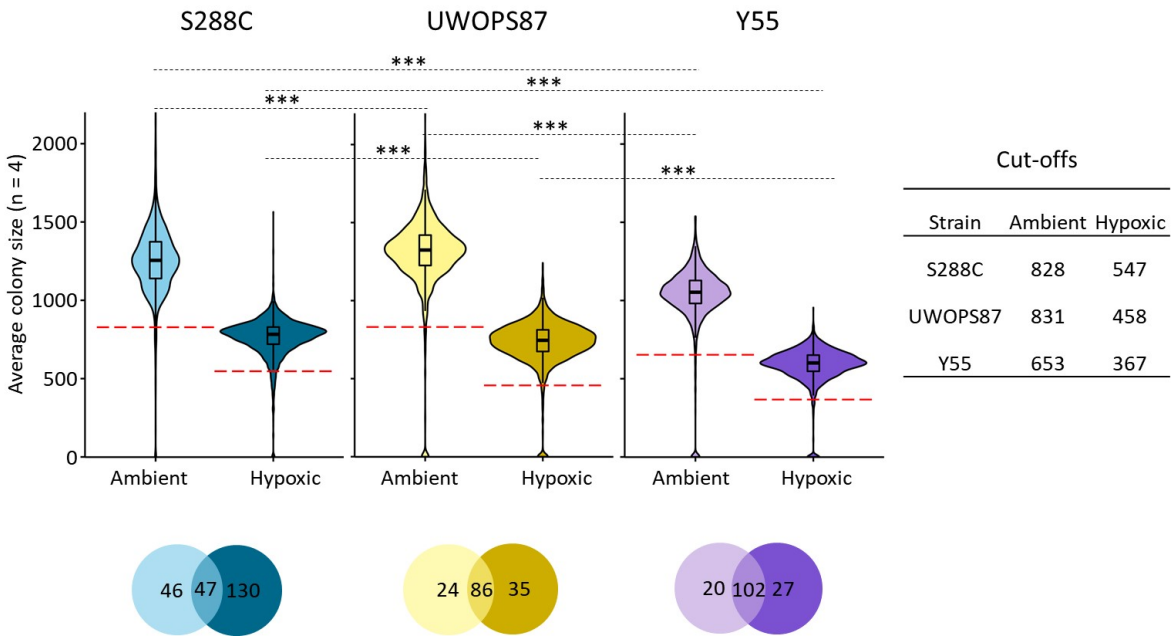

Figure 4.5: **The strength of synthetic sick/lethal interactions differs significantly in ambient and hypoxic conditions in three genetic backgrounds.** Violin plot distributions of average fitness of 12,900 strains as measured by average colony sizes (n = 4) of *xxx*Δ in ambient and hypoxic conditions where higher scores represent increased fitness and lower scores represent decreased fitness. The red dashed lines indicate the score cut-off values selected for validation in independent assays. Venn diagrams visualise the overlap in the number of genes below the cut-off lines. Statistical differences were evaluated with a Student's *t*-test (*, $P < 0.05$ **, $P < 0.01$ ***, $P < 0.001$).

1536-colony, growth of candidate *xxx*Δ strains was monitored in an independent assay where strains were grown individually as serial spot dilutions on agar (Figure 4.2B bottom row). Nine conditional genetic interactions with atorvastatin specific to hypoxia were apparent in the spot dilution assay (Figure 4.6). Only in UWOPS87 and Y55, the deletion of *ACF2*, *HRK1*, *MMT2*, *NHA1*, *NTO1*, *SND2*, *TKL1* or *TRS85* resulted in a minor growth defect in one dilution spot in hypoxia compared to control. In contrast, the deletion of *NDE1* resulted in a growth defect in hypoxia compared to control in all three backgrounds.

Functionally, these nine genes are involved in a diversity of processes (Table 4.1). *TKL1* has a role in the pentose phosphate pathway that is essential for the generation of NADPH. *NDE1* has the capacity to oxidise NADPH for entry to the mitochondrial respiratory chain, a cellular process that has been targeted to enhance the efficacy of anticancer therapy in hypoxic tumours (Kelly et al. 2014). This might explain that cells under hypoxia require genes involved in the production and oxidation of NADPH, particularly with atorvastatin being an inhibitor of the electron transport chain (Broniarek et al. 2020; Schirris et al. 2015). Though *NDE1* does not have a human orthologue, human orthologue variants of *TKL1* are candidate targets to trial in combination with atorvastatin in hypoxic tumours.

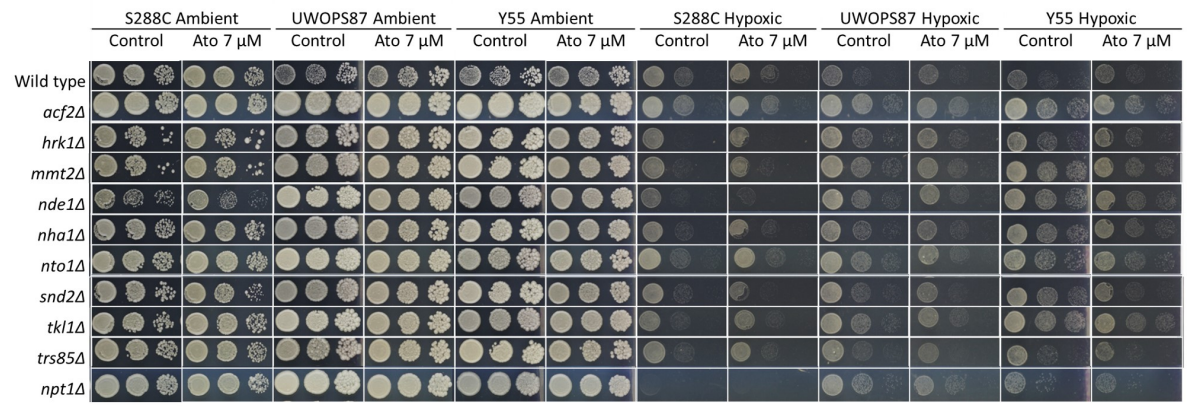

Figure 4.6: **Nine *xxx*△ single deletions were sensitive to atorvastatin treatment in hypoxia compared to control.** Haploid cells derived from DMA libraries were pinned on SC with or without supplementation of atorvastatin in serial dilution and incubated for 3 days at 30°C in ambient vs hypoxic conditions. The *npt1*△ strain was included as a control for effective hypoxia since this strain is inviable in anaerobiosis in S288C (Panozzo et al. 2002).

ORF	Gene	Name	Description	Human orthologue(s)
YLR144C	*ACF2*	Assembly Complementing Factor	Endoglucanase that may have a role in actin cytoskeleton assembly and increases protein abundance during DNA replication stress	None
YOR267C	*HRK1*	Hygromycin Resistance Kinase	Protein kinase with a role in ion homeostasis and its protein abundance increases during DNA replication stress	HUNK, PRKAA2
YPL224C	*MMT2*	Mitochondrial Metal Transporter	Mitochondrial metal transporter involved in iron accumulation	None
YMR145C	*NDE1*	NADH Dehydrogenase, External	Mitochondrial external NADH dehydrogenase that catalyzes the oxidation of cytosolic NADH and provides it to the mitochondrial respiratory chain	None
YLR138W	*NHA1*	Na+/H+ Antiporter	Involved in sodium and potassium efflux through the plasma membrane.	None
YPR031W	*NTO1*	NuA Three Orf	Subunit of the NuA3 histone acetyltransferase complex, which acetylates histone H3	JADE2, BRD1, BRPF3, MLLT6, BRPF1, JADE1, MLLT10, PHF14, JADE3
YLR065C	*SND2*	SRP-iNDependent targeting	Protein involved in signal recognition particle (SRP)-independent targeting of substrates to the ER, alternative ER targeting pathway that has partial functional redundancy with the GET pathway and has a role in the late endosome-vacuole interface.	TMEM208
YPR074C	*TKL1*	TransKetoLase	Transketolase with a role in the pentose phosphate pathway; needed for synthesis of aromatic amino acids	PDHB, TKT, TKTL1, TKTL2
YDR108W	*TRS85*	TRapp Subunit	Component of transport protein particle TRAPPIII, which activates the GTPase Ypt1p and regulates endosome-Golgi traffic; has a role in autophagy.	TRAPPC8

Table 4.1: **Annotation of *xxx*△ strains sensitive to atorvastatin in hypoxia.** Description was obtained from SGD (Cherry et al. 2012). Human orthologues were obtained from YeastMine (Balakrishnan et al. 2012).

Closely related, ATP production inhibited by hypoxia and potentially exacerbated by atorvastatin seems to be modulated by genes involved in Na^+/K^+ ion homeostasis (*e.g.*, *NHA1* deletion enhances toxicity of atorvastatin in hypoxia). Additionally important ion homeostasis mechanisms are mediated by *MMT2* and *HRK1* genes.

Another process that mediates atorvastatin-specific survival in hypoxia is autophagy. *TRS85* has a role in autophagy and the mTOR kinase signalling pathway, processes known to mediate the response of tumour cells to hypoxia (Chipurupalli et al. 2019). This gene and its human orthologue may enhance toxicity of atorvastatin in hypoxia. Likewise, *HRK1* deletion prevents UPR induction under ER stress (Tan et al. 2009), suggesting UPR is involved in atorvastatin toxicity in hypoxia. Endosomal transport is also involved as evidenced by the increased sensitivity upon deletion of *TRS85* or *SND2*. Additionally, DNA replication stress is involved based on the *ACF2* and *HRK1* deletion phenotypes. In summary, I identified specific gene modulators of NADPH and ATP production, autophagy, UPR pathway, endosomal transport and DNA replication that might enhance the toxicity of atorvastatin in hypoxic tumours, whereby the orthologues of these genes may be candidates for studies in human cancer cell lines and animal models.

4.3.4 Genome-wide analysis of suppressors of bts1Δ synthetic sick/lethal interactions shows the genes mediating statin sensitivity in hypoxia

Via the quantification of growth of *bts1Δ xxxΔ* double deletion mutant libraries, screening of SGAs reveal gene-gene interactions integral to the atorvastatin mechanism of action, since *BTS1* is a downstream target of atorvastatin. To investigate genetic epistasis in hypoxia, genome-wide *bts1Δ xxxΔ* double deletion libraries for the statin-susceptible (S288C) and the statin-resistant (UWOPS87 and Y55) backgrounds were screened in hypoxia (Figure 4.2A). Since deletion of *BTS1* confers synthetic lethality to S288C and synthetic sickness to UWOPS87 and Y55 (Figure 4.3), here I sought to detect enhanced growth due to phenotypic suppression of synthetic sickness/lethality that were unique to the hypoxic condition. SGA libraries of the three genetic backgrounds were grown in ambient and hypoxic conditions in quadruplicate.

The conditional genetic profiles of the double deletion strains were significantly different from that of the single deletion strains based on the distribution of average colony sizes where lower scores represent fitness defects (synthetic sick/lethal interactions) and higher values relate to increased fitness (suppressors) (Figure 4.7). Similar to previous sections, I decided to use average colony sizes of atorvastatin-treated strains in order to increase the chances of me finding sickness/lethality suppressor

interactions in hypoxia that were unique to *bts1*Δ *xxx*Δ strains. As expected, given that *bts1*Δ is lethal in S288C but only synthetic sick in Y55 and UWOPS87, the overall growth of colonies was reduced in S288C compared to UWOPS87 and Y55 (Figure 4.7).

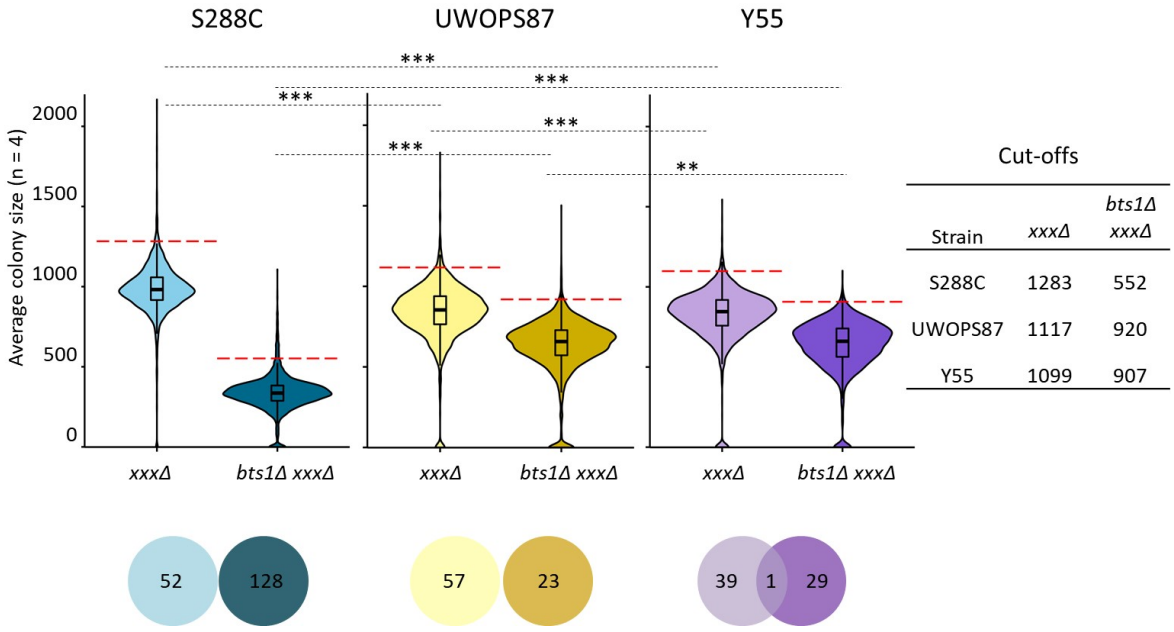

Figure 4.7: **The strength of synthetic sick/lethal and suppressor interactions differs significantly in ambient and hypoxic conditions in three genetic backgrounds.** Violin plot distributions of average fitness of ~12,900 strains as measured by average colony sizes (n = 4) of *bts1*Δ *xxx*Δ compared to *xxx*Δ single deletions in hypoxic conditions where higher scores represent increased fitness and lower scores represent decreased fitness. The red dashed lines indicate the cut-off values selected for validation in independent assays for interactions in hypoxia that did not overlap with the ones in *xxx*Δ. Venn diagrams visualise the overlap in the number of genes above the cut-off lines. Statistical differences were evaluated with a Student's *t*-test (*, $P < 0.05$ **, $P < 0.01$ ***, $P < 0.001$).

To validate the suppressor interactions identified in 1536-colony format, I established a cut-off for the average colony sizes of two standard deviations above the median for S288C and 1.5 standard deviations above the median for UWOPS87 and Y55; different standard deviation cut-offs were a consequence of the different shapes of violin plots (Figure 4.7). That way, genes with average colony sizes above 552 (pixel-based colony size values assigned in SGAtools via Gitter (Wagih and Parts 2014)) were considered hits for validation in S288C, 920 for UWOPS87 and 907 for Y55. There was only one interaction overlapping in *xxx*Δ and *bts1*Δ *xxx*Δ in Y55, which was excluded from further analyses, and none for the other two genetic backgrounds. This was somewhat surprising given that the five oxygen-dependent steps of the mevalonate pathway (Figure 4.1) may cause accumulation of oxygen-independent intermediates in both *xxx*Δ and *bts1*Δ *xxx*Δ strains and thus trigger similar survival pathways. If the *bts1*Δ strain would in theory exacerbate the accumulation of some of these intermediates, I expected to find more interactions common to the *xxx*Δ and *bts1*Δ *xxx*Δ strains.

4.3.5 Validation of hypoxia-specific suppressors of bts1Δ synthetic sick/lethal interactions

Using the cut-off criteria in the SGA analysis, I selected to validate hypoxia-specific suppressors of sickness/lethality in 128, 23 and 29 *BTS1*-deleted strains for S288C, UWOPS87, and Y55, respectively. To complement the high-throughput growth assay in 1536-colony, growth of candidate suppressor strains was monitored in an independent assay where strains were grown individually as serial dilution spots on agar (Figures 4.2B). Conditional genetic interactions conserved across the three genetic backgrounds provide insight into *BTS1*-mediated response to hypoxia. Thirteen conditional genetic interactions rescued sickness/lethality of *BTS1*-deleted strains in three genetic backgrounds (Figure 4.8; Table 4.2). Overall, *bts1*Δ *xxx*Δ double deletion conditional genetic interactions that rescued lethality in S288C also rescued synthetic sickness in UWOPS87 and Y55. Some double deletion interactions also rescued synthetic sickness of *xxx*Δ single deletions, for instance, *rpl21b*Δ, *ygr107w*Δ, *vps72*Δ and *mdm31*Δ, which was more evident in S288C than in UWOPS87 and Y55. As seen before (Figure 4.3), *bts1*Δ had similar growth to the wild types in all backgrounds in ambient conditions. As expected, *npt1*Δ was lethal in hypoxia in S288C and not in UWOPS87 and Y55; however, the double deletion *bts1*Δ *npt1*Δ was lethal for both UWOPS87 and Y55 in hypoxia, implying the need for NAD^+ biosynthesis by *NPT1* for geranylgeranylation-deficient *bts1*Δ strains. Given the phenotypes observed, I hypothesise that overexpression of the suppressor genes' human orthologues might selectively sensitise hypoxic cells to atorvastatin and potentially other anticancer treatments while having minimal effect in well oxygenated cells.

As presented in Figure 4.9, one possible explanation is that the suppressor genes are mediators of survival that are activated through a signal by either *BTS1* or an oxygen-dependent cellular metabolite, or both in the case of ambient conditions (Figure 4.9A, row 1). This would explain why deletion of *BTS1* barely affects cell fitness in ambient conditions (Figure 4.9A, row 2), the oxygen-dependent cellular metabolite would compensate and signal the suppressor gene to mediate cell survival. The suppressor genes or their products may also serve as repressors or inhibitors of buffering genes, metabolites or cellular processes (hereby, buffer genes) that only become activated when the suppressor genes are, for instance, underexpressed or deleted (Figure 4.9A, row 3). In such cases, buffer genes may become the mediators of cell survival, and hence the cells with *BTS1* and suppressor genes deleted show no fitness defect (Figure 4.9A, row 3).

In hypoxia (Figure 4.9B-C), *BTS1* also serves as a signal for the suppressor genes to mediate

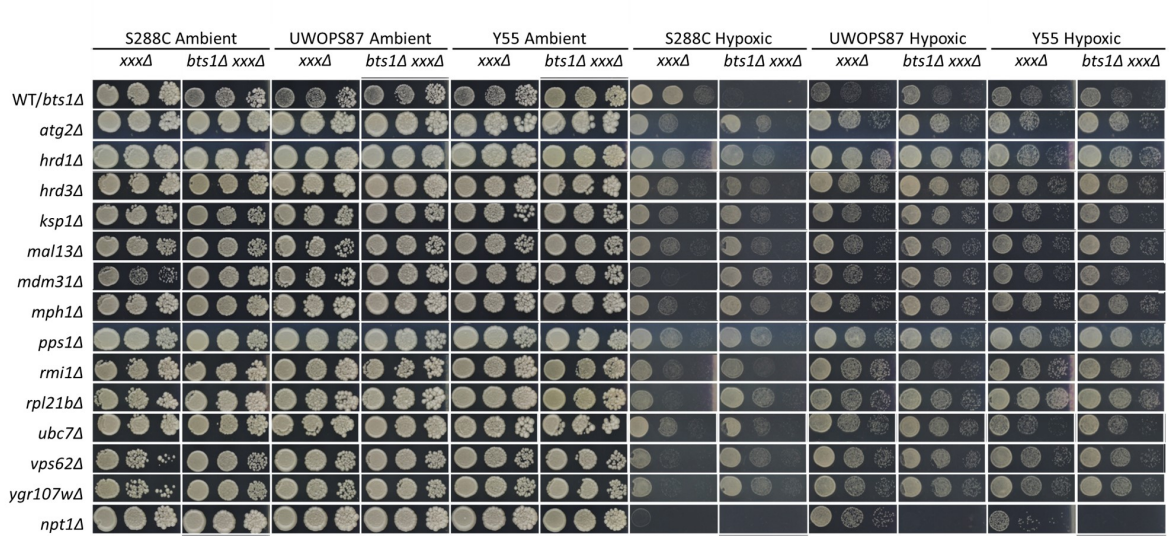

Figure 4.8: **Thirteen *bts1*Δ *xxx*Δ double deletion strains suppressed hypoxia-specific sickness/lethality of *bts1*Δ in three genetic backgrounds.** Haploid cells were pinned on SC in serial dilution and incubated for 3 days at 30°C in ambient vs hypoxic conditions. Top row shows either the wild type (WT) strains for the *xxx*Δ strain columns or the *bts1*Δ single deletions for the *bts1*Δ *xxx*Δ double deletion strain columns. The deletion *npt1*Δ was included as a control for effective hypoxia since this strain is inviable in anaerobiosis in S288C (Panozzo et al. 2002).

cell survival in S288C, but not for UWOPS87 and Y55. In turn, these may either be using a functional homologue, such as *ERG20*, which has been described as being capable of exerting a GGPP synthase function (Ye et al. 2007) or also possible is that the small concentration of oxygen may have stimulated a weak signal for the suppressor gene to mediate survival in UWOPS87 and Y55 (Figure 4.9C, row 1). The latter two genetic backgrounds do not seem to be reliant on the *BTS1* product in hypoxia to activate the suppressor genes. This explains the similar phenotypes observed regardless of *BTS1* (Figure 4.9C, rows 1 and 2) as opposed to the synthetic lethality observed in S288C genetic background upon deletion of *BTS1* in hypoxia (Figure 4.9B, row 2).

The suppressor genes being repressors or inhibitors of buffer genes that mediate cell survival would thus explain the rescued synthetic lethality in S288C (Figure 4.9B, row 3), since the lack of expression of the suppressor gene may be the signal for the buffer genes to be activated. Similarly, I hypothesise that the suppressor genes are as well repressors or inhibitors of buffering pathways in UWOSP87 and Y55 regardless of *BTS1* expression (Figure 4.9C, row 3), since deletion of the suppressor genes would also have served as a signal for the buffer genes (or metabolites) to be triggered enhancing cell survival and thus rescuing the synthetic sickness observed for the strains where the suppressor genes were not deleted (Figure 4.9C, rows 1 and 2). *BTS1* thus seems to participate in the signalling for suppressor genes to mediate cell survival in hypoxia in S288C and a weak signal from an oxygen-dependent metabolite but not in UWOPS87 and Y55. Regardless of the origin of this signal, the suppressor

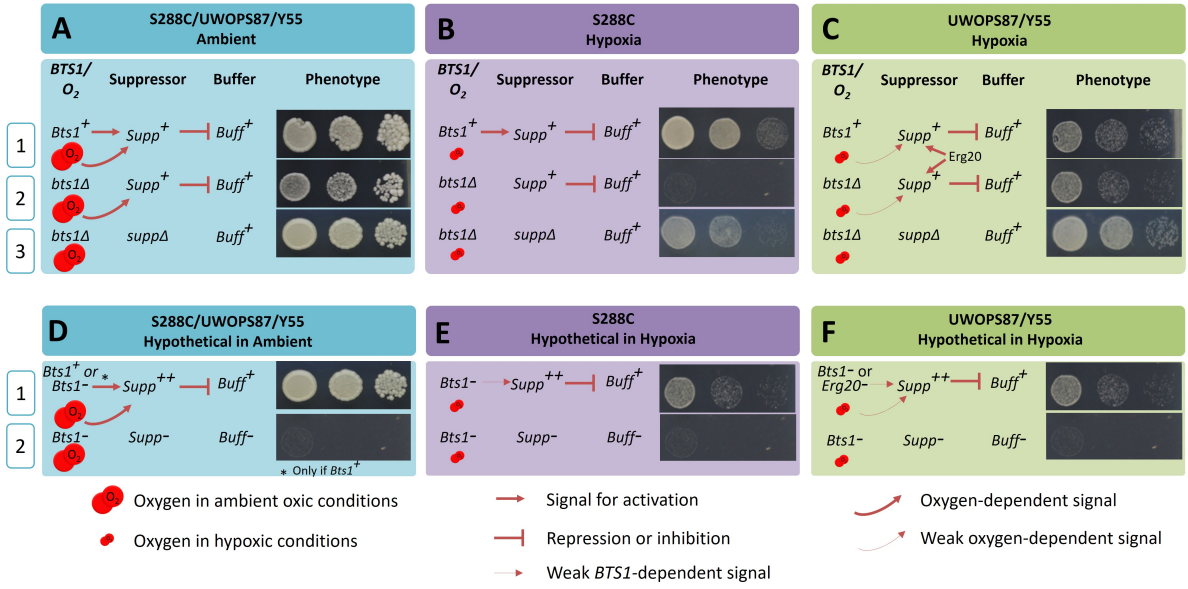

Figure 4.9: **Overexpression of suppressor genes conditionally mediates cell death in hypoxia.** Panel A shows the proposed *BTS1*- and oxygen-dependent regulation of the suppressor genes and the proposed repression/inhibition of buffer genes in ambient normoxic conditions. Panel B shows the proposed *BTS1*-dependent regulation of the suppressor genes in hypoxia in S288C and similarly, the repression/inhibition of buffer genes. Panel C shows the proposed weak oxygen-dependent regulation of the suppressor genes in hypoxia in UWOPS87 and Y55 and repression of the buffer genes. Panels D, E and F visualise the hypothesis proposed in this figure that overexpression of suppressor genes should inhibit growth in hypoxia but not in ambient normoxic conditions. This figure shows one example taken from Figure 4.8, but the hypotheses presented here should be applicable to all suppressors in Figure 4.8. *Bts1*$^{+}$ = non-mutated *BTS1* (wild type allele); *Supp*$^{+}$ = non-mutated suppressor gene (wild type allele); *Buff*$^{+}$ = non-mutated buffer gene (wild type allele); *bts1*Δ = deleted *BTS1*; *supp*Δ = deleted suppressor gene; *buff*Δ = deleted buffer gene; *Bts1*- = inhibited *BTS1* (*e.g.*, with atorvastatin); *Supp*- = inhibited suppressor gene; *Buff*- = inhibited buffer gene; *Supp*$^{++}$ = overexpression of the suppressor gene.

genes seem to be negative regulators of buffer genes or metabolic pathways for cell survival.

I thus hypothesise that overexpression of the suppressor genes with inhibited *BTS1*, *i.e.* atorvastatin treatment, should lead to a fitness defect (sickness or lethality) in all three genetic backgrounds specific to hypoxia (Figure 4.9D-F, row 1) because in every case the signal to activate the suppressors' cell survival activity would be weak (inhibited *BTS1*, *ERG20* or inhibited oxygen supply) but also overexpression would impede any triggering of the buffering metabolic pathway thus leading to cell death. Cells in ambient conditions should not undergo the same fate since the suppressor gene would be signalled from either *BTS1*, the oxygen-dependent metabolite, or both. Simultaneous inhibition of *BTS1*, the suppressor genes and buffering genes may also be lethal, however, this combination may also become too toxic for cells in ambient conditions (Figure 4.9D-F, row 2).

Annotation of suppressors

Of the 13 suppressors of hypoxia-specific atorvastatin lethality (Table 4.2), nine are involved in metabolic pathways having a role in cell survival. Three are subunits of the HRD1 complex (*HRD1*, *HRD3* and *UBC7*) that participate in the ER-associated degradation pathway (ERAD). Two other genes have roles in autophagy (*KSP1* and *ATG2*) and four genes are involved in cell cycle and responses to DNA stress (*PPS1*, *KSP1*, *ATG2* and *RMI1*). Two of these genes have contrasting roles emphasising the complexity of the responses to hypoxia; *PPS1* is a Ser/Thr/Tyr phosphatase involved in the DNA synthesis phase of the cell cycle (S phase) whereas *KSP1* is a Ser/Thr kinase involved in DNA replication stress. Interestingly, the DNA helicase *MPH1* is the yeast orthologue of the human FANCM Fanconi anemia gene in which mutations have been linked to increased incidence of cancer. Taken together, these results suggest that genes involved in the ERAD pathway, autophagy and cell cycle are mediators of lethality (or survival) in hypoxia that may be enhanced by atorvastatin and that the specific suppressors of lethality identified in this section should aid in the design of therapeutics or combination therapies to either suppress or enhance their activity to treat hypoxic tumours.

4.3.6 Multi-layer network analysis enhances connectivity of networks

Similar to a single-layer network, albeit just more complex, aggregated networks are n-dimensional matrices or tensors that can be investigated using mathematical methodologies as explained before. In this case, consistent with previous chapters, the first layer was derived from GINs, the second layer derived from PPINs, and the aggregated network was derived from both GINs and PPINs (Figures 4.2C). These networks were created for the nine *xxx*Δ single deletion genes that conferred hypersensitivity to atorvastatin treatment (Table 4.1), as well as the 13 *bts1*Δ *xxx*Δ double deletion strains that suppressed synthetic sickness/lethality in hypoxia (Table 4.2).

As expected, the aggregated network (Figure 4.10) contained 11 gene nodes that were common to both GINs and PPINs in the multi-layer analysis for the deletions sensitive to atorvastatin treatment. However, many more, specifically 57 genes were shared between GINs and PPINs for the suppressors of sickness/lethality, which included the input genes. These comprised mainly genes involved in ribosomal activity (*e.g.*, RPL genes), mitochondrial homeostasis (*e.g.*, MDM genes), proteasome degradation (*e.g.*, UBC and HRD genes) and secretory pathway (*e.g.*, ERV and SEC genes). The aggregated network for single deletions sensitive to atorvastatin comprised 274 nodes and 1281 edges (interactions), as opposed to the GIN (110 nodes, 500 edges) and PPIN (175 nodes, 814 edges) alone.

ORF	Gene	Name	Description	Human orthologue(s)
YNL242W	*ATG2*	AuTophaGy related	Peripheral membrane protein required for autophagic vesicle formation; also required for vesicle; contains an APT1 domain that binds phosphatidylinositol-3-phosphate; essential for cell cycle progression from G2/M to G1 under nitrogen starvation; forms cytoplasmic foci upon DNA replication stress	ATG2A, ATG2B
YOL013C	*HRD1*	HMG-coA Reductase Degradation	Ubiquitin-protein ligase involved in ER-associated degradation (ERAD) of misfolded proteins; upon autoubiquitination triggers retrotranslocation of misfolded proteins to cytosol for degradation; genetically linked to the unfolded protein response (UPR); regulated through association with Hrd3p; contains an H2 ring finger; likely plays a general role in targeting proteins that persistently associate with and potentially obstruct the ER-localized translocon	RNF145, AMFR, SYVN1
YLR207W	*HRD3*	HMG-coA Reductase Degradation	ER membrane protein that plays a central role in ERAD; forms HRD complex with Hrd1p and ER-associated protein degradation (ERAD) determinants that engages in lumen to cytosol communication and coordination of ERAD events	SEL1L, SEL1L2, SEL1L3
YHR082C	*KSP1*	Kinase Suppressing Prp20-10	Serine/threonine protein kinase; associates with TORC1, negative regulator of autophagy; protein abundance increases in DNA replication stress	None
YGR288W	*MAL13*	MALtose fermentation	Part of complex locus MAL1; nonfunctional in genomic reference strain S288C	None
YHR194W	*MDM31*	Mitochondrial Distribution and Morphology	Mitochondrial protein that may have a role in phospholipid metabolism; required for normal mitochondrial morphology and inheritance	None
YIR002C	*MPH1*	Mutator PHenotype	3'-5' DNA helicase involved in error-free bypass of DNA lesions; binds flap DNA, stimulates activity of Rad27p and Dna2p	FANCM
YBR276C	*PPS1*	Protein Phosphatase S phase	Protein phosphatase with specificity for serine, threonine, and tyrosine and a role in S phase of the cell cycle	DUSP14, DUSP10, PTPMT1, DUSP15, DUSP19, CCDC155, DUSP18, DUSP1, DUSP2, DUSP3, DUSP4, DUSP5, DUSP6, DUSP7, DUSP8, DUSP9, DUSP28, DUPD1, DUSP13, STYXL1, SSH1, SSH3, DUSP22, DUSP21, STYX, DUSP26, DUSP16, SSH2, DUSP27
YPL024W	*RMI1*	RecQ Mediated genome Instability	Stimulates superhelical relaxing, DNA catenation/decatenation and ssDNA binding activities of Top3p; involved in response to DNA damage; functions in S phase-mediated cohesion establishment via a pathway involving the Ctf18-RFC complex and Mrc1p; null mutants display increased rates of recombination and delayed S phase	None
YPL079W	*RPL21B*	Ribosomal Protein of the Large subunit	Ribosomal 60S subunit protein L21B	RPL21
YMR022W	*UBC7*	UBiquitin-Conjugating enzyme	Involved in the ERAD pathway and in the inner nuclear membrane-associated degradation (INMAD) pathway; proposed to be involved in chromatin assembly	UBE2G1, UBE2G2, UBE2R2, CDC34
YGR141W	*VPS62*	Vacuolar Protein Sorting	Required for cytoplasm to vacuole targeting of proteins	None
YGR107W	*YGR107W*	ORF, Dubious	Dubious open reading frame; unlikely to encode a functional protein	None

Table 4.2: **List of validated hypoxia-specific suppressors overlapping in three genetic backgrounds.** Description was obtained from SGD (Cherry et al. 2012). Human orthologues were obtained from YeastMine (Balakrishnan et al. 2012).

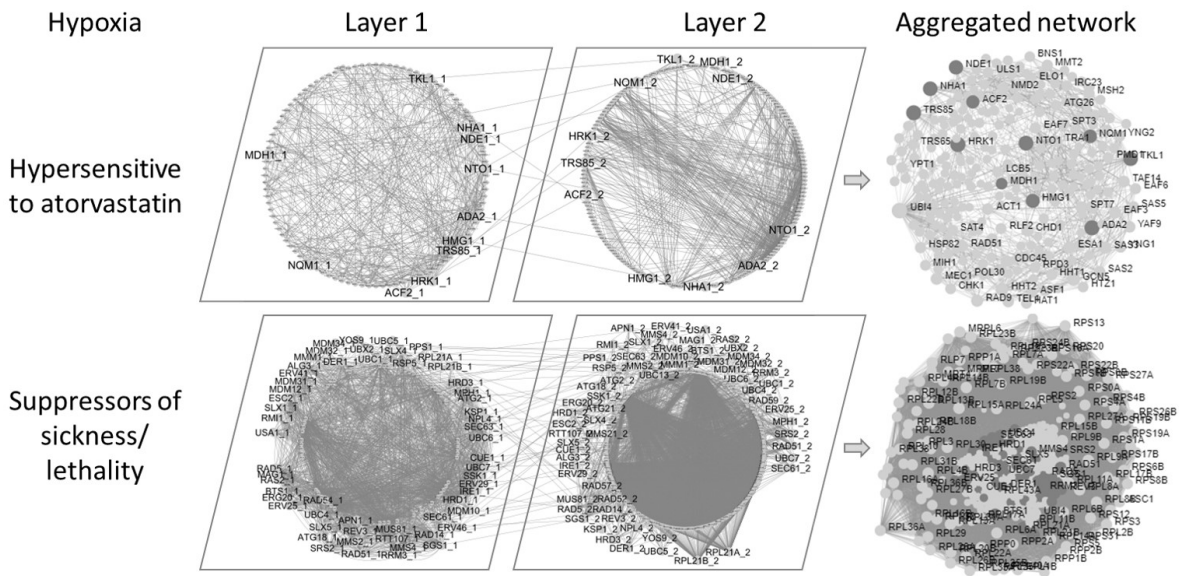

Figure 4.10: **Multi-layer networks of gene deletions that were either sensitive to atorvastatin in hypoxia or suppressed sickness/lethality of *bts1*Δ.** GINs (Layer 1), PPINs (Layer 2) and the edges between them were integrated in an aggregated network using TimeNexus. Edges between layers connect overlapping nodes in the two layers and the genes linking these edges are shown in the periphery of circular networks. Darker nodes in aggregated networks are validated hits.

For the suppressors of *BTS1*-mediated synthetic sickness/lethality, the aggregated network was highly interconnected with 420 nodes and 10,478 edges (GIN = 114 nodes, 1975 edges; PPIN = 363 nodes, 9260 edges) (Figure 4.10). This is expected given the highly interactive activity of genes involved in the aforementioned processes.

4.3.7 Network topology identifies bottleneck genes through centrality analyses

To obtain functional insight of the aggregated networks, three measurements of centrality (degree (deg), closeness (close) and betweenness (bet)) were obtained for every gene in each aggregated network (Figures 4.2D and 4.11). *UBI4* was excluded from the 3D plots, just as it was in Chapter 2, because it obscured the relevance of other genes due to its highly interacting nature. The protein kinase *HRK1* was the top ranked interaction based on centrality (bet = 0.14, close = 0.50, deg = 41) and was indeed one of the validated hits that showed enhanced toxicity of atorvastatin in hypoxia (Figure 4.6; Table 4.1), emphasising the importance of *HRK1* function in Na^+/K^+ ion homeostasis and the response to DNA replication stress. *HRK1* has two orthologue genes in humans, HUNK and PRKAA2 (Table 4.1), which I hypothesise are candidate targets to enhance the anticancer activity of statins in hypoxic tumours.

Other genes that were highly central to the network and thus important buffers of atorvastatin

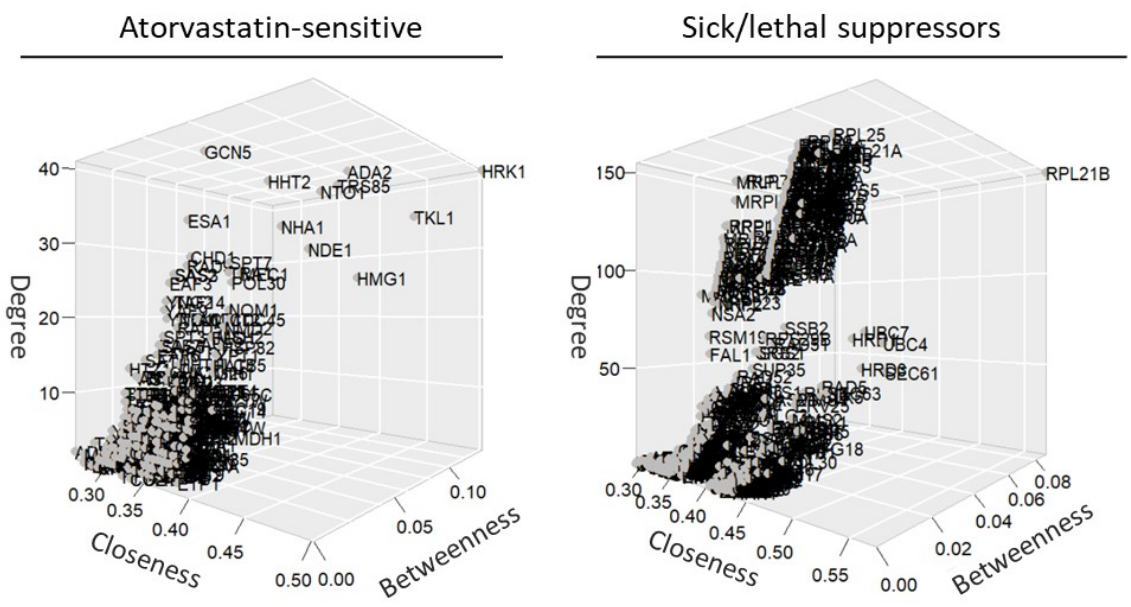

Figure 4.11: **Network topology centrality analyses of aggregated networks identify key interactors for atorvastatin sensitivity and suppressors of *BTS1*-mediated growth defects in hypoxia.** Centrality measurements (degree, closeness and betweenness) were calculated for each gene and visualised in a 3D plot.

treatment in hypoxia were *NTO1* (bet = 0.06, close = 0.42, deg = 36) and *TKL1* (bet = 0.09, close = 0.48, deg = 33) (Figure 4.11 left panel), both of which have human orthologues (Table 4.1) and *TRS85* (bet = 0.08, close = 0.41, deg = 38) that has one human orthologue TRAPPC8. These would all be potential candidate genes to target in human cell lines and animal models to enhance the anticancer activity of statins in hypoxic tumours, particularly with *TKL1*, *NTO1* and *TRS85* being involved in fundamental processes of the pentose phosphate pathway, histone acetylation and endosome-Golgi transport, respectively.

To identify the top central genes, I generated individual networks for the top ten betweenness, closeness and degree centralities (Figure 4.12). For the atorvastatin-sensitive single gene deletions, the atorvastatin target *HMG1* itself ranked as one of the top 10 genes for both betweenness and closeness (bet = 0.07, close = 0.45, deg = 25), supporting the idea that the interactors should enhance the anticancer activity or atorvastatin in hypoxic tumours (Figure 4.12 left panel). Other genes that showed their relevance in this analysis were *NTO1*, which has a role in the acetylation of histones (Table 4.1), and two other genes that were central to the network (not sensitive genes themselves) were *ADA2* (bet = 0.06, close = 0.45, deg = 38) and *HHT2* (bet = 0.02, close = 0.43, deg = 35), the former being a transcription coactivator with a role in the acetylation of histones (Sterner et al. 2002) and the latter a core histone protein required for chromatin assembly (Duan and Smerdon 2014). These

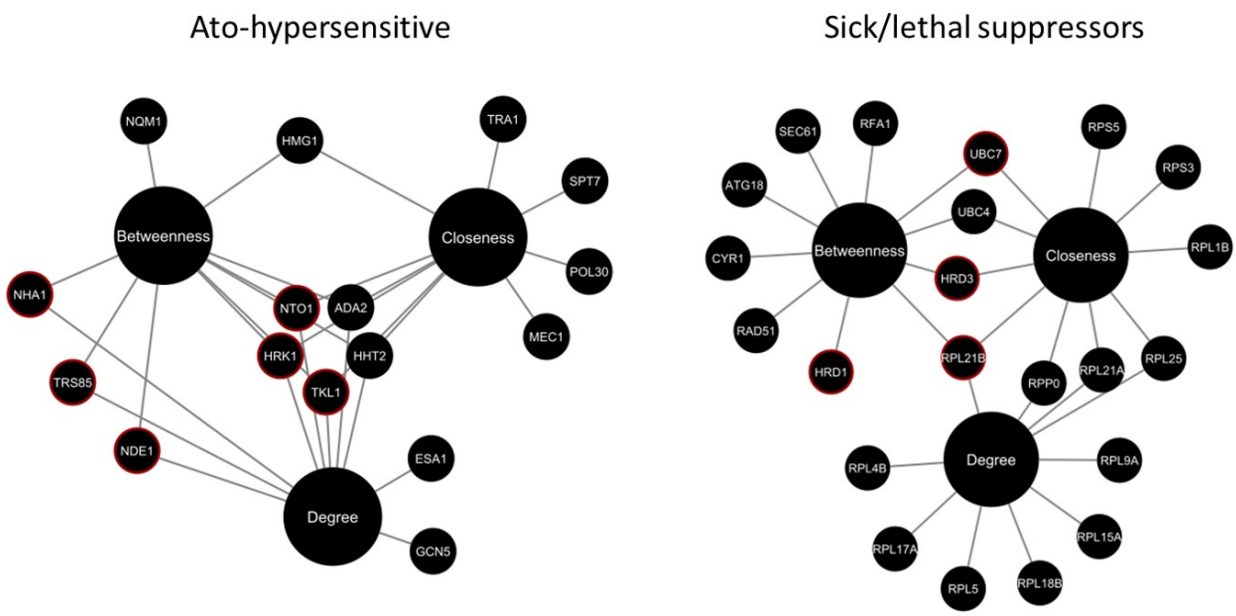

Figure 4.12: **Network centrality of genes behind sensitivity to atorvastatin in hypoxia and suppression of hypoxia-specific atorvastatin sensitivity in *bts1*△.** Genes that ranked in the top ten centrality measurements were found to confirm phenotypic findings. Centrality measurements (betweeness, closeness and degree) were calculated in NetworkAnalyzer app in Cytoscape (Boccaletti et al. 2014) and networks were built in Cytoscape. The red outline points to validated hypoxia-specific interactors.

observations suggest chromatin remodelling is an important biological process behind hypoxia-specific sensitivity to atorvastatin.

In the case of suppressors of hypoxia-specific sickness/lethality with *BTS1*-deficiency (Figure 4.12, right panel), I found that the top central gene to this network was *RPL21B* (bet = 0.09, close = 0.57, deg = 155), revealing the importance of ribosomal activity and translation in regulating cell death in hypoxia. Closer inspection of the top 10 centralities revealed that ERAD genes were also central to the network of *BTS1* suppressors including *HRD1* (bet = 0.02, close = 0.50, deg = 67), *HRD3* (bet = 0.02, close = 0.50, deg = 54) and *UBC7* (bet = 0.02, close = 0.50, deg = 70), which each contribute to cell survival. *UBC4* (bet = 0.03, close = 0.52, deg = 65) also appeared in the centrality analyses, and while *UBC4* mediates protein quality control, it does not participate in ERAD, thus perhaps uncovering another role of ubiquitination behind the hypoxia-induced sickness/lethality. Other high betweenness genes were *SEC61* (bet = 0.03, close = 0.50, deg = 51), *ATG18* (bet = 0.02, close = 0.45, deg = 17), *RAD51* (bet = 0.02, close = 0.42, deg = 64), *RFA1* (bet = 0.02, close = 0.46, deg = 30) and *CYR1* (bet = 0.02, close = 0.45, deg = 16) that are involved in protein secretion, autophagy, cell cycle and stress response, respectively.

4.3.8 Community analysis reveals pathways mediating atorvastatin hypersensitivity and BTS1-mediated suppression of lethality in hypoxia

To gain more insight into the structural organisation of the aggregated networks, the hypoxia-specific networks were partitioned through community analysis (Figure 4.2E). In this analysis, 3-4 modules were detected in each network with significant enrichment for metabolic pathways ($P < 0.05$), and in most cases, pathways enriched in the modules in the network pertaining to sensitivity to atorvastatin overlapped with the enriched modules in the network for suppressors of *BTS1*-mediated sickness/lethality (Figure 4.13). For instance, out of 17 pathways enriched in the former and 23 in the latter, 11 pathways overlapped, emphasising the relevance of these particular pathways to atorvastatin response in hypoxia. These pathways were autophagy, base excision repair, cell cycle, DNA replication, homologous recombination, meiosis, mismatch repair, mitophagy, non-homologous end-joining, nucleotide excision repair and terpenoid backbone synthesis. The latter serves as proof-of-principle that fundamental aspects of atorvastatin bioactivity are maintained in hypoxia.

Autophagy, DNA replication and endocytosis were three metabolic pathways enriched in the community analysis for the genes that enhanced the toxicity of atorvastatin in hypoxia (Figure 4.13), which show complementarity between centrality analyses and community analyses. I also found metabolic pathways relevant to the hypoxia-induced toxicity of atorvastatin that were not yet identified in this chapter such as longevity regulating pathway, MAPK signalling pathway, meiosis and cell cycle, proteasome and homologous recombination. Further characterisation of the involvement of these pathways in the modulation of cell death in hypoxia should be considered in future analyses in both yeast and human cells.

Similarly, the most important metabolic pathways that were identified in the previous sections were supported by the findings in the community analysis, such as ribosomal activity and translation (ribosome), DNA replication, cell cycle, protein processing in ER (ERAD) and ubiquitin-mediated proteolysis (Figure 4.13); the latter two confirm that not only ERAD is an important mediator of sickness/lethality in hypoxia but also non-ER proteasomal degradation. Some metabolic pathways that were enriched in the community analysis, but not yet with other analyses, were homologous recombination, protein export, meiosis and *N*-glycan biosynthesis; these should as well be interesting pathways to further characterise in future assays. These findings also emphasise the complementarity of centrality and community analyses, one confirming the results of the other, with each adding information that may have been overlooked in the original phenotypic assay (growth in hypoxia in

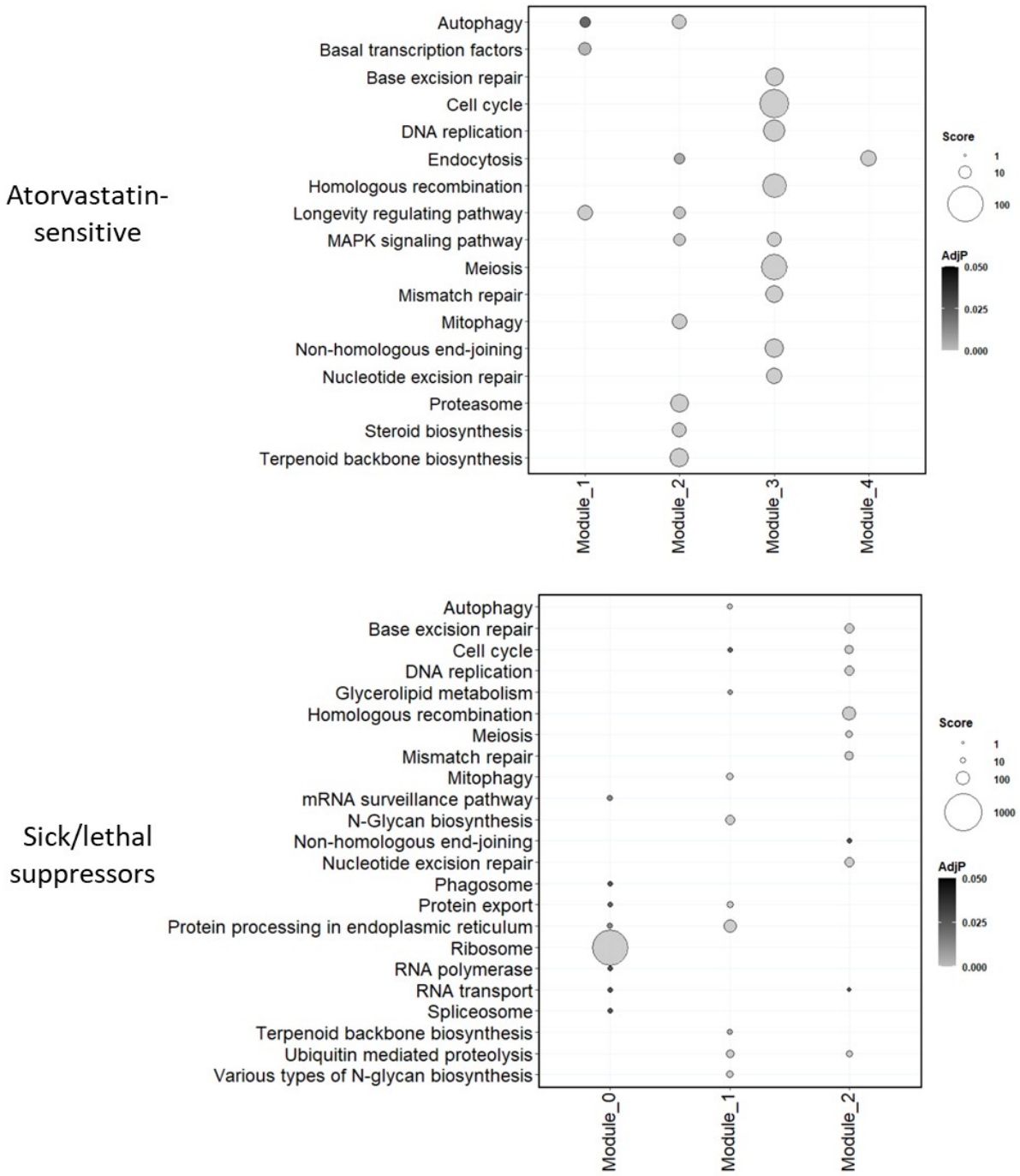

Figure 4.13: **Metabolic pathway enrichment of modules in hypoxia-specific aggregated networks.** Bubble plots showing enrichment for each of the modules identified through community analysis for *xxx*Δ interactions sensitive to atorvastatin in hypoxia (top panel) and suppressors of *bts1*Δ sickness/lethality in hypoxia (bottom panel). The size of the bubbles is relative to the enrichment score for each pathway, while the intensity of the grey scale is relative to the adjusted *P* value. The x axis shows modules that were significantly enriched for a pathway ($P < 0.05$). Module numbers were assigned by NetworkAnalyst.

this case).

4.3.9 Humanised enrichment analysis identifies candidate drugs to improve anticancer activity of statins in hypoxic tumours

Combination therapies increase efficacy of repurposed drugs (Sun et al. 2016). Synergy with statins has been previously examined (Agrawal et al. 2019; Jouve et al. 2019; Kim et al. 2014; Kim et al. 2019), but not in the context of building off genes identified in unbiased genome-wide analyses in hypoxia. Therefore, I identified the human orthologues of key hub/bottleneck genes identified in my yeast genomic analyses in three genetic backgrounds that suppressed sickness/lethality of *BTS1*-deleted strains (Table 4.3) and integrated these genes in an enrichment analysis in the gene set analysis database Drug Signature Database (Yoo et al. 2015), which detects over-representation of drugs and compounds with 'signature genes' integral to their bioactivity (Figure 4.2F). Given the subtle growth defect phenotypes of the atorvastatin-treated single deletions in hypoxia (Figure 4.6), these were excluded from this analysis. A total of 766 drugs and compounds were identified of which 82 had adjusted *P* values lower than 0.05. Of these, the maximum and minimum odd ratios were 77 and 3, respectively. I then selected a cut-off for the top 20 drugs and compounds based on the lowest adjusted *P* values since these represent the highest enrichment.

Yeast gene	Human orthologue	Yeast gene	Human orthologue	Yeast gene	Human orthologue
ATG2	ATG2A	*PPS1*	DUSP16	*PPS1*	SSH2
ATG2	ATG2B	*PPS1*	DUSP18	*PPS1*	SSH3
BTS1	GGPS1	*PPS1*	DUSP19	*PPS1*	STYX
HMG1	HMGCR	*PPS1*	DUSP2	*PPS1*	STYXL1
HRD1	AMFR	*PPS1*	DUSP21	*RPL21B*	RPL21
HRD1	RNF145	*PPS1*	DUSP22	*UBC4*	UBE2D1
HRD1	SYVN1	*PPS1*	DUSP26	*UBC4*	UBE2D2
HRD3	SEL1L	*PPS1*	DUSP27	*UBC4*	UBE2D3
HRD3	SEL1L2	*PPS1*	DUSP28	*UBC4*	UBE2D4
HRD3	SEL1L3	*PPS1*	DUSP3	*UBC4*	UBE2E1
MDM31	FANCM	*PPS1*	DUSP4	*UBC4*	UBE2E3
PPS1	CCDC155	*PPS1*	DUSP5	*UBC4*	UBE2L3
PPS1	DUPD1	*PPS1*	DUSP6	*UBC4*	UBE2L6
PPS1	DUSP1	*PPS1*	DUSP7	*UBC4*	UBE2W
PPS1	DUSP10	*PPS1*	DUSP8	*UBC7*	CDC34
PPS1	DUSP13	*PPS1*	DUSP9	*UBC7*	UBE2G1
PPS1	DUSP14	*PPS1*	PTPMT1	*UBC7*	UBE2G2
PPS1	DUSP15	*PPS1*	SSH1	*UBC7*	UBE2R2

Table 4.3: **Human orthologues of validated interactors and key network centrality genes used as input for enrichment analysis in Drug Signature Database.** Human orthologues were obtained from YeastMine (Balakrishnan et al. 2012). Yeast gene column comprises all validated hits, main network centrality genes and query genes.

To compare the chemical genetic profiles of the top-ranked drugs/compounds, the odds ratio values for the top 20 drugs/compounds and their signature genes were visualised in a bubble plot (Figure 4.14). The 23 signature genes represented five major processes. All drugs/compounds were correlated with at least two out of 11 members of the Dual Specificity Phosphatases (DUSPs) (Huang and Tan 2012). Twelve drugs/compounds (ciclopirox, trichostatin, vorinostat, astemizole, pimozide, monensin, niclosamide, deoxynivalenol, thioridazine, 0175029-0000, fluspirilene, mitoxantrone) were correlated with genes involved in the biosynthesis of lipids (HMGCR, PTPMT1). Six drugs/compounds (setraline, trichostatin, perphenazine, 0175029-0000, mitoxantrone, chlorprothixene) were correlated with genes involved in UPR and ubiquitin-mediated proteolysis (CDC34, SEL1L, SEL1L2, SYVN1, UBE2G1, UBE2G2). Five drugs/compounds (mebendazole, trichostatin, vorinostat, 8-azaguanine, 0175029-0000) were correlated with genes involved in autophagy (ATG2A, ATG2B). Three drugs/compounds (mebendazole, podophyllotoxin, 0175029-0000) were correlated with SSH1, a mediator of actin cytoskeleton.

All of the top 20 drugs/compounds identified in this analysis are either well established anticancer therapeutics (azacitidine, vorinostat) or have shown to exert anticancer activity. Of these, three compounds are under investigation for their antineoplastic activity (trichostatin A, 8-azaguanine, 0175029-0000), five are approved or retired drugs for the treatment of mental disorders (sertraline, pimozide, perphenazine, thioridazine, chlorprotixene), six are antibacterial, antifungal or antiparasitic drugs (primaquine, ciclopirox, mebendazole, monensin, niclosamide, mitoxantrone), one is a withdrawn antiallergic (astemizole) and one is used for the treatment of warts (podophyllotoxin). Sertraline ranked the highest of all drugs/compounds (P = 4.92E-06; odds ratio = 37), mainly due to dual specificity phosphatases and genes involved in UPR pathways. Sertraline is an antidepressant with anticancer activity (Table 4.4) (Zinnah et al. 2020). Clinical trial NCT02770378 is evaluating the safety of nine repurposed drugs, including sertraline in combination with metronomic temozolomide for recurrent glioblastoma. Azacitine, a well established antineoplastic, is in an active trial in combination with venetoclax and pitavastatin for the treatment of leukemia (NCT04512105). Mebendazole, an anthelmintic with anticancer activity, is being trialled (NCT02201381) for its safety, tolerabiliy and efficacy of combination therapies against cancer with metformin, atorvastatin and doxycline. Perphenazine, an antipsychotic with anticancer properties has been trialled in combination with simvastatin (NCT00802100) to limit treatment side effects in patients with schizophrenia, but not in the context of cancer. Mitoxantrone was also trialled (NCT01342887) for combination therapy with cyclosporine, pravastatin and etoposide in treating patients with acute myeloid leukemia but the study

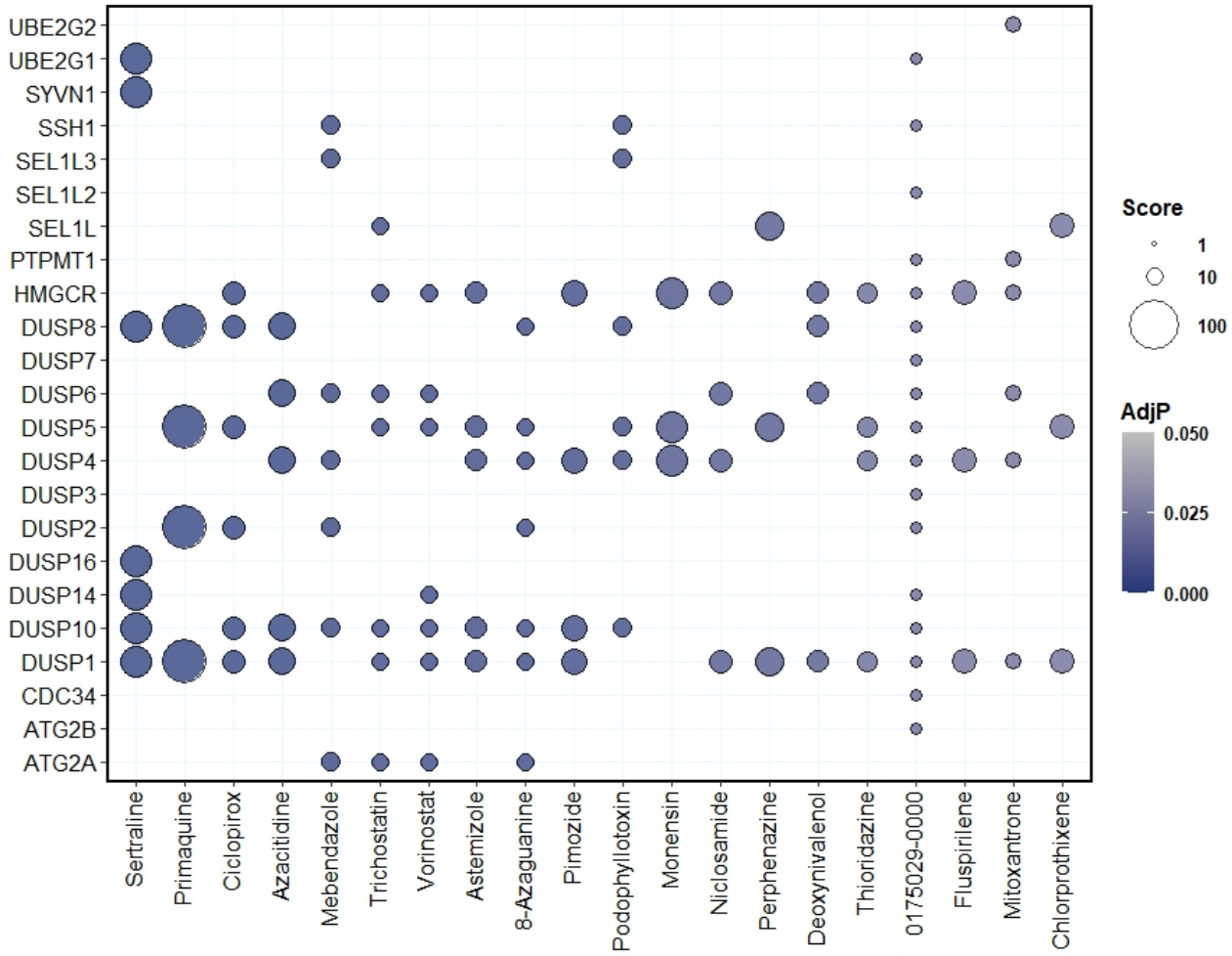

Figure 4.14: **Human orthologues of validated interactors and key network centrality genes reveal drugs/compounds to test for synergy with atorvastatin in hypoxia.** Human orthologues of validated genes and genes identified through centrality analyses were processed via an enrichment analysis for signature genes in the Drug Signature Database. Bubble plot representing the human orthologues (y-axis) that were enriched for drugs/compounds (x-axis). The colour of each bubble is determined by the *P*-value and the size of bubble reflects the odds ratio, where bigger bubbles represent greater enrichment.

was terminated for unstated reasons. None of these trials, however, involve the treatment of hypoxic tumours. Interestingly, vorinostat was also one of the top 20 drugs that share signature genes with atorvastatin in Chapter 2, and niclosamide was one of the top 20 drugs in both Chapters 2 and 3, giving proof of principle for their potential as candidate combination therapies with atorvastatin against cancer, which have not been trialled to date.

Drug/compound	Description	Approved	Intended use	Cancer clinical trials	Clinical trials with statin
Sertraline	Selective serotonin reuptake inhibitor (SSRI)	Yes	Depression, anxiety disorders and obsessive -compulsive disorder with anticancer properties	Yes	No
Primaquine	Synthetic, 8-aminoquinoline derivative	Yes	Anti-malaria that sensitises cancer cells to treatments	No	No
Ciclopirox	Inhibits availability of essential co-factors for enzymes	Yes	Broad-spectrum antifungal agent with additional antibacterial and anti-inflammatory activities and anticancer activity	Yes	No
Azacitidine	Pyrimidine nucleoside analogue of cytidine	Yes	Antineoplastic	NA	Yes
Mebendazole	Synthetic benzimidazole derivate	Yes	Anthelmintic agent with anticancer properties	Yes	Yes
Trichostatin A	Natural derivative of dienohydroxamic acid	No	Inhibition of tumor growth	Yes	No
Vorinostat	Synthetic hydroxamic acid derivative	Yes	Antineoplastic	NA	No
Astemizole	Synthetic piperidinyl-benzimidazol derivative	Retired	Antiallergic wit anticancer properties	No	No
8-Azaguanine	Purine analogue	No	Antineoplastic	No	No
Pimozide	Diphenylbutylpiperidine derivative and a dopamine antagonist	Yes	Antipsychotic with anticancer properties	No	No
Podophyllotoxin	Pure, stabilized form of podophyllin	Yes	For treatment of external genital warts with anticancer properties	Yes	No
Monensin	Polyether isolated from Streptomyces cinnamonensis	Yes	Antibiotic for ruminant animal feeds with anticancer propeties	No	No
Niclosamide	Orally bioavailable chlorinated salicylanilide	Yes	Anthelmintic and potential antineoplastic activity	Yes	No
Perphenazine	Phenothiazine derivative and a dopamine antagonist	Yes	Antipsychotic with anticancer properties	Yes	Yes
Deoxynivalenol	Natural-occurring mycotoxin	No	Mycoherbicide with anticancer properties	No	No
Thioridazine	Phenothiazine derivative	Retired	Antipsychotic with anticancer properties	Yes	No
0175029-0000	Cyclin-dependent kinase inhibitor	No	Potential anticancer properties	No	No
Fluspirilene	Diarylmethane	No	Antipsychotic agent	No	No
Mitoxantrone	Dihydroxyanthraquinone	Yes	Antibiotic with antineoplastic activity	Yes	Yes
Chlorprothixene	Organochlorine compound	Retired	Antipsychotic with anticancer properties	No	No

Table 4.4: **The top 20 drugs that share signature genes with atorvastatin identified have anticancer activity.** Description and intended uses were obtained from PubChem (Kim et al. 2021), while clinical trials were identified at https://clinicaltrials.gov/.

4.4 Discussion

4.4.1 Summary

In this chapter I have identified conditional genetic interactions that enhance the toxicity of atorvastatin in hypoxic conditions in three yeast genetic backgrounds, one that is naturally sensitive to atorvastatin treatment (S288C) and two that are naturally resistant to atorvastatin treatment (UWOPS87 and Y55). Because hypoxia is a mechanism of decreased sensitivity to anticancer treatments (*e.g.*, radiotherapy) and poor prognosis (Gray et al. 1953; Sørensen and Horsman 2020; Thomlinson and Gray 1955), my experimental strategy involved elucidating genes enhancing toxicity of atorvastatin in hypoxia while having low toxicity in normal oxygenated conditions. GGPPS1 enhances anticancer activity of statins when silenced in humans (Pandyra et al. 2015) and the yeast homologue of GGPPS1, *BTS1*, is synthetic lethal in hypoxia in the S288C yeast genetic background (Figure 4.3), thus I also sought suppressors of lethality in hypoxia. These complementary approaches may potentiate the anticancer activity of atorvastatin and potentially other cancer therapeutics. Since deletion of genes in the HRD complex rescued lethality of *BTS1*-deficient strains and deletion of *SND2* enhanced toxicity of atorvastatin in hypoxia, I identified the HRD complex as a major mediator of cell survival induced by the metabolic products of *BTS1* and possibly its paralogue *ERG20*. The HRD complex may be a repressor or inhibitor of compensatory pathways such as the SRP-independent alternative targeting pathway to the ER mediated by *SND2*. I also identified candidate combination therapies with established anticancer therapeutics (azacitidine, vorinostat), and drugs/compounds with other primary and intended uses but that have shown anticancer activity (*e.g.*, sertraline, primaquine, ciclopirox, mebendazole, astemizole, 8-azaguanine).

4.4.2 Yeast as a model to study hypoxic tumours and their response to statin therapy

Here, I have used yeast models for the study of the anticancer activity of atorvastatin in hypoxic tumours by screening for conditional genetic interactions with the additional environmental stress of hypoxia. The effect of anaerobic stress has been investigated in genome-wide analyses of the yeast deletion library in S288C (Munkacsi et al. 2011; Reiner et al. 2006). Here I have expanded the knowledge on how genetic background influences conditional genetic interactions in response to hypoxia. In good agreement with other environmental conditions (Costanzo et al. 2021), most of the interactions identified in my hypoxia condition were shared with the interactions identified in ambient

conditions, reiterating global robustness to environmental perturbation in yeast.

My model also added information pertaining to the influence of genetic background and the response to hypoxia. Fitness defects in temperature-sensitive alleles of yeast essential genes, for instance, have been shown to vary in different genetic backgrounds (Parts et al. 2021). I was able to identify conditional genetic and conditional chemical genetic interactions that were conserved across genetic backgrounds and some that were unique to each genetic background. Two findings that stood out were the phenotypes of *BTS1*- and *NPT1*-deleted strains. It has been acknowledged for years that these strains in S288C are inviable in anaerobiosis (Panozzo 2002, Ishtar Snoek and Yde Steensma 2006). Here I have shown that this phenotype is in fact dependent on genetic background with these strains being viable in UWOPS87 and Y55 in hypoxia. Interestingly, the double deletion of both genes in all three genetic backgrounds was inviable, indicating a highly conserved conditional genetic interaction specific to hypoxia.

4.4.3 ERAD-mediated cell survival is a potential target to enhance atorvastatin and other therapeutic treatments against hypoxic tumours

One of the main findings from this chapter was that specific genes involved in ERAD-mediated cell survival were suppressors of conditional lethality in hypoxia. I hypothesised that the yeast strains may be reliant on either *BTS1* or on a functional homologue, such as *ERG20*, to signal the suppressor genes to trigger cell survival pathways and that overexpression of the suppressor genes' human orthologues might selectively sensitise hypoxic cancer cells to atorvastatin and potentially other anticancer treatments. Interestingly, *ERG20* along with *BTS1* and the atorvastatin target *HMG1* were within module 2 of the community analysis that was over-represented for terpenoid backbone synthesis (Figure 4.13 top panel), further supporting the involvement of *ERG20* as a functional backup of *BTS1* in hypoxia.

In good agreement with my hypothesis that *BTS1* or *ERG20* signalled suppressor genes to trigger cell survival pathways, I identified top central genes and experimentally validated these genes that form part of the HMGCR degradation (HRD) complex (*HRD1*, *HRD3* and *UBC7*). This is a conserved complex that participates in the ERAD pathway, which ubiquitinates misfolded proteins (usually upon ER stress) to be degraded by the proteasome (Neal et al. 2020). Auto-ubiquitination of *HRD1* triggers retro-translocation of misfolded proteins from the ER lumen to the cytosol to be ubiquitinated and degraded by the proteasome (Baldridge and Rapoport 2016). As explained in Chapter 1 (Figure 1.7), *HMG2*, the dominant isozyme of HMGCR in hypoxia, is regulated by this complex (Gardner

et al. 2001; Garza et al. 2009), and in fact the HRD-dependent degradation of Hmg2 is enhanced in hypoxia (Theesfeld and Hampton 2013). Accumulation of GGPP changes the conformation of Hmg2, and accumulation of oxysterols also enhances the signal for the HRD complex to ubiquitinate the misfolded Hmg2 for proteasomal degradation (Gardner et al. 2001; Garza et al. 2009). In the absence of sterols, particularly lanosterol, accumulation of GGPP induces the HRD-mediated degradation of Hmg2. Both sterol depletion and accumulation of GGPP occur in anaerobiosis, given that synthesis of sterols is oxygen-dependent and the synthesis of GGPP (not dependent on oxygen) is upstream to the oxygen-dependent part of the mevalonate pathway (see Figure 4.1). It is thus possible that deletion of *BTS1* further caused upstream intermediates to accumulate inducing toxicity (***e.g.***, FPP, mevalonate and HMGCR itself) and also that the HRD complex was not able to tag Hmg2 for degradation due to the lack of *BTS1*-mediated signal, GGPP, also contributing to *HMG2*-dependent toxicity.

My results may thus indicate that cell survival in hypoxia is maintained by the HRD complex signalled by the accumulation of GGPP (Figure 4.9B, row 1). This is in line with findings that GGPP enhances Hmg2 ubiquitination (Garza et al. 2009). Hence, when *BTS1* is deleted and GGPP is no longer synthesised (unless it is by *ERG20* as I have hypothesised for UWOPS87 and Y55 genetic backgrounds), ubiquitination and degradation of Hmg2 are not activated. Oxysterols would also have been low, thus only weakly stimulating HRD degradation (Figure 4.9C, row 1 and 2).

Lack of signal to stimulate the HRD complex, however, only partially explains my results. It may explain the synthetic sickness or lethality upon *BTS1* deletion in hypoxia but does not explain why deletion of *HRD1* suppresses lethality. Therefore, I propose that suppressor genes potentially are negative regulators of a second compensatory pathway that is only activated upon deletion of the suppressor genes or pathways. In this case, I believe that the HRD complex (specifically the *HRD1*, *HRD3* and *UBC7* genes) are repressors or inhibitors of a compensatory pathway that also participate in retro-translocation, ubiquitination and degradation of Hmg2. In my results, *SND2* is one of the validated genes that enhanced lethality in hypoxia upon atorvastatin treatment (Figure 4.6). Since *SND2* participates in the SRP-independent (SND) pathway that targets proteins to the ER via an alternative to the SRP and GET pathways (Aviram et al. 2016), the SND pathway is clearly a critical pathway to atorvastatin bioactivity in hypoxia where future research can determine whether Hmg2 is cargo in this pathway in hypoxia.

Snd2 is also a physical interactor of Dfm1 (Aviram et al. 2016), which is involved in ERAD and in fact a physical interactor of Hrd1 and Hrd3 (Goder et al. 2008; Stolz et al. 2010). Hrd1 forms a tunnel for retro-translocation from the lumen to the cytoplasm (ERAD-L), whereas substrates integral

to the membrane (such as HMGCR), exit through the *DFM1*-mediated pathway (Neal et al. 2020). In the absence of *DFM1*, the HRD complex remodels to mediate ERAD-M, emphasising the plasticity of these pathways to compensate for one another. Although the full mechanism of the Snd2-Dfm1 interaction is not known, I believe *SND2* might mediate the switch to a compensatory pathway in the absence of HRD complex components in hypoxia. In line with this hypothesis, the Snd2 human orthologue TMEM208 is localised to the ER membrane (Zhao et al. 2013) and regulated by HIF1A, and hence transcribed under hypoxia (Lei et al. 2020).

Although *SND2* was not a central gene in my network analysis, the construction of networks was limited to interactions in databases under normal ambient conditions. It is thus possible that *SND2* is a gene central to the hypoxia network albeit not detectable. The importance of *SND2* in hypoxia but not in ambient normoxic conditions would be consistent with conditional genetic interaction networks being rewired in different environmental conditions (Costanzo et al. 2021). In fact, *SND2* has been reported to be synthetic sick with *HMG1* in aerobic experiments (Costanzo et al. 2016), which points to a potential genetic interaction with *HMG2* in hypoxia. Snd2 has also been reported as a physical interactor with five of the six proteins coded by ERG genes that are oxygen dependent (*ERG1*, *ERG3*, *ERG5*, *ERG11* and *ERG25*) and three out of the 12 that are not oxygen-dependent (*ERG2*, *ERG9*, and *ERG27*) (Aviram et al. 2016), further supporting the involvement of *SND2* in the regulation of genes in the mevalonate pathway.

I thus propose that overexpression of *HRD1*, *HRD3* or *UBC7* in combination with atorvastatin-mediated inhibition of *BTS1* and *ERG20* may prevent the compensatory pathway from activating, likely via *SND2*. Based on the phenotypes observed in my validations (Figures 4.6 and 4.8), atorvastatin or other inhibitors of *BTS1* and *ERG20* should also limit signalling for ubiquitination in hypoxia, which is GGPP-dependent, thus causing toxic accumulation of HMGCR and potential cell death while having minimal impact in ambient conditions. This is a hypothesis that should be tested in order to determine at what cellular level (*e.g.*, the level of transcription, translation or post-translation) *HRD1*, *HRD3* and *UBC7* represses or inhibits *SND2* (if this were indeed the compensatory pathway).

The translation of this process to humans is complex because although humans have a similar form of regulation of HMGCR in hypoxia, the signal for this is accumulation of sterols (mainly lanosterol) that triggers the binding of INSIGs to HMGCR and subsequent ubiquitination (Figure 1.11 in Chapter 1) (Nguyen et al. 2007). Furthermore, human orthologues of genes identified here are upregulated in hypoxia. SYVN1, AMFR and SEL1L, for instance, are human orthologues of *HRD1* that regulate HMGCR ubiquitination (Menzies et al. 2018) and have been found upregulated in mouse

models of hypoxic-ischemia (Qi et al. 2004), colon carcinoma cells in hypoxia (Liu et al. 2007), hypoxia-induced cardiomyocytes (Liu et al. 2018) and glioblastoma cells in hypoxia also stimulating cell migration and invasion (Kathagen-Buhmann et al. 2018). This might be in contrast to my hypothesis that overexpression of these genes in combination with atorvastatin should inhibit cell growth since they already are overexpressed in hypoxia, although their expression in atorvastatin-treated or GGPPS1-inhibited cells or models has not been explored.

Overexpression of other E3-ubiquitin ligases that are buffers of genes identified here may also be potential targets to enhance anticancer activity of atorvastatin in hypoxia. MARCH6, for instance, is a regulator of HMGCR, squalene monooxygenase and cytochrome P450 family 51 (CYP51) that catalyses the conversion of lanosterol to 4,4 dimethyl cholesta-8,14,24-trienol (Scott et al. 2020; Zelcer et al. 2014). MARCH6 is human orthologue of *SSM4*, which is a negative genetic interactor of *HRD1* (Buck et al. 2010; Swanson et al. 2001), *UBC4* (Xie et al. 2010), *UBC7* (Swanson et al. 2001) and notably *SND2* (Costanzo et al. 2016) identified here. Substrates of CYP51 accumulated and CYP51 expression was repressed in 3T3L1 cells in hypoxia (Nguyen et al. 2007; Zhu et al. 2014), while CYP51 protein levels were not altered in HeLa and HepG2 cells in hypoxia (Scott et al. 2020). It was not explored whether overexpression of MARCH6 would repress CYP51 in hypoxia, and if so, it may indeed be an anticancer strategy since CYP51 is overexpressed in liver and ovary cancers (Downie et al. 2005; Kumarakulasingham et al. 2005) and its inhibition has been proposed as a potential anticancer therapy (Hargrove et al. 2016). In contrast to genes discussed above, MARCH6 has been found downregulated in melanoma (Roesch et al. 2003), which may deem this gene a candidate for overexpression in combination with atorvastatin and potentially other anticancer therapeutics.

All these hypotheses should be tested, but my results thus far suggest that human orthologues of the yeast suppressor genes identified herein are good candidates for overexpression assays to conditionally targeting hypoxic cells, which may or may not be enhanced by inhibition of the human orthologue of *BTS1* (GGPPS1) with atorvastatin or any other inhibitor, and this may be genetic background dependent. These results could be used to design pre-clinical experimental treatment strategies. For instance, sertraline, the top drug identified to share signature genes with atorvastatin, induced overexpression of SYVN1 and UBE2G1 in liver cell cultures (Chen et al. 2014), which are human orthologues of *HRD1* and *UBC7*, respectively. Mebendazole and podophyllotoxin have also shown to upregulate SEL1L3 in HL60 cells, an perphenazine and chlorprothixene upregulated SEL1L in PC3 cells (Yoo et al. 2015), both human orthologues of *HRD3* thus supporting them as candidate combination therapy with atorvastatin. However, the identification of therapeutics that are active in

hypoxic tumours is intricate given the complex biology of hypoxic tumours (Sørensen and Horsman 2020). One common strategy, for instance, is hypoxia alleviation to sensitise hypoxic cells to known general anticancer drugs (Graham and Unger 2018). In such case, the therapeutics to be used may need to suppress rather than overexpress the human orthologues of yeast genes identified here. Mitoxantrone, for instance, downregulated UBE2G2, whereas the compound 0175029-0000 downregulated UBE2G1, SEL1L2 and CDC34 (Yoo et al. 2015). Human orthologues of targets identified here may also serve as targets for the design of hypoxia-activated prodrugs.

4.4.4 Targeting mitophagy as a mechanism to enhance the anticancer activity of atorvastatin in hypoxic tumours

I expected to find genes involved in ER stress/UPR and autophagy to play a role in atorvastatin sensitivity in hypoxia since these have been associated with statin bioactivity in yeast (Busby et al. 2019) and these are the main pathways that allow hypoxic tumours an increased survival (Daskalaki et al. 2018; Tan et al. 2016a; Wouters and Koritzinsky 2008). Notably, the exact mechanism by which UPR mediates cell survival of hypoxic tumours is not well characterised (Chipurupalli et al. 2019). I found autophagy-related genes such as *ATG2* and *KSP1*, which were suppressors of lethality of *BTS1* as well as central genes in networks. Additionally, *ATG18* appeared as one of the top betweenness genes. I also found *TRS85*, which enhanced lethality of atorvastatin treatment in hypoxia, and also showed as one of the top betweenness genes. Accumulating evidence points to autophagy selectivity to degrade specific cellular components (Suzuki 2013), and thus I sought to define if there was a specific type of autophagy identified in this study. Interestingly, *ATG2*, *ATG18* and *TRS85* have shown to be required for a more selective type of autophagy, mitophagy (Kanki et al. 2009; Kanki et al. 2015; Okamoto et al. 2009). Indeed I found mitophagy to be enriched in both networks, the one generated for atorvastatin-hypersensitive strains and for suppressors of synthetic sickness/lethality. I thus propose that mitophagy confers a protective effect against atorvastatin-induced toxicity and may be a target to inhibit in combination with atorvastatin to enhance the anticancer activity of atorvastatin in hypoxic tumours.

In line with my hypothesis, mitophagy has been shown to exert a protective effect against statin-induced toxicity in skeletal muscle cells (Ramesh et al. 2019) and simvastatin has been shown to trigger mitophagy in cardiomyocytes inducing cardioprotection (Andres et al. 2014). Furthermore, vorinostat identified here as a potential combination therapy with atorvastatin, has shown to inhibit mitophagy in combination with quinacrine inducing apoptosis of T-cell acute lymphoblastic leukemia

cells (Jing et al. 2018). Other autophagy inhibitors, such as chloroquine, have been used in combination with anticancer therapeutics to enhance survival of glioblastoma patients (Pascolo 2016). However, the contribution of mitophagy is not fully understood and should be subject to future studies of hypoxic tumours with atorvastatin.

I also believe that modulation of mitophagy may be achieved by specifically targeting human orthologues of the genes mentioned above (*ATG2*, *ATG18* and *TRS85*) or also genes I found to be involved in ion homeostasis, *TKL1*, *NDE1*, *NHA1*, *MMT2*, and *HRK1*. Some of these genes (*NDE1*, *MMT2*) also have mitochondrial functions (*NDE1*, *MMT2*) and hence could be mediators of mitophagy since changes in ion homeostasis triggered both mitophagy and autophagy (Nowikovsky et al. 2007) and disruption of mitochondrial activity in anaerobiosis has been found to induced mitophagy (Priault et al. 2005). NAD^+ is also known to induce and boost mitophagy (Fang et al. 2016; Vannini et al. 2019), and I found *NDE1* as one of the genes that enhanced toxicity of atorvastatin in hypoxia (Figure 4.6). *NDE1* codes for a NADH dehydrogenase that oxidises NADH to provide it to the mitochondria. Without this gene, the levels of NAD^+ would have been limited and thus preventing mitophagy from activating. *NDE1* does not have a human orthologue in terms of sequence homology, but components of the NADH dehydrogenase complex may also serve as potential targets. Metformin, for instance, inhibits human NADH dehydrogenase activity and also proliferation of human cancer cells (Wheaton et al. 2014). Its mechanism was not associated with mitophagy but it cannot be ruled out since it was not investigated. The mechanism by which statins induce mitophagy is unknown, but it has been suggested that ubiquinone depletion by statins triggers mitophagy (Andres et al. 2014). I believe another possible mechanism could be mediated through AMPK since statins induce AMPK and AMPK activates mitophagy (Pei et al. 2018; Toyama et al. 2016). It contrasts, however, that statins also activate the tumour suppressor PTEN, which is negative regulator of mitophagy (Wang et al. 2020).

4.4.5 Conclusion

Taken together, I developed a method to study hypoxic tumours and their response to atorvastatin treatment using yeast models in three genetic backgrounds. I identified ERAD and mitophagy pathways as potential targets to enhance the anticancer activity of atorvastatin in hypoxic tumours and potentially of other anticancer therapeutics. Although I focused the role of autophagy in mitophagy, it is possible that other types of autophagy might play a role, since *TRS85* has also shown a role in ER-phagy (Lipatova et al. 2013) and *ATG2* and *ATG18* also have a role in pexophagy (autophagy of the peroxisome) (Wang et al. 2001; Guan et al. 2001), and both ER-phagy and pexophagy are known to

be activated in hypoxia (Daskalaki et al. 2018). To summarise, these genes and pathways in particular interacting with the ubiquitination and degradation of HMGCR could be used to design pre-clinical experiments with the potential to aid in two purposes: (i) overexpression of these targets may assist the design of hypoxia-activated prodrugs to promote cell death in hypoxic tumours; or (ii) inhibition of such targets may alleviate hypoxia to sensitise hypoxic tumours to anticancer therapeutics such as atorvastatin.

Chapter 5

Synthesis and Future Directions

5.1 Synthesis

In this dissertation, I have investigated how atorvastatin acts in anti-cancer and pro-diabetes processes. These are genetically complex diseases, requiring analysis methodologies that account for the action of multiple diverse genes both additively and, just as importantly, epistatically. I used quantitative growth phenotypes under a variety of conditions in the presence and absence of statins to assemble multi-layer networks (n-dimensional tensors) representing genetic and protein-protein interaction networks that were then analysed for topological centrality, community clustering and metabolic pathway enrichment to address this complexity. Previous studies have produced baseline interaction data to yield initial insight into the genes involved in atorvastatin bioactivity in one genetic background (Giaever et al. 2004; Maciejak et al. 2013). My thesis has expanded on this via the identification of genetic, chemical genetic and conditional interactions in three genetic backgrounds, and the subsequent network analyses of these interactions to distinguish key genes and compounds that mediate the anticancer and pro-diabetes activities of atorvastatin. I used specific queries for the mevalonate pathway under ambient conditions (Chapter 2) as well as hypoxic conditions (Chapter 4) to investigate anticancer activity, and also specific queries for interrogating obese and anorexic yeast models to investigate pro-diabetes activity.

The target of statins is HMGCR, the rate-limiting enzyme in the well characterised mevalonate pathway integral to the synthesis of cholesterol. This pathway has several branches at farnesyl pyrophosphate (FPP) to five other possible outcomes potentially affecting diabetes and cancer (Chapter 1 Figure 1.4). Defining complex genetics in an unbiased manner requires genome-wide analysis that may be achieved by building interactive gene networks utilising genome-wide deletion

libraries. Such libraries do not yet exist in human cells, so I used the well-studied and conceptually productive genetic model Baker's yeast (*S. cerevisiae*) in lieu as a 'pre-screen' to help unravel the genetic complexity mediating atorvastatin bioactivity. I increased functional interpretation, by performing studies with genome-wide deletion libraries in three genetic backgrounds namely S288C, UWOPS87, and Y55 that were variably sensitive to statins, thus providing an extra parameter to assess the importance of specific genetic, chemical genetic and conditional genetic interactions identified in the three results chapters of this thesis.

Genome-wide deletion-mutant libraries in three genetic backgrounds were investigated here in the condition of hypoxia, including the two novel ones, UWOPS87 and Y55. These were recently developed but their use has been limited (Busby et al. 2019; Galardini et al. 2019; Joblin-Mills 2020). This thesis adds evidence to the reliability and utility of these libraries by confirming expected fundamental biology in their use but also by discovery of new biology and insights as summarised above in this chapter. The importance of genetic background can be seen using single deletions of *BTS1* or the NAD^+ salvage *NPT1* that are each lethal in hypoxia in S288C, a phenotype that is not conserved in UWOPS87 and Y55.

In **Chapter 2**, I focused on **the anticancer activity of atorvastatin** and sought atorvastatin-specific epistasis by generating 25,800 double deletion strains, each lacking a gene in the statin pathway and a second gene from the wider yeast genome. The selected genes in the statin pathway were *HMG1*, the main target of atorvastatin in aerobic conditions, and *BTS1*, an important gene downstream of *HMG1* where silencing of the human orthologue, GGPPS1, enhances the anticancer activity of statins (Pandyra et al. 2015).

Building off the validation of 17 and 23 epistatic interactions for *HMG1* and *BTS1*, respectively, network topological analyses, and community clustering of GIN and PPIN interactions were enhanced by adding interactors up to a path-length of two from established yeast global interaction networks. I then aggregated these two networks in one multi-layered network that was analysed for centrality and community clustering. I determined that the multi-layered approach was more informative to biological function than analysing GINs or PPINs alone. For instance, *HMG1* was identified as a central gene in response to atorvastatin treatment in three genetic backgrounds in the multi-layer analysis. This also should have been expected in single-layered matrix analysis given that *HMG1* is the target of atorvastatin, hence indicating the total number of interactions in single layer networks was insufficient to represent the fundamental chemical biology of atorvastatin. Similar comments can be made about pathway enrichment analysis where the specific KEGG metabolic pathway 'terpenoid backbone

synthesis' specific to the mevalonate pathway was enriched for both *HMG1* and *BTS1* queries in the aggregated networks, but was not enriched for the corresponding single-layered networks. This is a major conclusion from the studies in this thesis about the network complexity needed to get sensible interpretations of function, and thus the reason that multi-layered aggregated networks were chosen for computational analyses in this and other chapters. It should also present avenues for future studies on how and if networks contribute to phenotypes, an area that is currently not well studied.

Using multi-layered network methodology, I identified ribophagy and ageing pathways as buffers of atorvastatin bioactivity. *RIM15* was identified as a key statin modulator in positively regulating autophagy, thereby mediating ribophagy through phosphorylation of a histone deacetylase complex subunit (Li et al. 2021; Waliullah et al. 2017). I thus deduced that human orthologues of *RIM15* (MASTL, MAST1, MAST2, MAST3, and MAST4) and genes involved in ribophagy (NFIP1, ZNHIT3) should be potential targets to enhance the anticancer activity of atorvastatin through inhibition of these buffering pathways. I similarly identified a role for actin, endocytosis and autophagy, mediated by *TPM1* as well as a role for *CDC28*, a master regulator of mitotic and meiotic cycles that contributes to the induction of UPR. Using the Drug Signature Database (Yoo et al. 2015), I identified potential anticancer combination therapies with atorvastatin that revealed approved anticancer (*e.g.*, lestaurtinib, sunitinib), approved non-anticancer (*e.g.*, probenecid), and also relatively understudied compounds (*e.g.*, GW779439X, verlukast, hesperetin) that could form the basis of testing these combination therapies in human cells.

In **Chapter 3**, I focused on **the diabetogenic activity of atorvastatin** and also sought atorvastatin-specific epistasis by generating 25,800 triple deletion strains, comprising double deletion query strains to identify additional hypersensitivity in the resultant triple deletions genome-wide in the three genetic backgrounds. The query double deletions were established models for metabolic syndrome namely *TGL3* and *TGL4* genes required for triacylglyceride (fat) degradation comprising the 'obese' yeast model characterised by oversized lipid droplets (Kurat et al. 2006); and correspondingly the deletion of the *DGA1* and *LRO1* triacylglyceride synthesis genes comprising the 'anorexic' model. The 'obese' and 'anorexic' yeast models have been used to study lipotoxicity and metabolic syndrome (Garbarino and Sturley 2006; Joblin-Mills 2020; Kohlwein 2010) that are tightly linked to the development of type 2 diabetes. This thesis is the first time that such models have been used to gain insight into the genetic interactions mediating the diabetogenic activity of statins.

As in the previous chapter, I used multi-layer networks for topology centrality metrics and community analyses to investigate experimentally validated growth phenotypes. Based on atorvastatin-hypersensitive interactions in the 'anorexic' yeast model, I proposed that lipotoxicity

is a mechanism for atorvastatin-induced insulin resistance via accumulation of acetoacetyl-CoA and increased synthesis of fatty acids. Inhibition of diacylglycerol acyltransferase resulting in the accumulation of lipotoxic intermediates may explain induction of insulin resistance. Statins have indeed increased fatty acid synthesis leading to defective insulin signalling (Kain et al. 2015; Williams et al. 1992), and simvastatin has induced insulin resistance via lipotoxic accumulation of fatty acids and diacylglycerol (Larsen et al. 2018). However, this complex trait of lipotoxicity/insulin resistance cannot be explained by the accumulation of fatty acids alone and may depend on other compensatory metabolic pathways such as lipid droplet homeostasis and mitochondrial oxidative phosphorylation. Regarding the latter, *MCP2*, *MDM38* and *COQ10* were identified in this chapter as buffering toxicity of atorvastatin potentially through mitigation of lipotoxicity and mitophagy. Interestingly, these genes were identified in Y55 and UWOPS87 only, which although naturally resistant to atorvastatin treatment (Busby et al. 2019) the DGAT deletion was more sensitive to statins than in S288C implying that Y55 and UWOPS87 may have less redundancy of pathways to mitigate lipotoxicity than S288C. The involvement of *GYP1*-mediated autophagy and protein secretion was also made apparent, suggesting *GYP1* may be a mediator of protein secretion under lipotoxic conditions.

Similar to the findings in Chapter 2 where I found potential combination therapies with known anticancer therapeutics, some of the drug activities revealed in Chapter 3 are known antidiabetic therapeutics, namely glibenclamide and pioglitazone that validate my methodology. I also identified drugs with potential antidiabetic activity, namely bafilomycin and niclosamide. Interestingly, bafilomycin and niclosamide exert both anticancer and antidiabetic activity and are strong candidates for testing synergy with atorvastatin.

Fitness defects were expected in both DGAT and TGL double deletion strains, *dga1*∆ *lro1*∆ and *tgl3*∆ *tgl4*∆ respectively, because atorvastatin treatment should further impair the metabolism of sterols in these strains with already impaired triacylglyceride and sterol ester metabolism. DGAT and TGL spot dilution phenotypes are affected by lipid droplet buffering (Kohlwein 2010; Kohlwein et al. 2013) and I found here that this is dependent on genetic background, a pertinent finding in its own right to diabetogenic pathways. However, I was surprised to find nearly identical growth phenotypes of the statin-treated *triple deletion tgl3Δ tgl4Δ xxxΔ* strains compared to the *single deletion xxxΔ* strains in all three genetic backgrounds. An explanation of this lack of atorvastatin-enhanced toxicity is unclear for diabetogenic pathways because of too many interactive uncontrolled variables. These include lipid droplet buffering, the high redundancy of triacylglyceride lipases (at least 5 of them) and that the double deletion query *tgl3Δ tgl4Δ* are not themselves epistatic (Figure 3.3 Chapter 3), which independently as

well as combinatorially affect the expected total number of trigenic interactions. I conclude that it may be necessary to investigate fitness defects in multi-layer vs single-layer networks that would comprise trigenic or quadrigenic query gene deletions for the triacylglyceride lipases to be able to get a better picture for potential targets in diabetes potentiated by statins. I note *inter alia* the reinforcement of the rationale of using yeast for complex genetic studies as guidance prior to the much less genetically tractable human cell systems.

In **Chapter 4**, I focused on **conditional genetic interactions in the mevalonate pathway and its branches under hypoxia** in my yeast model because hypoxia decreases sensitivity to anticancer therapeutics. Since I identified that the *BTS1* deletion is synthetic lethal with statins under hypoxia, I generated 12,900 *bts1*Δ *xxx*Δ double deletion strains looking for suppressors of *BTS1*-deletion synthetic sickness/lethality in hypoxia in the three genetic backgrounds. I identified the HRD complex as a major mediator of cell survival induced by the metabolic products of *BTS1* and possibly its paralogue *ERG20*. The HRD complex may be a repressor or inhibitor of compensatory pathways such as the SRP-independent alternative targeting pathway to the ER mediated by *SND2* since deletion of genes in the HRD complex rescued lethality of *BTS1*-deficient strains and deletion of *SND2* enhanced toxicity of atorvastatin in hypoxia. I also identified drugs that upregulate human orthologues of *HRD3* (mebendazole, podophyllotoxin, perphenazine and chlorprothixene) that are candidate combination therapies with atorvastatin to target hypoxic tumours.

Given the specific hypersensitive interactions to atorvastatin in hypoxia, I conclude mitophagy has a protective effect against atorvastatin-induced toxicity in hypoxic conditions. The involvement of mitophagy seen in the hypoxia model and also the lipotoxic model suggest that mitochondrial UPR (UPR^{mt}) is the main mediator of survival in these conditions, since mitophagy requires UPR^{mt} activation. This prediction would be consistent with UPR^{mt} activation that has protected yeast, worm and human cells from statin-induced toxicity (Rauthan et al. 2013). Thus it is plausible that accumulation of lipotoxic precursors may be a mechanism for the hypoxia, obese and anorexic models considering that oxygen-dependent enzymes in the mevalonate pathway result in accumulation of oxygen-independent precursors upstream of squalene (see Figure 1.4 in Chapter 1). Inhibition with atorvastatin would thus lead to reduced levels of intermediates between squalene and mevalonate but may cause accumulation of precursors upstream to HMG-CoA. This accumulation would include acetoacetyl-CoA that is the link between the mevalonate and the fatty acid synthesis pathways (Figure 3.1 in Chapter 3), thus resulting in enhanced synthesis of fatty acids and accumulation of lipotoxic intermediates since atorvastatin may also inhibit the diacylglycerol acyltransferase.

It is important to acknowledge that yeast is a powerful model to study fundamental biology of eukaryotes in a simple genetic model, albeit limited to its own cell biology, where some relevant genes and pathways are conserved with human cells but others may differ greatly (*i.e.*, 6,200 yeast genes compared to 20,000 human genes). Yeast have been used for decades, however, as models for the discovery of anticancer drugs (Ferreira et al. 2019; Hartwell et al. 1997; Simon 2001). It is clear that yeast do not develop cancer, and the complexity behind cancer cell biology cannot be completely studied in yeast. Though *BTS1*-deleted mutants, for instance, were used in this study because GGPPS1-silenced cancer cells have shown increased sensitivity to atorvastatin treatment (Pandyra et al. 2015), this is only one of the genes that have shown a similar response, such as SREBF2, which is not conserved in yeast (Pandyra et al. 2015). My yeast model was also not cancer engineered, for instance, yeast models expressing human p53 have been used to study some of its mutant alleles (Hekmat-Scafe et al. 2017). I have also developed a model as a proxy for hypoxic tumours, though tumour hypoxia is only one of many factors influencing the tumour microenvironment (Sørensen and Horsman 2020). The complexity of tumour hypoxia goes beyond limited oxygen supply, as hypoxia can be acute (minutes to hours), chronic (days) or cyclic (intermittent hypoxia) (Saxena and Jolly 2019), and such differences were not studied here. Similarly, yeast are not a complete model for diabetes, as they cannot mimic the entirety of beta cell biology, and thus I focused on one characteristic only, lipotoxicity. In the particular case of statin-mediated insulin resistance, lipotoxicity has been suggested as one factor contributing to insulin resistance (Hegarty et al. 2003; Kelley and Simoneau 1994), but also inhibition of IRS-1 (Henriksbo et al. 2014), inhibition of isoprenylation of Rab and Rho GTPases, and impaired translocation of GLUT4 (Betteridge and Carmena 2016) are other contributing factors that were not studied in this model.

Overall, it is impossible at this stage to develop a perfect model for the study of diabetes and cancer, as even mammalian cell cultures have their own shortcomings. For example, a major shortcoming is that genetic interaction networks are not completely known for mammalian cells and therefore cannot be interrogated genome-wide for network topological properties for key genes. Upon identification of key network genes, yeast genetics makes follow-up relatively simple but the same cannot be said for mammalian cell genetic manipulation. There has been progress in mammalian cell genetic manipulations, large scale CRISPR knockout screens, for instance, have retrieved limited genetic interaction networks of around 200,000 gene pairs in cancer cell lines (Horlbeck et al. 2018), while computational frameworks have integrated CRISPR knockout screens in 60 human cancer cell lines identifying more than 2 million genetic interactions that point to vulnerabilities in cancer cells (Rauscher

et al. 2018), yet representing only a small proportion of the possible ~2 × 10^8 interactions for protein coding genes. Other cost effective approaches are being explored, such as sequencing of nascent human radiation hybrid clones, which thus far has retrieved a limited number of interactions (Khan and Smith 2021), but seems a promising approach to accelerate our knowledge of human genetic interaction networks in the near future. The specificity of interactions identified in my study have surely shed light on the basic cell biological molecular mechanisms behind the anticancer and diabetogenic activity of atorvastatin that establish a solid basis for future studies in yeast and human cell models, some of which are presented below.

5.2 Future Directions

Taken together, I have identified genetic, chemical genetic and conditional interactions relevant to the anticancer and diabetogenic activity of atorvastatin. These interactions suggest specific pathways and combination therapies to enhance the anticancer and reduce the diabetogenic activity of atorvastatin. Intriguingly, many of the key gene interactors and metabolic pathways identified by the yeast model in this thesis are conserved in humans. This section therefore discusses possible experiments to conduct in the future to follow up on my thesis results.

5.2.1 Characterising the role of actin and ageing in the UPR-mediated autophagy response to atorvastatin

I proposed a model whereby atorvastatin, via actin- and ageing-related processes, activates UPR leading to autophagy. UPR and autophagy are indeed known pathways for the anticancer activity of statins (Okubo et al. 2020; Yang et al. 2010; Yang and Chen 2011), but inclusion of actin and ageing are not fully understood at the molecular level. Here specific experiments can be conducted to further characterise relevant genetic interactions identified in this thesis. For example, the *HMG1-SLG1* and *HMG1-TPM1* interactions involved in actin and the *HMG1-RIM15* interaction involved in ageing and autophagy can each be investigated for their contributions to UPR activation.

If my proposed model is correct, double deletions of these genes should induce UPR and autophagy in atorvastatin-treated strains. It should be determined whether double deletion with functional *HMG1* is necessary for this to happen or if the concentrations of atorvastatin tested here or higher would produce the same levels of UPR and autophagy in *slg1*△, *tpm1*△ and *rim15*△ single deletions. Furthermore, the double deletions treated with atorvastatin should also show reduced levels

of actin-related proteins (Meiling-Wesse et al. 2002), reduced levels of actin filaments (Higuchi et al. 2013), and ultimately decreased lifespan (Powers et al. 2006). Similar studies in human cell models could be performed using orthologous gene deletions (*e.g.*, CRISPR technology) in order to confirm whether UPR (Dastghaib et al. 2020) and autophagy (Parikh et al. 2010) are induced and contribute to apoptosis and cell cycle arrest (Hoque et al. 2008) of cancer cells compared to healthy cells.

5.2.2 Investigating hypoxia-specific interactions within ERAD- and mitophagy-mediated cell survival

ERAD-mediated cell survival

In hypoxia, deletion of *BTS1* leads to inviability for S288C and decreased growth for Y55 and UWOPS87. Rescue of these growth defects was achieved by deleting genes in the ERAD pathway (*HRD1*, *HRD3* and *UBC7*). This led to my hypothesis that products of *BTS1* and its functional homologue *ERG20* signal this pathway to mediate cell survival in hypoxia. To test this model, it will be interesting to alter the levels of gene products of *ERG20* (encodes farnesyl pyrophosphate synthetase, FPPS) and *BTS1* (encodes geranylgeranyl diphosphate synthase, GGPPS) in the presence and absence of hypoxia, and then measure growth defects. The results will uncover the contribution of these genes (*BTS1* and *ERG20*) in each genetic background and provide additional insight into the thesis results herein that found *ERG20* is a stronger mediator in UWOPS87 and Y55 genetic backgrounds than S288C.

One of the potential statin compensatory pathways that I proposed from the results of Chapter 4 is mediated by *SND2*. To test this, double deletion strains should be constructed to determine whether there is a genetic interaction of *SND2* with the ERAD genes *HRD1*, *HRD3* or *UBC7* genes. *UBC7*, for instance, has been reported as a negative genetic interactor in ambient conditions (Costanzo et al. 2010) but it is not known if there is a genetic interaction in hypoxia.

Future experimentation should also test whether overexpression of *HRD1*, *HRD3* or *UBC7* in combination with atorvastatin-mediated inhibition of *BTS1* and *ERG20* (or direct inhibition with other compounds, such as digeranyl bisphosphonate) induces death in hypoxia. Yeast strains in the three genetic backgrounds overexpressing *HRD1*, *HRD3*, *UBC7* or a combination of these, should be highly sensitive to atorvastatin treatment in hypoxia. Should these hypotheses be proven in yeast, equivalent assays in humans will be tested, bearing in mind that the closest equivalent to HRD complex for humans is the INSIGs for the sterol pathway regulation. This is because INSIGs regulate the transcription of

HMGCR in humans alongside with SREBPs and SCAP (Figure 1.8 in Chapter 1) and its degradation in hypoxia (Figure 1.11 in Chapter 1).

Mitophagy-mediated cell survival

I proposed that mitophagy confers a protective effect against atorvastatin-induced toxicity and may thus be a target to enhance the anticancer activity of atorvastatin in hypoxic tumours. I therefore suggest that mitophagy inhibition through deletion of specific genes (*e.g.*, *ATG2*, *ATG18*, *TRS85*, *TKL1*, *NDE1*, *NHA1*, *MMT2*, or *HRK1*) or through the supplementation of a mitophagy inhibitor such as chloroquine (Pascolo 2016) or liensinine (Zhou et al. 2015), should enhance toxicity of atorvastatin treatment in hypoxia. Chloroquine has indeed shown a synergy with small-molecule inhibitors against bladder cancer and interestingly lethality of these cancer cells was rescued by addition of cholesterol and recapitulated upon atorvastatin supplementation (King et al. 2016). Liensinine is a blocker of autophagosome-lysosome fusion that inhibits late stage of autophagy/mitophagy that has not been used in combination with statins to enhance its anticancer activity but that has enhanced the activity of the chemotherapeutic doxorubicin (Zhou et al. 2015). NAD^+ supplementation may be used as a positive control since NAD^+ is known to induce and boost mitophagy (Fang et al. 2016; Vannini et al. 2019) and should thus inhibit toxicity of atorvastatin treatment in hypoxia. Measurement of the induction of mitophagy could be achieved by using fluorescence microscopy and western blotting (Eiyama and Okamoto 2017). Results from these assays should guide future assays in human cell models (*e.g.*, Western blot and microscopy (Ramesh et al. 2019)) measuring the contribution of orthologous gene deletions to statin-induced mitophagy.

5.2.3 Characterising atorvastatin-induced lipotoxicity and its involvement in insulin resistance hypoxia, and diabetogenic pathways

I proposed that lipotoxicity is a mechanism for atorvastatin-induced insulin resistance and enhanced lipotoxicity in hypoxia would occur through inhibition of diacylglycerol acyltransferase, accumulation of acetoacetyl-CoA, fatty acids and other lipotoxic intermediates. To test this, neutral lipids could be investigated through thin layer chromatography (Fried and Sherma 1996) or mass spectrometry (Alzeer et al. 2016) in extracts of non-mutated, DGAT and TGL yeast strains treated with atorvastatin in normoxic and hypoxic conditions. Accumulation of acetyl-CoA and fatty acids in tandem with decreased diacylglycerol and triacylglycerol levels will be indicative that lipotoxicity is indeed a mechanism for atorvastatin-induced toxicity in hypoxia. Similar approaches may be used in human

cells where the glucose-stimulated insulin secretion and glucose uptake should also be measured (Yaluri et al. 2015).

The link between lipotoxic intermediates and insulin resistance probably is not caused by accumulation of diacylglycerols and fatty acids alone but might also depend on related complementary metabolic pathways such as lipid droplet dynamics as well as *GYP1*-mediated autophagy and mitophagy. Lipid droplets could be investigated by microscopy in single, DGAT triple mutants and TGL triple mutants treated with atorvastatin in the presence and absence of autophagy/mitophagy inhibitors, such as chloroquine or liensinine (Pascolo 2016; Zhou et al. 2015). A role for lipid droplets in atorvastatin bioactivity would be conferred by either the inability to synthesise triacylglycerides ('anorexic' phenotype) and only one small lipid droplet per yeast cell (Kohlwein 2010; Petschnigg et al. 2009) or by accumulation of oversized lipid droplets given the inability to degrade triacylglycerides ('obese' phenotype) (Kurat et al. 2006).

5.2.4 Further applications towards human therapeutic use

Beyond the genetic, chemical-genetic and conditional-genetic interactions proposed above that can be applied to human cell models using orthologous gene deletions, I have proposed combination therapies to enhance the anticancer or decrease the diabetogenic activity of statins in previous chapters. Probenecid, for instance, identified in Chapter 2, is prescribed for the prevention of gout as it increases uric acid excretion and inhibits drug renal excretion. Given that high lipid profiles, including high serum cholesterol have been correlated with hyperuricemia (Peng et al. 2015), it is likely that many patients worldwide are prescribed probenecid and statins simultaneously. Similarly, many patients should be under treatment with at least one of the antidiabetic drugs identified in Chapter 3, glibenclamide or pioglitazone alongside with statin treatment as diabetes and high cholesterol are commonly found together. Though not having an obvious correlation, it is also possible that patients under treatment for depression or anxiety disorders with sertraline identified in Chapter 4 may also be treated with statins. Databases such as UK Biobank (Sudlow et al. 2015) could be used to reveal whether simultaneous treatment of probenecid, glibenclamide, pioglitazone or sertraline with statins has been associated with reduced rates of cancer. Other drugs, such as minoxidil for hypertension and digoxin for heart conditions found in Chapter 3 are also likely to be taken in combination with statins by patients worldwide; making them attractive combinations to search in databases for potential reduced rates of incidence to type 2 diabetes.

5.3 Conclusion

To conclude, this thesis constructed genetic, chemical genetic and conditional interaction networks as models for the study of the mevalonate pathway and atorvastatin relative to cancer, hypoxic tumours and diabetes. This interaction network-based approach utilised a sophisticated combination of genetic and computational analyses, not commonly found altogether in the literature, comprising:

- Synthetic Genetic Array (SGA) analyses to generate pairwise combinations of double and triple deletions representing the genomes of three genetic backgrounds.
- Experimental validation of positive and negative genetic, chemical genetic and conditional interactions specific to atorvastatin and/or hypoxia.
- Multi-layered network construction followed by centrality analysis, community clustering and pathway enrichment.
- Humanising key yeast genes to identify drugs that potentially enhance atorvastatin activity.

This methodology allowed identification of interactions that could enhance or reduce toxicity of atorvastatin treatment in cancer or diabetes, respectively, when applied to human cell and animal model systems. It also detailed metabolic pathways that might be required for viability in atorvastatin-treated human cells, and processes that could enhance lethality in hypoxic tumours. One example is the identification of specific genes mediating actin and ageing pathways leading to UPR and potential autophagic cell death. Another example is the identification of conditional genetic interactions that mediate ERAD- and mitophagy-associated cell survival in hypoxia pointing to future experiments to enhance the toxicity of atorvastatin in hypoxic tumours. Finally, I identified a potential mechanism by which atorvastatin induces lipotoxicity, pointing to lipotoxic-induced insulin resistance as another mechanism for the diabetogenic activity of atorvastatin.

Bibliography

Abudugupur, A., K. Mitsui, S. Yokota, and K. Tsurugi (2002). An *ARL1* mutation affected autophagic cell death in yeast, causing a defect in central vacuole formation. *Cell Death and Differentiation* **9**, 158–68.

Agrawal, S., P. Vamadevan, N. Mazibuko, R. Bannister, R. Swery, S. Wilson, and S. Edwards (2019). A new method for ethical and efficient evidence generation for off-label medication use in oncology (a case study in glioblastoma). *Frontiers in Pharmacology* **10**, 681.

Ahangari, N., M. Doosti, M. Ghayour Mobarhan, A. Sahebkar, G. A. Ferns, and A. Pasdar (2020). Personalised medicine in hypercholesterolaemia: the role of pharmacogenetics in statin therapy. *Annals of Medicine* **52**, 462–470.

Ahern, T. P., L. Pedersen, M. Tarp, D. P. Cronin-Fenton, J. P. Garne, R. A. Silliman, H. T. Sørensen, and T. L. Lash (2011). Statin prescriptions and breast cancer recurrence risk: a Danish nationwide prospective cohort study. *Journal of the National Cancer Institute* **103**, 1461–8.

Ahmadi, M., S. Amiri, S. Pecic, F. Machaj, J. Rosik, M. J. Łos, J. Alizadeh, R. Mahdian, S. C. da Silva Rosa, D. Schaafsma, et al. (2020). Pleiotropic effects of statins: A focus on cancer. *Biochimica et Biophysica Acta Molecular Basis of Disease* **1866**, 165968.

Alberts, A. W., J. Chen, G. Kuron, V. Hunt, J. Huff, C. Hoffman, J. Rothrock, M. Lopez, H. Joshua, E. Harris, et al. (1980). Mevinolin: a highly potent competitive inhibitor of hydroxymethylglutaryl-coenzyme A reductase and a cholesterol-lowering agent. *Proceedings of the National Academy of Sciences of the United States of America* **77**, 3957–61.

Alupei, M. C., E. Licarete, F. B. Cristian, and M. Banciu (2014). Cytotoxicity of lipophilic statins depends on their combined actions on HIF-1α expression and redox status in B16.F10 melanoma cells. *Anti-Cancer Drugs* **25**, 393–405.

Alzeer, M. I., K. J. MacKenzie, and R. A. Keyzers (2016). Porous aluminosilicate inorganic polymers (geopolymers): a new class of environmentally benign heterogeneous solid acid catalysts. *Applied Catalysis A* **524**, 173–181.

Amemiya-Kudo, M., H. Shimano, A. H. Hasty, N. Yahagi, T. Yoshikawa, T. Matsuzaka, H. Okazaki, Y. Tamura, Y. Iizuka, K. Ohashi, et al. (2002). Transcriptional activities of nuclear SREBP-1a, -1c, and -2 to different target promoters of lipogenic and cholesterogenic genes. *Journal of Lipid Research* **43**, 1220–35.

Anderson, C. M., M. Kazantzis, J. Wang, S. Venkatraman, R. L. S. Goncalves, C. L. Quinlan, R. Ng, M. Jastroch, D. I. Benjamin, B. Nie, et al. (2015). Dependence of brown adipose tissue function on CD36-mediated coenzyme Q uptake. *Cell Reports* **10**, 505–15.

Anderson, M. S., M. Muehlbacher, I. P. Street, J. Proffitt, and C. D. Poulter (1989). Isopentenyl diphosphate:dimethylallyl diphosphate isomerase. An improved purification of the enzyme and isolation of the gene from *Saccharomyces cerevisiae*. *The Journal of Biological Chemistry* **264**, 19169–75.

Andres, A. M., G. Hernandez, P. Lee, C. Huang, E. P. Ratliff, J. Sin, C. A. Thornton, M. V. Damasco, and R. A. Gottlieb (2014). Mitophagy is required for acute cardioprotection by simvastatin. *Antioxidants & Redox Signaling* **21**, 1960–73.

Andres, D. A., A. Milatovich, T. Ozçelik, J. M. Wenzlau, M. S. Brown, J. L. Goldstein, and U. Francke (1993). cDNA cloning of the two subunits of human CAAX farnesyltransferase and chromosomal mapping of FNTA and FNTB loci and related sequences. *Genomics* **18**, 105–12.

Anitschkow, N. (1913). Über die Veränderungen der Kaninchenaorta bei experimenteller Cholesterinsteatose. *Beitrage zur Pathologischen Anatomie* **56**, 379–404.

Arrell, D. K. and A. Terzic (2010). Network systems biology for drug discovery. *Clinical Pharmacology and Therapeutics* **88**, 120–5.

Athenstaedt, K. and G. Daum (2005). Tgl4p and Tgl5p, two triacylglycerol lipases of the yeast *Saccharomyces cerevisiae* are localized to lipid particles. *The Journal of Biological Chemistry* **280**, 37301–9.

Athenstaedt, K. and G. Daum (2003). YMR313c/*TGL3* encodes a novel triacylglycerol lipase located in lipid particles of *Saccharomyces cerevisiae*. *The Journal of Biological Chemistry* **278**, 23317–23.

Aviram, N., T. Ast, E. A. Costa, E. C. Arakel, S. G. Chuartzman, C. H. Jan, S. Haßdenteufel, J. Dudek, M. Jung, S. Schorr, et al. (2016). The SND proteins constitute an alternative targeting route to the endoplasmic reticulum. *Nature* **540**, 134–138.

El-Awady, R., E. Saleh, A. Hashim, N. Soliman, A. Dallah, A. Elrasheed, and G. Elakraa (2016). The role of eukaryotic and prokaryotic ABC transporter family in failure of chemotherapy. *Frontiers in Pharmacology* **7**, 535.

Balakrishnan, R., J. Park, K. Karra, B. C. Hitz, G. Binkley, E. L. Hong, J. Sullivan, G. Micklem, and J. M. Cherry (2012). YeastMine-an integrated data warehouse for *Saccharomyces cerevisiae* data as a multipurpose tool-kit. *Database The Journal of Biological Databases and Curation* **2012**, bar062.

Baldridge, R. D. and T. A. Rapoport (2016). Autoubiquitination of the Hrd1 ligase triggers protein retrotranslocation in ERAD. *Cell* **166**, 394–407.

Barakat, R., I. Goubet, S. Manon, T. Berges, and E. Rosenfeld (2014). Unsuspected pyocyanin effect in yeast under anaerobiosis. *Microbiology Open* **3**, 1–14.

Baron, J. A. (2010). Statins and the colorectum: hope for chemoprevention? *Cancer Prevention Research* **3**, 573–5.

Basson, M. E., M. Thorsness, J. Finer-Moore, R. M. Stroud, and J. Rine (1988). Structural and functional conservation between yeast and human 3-hydroxy-3-methylglutaryl coenzyme A reductases, the rate-limiting enzyme of sterol biosynthesis. *Molecular and Cellular Biology* **8**, 3797–808.

Basson, M. E., M. Thorsness, and J. Rine (1986). *Saccharomyces cerevisiae* contains two functional genes encoding 3-hydroxy-3-methylglutaryl-coenzyme A reductase. *Proceedings of the National Academy of Sciences of the United States of America* **83**, 5563–7.

Benjamini, Y. and Y. Hochberg (1995). Controlling the false discovery rate: A practical and powerful approach to multiple testing. *Journal of the Royal Statistical Society* **57**, 289–300.

Bennetzen, M. V., G. Mariño, D. Pultz, E. Morselli, N. J. Færgeman, G. Kroemer, and J. S. Andersen (2012). Phosphoproteomic analysis of cells treated with longevity-related autophagy inducers. *Cell Cycle* **11**, 1827–40.

Berben, L., G. Floris, H. Wildiers, and S. Hatse (2021). Cancer and aging: Two tightly interconnected biological processes. *Cancers* **13**, 1–20.

Bergamini, E., R. Bizzarri, G. Cavallini, B. Cerbai, E. Chiellini, A. Donati, Z. Gori, A. Manfrini, I. Parentini, F. Signori, et al. (2004). Ageing and oxidative stress: a role for dolichol in the antioxidant machinery of cell membranes? *Journal of Alzheimer's Disease* **6**, 129–35.

Bergès, T., D. Guyonnet, and F. Karst (1997). The *Saccharomyces cerevisiae* mevalonate diphosphate decarboxylase is essential for viability, and a single Leu-to-Pro mutation in a conserved sequence leads to thermosensitivity. *Journal of Bacteriology* **179**, 4664–70.

Bertolini, F., V. P. Sukhatme, and G. Bouche (2015). Drug repurposing in oncology-patient and health systems opportunities. *Nature Reviews Clinical Oncology* **12**, 732–42.

Betteridge, D. J. and R. Carmena (2016). The diabetogenic action of statins - mechanisms and clinical implications. *Nature Reviews Endocrinology* **12**, 99–110.

Biden, T. J., E. Boslem, K. Y. Chu, and N. Sue (2014). Lipotoxic endoplasmic reticulum stress, β cell failure, and type 2 diabetes mellitus. *Trends in Endocrinology and Metabolism* **25**, 389–98.

Bisschops, M. M. M., P. Zwartjens, S. G. F. Keuter, J. T. Pronk, and P. Daran-Lapujade (2014). To divide or not to divide: a key role of Rim15 in calorie-restricted yeast cultures. *Biochimica et Biophysica Acta* **1843**, 1020–30.

Bloch, K. (1965). The biological synthesis of cholesterol. *Science* **150**, 19–28.

Blondel, V. D., J. L. Guillaume, R. Lambiotte, and E. Lefebvre (2008). Fast unfolding of communities in large networks. *Journal of Statistical Mechanics Theory and Experiment* **2008**, 10008.

Boccaletti, S., G. Bianconi, R. Criado, C. I. Del Genio, J. Gómez-Gardeñes, M. Romance, I. Sendiña-Nadal, Z. Wang, and M. Zanin (2014). The structure and dynamics of multilayer networks. *Physics Reports* **544**, 1–122.

Boccardi, V., M. Barbieri, M. R. Rizzo, R. Marfella, A. Esposito, L. Marano, and G. Paolisso (2013). A new pleiotropic effect of statins in elderly: modulation of telomerase activity. *Federation of American Societies for Experimental Biology* **27**, 3879–85.

Boerma, M., Q. Fu, J. Wang, D. S. Loose, A. Bartolozzi, J. L. Ellis, S. McGonigle, E. Paradise, P. Sweetnam, L. M. Fink, et al. (2008). Comparative gene expression profiling in three primary human cell lines after treatment with a novel inhibitor of Rho kinase or atorvastatin. *Blood Coagulation & Fibrinolysis* **19**, 709–18.

Boone, C., H. Bussey, and B. J. Andrews (2007). Exploring genetic interactions and networks with yeast. *Nature Reviews Genetics* **8**, 437–49.

Botstein, D., S. A. Chervitz, and J. M. Cherry (1997). Yeast as a model organism. *Science* **277**, 1259–60.

Bouchez, C. L., N. Hammad, S. Cuvellier, S. Ransac, M. Rigoulet, and A. Devin (2020). The Warburg effect in yeast: repression of mitochondrial metabolism is not a prerequisite to promote cell proliferation. *Frontiers in Oncology* **10**, 1333.

Boudreau, D. M., O. Yu, J. Chubak, H. S. Wirtz, E. J. A. Bowles, M. Fujii, and D. S. M. Buist (2014). Comparative safety of cardiovascular medication use and breast cancer outcomes among women with early stage breast cancer. *Breast Cancer Research and Treatment* **144**, 405–16.

Brandes, U. (2001). A faster algorithm for betweenness centrality. *Journal of Mathematical Sociology* **25**, 163–177.

Brasaemle, D. L., G. Dolios, L. Shapiro, and R. Wang (2004). Proteomic analysis of proteins associated with lipid droplets of basal and lipolytically stimulated 3T3-L1 adipocytes. *The Journal of Biological Chemistry* **279**, 46835–42.

Brea-Calvo, G., A. Rodríguez-Hernández, D. J. M. Fernández-Ayala, P. Navas, and J. A. Sánchez-Alcázar (2006). Chemotherapy induces an increase in coenzyme Q10 levels in cancer cell lines. *Free Radical Biology & Medicine* **40**, 1293–302.

Broniarek, I., K. Dominiak, L. Galganski, and W. Jarmuszkiewicz (2020). The influence of statins on the aerobic metabolism of endothelial cells. *International Journal of Molecular Sciences* **21**, 1485.

Brosh, R. and V. Rotter (2009). When mutants gain new powers: news from the mutant p53 field. *Nature Reviews Cancer* **9**, 701–13.

Brown, M. S. and J. L. Goldstein (1980). Multivalent feedback regulation of HMG CoA reductase, a control mechanism coordinating isoprenoid synthesis and cell growth. *Journal of Lipid Research* **21**, 505–17.

Brown, M. S. and J. L. Goldstein (1986). A receptor-mediated pathway for cholesterol homeostasis. *Science* **232**, 34–47.

Bryant, H. E., N. Schultz, H. D. Thomas, K. M. Parker, D. Flower, E. Lopez, S. Kyle, M. Meuth, N. J. Curtin, and T. Helleday (2005). Specific killing of BRCA2-deficient tumours with inhibitors of poly(ADP-ribose) polymerase. *Nature* **434**, 913–7.

Buck, T. M., A. R. Kolb, C. R. Boyd, T. R. Kleyman, and J. L. Brodsky (2010). The endoplasmic reticulum-associated degradation of the epithelial sodium channel requires a unique complement of molecular chaperones. *Molecular Biology of the Cell* **21**, 1047–58.

Burg, J. S. and P. J. Espenshade (2011). Regulation of HMG-CoA reductase in mammals and yeast. *Progress in Lipid Research* **50**, 403–10.

Busby, B. P., E. Niktab, C. A. Roberts, J. P. Sheridan, N. V. Coorey, D. S. Senanayake, L. M. Connor, A. B. Munkacsi, and P. H. Atkinson (2019). Genetic interaction networks mediate individual statin drug response in *Saccharomyces cerevisiae*. *NPJ Systems Biology and Applications* **5**, 35.

Cao, L., Y. Tang, Z. Quan, Z. Zhang, S. G. Oliver, and N. Zhang (2016). Chronological lifespan in yeast is dependent on the accumulation of storage carbohydrates mediated by Yak1, Mck1 and Rim15 kinases. *PLoS Genetics* **12**, e1006458.

Cartee, G. D. (2015). AMPK-TBC1D4-dependent mechanism for increasing insulin sensitivity of skeletal muscle. *Diabetes* **64**, 1901–3.

Chae, Y. K., M. E. Valsecchi, J. Kim, A. L. Bianchi, D. Khemasuwan, A. Desai, and W. Tester (2011). Reduced risk of breast cancer recurrence in patients using ACE inhibitors, ARBs, and/or statins. *Cancer Investigation* **29**, 585–93.

Chakrabarty, J. K., A. H. M. Kamal, A. D. A. Shahinuzzaman, and S. M. Chowdhury (2020). Proteomics network analysis of polarized macrophages. *Methods in Molecular Biology* **2184**, 61–75.

Chalkiadaki, A. and L. Guarente (2015). The multifaceted functions of sirtuins in cancer. *Nature Reviews Cancer* **15**, 608–24.

Chambers, C. M. and G. C. Ness (1998). Dietary cholesterol regulates hepatic 3-hydroxy-3-methylglutaryl coenzyme A reductase gene expression in rats primarily at the level of translation. *Archives of Biochemistry and Biophysics* **354**, 317–22.

Chambon, C., V. Ladeveze, M. Servouse, L. Blanchard, C. Javelot, B. Vladescu, and F. Karst (1991). Sterol pathway in yeast. Identification and properties of mutant strains defective in mevalonate diphosphate decarboxylase and farnesyl diphosphate synthetase. *Lipids* **26**, 633–6.

Chang, H.-L., C.-Y. Chen, Y.-F. Hsu, W.-S. Kuo, G. Ou, P.-T. Chiu, Y.-H. Huang, and M.-J. Hsu (2013). Simvastatin induced HCT116 colorectal cancer cell apoptosis through p38MAPK-p53-survivin signaling cascade. *Biochimica et Biophysica Acta* **1830**, 4053–64.

Chen, B., M. Zhang, D. Xing, and Y. Feng (2017). Atorvastatin enhances radiosensitivity in hypoxia-induced prostate cancer cells related with HIF-1α inhibition. *Bioscience Reports* **37**, BSR20170340.

Chen, E. Y., C. M. Tan, Y. Kou, Q. Duan, Z. Wang, G. V. Meirelles, N. R. Clark, and A. Ma'ayan (2013). Enrichr: interactive and collaborative HTML5 gene list enrichment analysis tool. *BMC Bioinformatics* **14**, 128.

Chen, J. and B. Yuan (2006). Detecting functional modules in the yeast protein-protein interaction network. *Bioinformatics* **22**, 2283–90.

Chen, M.-J., A.-C. Cheng, M.-F. Lee, and Y.-C. Hsu (2018). Simvastatin induces G1 arrest by up-regulating GSK3β and down-regulating CDK4/cyclin D1 and CDK2/cyclin E1 in human primary colorectal cancer cells. *Journal of Cellular Physiology* **233**, 4618–4625.

Chen, S., J. Xuan, L. Couch, A. Iyer, Y. Wu, Q.-Z. Li, and L. Guo (2014). Sertraline induces endoplasmic reticulum stress in hepatic cells. *Toxicology* **322**, 78–88.

Cherry, J. M., E. L. Hong, C. Amundsen, R. Balakrishnan, G. Binkley, E. T. Chan, K. R. Christie, M. C. Costanzo, S. S. Dwight, S. R. Engel, et al. (2012). *Saccharomyces* Genome Database: the genomics resource of budding yeast. *Nucleic Acids Research* **40**, D700–5.

Chipurupalli, S., E. Kannan, V. Tergaonkar, R. D'Andrea, and N. Robinson (2019). Hypoxia induced ER stress tesponse as an adaptive mechanism in cancer. *International Journal of Molecular Sciences* **20**, 749.

Choi, S.-E., S.-M. Lee, Y.-J. Lee, L.-J. Li, S.-J. Lee, J.-H. Lee, Y. Kim, H.-S. Jun, K.-W. Lee, and Y. Kang (2009). Protective role of autophagy in palmitate-induced INS-1 beta-cell death. *Endocrinology* **150**, 126–34.

Chojnacki, T. and G. Dallner (1988). The biological role of dolichol. *The Biochemical Journal* **251**, 1–9.

Chou, C.-W., C.-H. Lin, T.-H. Hsiao, C.-C. Lo, C.-Y. Hsieh, C.-C. Huang, and Y.-P. Sher (2019). Therapeutic effects of statins against lung adenocarcinoma via p53 mutant-mediated apoptosis. *Scientific Reports* **9**, 20403.

Chubinskiy-Nadezhdin, V. I., Y. A. Negulyaev, and E. A. Morachevskaya (2017). Simvastatin induced actin cytoskeleton disassembly in normal and transformed fibroblasts without affecting lipid raft integrity. *Cell Biology International* **41**, 1020–1029.

Chung, J., E. P. Brass, R. G. Ulrich, and W. R. Hiatt (2008). Effect of atorvastatin on energy expenditure and skeletal muscle oxidative metabolism at rest and during exercise. *Clinical Pharmacology and Therapeutics* **83**, 243–50.

Coleman, C. I., K. Reinhart, J. Kluger, and C. M. White (2008). The effect of statins on the development of new-onset type 2 diabetes: a meta-analysis of randomized controlled trials. *Current Medical Research and Opinion* **24**, 1359–62.

Cordenonsi, M., F. Zanconato, L. Azzolin, M. Forcato, A. Rosato, C. Frasson, M. Inui, M. Montagner, A. R. Parenti, A. Poletti, et al. (2011). The Hippo transducer TAZ confers cancer stem cell-related traits on breast cancer cells. *Cell* **147**, 759–72.

Costa Verdera, H., J. J. Gitz-Francois, R. M. Schiffelers, and P. Vader (2017). Cellular uptake of extracellular vesicles is mediated by clathrin-independent endocytosis and macropinocytosis. *Journal of Controlled Release* **266**, 100–108.

Costanzo, M., A. Baryshnikova, J. Bellay, Y. Kim, E. D. Spear, C. S. Sevier, H. Ding, J. L. Y. Koh, K. Toufighi, S. Mostafavi, et al. (2010). The genetic landscape of a cell. *Science* **327**, 425–31.

Costanzo, M., J. Hou, V. Messier, J. Nelson, M. Rahman, B. VanderSluis, W. Wang, C. Pons, C. Ross, M. Ušaj, et al. (2021). Environmental robustness of the global yeast genetic interaction network. *Science* **372**, eabf8424.

Costanzo, M., E. Kuzmin, J. van Leeuwen, B. Mair, J. Moffat, C. Boone, and B. Andrews (2019). Global genetic networks and the genotype-to-phenotype relationship. *Cell* **177**, 85–100.

Costanzo, M., B. VanderSluis, E. N. Koch, A. Baryshnikova, C. Pons, G. Tan, W. Wang, M. Usaj, J. Hanchard, S. D. Lee, et al. (2016). A global genetic interaction network maps a wiring diagram of cellular function. *Science* **353**, aaf1420.

Cox, A. D., S. W. Fesik, A. C. Kimmelman, J. Luo, and C. J. Der (2014). Drugging the undruggable RAS: Mission possible? *Nature Reviews Drug Discovery* **13**, 828–51.

Culhane, A. C., T. Schwarzl, R. Sultana, K. C. Picard, S. C. Picard, T. H. Lu, K. R. Franklin, S. J. French, G. Papenhausen, M. Correll, et al. (2010). GeneSigDB - a curated database of gene expression signatures. *Nucleic Acids Research* **38**, D716–25.

Culotti, J. and L. H. Hartwell (1971). Genetic control of the cell division cycle in yeast. 3. Seven genes controlling nuclear division. *Experimental Cell Research* **67**, 389–401.

da Silva Rosa, S. C., M. D. Martens, J. T. Field, L. Nguyen, S. M. Kereliuk, Y. Hai, D. Chapman, W. Diehl-Jones, M. Aliani, A. R. West, et al. (2020). BNIP3L/Nix-induced mitochondrial fission, mitophagy, and impaired myocyte glucose uptake are abrogated by PRKA/PKA phosphorylation. *Autophagy*, 1–16.

Dam, H. (1958). Historical introduction to cholesterol. *Chemistry, Biochemistry and Pathology*. New York, NY: Academic Press, 1–14.

Damacharla, D., V. Thamilselvan, X. Zhang, A. Mestareehi, Z. Yi, and A. Kowluru (2019). Quantitative proteomics reveals novel interaction partners of Rac1 in pancreatic β-cells: Evidence for increased interaction with Rac1 under hyperglycemic conditions. *Molecular and Cellular Endocrinology* **494**, 110489.

Daskalaki, I., I. Gkikas, and N. Tavernarakis (2018). Hypoxia and selective autophagy in cancer development and therapy. *Frontiers in Cell and Developmental Biology* **6**, 104.

Dastghaib, S., S. Shojaei, Z. Mostafavi-Pour, P. Sharma, J. B. Patterson, A. Samali, P. Mokarram, and S. Ghavami (2020). Simvastatin induces unfolded protein response and enhances temozolomide-induced cell death in glioblastoma cells. *Cells* **9**, 2339.

Debelyy, M. O., S. Thoms, M. Connerth, G. Daum, and R. Erdmann (2011). Involvement of the *Saccharomyces cerevisiae* hydrolase Ldh1p in lipid homeostasis. *Eukaryotic Cell* **10**, 776–81.

Deegan, S., S. Saveljeva, A. M. Gorman, and A. Samali (2013). Stress-induced self-cannibalism: on the regulation of autophagy by endoplasmic reticulum stress. *Cellular and Molecular Life Sciences* **70**, 2425–41.

Dengler, V. L., M. Galbraith, and J. M. Espinosa (2014). Transcriptional regulation by hypoxia inducible factors. *Critical Reviews in Biochemistry and Molecular Biology* **49**, 1–15.

Denoyelle, C., P. Albanese, G. Uzan, L. Hong, J.-P. Vannier, J. Soria, and C. Soria (2003). Molecular mechanism of the anti-cancer activity of cerivastatin, an inhibitor of HMG-CoA reductase, on aggressive human breast cancer cells. *Cellular Signalling* **15**, 327–38.

Desai, P., R. Wallace, M. L. Anderson, B. V. Howard, R. M. Ray, C. Wu, M. Safford, L. W. Martin, T. Rohan, J. E. Manson, et al. (2018). An analysis of the association between statin use and risk of endometrial and ovarian cancers in the Women's Health Initiative. *Gynecologic Oncology* **148**, 540–546.

Deutschbauer, A. M. and R. W. Davis (2005). Quantitative trait loci mapped to single-nucleotide resolution in yeast. *Nature Genetics* **37**, 1333–40.

Dey, N., P. De, and B. Leyland-Jones (2017). PI3K-AKT-mTOR inhibitors in breast cancers: From tumor cell signaling to clinical trials. *Pharmacology & Therapeutics* **175**, 91–106.

Diaz-Ruiz, R., S. Uribe-Carvajal, A. Devin, and M. Rigoulet (2009). Tumor cell energy metabolism and its common features with yeast metabolism. *Biochimica et biophysica acta* **1796**, 252–65.

Diaz-Ruiz, R., M. Rigoulet, and A. Devin (2011). The Warburg and Crabtree effects: On the origin of cancer cell energy metabolism and of yeast glucose repression. *Biochimica et Biophysica Acta* **1807**, 568–76.

Dieli, F., D. Vermijlen, F. Fulfaro, N. Caccamo, S. Meraviglia, G. Cicero, A. Roberts, S. Buccheri, M. D'Asaro, N. Gebbia, et al. (2007). Targeting human gamma/delta T cells with zoledronate and interleukin-2 for immunotherapy of hormone-refractory prostate cancer. *Cancer Research* **67**, 7450–7.

Diepart, C., O. Karroum, J. Magat, O. Feron, J. Verrax, P. B. Calderon, V. Grégoire, P. Leveque, J. Stockis, N. Dauguet, et al. (2012). Arsenic trioxide treatment decreases the oxygen consumption rate of tumor cells and radiosensitizes solid tumors. *Cancer Research* **72**, 482–90.

Dimitroulakos, J., D. Nohynek, K. L. Backway, D. W. Hedley, H. Yeger, M. H. Freedman, M. D. Minden, and L. Z. Penn (1999). Increased sensitivity of acute myeloid leukemias to lovastatin-induced apoptosis: A potential therapeutic approach. *Blood* **93**, 1308–18.

Dimster-Denk, D., M. K. Thorsness, and J. Rine (1994). Feedback regulation of 3-hydroxy-3-methylglutaryl coenzyme A reductase in *Saccharomyces cerevisiae*. *Molecular Biology of the Cell* **5**, 655–65.

DiSilvestro, P. A., S. Ali, P. S. Craighead, J. A. Lucci, Y.-C. Lee, D. E. Cohn, N. M. Spirtos, K. S. Tewari, C. Muller, W. H. Gajewski, et al. (2014). Phase III randomized trial of weekly cisplatin and irradiation versus cisplatin and tirapazamine and irradiation in stages IB2, IIA, IIB, IIIB, and IVA cervical carcinoma limited to the pelvis: a Gynecologic Oncology Group study. *Journal of Clinical Oncology* **32**, 458–64.

Dobzhansky, T. (1946). Genetics of natural populations; recombination and variability in populations of *Drosophila pseudoobscura*. *Genetics* **31**, 269–90.

Dong, J. and S. Horvath (2007). Understanding network concepts in modules. *BMC Systems Biology* **1**, 24.

Downie, D., M. C. E. McFadyen, P. H. Rooney, M. E. Cruickshank, D. E. Parkin, I. D. Miller, C. Telfer, W. T. Melvin, and G. I. Murray (2005). Profiling cytochrome P450 expression in ovarian cancer: identification of prognostic markers. *Clinical Cancer Research* **11**, 7369–75.

Duan, M.-R. and M. J. Smerdon (2014). Histone H3 lysine 14 (H3K14) acetylation facilitates DNA repair in a positioned nucleosome by stabilizing the binding of the chromatin Remodeler RSC (Remodels Structure of Chromatin). *The Journal of Biological Chemistry* **289**, 8353–63.

Dunn, R., F. Dudbridge, and C. M. Sanderson (2005). The use of edge-betweenness clustering to investigate biological function in protein interaction networks. *BMC Bioinformatics* **6**, 39.

Durr, I. F. and H. Rudney (1960). The reduction of beta-hydroxy-beta-methyl-glutaryl coenzyme A to mevalonic acid. *The Journal of Biological Chemistry* **235**, 2572–8.

Eiyama, A. and K. Okamoto (2017). Assays for mitophagy in yeast. *Methods in Molecular Biology* **1567**, 337–347.

Eli Lilly (2007). *FDA approves Lilly's osteoporosis drug EVISTA(R) (raloxifene HCl) to reduce the risk of invasive breast cancer in two populations of postmenopausal women.*

Endo, A., Y. Tsujita, M. Kuroda, and K. Tanzawa (1979). Effects of ML-236B on cholesterol metabolism in mice and rats: lack of hypocholesterolemic activity in normal animals. *Biochimica et Biophysica Acta* **575**, 266–76.

Endo, A. (1992). The discovery and development of HMG-CoA reductase inhibitors. *Journal of Lipid Research* **33**, 1569–82.

Endo, A. (2008). A gift from nature: the birth of the statins. *Nature Medicine* **14**, 1050–2.

Endo, A. (2010). A historical perspective on the discovery of statins. *Proceedings of the Japan Academy Series B, Physical and Biological Bciences* **86**, 484–93.

Endo, A., M. Kuroda, and K. Tanzawa (1976a). Competitive inhibition of 3-hydroxy-3-methylglutaryl coenzyme A reductase by ML-236A and ML-236B fungal metabolites, having hypocholesterolemic activity. *Federation of European Biochemical Societies Letters* **72**, 323–6.

Endo, A., M. Kuroda, and Y. Tsujita (1976b). ML-236A, ML-236B, and ML-236C, new inhibitors of cholesterogenesis produced by *Penicillium citrinium*. *The Journal of Antibiotics* **29**, 1346–8.

Endo, S., Y.-W. Zhang, S. Takahashi, and T. Koyama (2003). Identification of human dehydrodolichyl diphosphate synthase gene. *Biochimica et Biophysica Acta* **1625**, 291–5.

Engin, A. B. (2017). What is lipotoxicity? *Advances in Experimental Medicine and Biology* **960**, 197–220.

Erler, J. T., C. J. Cawthorne, K. J. Williams, M. Koritzinsky, B. G. Wouters, C. Wilson, C. Miller, C. Demonacos, I. J. Stratford, and C. Dive (2004). Hypoxia-mediated down-regulation of Bid and Bax in tumors occurs via hypoxia-inducible factor 1-dependent and -independent mechanisms and contributes to drug resistance. *Molecular and Cellular Biology* **24**, 2875–89.

Estébanez, B., J. A. de Paz, M. J. Cuevas, and J. González-Gallego (2018). Endoplasmic reticulum unfolded protein response, aging and exercise: an update. *Frontiers in Physiology* **9**, 1744.

Fan, J., Y. Wang, L. Liu, H. Zhang, F. Zhang, L. Shi, M. Yu, F. Gao, and Z. Xu (2017). cTAGE5 deletion in pancreatic β cells impairs proinsulin trafficking and insulin biogenesis in mice. *The Journal of Cell Biology* **216**, 4153–4164.

Fang, E. F., H. Kassahun, D. L. Croteau, M. Scheibye-Knudsen, K. Marosi, H. Lu, R. A. Shamanna, S. Kalyanasundaram, R. C. Bollineni, M. A. Wilson, et al. (2016). NAD+ replenishment improves lifespan and healthspan in ataxia telangiectasia models via mitophagy and DNA repair. *Cell Metabolism* **24**, 566–581.

Farmer, H., N. McCabe, C. J. Lord, A. N. J. Tutt, D. A. Johnson, T. B. Richardson, M. Santarosa, K. J. Dillon, I. Hickson, C. Knights, et al. (2005). Targeting the DNA repair defect in BRCA mutant cells as a therapeutic strategy. *Nature* **434**, 917–21.

FDA (2012). *FDA drug safety communication: important safety label changes to cholesterol-lowering statin drugs.*

Feldt, M., J. Menard, A. H. Rosendahl, B. Lettiero, P.-O. Bendahl, M. Belting, and S. Borgquist (2020). The effect of statin treatment on intratumoral cholesterol levels and LDL receptor expression: a window-of-opportunity breast cancer trial. *Cancer & Metabolism* **8**, 25.

Ferreira, R., A. Limeta, and J. Nielsen (2019). Tackling cancer with yeast-based technologies. *Trends in Biotechnology* **37**, 592–603.

Fisher, N. M., K. Meksawan, A. Limprasertkul, P. J. Isackson, D. R. Pendergast, and G. D. Vladutiu (2007). Statin therapy depresses total body fat oxidation in the absence of genetic limitations to fat oxidation. *Journal of Inherited Metabolic Disease* **30**, 388–99.

Fleischmann, M. and P. B. Iynedjian (2000). Regulation of sterol regulatory-element binding protein 1 gene expression in liver: role of insulin and protein kinase B/cAkt. *The Biochemical Journal* **349**, 13–7.

Forsburg, S. L. (2001). The art and design of genetic screens: yeast. *Nature Reviews Genetics* **2**, 659–68.

Freed-Pastor, W. and C. Prives (2016). Targeting mutant p53 through the mevalonate pathway. *Nature Cell Biology* **18**, 1122–1124.

Freeman, L. C. (1977). A set of measures of centrality based on betweenness. *Sociometry* **40**, 35.

Fried, B. and J. Sherma (1996). *Practical thin-layer chromatography : a multidisciplinary approach*, 288.

Funato, K. and H. Riezman (2001). Vesicular and nonvesicular transport of ceramide from ER to the Golgi apparatus in yeast. *The Journal of Cell Biology* **155**, 949–59.

Furberg, C. D. and B. Pitt (2001). Withdrawal of cerivastatin from the world market. *Current Controlled Trials in Cardiovascular Medicine* **2**, 205–207.

Galardini, M., B. P. Busby, C. Vieitez, A. S. Dunham, A. Typas, and P. Beltrao (2019). The impact of the genetic background on gene deletion phenotypes in *Saccharomyces cerevisiae*. *Molecular Systems Biology* **15**, e8831.

Gallez, B., M.-A. Neveu, P. Danhier, and B. F. Jordan (2017). Manipulation of tumor oxygenation and radiosensitivity through modification of cell respiration. A critical review of approaches and imaging biomarkers for therapeutic guidance. *Biochimica et Biophysica Acta Bioenergetics* **1858**, 700–711.

Ganesan, S. and M. K. Ito (2013). Coenzyme Q10 ameliorates the reduction in GLUT4 transporter expression induced by simvastatin in 3T3-L1 adipocytes. *Metabolic Syndrome and Related Disorders* **11**, 251–5.

Garbarino, J. A. and S. L. Sturley (2006). Mechanisms of lipotoxicity in yeast *Saccharomyces cerevisiae*. *The Federation of American Societies for Experimental Biology Journal* **20**, A948–A948.

Gardner, R. G., H. Shan, S. P. Matsuda, and R. Y. Hampton (2001). An oxysterol-derived positive signal for 3-hydroxy- 3-methylglutaryl-CoA reductase degradation in yeast. *The Journal of Biological Chemistry* **276**, 8681–94.

Garza, R. M., B. K. Sato, and R. Y. Hampton (2009). In vitro analysis of Hrd1p-mediated retrotranslocation of its multispanning membrane substrate 3-hydroxy-3-methylglutaryl (HMG)-CoA reductase. *The Journal of Biological Chemistry* **284**, 14710–22.

Giaever, G., A. M. Chu, L. Ni, C. Connelly, L. Riles, S. Véronneau, S. Dow, A. Lucau-Danila, K. Anderson, B. André, et al. (2002). Functional profiling of the *Saccharomyces cerevisiae* genome. *Nature* **418**, 387–91.

Giaever, G., P. Flaherty, J. Kumm, M. Proctor, C. Nislow, D. F. Jaramillo, A. M. Chu, M. I. Jordan, A. P. Arkin, and R. W. Davis (2004). Chemogenomic profiling: identifying the functional interactions of small molecules in yeast. *Proceedings of the National Academy of Sciences of the United States of America* **101**, 793–8.

Giaever, G., D. D. Shoemaker, T. W. Jones, H. Liang, E. A. Winzeler, A. Astromoff, and R. W. Davis (1999). Genomic profiling of drug sensitivities via induced haploinsufficiency. *Nature Genetics* **21**, 278–83.

Gietz, R. D. and R. H. Schiestl (2007). High-efficiency yeast transformation using the LiAc/SS carrier DNA/PEG method. *Nature Protocols* **2**, 31–34.

Gil, G., J. R. Faust, D. J. Chin, J. L. Goldstein, and M. S. Brown (1985). Membrane-bound domain of HMG CoA reductase is required for sterol-enhanced degradation of the enzyme. *Cell* **41**, 249–58.

Gillies, P. S. and C. J. Dunn (2000). Pioglitazone. *Drugs* **60**, 333–43.

Girvan, M. and M. E. J. Newman (2002). Community structure in social and biological networks. *Proceedings of the National Academy of Sciences of the United States of America* **99**, 7821–6.

Göbel, A., D. Breining, M. Rauner, L. C. Hofbauer, and T. D. Rachner (2019). Induction of 3-hydroxy-3-methylglutaryl-CoA reductase mediates statin resistance in breast cancer cells. *Cell Death & Disease* **10**, 91.

Göbel, A., M. Rauner, L. C. Hofbauer, and T. D. Rachner (2020). Cholesterol and beyond - The role of the mevalonate pathway in cancer biology. *Biochimica et Biophysica Acta Reviews on Cancer* **1873**, 188351.

Goder, V., P. Carvalho, and T. A. Rapoport (2008). The ER-associated degradation component Der1p and its homolog Dfm1p are contained in complexes with distinct cofactors of the ATPase Cdc48p. *Federation of European Biochemical Societies Letters* **582**, 1575–80.

Goffeau, A., B. G. Barrell, H. Bussey, R. W. Davis, B. Dujon, H. Feldmann, F. Galibert, J. D. Hoheisel, C. Jacq, M. Johnston, et al. (1996). Life with 6000 genes. *Science* **274**, 546, 563–7.

Gofman, J. W., F. T. Lindgren, and H. Elliot (1949). Ultracentrifugal studies of lipoproteins of human serum. *The Journal of biological chemistry* **179**, 973–9.

Gofman, J. W. (1956). Serum lipoproteins and the evaluation of atherosclerosis. *Annals of the New York Academy of Sciences* **64**, 590–5.

Gogola, E., A. A. Duarte, J. R. de Ruiter, W. W. Wiegant, J. A. Schmid, R. de Bruijn, D. I. James, S. Guerrero Llobet, D. J. Vis, S. Annunziato, et al. (2018). Selective loss of PARG restores PARylation and counteracts PARP inhibitor-mediated synthetic lethality. *Cancer Cell* **33**, 1078–1093.e12.

Goldstein, A. L. and J. H. McCusker (1999). Three new dominant drug resistance cassettes for gene disruption in *Saccharomyces cerevisiae*. *Yeast* **15**, 1541–53.

Goldstein, J. L., R. G. Anderson, and M. S. Brown (1982). Receptor-mediated endocytosis and the cellular uptake of low density lipoprotein. *Ciba Foundation Symposium*, 77–95.

Goldstein, J. L. and H. S. Brown (2003). Cholesterol: a century of research. *Howard Hughes Medical Institute Bulletin* **16**, 10–19.

Goldstein, J. L. and M. S. Brown (1973). Familial hypercholesterolemia: identification of a defect in the regulation of 3-hydroxy-3-methylglutaryl coenzyme A reductase activity associated with overproduction of cholesterol. *Proceedings of the National Academy of Sciences of the United States of America* **70**, 2804–8.

Gorman, J. W. and F. Lindgren (1950). The role of lipids and lipoproteins in atherosclerosis. *Science* **111**, 166–71.

Graham, K. and E. Unger (2018). Overcoming tumor hypoxia as a barrier to radiotherapy, chemotherapy and immunotherapy in cancer treatment. *International Journal of Nanomedicine* **13**, 6049–6058.

Gray, L. H., A. D. Conger, M. Ebert, S. Hornsey, and O. C. Scott (1953). The concentration of oxygen dissolved in tissues at the time of irradiation as a factor in radiotherapy. *The British Journal of Radiology* **26**, 638–48.

Greninger, A. L., G. M. Knudsen, M. Betegon, A. L. Burlingame, and J. L. DeRisi (2013). ACBD3 interaction with TBC1 domain 22 protein is differentially affected by enteroviral and kobuviral 3A protein binding. *mBio* **4**, e00098–13.

Guan, J., P. E. Stromhaug, M. D. George, P. Habibzadegah-Tari, A. Bevan, W. A. Dunn, and D. J. Klionsky (2001). Cvt18/Gsa12 is required for cytoplasm-to-vacuole transport, pexophagy, and autophagy in *Saccharomyces cerevisiae* and *Pichia pastoris*. *Molecular Biology of the Cell* **12**, 3821–38.

Guan, Z.-W., K.-R. Wu, R. Li, Y. Yin, X.-L. Li, S.-F. Zhang, and Y. Li (2019). Pharmacogenetics of statins treatment: Efficacy and safety. *Journal of Clinical Pharmacy and Therapeutics* **44**, 858–867.

Guarente, L. (1993). Synthetic enhancement in gene interaction: a genetic tool come of age. *Trends in Genetics* **9**, 362–6.

Haber, J. E. (2012). Mating-type genes and MAT switching in *Saccharomyces cerevisiae*. *Genetics* **191**, 33–64.

Hampton, R. Y. and J. Rine (1994). Regulated degradation of HMG-CoA reductase, an integral membrane protein of the endoplasmic reticulum, in yeast. *The Journal of Cell Biology* **125**, 299–312.

Han, J. and R. J. Kaufman (2016). The role of ER stress in lipid metabolism and lipotoxicity. *Journal of Lipid Research* **57**, 1329–38.

Hargrove, T. Y., L. Friggeri, Z. Wawrzak, S. Sivakumaran, E. M. Yazlovitskaya, S. W. Hiebert, F. P. Guengerich, M. R. Waterman, and G. I. Lepesheva (2016). Human sterol 14α-demethylase as a target for anticancer chemotherapy: towards structure-aided drug design. *Journal of Lipid Research* **57**, 1552–63.

Hart, T., M. Chandrashekhar, M. Aregger, Z. Steinhart, K. R. Brown, G. MacLeod, M. Mis, M. Zimmermann, A. Fradet-Turcotte, S. Sun, et al. (2015). High-resolution CRISPR screens reveal fitness genes and genotype-specific cancer liabilities. *Cell* **163**, 1515–26.

Hartwell, L. H. (1971a). Genetic control of the cell division cycle in yeast. IV. Genes controlling bud emergence and cytokinesis. *Experimental Cell Research* **69**, 265–76.

Hartwell, L. H. (1971b). Genetic control of the cell division cycle in yeast. II. Genes controlling DNA replication and its initiation. *Journal of Molecular Biology* **59**, 183–94.

Hartwell, L. H., P. Szankasi, C. J. Roberts, A. W. Murray, and S. H. Friend (1997). Integrating genetic approaches into the discovery of anticancer drugs. *Science* **278**, 1064–8.

He, B., P. Chen, S. Y. Chen, K. L. Vancura, S. Michaelis, and S. Powers (1991). *RAM2*, an essential gene of yeast, and *RAM1* encode the two polypeptide components of the farnesyltransferase that prenylates a-factor and Ras proteins. *Proceedings of the National Academy of Sciences of the United States of America* **88**, 11373–7.

Head, A., P. M. Jakeman, M. J. Kendall, R. Cramb, and S. Maxwell (1993). The impact of a short course of three lipid lowering drugs on fat oxidation during exercise in healthy volunteers. *Postgraduate Medical Journal* **69**, 197–203.

Heeke, A. L., J. Xiu, A. Elliott, W. M. Korn, F. Lynce, P. R. Pohlmann, C. Isaacs, S. M. Swain, G. Vidal, L. S. Schwartzberg, et al. (2020). Actionable co-alterations in breast tumors with pathogenic mutations in the homologous recombination DNA damage repair pathway. *Breast Cancer Research and Treatment* **184**, 265–275.

Hegarty, B. D., S. M. Furler, J. Ye, G. J. Cooney, and E. W. Kraegen (2003). The role of intramuscular lipid in insulin resistance. *Acta Physiologica Scandinavica* **178**, 373–83.

Hekmat-Scafe, D. S., S. E. Brownell, P. C. Seawell, S. Malladi, J. F. Imam, V. Singla, N. Bradon, M. S. Cyert, and T. Stearns (2017). Using yeast to determine the functional consequences of mutations in the human p53 tumor suppressor gene: An introductory course-based undergraduate research experience in molecular and cell biology. *Biochemistry and Molecular Biology Education* **45**, 161–178.

Hellig, H. and G. Popják (1961). Studies on the biosynthesis of cholesterol: XIII. phosphomevalonic kinase from liver. *Journal of Lipid Research* **2**, 235–243.

Henriksbo, B. D., T. C. Lau, J. F. Cavallari, E. Denou, W. Chi, J. S. Lally, J. D. Crane, B. M. Duggan, K. P. Foley, M. D. Fullerton, et al. (2014). Fluvastatin causes NLRP3 inflammasome-mediated adipose insulin resistance. *Diabetes* **63**, 3742–7.

Higuchi, R., J. D. Vevea, T. C. Swayne, R. Chojnowski, V. Hill, I. R. Boldogh, and L. A. Pon (2013). Actin dynamics affect mitochondrial quality control and aging in budding yeast. *Current Biology* **23**, 2417–22.

Hillenmeyer, M. E., E. Fung, J. Wildenhain, S. E. Pierce, S. Hoon, W. Lee, M. Proctor, R. P. St Onge, M. Tyers, D. Koller, et al. (2008). The chemical genomic portrait of yeast: uncovering a phenotype for all genes. *Science* **320**, 362–5.

Ho, J. and A. Bretscher (2001). Ras regulates the polarity of the yeast actin cytoskeleton through the stress response pathway. *Molecular Biology of the Cell* **12**, 1541–55.

Hohmann, S. (2016). Nobel yeast research. *Federation of European Microbiological Societies Yeast Research* **16**. Ed. by J. Nielsen, fow094.

Hopkins, A. L. (2008). Network pharmacology: the next paradigm in drug discovery. *Nature Chemical Biology* **4**, 682–90.

Hoque, A., H. Chen, and X.-C. Xu (2008). Statin induces apoptosis and cell growth arrest in prostate cancer cells. *Cancer Epidemiology, Biomarkers & Prevention* **17**, 88–94.

Horlbeck, M. A., A. Xu, M. Wang, N. K. Bennett, C. Y. Park, D. Bogdanoff, B. Adamson, E. D. Chow, M. Kampmann, T. R. Peterson, et al. (2018). Mapping the genetic landscape of human cells. *Cell* **174**, 953–967.

Hu, Y., A. Comjean, S. E. Mohr, FlyBase Consortium, and N. Perrimon (2017). Gene2Function: An integrated online resource for gene function discovery. *Genes, Genomes, Genetics* **7**, 2855–2858.

Hua, X., C. Yokoyama, J. Wu, M. R. Briggs, M. S. Brown, J. L. Goldstein, and X. Wang (1993). SREBP-2, a second basic-helix-loop-helix-leucine zipper protein that stimulates transcription by binding to a sterol regulatory element. *Proceedings of the National Academy of Sciences of the United States of America* **90**, 11603–7.

Huang, C.-Y. and T.-H. Tan (2012). DUSPs, to MAP kinases and beyond. *Cell & Bioscience* **2**, 24.

Hwang, S., A. D. Nguyen, Y. Jo, L. J. Engelking, J. Brugarolas, and R. A. DeBose-Boyd (2017). Hypoxia-inducible factor 1α activates insulin-induced gene 2 (Insig-2) transcription for degradation of 3-hydroxy-3-methylglutaryl (HMG)-CoA reductase in the liver. *The Journal of Biological Chemistry* **292**, 9382–9393.

Imai, S.-i. and L. Guarente (2016). It takes two to tango: NAD+ and sirtuins in aging/longevity control. *NPJ Aging and Mechanisms of Disease* **2**, 16017.

Inoue, S., S. Bar-Nun, J. Roitelman, and R. D. Simoni (1991). Inhibition of degradation of 3-hydroxy-3-methylglutaryl-coenzyme A reductase in vivo by cysteine protease inhibitors. *The Journal of Biological Chemistry* **266**, 13311–7.

Jacobs, J. M., A. Cohen, E. Ein-Mor, and J. Stessman (2013). Cholesterol, statins, and longevity from age 70 to 90 years. *Journal of the American Medical Directors Association* **14**, 883–8.

Jahn, A., B. Scherer, G. Fritz, and S. Honnen (2020). Statins induce a DAF-16/Foxo-dependent longevity phenotype via JNK-1 through mevalonate depletion in C. elegans. *Aging and Dsease* **11**, 60–72.

Jaishy, B. and E. D. Abel (2016). Lipids, lysosomes, and autophagy. *Journal of Lipid Research* **57**, 1619–35.

Jiang, Y., P. Proteau, D. Poulter, and S. Ferro-Novick (1995). *BTS1* encodes a geranylgeranyl diphosphate synthase in *Saccharomyces cerevisiae*. *The Journal of Biological Chemistry* **270**, 21793–9.

Jin, L., J. Chun, C. Pan, D. Li, R. Lin, G. N. Alesi, X. Wang, H.-B. Kang, L. Song, D. Wang, et al. (2018). MAST1 drives cisplatin resistance in human cancers by rewiring cRaf-independent MEK activation. *Cancer Cell* **34**, 315–330.e7.

Jing, B., J. Jin, R. Xiang, M. Liu, L. Yang, Y. Tong, X. Xiao, H. Lei, W. Liu, H. Xu, et al. (2018). Vorinostat and quinacrine have synergistic effects in T-cell acute lymphoblastic leukemia through reactive oxygen species increase and mitophagy inhibition. *Cell Death & Disease* **9**, 589.

Jing, X., F. Yang, C. Shao, K. Wei, M. Xie, H. Shen, and Y. Shu (2019). Role of hypoxia in cancer therapy by regulating the tumor microenvironment. *Molecular Cancer* **18**, 157.

Jo, Y. and R. A. Debose-Boyd (2010). Control of cholesterol synthesis through regulated ER-associated degradation of HMG CoA reductase. *Critical Reviews in Biochemistry and Molecular Biology* **45**, 185–98.

Joblin-Mills, A. (2020). Identintification and characterisation of the eukaryotic lipotoxicity interaction network (LIN) and modifiers of diacylglycerol-acyltransferase (DGAT)-mediated diseases. PhD thesis. Victoria University of Wellington, 282.

Jones, K. D., W. T. Couldwell, D. R. Hinton, Y. Su, S. He, L. Anker, and R. E. Law (1994). Lovastatin induces growth inhibition and apoptosis in human malignant glioma cells. *Biochemical and Biophysical Research Communications* **205**, 1681–7.

Jouve, J.-L., T. Lecomte, O. Bouché, E. Barbier, F. Khemissa Akouz, G. Riachi, E. Nguyen Khac, I. Ollivier-Hourmand, M. Debette-Gratien, R. Faroux, et al. (2019). Pravastatin combination with sorafenib does not improve survival in advanced hepatocellular carcinoma. *Journal of Hepatology* **71**, 516–522.

Juanes, M. A., R. Khoueiry, T. Kupka, A. Castro, I. Mudrak, E. Ogris, T. Lorca, and S. Piatti (2013). Budding yeast greatwall and endosulfines control activity and spatial regulation of PP2A(Cdc55) for timely mitotic progression. *PLoS Genetics* **9**, e1003575.

Juarez, D. and D. A. Fruman (2021). Targeting the mevalonate pathway in cancer. *Trends in Cancer* **7**, 525–540.

Kachroo, A. H., J. M. Laurent, C. M. Yellman, A. G. Meyer, C. O. Wilke, and E. M. Marcotte (2015). Evolution. Systematic humanization of yeast genes reveals conserved functions and genetic modularity. *Science* **348**, 921–5.

Kaelin, W. G. (2005). The concept of synthetic lethality in the context of anticancer therapy. *Nature Reviews Cancer* **5**, 689–98.

Kain, V., B. Kapadia, P. Misra, and U. Saxena (2015). Simvastatin may induce insulin resistance through a novel fatty acid mediated cholesterol independent mechanism. *Scientific Reports* **5**, 13823.

Kainou, T., K. Kawamura, K. Tanaka, H. Matsuda, and M. Kawamukai (1999). Identification of the GGPS1 genes encoding geranylgeranyl diphosphate synthases from mouse and human. *Biochimica et Biophysica Acta* **1437**, 333–40.

Kamal, A. H. M., J. K. Chakrabarty, S. M. N. Udden, M. H. Zaki, and S. M. Chowdhury (2018). Inflammatory proteomic network analysis of statin-treated and lipopolysaccharide-activated macrophages. *Scientific Reports* **8**, 164.

Kandutsch, A. A., H. W. Chen, and H. J. Heiniger (1978). Biological activity of some oxygenated sterols. *Science* **201**, 498–501.

Kanehisa, M., M. Furumichi, Y. Sato, M. Ishiguro-Watanabe, and M. Tanabe (2021). KEGG: integrating viruses and cellular organisms. *Nucleic Acids Research* **49**, D545–D551.

Kanehisa, M. and S. Goto (2000). KEGG: kyoto encyclopedia of genes and genomes. *Nucleic Acids Research* **28**, 27–30.

Kanki, T., K. Furukawa, and S.-i. Yamashita (2015). Mitophagy in yeast: Molecular mechanisms and physiological role. *Biochimica et Biophysica Acta* **1853**, 2756–65.

Kanki, T., K. Wang, M. Baba, C. R. Bartholomew, M. A. Lynch-Day, Z. Du, J. Geng, K. Mao, Z. Yang, W.-L. Yen, et al. (2009). A genomic screen for yeast mutants defective in selective mitochondria autophagy. *Molecular Biology of the Cell* **20**, 4730–8.

Kanugula, A. K., V. M. Dhople, U. Völker, R. Ummanni, and S. Kotamraju (2014). Fluvastatin mediated breast cancer cell death: a proteomic approach to identify differentially regulated proteins in MDA-MB-231 cells. *PloS One* **9**, e108890.

Karst, F. and F. Lacroute (1977). Ergosterol biosynthesis in *Saccharomyces cerevisiae*: mutants deficient in the early steps of the pathway. *Molecular & General Genetics* **154**, 269–77.

Kathagen-Buhmann, A., C. L. Maire, J. Weller, A. Schulte, J. Matschke, M. Holz, K. L. Ligon, M. Glatzel, M. Westphal, and K. Lamszus (2018). The secreted glycolytic enzyme GPI/AMF stimulates glioblastoma cell migration and invasion in an autocrine fashion but can have anti-proliferative effects. *Neuro-Oncology* **20**, 1594–1605.

Kaymak, I., C. R. Maier, W. Schmitz, A. D. Campbell, B. Dankworth, C. P. Ade, S. Walz, M. Paauwe, C. Kalogirou, H. Marouf, et al. (2020). Mevalonate pathway provides ubiquinone to maintain pyrimidine synthesis and survival in p53-deficient cancer cells exposed to metabolic stress. *Cancer Research* **80**, 189–203.

Kelley, D. E. and J. A. Simoneau (1994). Impaired free fatty acid utilization by skeletal muscle in non-insulin-dependent diabetes mellitus. *The Journal of Clinical Investigation* **94**, 2349–56.

Kelley, R. and T. Ideker (2005). Systematic interpretation of genetic interactions using protein networks. *Nature Biotechnology* **23**, 561–6.

Kelly, C. J., K. Hussien, E. Fokas, P. Kannan, R. J. Shipley, T. M. Ashton, M. Stratford, N. Pearson, and R. J. Muschel (2014). Regulation of O2 consumption by the PI3K and mTOR pathways contributes to tumor hypoxia. *Radiotherapy and Oncology* **111**, 72–80.

Kessler, A., E. Tomas, D. Immler, H. E. Meyer, A. Zorzano, and J. Eckel (2000). Rab11 is associated with GLUT4-containing vesicles and redistributes in response to insulin. *Diabetologia* **43**, 1518–27.

Khan, A. H. and D. J. Smith (2021). Cost-effective mapping of genetic interactions in mammalian cells. *Frontiers in Genetics* **12**, 703738.

Kilic, U., O. Gok, B. Elibol-Can, O. Uysal, and A. Bacaksiz (2015). Efficacy of statins on sirtuin 1 and endothelial nitric oxide synthase expression: the role of sirtuin 1 gene variants in human coronary atherosclerosis. *Clinical and Experimental Pharmacology & Physiology* **42**, 321–30.

Kim, E.-H., H. Y. Ko, A. R. Yu, H. Kim, J. Zaheer, H. J. Kang, Y.-C. Lim, K. D. Cho, H.-Y. Joo, M. K. Kang, et al. (2020). Inhibition of HIF-1α by atorvastatin during 131I-RTX therapy in Burkitt's lymphoma model. *Cancers* **12**, 1203.

Kim, S. T., J. H. Kang, J. Lee, S. H. Park, J. O. Park, Y. S. Park, H. Y. Lim, I. G. Hwang, S.-C. Lee, K.-W. Park, et al. (2014). Simvastatin plus capecitabine-cisplatin versus placebo plus capecitabine-cisplatin in patients with previously untreated advanced gastric cancer: a double-blind randomised phase 3 study. *European Journal of Cancer* **50**, 2822–30.

Kim, S., J. Chen, T. Cheng, A. Gindulyte, J. He, S. He, Q. Li, B. A. Shoemaker, P. A. Thiessen, B. Yu, et al. (2021). PubChem in 2021: new data content and improved web interfaces. *Nucleic Acids Research* **49**, D1388–D1395.

Kim, Y., T. W. Kim, S. W. Han, J. B. Ahn, S. T. Kim, J. Lee, J. O. Park, Y. S. Park, H. Y. Lim, and W. K. Kang (2019). A single arm, phase II study of simvastatin plus XELOX and bevacizumab as first-line chemotherapy in metastatic colorectal cancer patients. *Cancer Research and Treatment* **51**, 1128–1134.

King, M. A., I. G. Ganley, and V. Flemington (2016). Inhibition of cholesterol metabolism underlies synergy between mTOR pathway inhibition and chloroquine in bladder cancer cells. *Oncogene* **35**, 4518–28.

Kloudova-Spalenkova, A., P. Holy, and P. Soucek (2021). Oxysterols in cancer management: from therapy to biomarkers. *British Journal of Pharmacology* **178**, 3235–3247.

Ko, Y. J. and S. P. Balk (2004). Targeting steroid hormone receptor pathways in the treatment of hormone dependent cancers. *Current Pharmaceutical Biotechnology* **5**, 459–70.

Koedoot, E., M. Fokkelman, V.-M. Rogkoti, M. Smid, I. van de Sandt, H. de Bont, C. Pont, J. E. Klip, S. Wink, M. A. Timmermans, et al. (2019). Uncovering the signaling landscape controlling breast cancer cell migration identifies novel metastasis driver genes. *Nature Communications* **10**, 2983.

Kohlwein, S. D. (2010). Obese and anorexic yeasts: experimental models to understand the metabolic syndrome and lipotoxicity. *Biochimica et Biophysica Acta* **1801**, 222–9.

Kohlwein, S. D., M. Veenhuis, and I. J. van der Klei (2013). Lipid droplets and peroxisomes: key players in cellular lipid homeostasis or a matter of fat-store 'em up or burn 'em down. *Genetics* **193**, 1–50.

Kolda, T. G. and B. W. Bader (2009). Tensor decompositions and applications. *Society for Industrial and Applied Mathematics Review* **51**, 455–500.

Kostova, Z., Y. C. Tsai, and A. M. Weissman (2007). Ubiquitin ligases, critical mediators of endoplasmic reticulum-associated degradation. *Seminars in Cell & Developmental Biology* **18**, 770–9.

Kuleshov, M. V., M. R. Jones, A. D. Rouillard, N. F. Fernandez, Q. Duan, Z. Wang, S. Koplev, S. L. Jenkins, K. M. Jagodnik, A. Lachmann, et al. (2016). Enrichr: a comprehensive gene set enrichment analysis web server 2016 update. *Nucleic Acids Research* **44**, W90–7.

Kumarakulasingham, M., P. H. Rooney, S. R. Dundas, C. Telfer, W. T. Melvin, S. Curran, and G. I. Murray (2005). Cytochrome p450 profile of colorectal cancer: identification of markers of prognosis. *Clinical Cancer Research* **11**, 3758–65.

Kurat, C. F., K. Natter, J. Petschnigg, H. Wolinski, K. Scheuringer, H. Scholz, R. Zimmermann, R. Leber, R. Zechner, and S. D. Kohlwein (2006). Obese yeast: triglyceride lipolysis is functionally conserved from mammals to yeast. *The Journal of Biological Chemistry* **281**, 491–500.

Kurat, C. F., H. Wolinski, J. Petschnigg, S. Kaluarachchi, B. Andrews, K. Natter, and S. D. Kohlwein (2009). Cdk1/Cdc28-dependent activation of the major triacylglycerol lipase Tgl4 in yeast links lipolysis to cell-cycle progression. *Molecular Cell* **33**, 53–63.

Kuzmin, E., B. VanderSluis, W. Wang, G. Tan, R. Deshpande, Y. Chen, M. Usaj, A. Balint, M. Mattiazzi Usaj, J. van Leeuwen, et al. (2018). Systematic analysis of complex genetic interactions. *Science* **360**, eaao1729.

Lancichinetti, A. and S. Fortunato (2009). Community detection algorithms: A comparative analysis. *Physical Review Statistical, Nonlinear, and Soft Matter Physics* **80**, 056117.

Langhi, C., T. J. Marquart, R. M. Allen, and A. Baldán (2014). Perilipin-5 is regulated by statins and controls triglyceride contents in the hepatocyte. *Journal of Hepatology* **61**, 358–65.

Larsen, S., N. Stride, M. Hey-Mogensen, C. N. Hansen, L. E. Bang, H. Bundgaard, L. B. Nielsen, J. W. Helge, and F. Dela (2013). Simvastatin effects on skeletal muscle: relation to decreased mitochondrial function and glucose intolerance. *Journal of the American College of Cardiology* **61**, 44–53.

Larsen, S., A. Vigelsø, S. Dandanell, C. Prats, F. Dela, and J. W. Helge (2018). Simvastatin-induced insulin resistance may be linked to decreased lipid uptake and lipid synthesis in human skeletal muscle: the LIFESTAT study. *Journal of Diabetes Research* **2018**, 9257874.

Lee, A. Y., R. P. St Onge, M. J. Proctor, I. M. Wallace, A. H. Nile, P. A. Spagnuolo, Y. Jitkova, M. Gronda, Y. Wu, M. K. Kim, et al. (2014). Mapping the cellular response to small molecules using chemogenomic fitness signatures. *Science* **344**, 208–11.

Lee, Y., H. Hirose, M. Ohneda, J. H. Johnson, J. D. McGarry, and R. H. Unger (1994). Beta-cell lipotoxicity in the pathogenesis of non-insulin-dependent diabetes mellitus of obese rats: impairment in adipocyte-beta-cell relationships. *Proceedings of the National Academy of Sciences of the United States of America* **91**, 10878–82.

Leeuwen, J. van, C. Boone, and B. J. Andrews (2017). Mapping a diversity of genetic interactions in yeast. *Current Opinion in Systems Biology* **6**, 14–21.

Lei, P., Y. Xiao, P. Li, P. Xie, H. Wang, S. Huang, P. Song, and Y. Zhao (2020). hSnd2/TMEM208 is an HIF-1α-targeted gene and contains a WH2 motif. *Acta Biochimica et Biophysica Sinica* **52**, 328–331.

Leitzmann, M. F., C.-J. Tsai, M. J. Stampfer, W. C. Willett, and E. Giovannucci (2005). Thiazide diuretics and the risk of gallbladder disease requiring surgery in women. *Archives of Internal Medicine* **165**, 567–73.

Li, H. Y., F. R. Appelbaum, C. L. Willman, R. A. Zager, and D. E. Banker (2003). Cholesterol-modulating agents kill acute myeloid leukemia cells and sensitize them to therapeutics by blocking adaptive cholesterol responses. *Blood* **101**, 3628–34.

Li, S., W. Topatana, S. Juengpanich, J. Cao, J. Hu, B. Zhang, D. Ma, X. Cai, and M. Chen (2020). Development of synthetic lethality in cancer: molecular and cellular classification. *Signal Transduction and Targeted Therapy* **5**, 241.

Li, W., P. He, Y. Huang, Y.-F. Li, J. Lu, M. Li, H. Kurihara, Z. Luo, T. Meng, M. Onishi, et al. (2021). Selective autophagy of intracellular organelles: recent research advances. *Theranostics* **11**, 222–256.

Limprasertkul, A., N. M. Fisher, A. B. Awad, and D. R. Pendergast (2012). Statin therapy depresses fat metabolism in older individuals. *Journal of the American College of Nutrition* **31**, 32–8.

Lipatova, Z., A. H. Shah, J. J. Kim, J. W. Mulholland, and N. Segev (2013). Regulation of ER-phagy by a Ypt/Rab GTPase module. *Molecular Biology of the Cell* **24**, 3133–44.

Liscum, L., J. Finer-Moore, R. M. Stroud, K. L. Luskey, M. S. Brown, and J. L. Goldstein (1985). Domain structure of 3-hydroxy-3-methylglutaryl coenzyme A reductase, a glycoprotein of the endoplasmic reticulum. *The Journal of Biological Chemistry* **260**, 522–30.

Litton, J. K., H. S. Rugo, J. Ettl, S. A. Hurvitz, A. Gonçalves, K.-H. Lee, L. Fehrenbacher, R. Yerushalmi, L. A. Mina, M. Martin, et al. (2018). Talazoparib in patients with advanced breast cancer and a germline BRCA mutation. *The New England Journal of Medicine* **379**, 753–763.

Liu, H. P. and A. Bretscher (1989). Disruption of the single tropomyosin gene in yeast results in the disappearance of actin cables from the cytoskeleton. *Cell* **57**, 233–42.

Liu, L.-K., V. Choudhary, A. Toulmay, and W. A. Prinz (2017). An inducible ER-Golgi tether facilitates ceramide transport to alleviate lipotoxicity. *The Journal of Cell Biology* **216**, 131–147.

Liu, T., C. Laurell, G. Selivanova, J. Lundeberg, P. Nilsson, and K. G. Wiman (2007). Hypoxia induces p53-dependent transactivation and Fas/CD95-dependent apoptosis. *Cell Death and Differentiation* **14**, 411–21.

Liu, X., N. Zhou, X. Sui, Y. Pei, Z. Liang, and S. Hao (2018). Hrd1 induces cardiomyocyte apoptosis via regulating the degradation of IGF-1R by sema3a. *Biochimica et Biophysica Acta Molecular Basis of Disease* **1864**, 3615–3622.

Loebrich, S. (2014). The role of F-actin in modulating Clathrin-mediated endocytosis: Lessons from neurons in health and neuropsychiatric disorder. *Communicative & Integrative Biology* **7**, e28740.

Longley, R. P., R. R. Dennis, M. S. Heyer, and J. J. Wren (1978). Selective *Saccharomyces media* containing ergosterol and Tween 80. *Journal of the Institute of Brewing* **84**, 341–345.

Longo, J., R. J. Hamilton, M. Masoomian, N. Khurram, E. Branchard, P. J. Mullen, M. Elbaz, K. Hersey, D. Chadwick, S. Ghai, et al. (2020). A pilot window-of-opportunity study of preoperative fluvastatin in localized prostate cancer. *Prostate cancer and prostatic diseases* **23**, 630–637.

Longo, J., P. J. Mullen, R. Yu, J. E. van Leeuwen, M. Masoomian, D. T. S. Woon, Y. Wang, E. X. Chen, R. J. Hamilton, J. M. Sweet, et al. (2019). An actionable sterol-regulated feedback loop modulates statin sensitivity in prostate cancer. *Molecular Metabolism* **25**, 119–130.

Longo, V. D. and B. K. Kennedy (2006). Sirtuins in aging and age-related disease. *Cell* **126**, 257–68.

Loregger, A., M. Raaben, J. Tan, S. Scheij, M. Moeton, M. van den Berg, H. Gelberg-Etel, E. Stickel, J. Roitelman, T. Brummelkamp, et al. (2017). Haploid mammalian genetic screen identifies UBXD8 as a key determinant of HMGCR degradation and cholesterol biosynthesis. *Arteriosclerosis, Thrombosis, and Vascular Biology* **37**, 2064–2074.

Lorenz, R. T. and L. W. Parks (1987). Regulation of ergosterol biosynthesis and sterol uptake in a sterol-auxotrophic yeast. *Journal of Bacteriology* **169**, 3707–11.

Luu, W., L. J. Sharpe, J. Stevenson, and A. J. Brown (2012). Akt acutely activates the cholesterogenic transcription factor SREBP-2. *Biochimica et Biophysica Acta* **1823**, 458–64.

Luzi, L. and G. Pozza (1997). Glibenclamide: an old drug with a novel mechanism of action? *Acta Diabetologica* **34**, 239–44.

Maciejak, A., A. Leszczynska, I. Warchol, M. Gora, J. Kaminska, D. Plochocka, M. Wysocka-Kapcinska, D. Tulacz, J. Siedlecka, E. Swiezewska, et al. (2013). The effects of statins on the mevalonic acid pathway in recombinant yeast strains expressing human HMG-CoA reductase. *BMC Biotechnology* **13**, 68.

Mackay, T. F. and J. H. Moore (2014). Why epistasis is important for tackling complex human disease genetics. *Genome Medicine* **6**, 124.

Maiuri, M. C. and G. Kroemer (2015). Essential role for oxidative phosphorylation in cancer progression. *Cell Metabolism* **21**, 11–2.

Majmundar, A. J., W. J. Wong, and M. C. Simon (2010). Hypoxia-inducible factors and the response to hypoxic stress. *Molecular Cell* **40**, 294–309.

Mannino, G. C., F. Andreozzi, and G. Sesti (2019). Pharmacogenetics of type 2 diabetes mellitus, the route toward tailored medicine. *Diabetes/Metabolism Research and Reviews* **35**, e3109.

Mattiazzi Usaj, M., N. Sahin, H. Friesen, C. Pons, M. Usaj, M. P. D. Masinas, E. Shuteriqi, A. Shkurin, P. Aloy, Q. Morris, et al. (2020). Systematic genetics and single-cell imaging reveal widespread morphological pleiotropy and cell-to-cell variability. *Molecular Systems Biology* **16**, e9243.

Mayer, M. P., F. M. Hahn, D. J. Stillman, and C. D. Poulter (1992). Disruption and mapping of IDI1, the gene for isopentenyl diphosphate isomerase in *Saccharomyces cerevisiae*. *Yeast* **8**, 743–8.

Meiling-Wesse, K., H. Barth, and M. Thumm (2002). Ccz1p/Aut11p/Cvt16p is essential for autophagy and the cvt pathway. *Federation of European Biochemical Societies Letters* **526**, 71–6.

Menzies, S. A., N. Volkmar, D. J. van den Boomen, R. T. Timms, A. S. Dickson, J. A. Nathan, and P. J. Lehner (2018). The sterol-responsive RNF145 E3 ubiquitin ligase mediates the degradation of HMG-CoA reductase together with gp78 and Hrd1. *eLife* **7**.

Meraviglia, S., M. Eberl, D. Vermijlen, M. Todaro, S. Buccheri, G. Cicero, C. La Mendola, G. Guggino, M. D'Asaro, V. Orlando, et al. (2010). In vivo manipulation of Vgamma9Vdelta2 T cells with zoledronate and low-dose interleukin-2 for immunotherapy of advanced breast cancer patients. *Clinical and Experimental Immunology* **161**, 290–7.

Metz, S. A., M. E. Rabaglia, J. B. Stock, and A. Kowluru (1993). Modulation of insulin secretion from normal rat islets by inhibitors of the post-translational modifications of GTP-binding proteins. *The Biochemical Journal* **295 (Pt 1**, 31–40.

Minakshi, R., S. Rahman, A. T. Jan, A. Archana, and J. Kim (2017). Implications of aging and the endoplasmic reticulum unfolded protein response on the molecular modality of breast cancer. *Experimental & Molecular Medicine* **49**, e389.

Miner, G. E., M. L. Starr, L. R. Hurst, and R. A. Fratti (2017). Deleting the DAG kinase Dgk1 augments yeast vacuole fusion through increased Ypt7 activity and altered membrane fluidity. *Traffic* **18**, 315–329.

Mitter, A. L., P. Schlotterhose, and R. Krick (2019). Gyp1 has a dual function as Ypt1 GAP and interaction partner of Atg8 in selective autophagy. *Autophagy* **15**, 1031–1050.

Möhlig, M., F. Isken, and M. Ristow (2004). Impaired mitochondrial activity and insulin-resistant offspring of patients with type 2 diabetes. *The New England Journal of Medicine* **350**, 2419–21, author reply 2419–21.

Montgomery, M. K., W. De Nardo, and M. J. Watt (2019). Impact of lipotoxicity on tissue "cross talk" and metabolic regulation. *Physiology* **34**, 134–149.

Moon, S.-H., C.-H. Huang, S. L. Houlihan, K. Regunath, W. A. Freed-Pastor, J. P. Morris, D. F. Tschaharganeh, E. R. Kastenhuber, A. M. Barsotti, R. Culp-Hill, et al. (2019). p53 represses the mevalonate pathway to mediate tumor suppression. *Cell* **176**, 564–580.e19.

Mooren, O. L., B. J. Galletta, and J. A. Cooper (2012). Roles for actin assembly in endocytosis. *Annual Review of Biochemistry* **81**, 661–86.

Morselli, E., M. C. Maiuri, M. Markaki, E. Megalou, A. Pasparaki, K. Palikaras, A. Criollo, L. Galluzzi, S. A. Malik, I. Vitale, et al. (2010). Caloric restriction and resveratrol promote longevity through the Sirtuin-1-dependent induction of autophagy. *Cell Death & Disease* **1**, e10.

Mudassar, F., H. Shen, G. O'Neill, and E. Hau (2020). Targeting tumor hypoxia and mitochondrial metabolism with anti-parasitic drugs to improve radiation response in high-grade gliomas. *Journal of Experimental & Clinical Cancer Research* **39**, 208.

Mullen, P. J., R. Yu, J. Longo, M. C. Archer, and L. Z. Penn (2016). The interplay between cell signalling and the mevalonate pathway in cancer. *Nature Reviews Cancer* **16**, 718–731.

Munkacsi, A. B., F. W. Chen, M. A. Brinkman, K. Higaki, G. D. Gutiérrez, J. Chaudhari, J. V. Layer, A. Tong, M. Bard, C. Boone, et al. (2011). An "exacerbate-reverse" strategy in yeast identifies histone deacetylase inhibition as a correction for cholesterol and sphingolipid transport defects in human Niemann-Pick type C disease. *The Journal of Biological Chemistry* **286**, 23842–51.

Nakanishi, M., J. L. Goldstein, and M. S. Brown (1988). Multivalent control of 3-hydroxy-3-methylglutaryl coenzyme A reductase. Mevalonate-derived product inhibits translation of mRNA and accelerates degradation of enzyme. *The Journal of Biological Chemistry* **263**, 8929–37.

Nakatogawa, H., K. Suzuki, Y. Kamada, and Y. Ohsumi (2009). Dynamics and diversity in autophagy mechanisms: lessons from yeast. *Nature Reviews Molecular Cell Biology* **10**, 458–67.

Neal, S., D. Syau, A. Nejatfard, S. Nadeau, and R. Y. Hampton (2020). HRD complex self-remodeling enables a novel route of membrane protein retrotranslocation. *iScience* **23**, 101493.

Ness, G. C., S. J. Eales, L. C. Pendleton, and M. Smith (1985). Activation of rat liver microsomal 3-hydroxy-3-methylglutaryl coenzyme A reductase by NADPH. Effects of dietary treatments. *The Journal of Biological Chemistry* **260**, 12391–3.

Ness, G. C. (2015). Physiological feedback regulation of cholesterol biosynthesis: Role of translational control of hepatic HMG-CoA reductase and possible involvement of oxylanosterols. *Biochimica et Biophysica Acta* **1851**, 667–73.

Ness, G. C., C. M. Chambers, and D. Lopez (1998). Atorvastatin action involves diminished recovery of hepatic HMG-CoA reductase activity. *Journal of Lipid Research* **39**, 75–84.

Newman, M. E. (2005). A measure of betweenness centrality based on random walks. *Social Networks* **27**, 39–54.

Nguyen, A. D., J. G. McDonald, R. K. Bruick, and R. A. DeBose-Boyd (2007). Hypoxia stimulates degradation of 3-hydroxy-3-methylglutaryl-coenzyme A reductase through accumulation of lanosterol and hypoxia-inducible factor-mediated induction of insigs. *The Journal of Biological Chemistry* **282**, 27436–27446.

Nishikawa, S. and A. Nakano (1993). Identification of a gene required for membrane protein retention in the early secretory pathway. *Proceedings of the National Academy of Sciences of the United States of America* **90**, 8179–83.

Nosengo, N. (2016). Can you teach old drugs new tricks? *Nature* **534**, 314–6.

Novak, A., B. Binnington, B. Ngan, K. Chadwick, N. Fleshner, and C. A. Lingwood (2013). Cholesterol masks membrane glycosphingolipid tumor-associated antigens to reduce their immunodetection in human cancer biopsies. *Glycobiology* **23**, 1230–9.

Novick, P. and R. Schekman (1979). Secretion and cell-surface growth are blocked in a temperature-sensitive mutant of *Saccharomyces cerevisiae*. *Proceedings of the National Academy of Sciences of the United States of America* **76**, 1858–62.

Novick, P., C. Field, and R. Schekman (1980). Identification of 23 complementation groups required for post-translational events in the yeast secretory pathway. *Cell* **21**, 205–15.

Nowikovsky, K., S. Reipert, R. J. Devenish, and R. J. Schweyen (2007). Mdm38 protein depletion causes loss of mitochondrial K+/H+ exchange activity, osmotic swelling and mitophagy. *Cell Death and Differentiation* **14**, 1647–56.

Ohsumi, Y. (2014). Historical landmarks of autophagy research. *Cell Research* **24**, 9–23.

Okada, S., T. Morimoto, H. Ogawa, H. Soejima, C. Matsumoto, M. Sakuma, M. Nakayama, N. Doi, H. Jinnouchi, M. Waki, et al. (2021). Association between statins and cancer incidence in diabetes: a cohort study of Japanese patients with type 2 diabetes. *Journal of General Internal Medicine* **36**, 632–639.

Okamoto, K., N. Kondo-Okamoto, and Y. Ohsumi (2009). Mitochondria-anchored receptor Atg32 mediates degradation of mitochondria via selective autophagy. *Developmental Cell* **17**, 87–97.

Okubo, K., M. Isono, K. Miyai, T. Asano, and A. Sato (2020). Fluvastatin potentiates anticancer activity of vorinostat in renal cancer cells. *Cancer Science* **111**, 112–126.

Olzmann, J. A. and P. Carvalho (2019). Dynamics and functions of lipid droplets. *Nature Reviews Molecular Cell Biology* **20**, 137–155.

Pan, C., J. Chun, D. Li, A. C. Boese, J. Li, J. Kang, A. Umano, Y. Jiang, L. Song, K. R. Magliocca, et al. (2019). Hsp90B enhances MAST1-mediated cisplatin resistance by protecting MAST1 from proteosomal degradation. *The Journal of Clinical Investigation* **129**, 4110–4123.

Pan, H., L. Gu, B. Liu, Y. Li, Y. Wang, X. Bai, L. Li, B. Wang, Q. Peng, Z. Yao, et al. (2017). Tropomyosin-1 acts as a potential tumor suppressor in human oral squamous cell carcinoma. *PloS One* **12**. Ed. by C.-H. Tang, e0168900.

Pan, X., P. Ye, D. S. Yuan, X. Wang, J. S. Bader, and J. D. Boeke (2006). A DNA integrity network in the yeast *Saccharomyces cerevisiae*. *Cell* **124**, 1069–81.

Panciera, T., L. Azzolin, A. Fujimura, D. Di Biagio, C. Frasson, S. Bresolin, S. Soligo, G. Basso, S. Bicciato, A. Rosato, et al. (2016). Induction of expandable tissue-specific stem/progenitor cells through transient expression of YAP/TAZ. *Cell Stem Cell* **19**, 725–737.

Panduro, J., M. Kjaer, J. Wolff-Jensen, and H. H. Hansen (1983). Misonidazole combined with radiotherapy in the treatment of inoperable squamous cell carcinoma of the lung. A double-blind randomized trial. *Cancer* **52**, 20–4.

Pandyra, A. A., P. J. Mullen, C. A. Goard, E. Ericson, P. Sharma, M. Kalkat, R. Yu, J. T. Pong, K. R. Brown, T. Hart, et al. (2015). Genome-wide RNAi analysis reveals that simultaneous inhibition of specific mevalonate pathway genes potentiates tumor cell death. *Oncotarget* **6**, 26909–21.

Panozzo, C., M. Nawara, C. Suski, R. Kucharczyka, M. Skoneczny, A. M. Bécam, J. Rytka, and C. J. Herbert (2002). Aerobic and anaerobic NAD+ metabolism in *Saccharomyces cerevisiae*. *Federation of European Biochemical Societies Letters* **517**, 97–102.

Parameswaran, S., D. Kundapur, F. S. Vizeacoumar, A. Freywald, M. Uppalapati, and F. J. Vizeacoumar (2019). A road map to personalizing targeted cancer therapies using synthetic lethality. *Trends in Cancer* **5**, 11–29.

Parikh, A., C. Childress, K. Deitrick, Q. Lin, D. Rukstalis, and W. Yang (2010). Statin-induced autophagy by inhibition of geranylgeranyl biosynthesis in prostate cancer PC3 cells. *The Prostate* **70**, 971–81.

Parrales, A., A. Ranjan, S. V. Iyer, S. Padhye, S. J. Weir, A. Roy, and T. Iwakuma (2016). DNAJA1 controls the fate of misfolded mutant p53 through the mevalonate pathway. *Nature Cell Biology* **18**, 1233–1243.

Parsons, A. B., R. L. Brost, H. Ding, Z. Li, C. Zhang, B. Sheikh, G. W. Brown, P. M. Kane, T. R. Hughes, and C. Boone (2004). Integration of chemical-genetic and genetic interaction data links bioactive compounds to cellular target pathways. *Nature Biotechnology* **22**, 62–9.

Parsons, A. B., A. Lopez, I. E. Givoni, D. E. Williams, C. A. Gray, J. Porter, G. Chua, R. Sopko, R. L. Brost, C.-H. Ho, et al. (2006). Exploring the mode-of-action of bioactive compounds by chemical-genetic profiling in yeast. *Cell* **126**, 611–25.

Parts, L., A. Batté, M. Lopes, M. W. Yuen, M. Laver, B.-J. San Luis, J.-X. Yue, C. Pons, E. Eray, P. Aloy, et al. (2021). Natural variants suppress mutations in hundreds of essential genes. *Molecular Systems Biology* **17**, e10138.

Pascolo, S. (2016). Time to use a dose of Chloroquine as an adjuvant to anti-cancer chemotherapies. *European Journal of Pharmacology* **771**, 139–44.

Patel, O. P. S., O. J. Jesumoroti, L. J. Legoabe, and R. M. Beteck (2021). Metronidazole-conjugates: A comprehensive review of recent developments towards synthesis and medicinal perspective. *European Journal of Medicinal Chemistry* **210**, 112994.

Pearson, E. R. (2016). Personalized medicine in diabetes: the role of 'omics' and biomarkers. *Diabetic Medicine* **33**, 712–7.

Pedersen, T. R., L. Wilhelmsen, O. Faergeman, T. E. Strandberg, G. Thorgeirsson, L. Troedsson, J. Kristianson, K. Berg, T. J. Cook, T. Haghfelt, et al. (2000). Follow-up study of patients randomized in the Scandinavian simvastatin survival study (4S) of cholesterol lowering. *The American Journal of Cardiology* **86**, 257–62.

Pei, S., M. Minhajuddin, B. Adane, N. Khan, B. M. Stevens, S. C. Mack, S. Lai, J. N. Rich, A. Inguva, K. M. Shannon, et al. (2018). AMPK/FIS1-mediated mitophagy is required for self-renewal of human AML stem cells. *Cell Stem Cell* **23**, 86–100.e6.

Peltomaa, A. I., P. Raittinen, K. Talala, K. Taari, T. L. J. Tammela, A. Auvinen, and T. J. Murtola (2021). Prostate cancer prognosis after initiation of androgen deprivation therapy among statin users. A population-based cohort study. *Prostate Cancer and Prostatic Diseases*, 1–8.

Peng, T.-C., C.-C. Wang, T.-W. Kao, J. Y.-H. Chan, Y.-H. Yang, Y.-W. Chang, and W.-L. Chen (2015). Relationship between hyperuricemia and lipid profiles in US adults. *BioMed Research International* **2015**. Ed. by A. Romero-Corral, 127596.

Petschnigg, J., H. Wolinski, D. Kolb, G. Zellnig, C. F. Kurat, K. Natter, and S. D. Kohlwein (2009). Good fat, essential cellular requirements for triacylglycerol synthesis to maintain membrane homeostasis in yeast. *The Journal of Biological Chemistry* **284**, 30981–93.

Petsko, G. A. (2010). When failure should be the option. *BMC Biology* **8**, 61.

Pezzuto, A. and E. Carico (2018). Role of HIF-1 in cancer progression: novel insights. A review. *Current Molecular Medicine* **18**, 343–351.

Phillips, P. C. (1998). The language of gene interaction. *Genetics* **149**, 1167–71.

Pierrelée, M., A. Reynders, F. Lopez, A. Moqrich, L. Tichit, and B. H. Habermann (2021). Introducing the novel Cytoscape app TimeNexus to analyze time-series data using temporal MultiLayer Networks (tMLNs). *Scientific Reports* **11**, 13691.

Pinho, S. S. and C. A. Reis (2015). Glycosylation in cancer: mechanisms and clinical implications. *Nature Reviews Cancer* **15**, 540–55.

Ploier, B., M. Scharwey, B. Koch, C. Schmidt, J. Schatte, G. Rechberger, M. Kollroser, A. Hermetter, and G. Daum (2013). Screening for hydrolytic enzymes reveals Ayr1p as a novel triacylglycerol lipase in *Saccharomyces cerevisiae*. *The Journal of Biological Chemistry* **288**, 36061–72.

Pollastro, C., C. Ziviello, V. Costa, and A. Ciccodicola (2015). Pharmacogenomics of drug response in type 2 diabetes: toward the definition of tailored therapies? *PPAR Research* **2015**, 415149.

Popovic, D., M. Akutsu, I. Novak, J. W. Harper, C. Behrends, and I. Dikic (2012). Rab GTPase-activating proteins in autophagy: regulation of endocytic and autophagy pathways by direct binding to human ATG8 modifiers. *Molecular and Cellular Biology* **32**, 1733–44.

Powers, R. W., M. Kaeberlein, S. D. Caldwell, B. K. Kennedy, and S. Fields (2006). Extension of chronological life span in yeast by decreased TOR pathway signaling. *Genes & Development* **20**, 174–84.

Preiss, D., S. R. K. Seshasai, P. Welsh, S. A. Murphy, J. E. Ho, D. D. Waters, D. A. DeMicco, P. Barter, C. P. Cannon, M. S. Sabatine, et al. (2011). Risk of incident diabetes with intensive-dose compared with moderate-dose statin therapy: a meta-analysis. *Journal of the American Medical Association* **305**, 2556–64.

Priault, M., B. Salin, J. Schaeffer, F. M. Vallette, J.-P. di Rago, and J.-C. Martinou (2005). Impairing the bioenergetic status and the biogenesis of mitochondria triggers mitophagy in yeast. *Cell Death and Differentiation* **12**, 1613–21.

Pushpakom, S., F. Iorio, P. A. Eyers, K. J. Escott, S. Hopper, A. Wells, A. Doig, T. Guilliams, J. Latimer, C. McNamee, et al. (2019). Drug repurposing: progress, challenges and recommendations. *Nature Reviews Drug Discovery* **18**, 41–58.

Qi, X., Y. Okuma, T. Hosoi, M. Kaneko, and Y. Nomura (2004). Induction of murine HRD1 in experimental cerebral ischemia. *Brain Research Molecular Brain Research* **130**, 30–8.

Qian, L., K. Zhu, Y. Lin, L. An, F. Huang, Y. Yao, and L. Ren (2019). Insulin secretion impairment induced by rosuvastatin partly though autophagy in INS-1E cells. *Cell Biology International* **44**, 127–136.

Rahiminejad, S., M. R. Maurya, and S. Subramaniam (2019). Topological and functional comparison of community detection algorithms in biological networks. *BMC Bioinformatics* **20**, 212.

Raittinen, P., K. Niemistö, E. Pennanen, H. Syvälä, S. Auriola, J. Riikonen, T. Lehtimäki, P. Ilmonen, and T. Murtola (2020). Circulatory and prostatic tissue lipidomic profiles shifts after high-dose atorvastatin use in men with prostate cancer. *Scientific Reports* **10**, 12016.

Raju, T. N. (2000). The Nobel chronicles. 1988: James Whyte Black, (b 1924), Gertrude Elion (1918-99), and George H Hitchings (1905-98). *Lancet* **355**, 1022.

Ramesh, M., J. C. Campos, P. Lee, Y. Song, G. Hernandez, J. Sin, K. C. Tucker, H. Saadaeijahromi, M. Gurney, J. C. B. Ferreira, et al. (2019). Mitophagy protects against statin-mediated skeletal muscle toxicity. *Federation of American Societies for Experimental Biology* **33**, 11857–11869.

Rauscher, B., F. Heigwer, L. Henkel, T. Hielscher, O. Voloshanenko, and M. Boutros (2018). Toward an integrated map of genetic interactions in cancer cells. *Molecular Systems Biology* **14**, e7656.

Rauthan, M., P. Ranji, N. Aguilera Pradenas, C. Pitot, and M. Pilon (2013). The mitochondrial unfolded protein response activator ATFS-1 protects cells from inhibition of the mevalonate pathway. *Proceedings of the National Academy of Sciences of the United States of America* **110**, 5981–6.

Reiner, S., D. Micolod, G. Zellnig, and R. Schneiter (2006). A genomewide screen reveals a role of mitochondria in anaerobic uptake of sterols in yeast. *Molecular Biology of the Cell* **17**, 90–103.

Rizzolo, K., J. Huen, A. Kumar, S. Phanse, J. Vlasblom, Y. Kakihara, H. A. Zeineddine, Z. Minic, J. Snider, W. Wang, et al. (2017). Features of the chaperone cellular network revealed through systematic interaction mapping. *Cell Reports* **20**, 2735–2748.

Roesch, A., T. Vogt, W. Stolz, M. Dugas, M. Landthaler, and B. Becker (2003). Discrimination between gene expression patterns in the invasive margin and the tumour core of malignant melanomas. *Melanoma Research* **13**, 503–9.

Roitelman, J. and R. D. Simoni (1992). Distinct sterol and nonsterol signals for the regulated degradation of 3-hydroxy-3-methylglutaryl-CoA reductase. *The Journal of Biological Chemistry* **267**, 25264–73.

Rosenwald, A. G., M. A. Rhodes, H. Van Valkenburgh, V. Palanivel, G. Chapman, A. Boman, C.-j. Zhang, and R. A. Kahn (2002). *ARL1* and membrane traffic in *Saccharomyces cerevisiae*. *Yeast* **19**, 1039–56.

Rosvall, M. and C. T. Bergstrom (2008). Maps of random walks on complex networks reveal community structure. *Proceedings of the National Academy of Sciences of the United States of America* **105**, 1118–23.

Rudney, H. and J. J. Ferguson (1959). The biosynthesis of beta-hydroxy-beta-methylglutaryl coenzyme A in yeast. II. The formation of hydroxymethylglutaryl coenzyme A via the condensation of acetyl coenzyme A and acetoacetyl coenzyme A. *The Journal of Biological Chemistry* **234**, 1076–80.

Salar, U., K. M. Khan, M. Taha, N. H. Ismail, B. Ali, Qurat-Ul-Ain, S. Perveen, M. Ghufran, and A. Wadood (2017). Biology-oriented drug synthesis (BIODS): In vitro β-glucuronidase inhibitory and in silico studies on 2-(2-methyl-5-nitro-1H-imidazol-1-yl)ethyl aryl carboxylate derivatives. *European Journal of Medicinal Chemistry* **125**, 1289–1299.

Samuel, V. T., K. F. Petersen, and G. I. Shulman (2010). Lipid-induced insulin resistance: unravelling the mechanism. *Lancet* **375**, 2267–77.

Santos, S. M. and J. L. Hartman (2019). A yeast phenomic model for the influence of Warburg metabolism on genetic buffering of doxorubicin. *Cancer & Metabolism* **7**, 9.

Sawyers, C. (2004). Targeted cancer therapy. *Nature* **432**, 294–7.

Saxena, K. and M. K. Jolly (2019). Acute vs. chronic vs. cyclic hypoxia: Their differential dynamics, molecular mechanisms, and effects on tumor progression. *Biomolecules* **9**, 339.

Scandinavian Simvastatin Survival Study Group (1994). Randomised trial of cholesterol lowering in 4444 patients with coronary heart disease: the Scandinavian Simvastatin Survival Study (4S). *Lancet* **344**, 1383–9.

Schekman, R., B. Esmon, S. Ferro-Novick, C. Field, and P. Novick (1983). Yeast secretory mutants: isolation and characterization. *Methods in Enzymology* **96**, 802–15.

Schirris, T. J. J., G. H. Renkema, T. Ritschel, N. C. Voermans, A. Bilos, B. G. M. van Engelen, U. Brandt, W. J. H. Koopman, J. D. Beyrath, R. J. Rodenburg, et al. (2015). Statin-induced myopathy is associated with mitochondrial complex III inhibition. *Cell Metabolism* **22**, 399–407.

Schrauwen, P., V. Schrauwen-Hinderling, J. Hoeks, and M. K. C. Hesselink (2010). Mitochondrial dysfunction and lipotoxicity. *Biochimica et Biophysica Acta* **1801**, 266–71.

Schwenk, R. W. and J. Eckel (2007). A novel method to monitor insulin-stimulated GTP-loading of Rab11a in cardiomyocytes. *Cellular Signalling* **19**, 825–30.

Scott, N. A., L. J. Sharpe, I. M. Capell-Hattam, S. J. Gullo, W. Luu, and A. J. Brown (2020). The cholesterol synthesis enzyme lanosterol 14α-demethylase is post-translationally regulated by the E3 ubiquitin ligase MARCH6. *The Biochemical Journal* **477**, 541–555.

Seeger, H., D. Wallwiener, and A. O. Mueck (2003). Statins can inhibit proliferation of human breast cancer cells in vitro. *Experimental and Clinical Endocrinology & Diabetes* **111**, 47–8.

Semenza, G. L. (2010). Defining the role of hypoxia-inducible factor 1 in cancer biology and therapeutics. *Oncogene* **29**, 625–34.

Senft, D. and Z. A. Ronai (2015). UPR, autophagy, and mitochondria crosstalk underlies the ER stress response. *Trends in Biochemical Sciences* **40**, 141–8.

Serratore, N. D., K. M. Baker, L. A. Macadlo, A. R. Gress, B. L. Powers, N. Atallah, K. M. Westerhouse, M. C. Hall, V. M. Weake, and S. D. Briggs (2018). A novel sterol-signaling pathway governs azole antifungal drug resistance and hypoxic gene repression in *Saccharomyces cerevisiae*. *Genetics* **208**, 1037–1055.

Sever, N., T. Yang, M. S. Brown, J. L. Goldstein, and R. A. DeBose-Boyd (2003). Accelerated degradation of HMG CoA reductase mediated by binding of insig-1 to its sterol-sensing domain. *Molecular Cell* **11**, 25–33.

Shannon, P., A. Markiel, O. Ozier, N. S. Baliga, J. T. Wang, D. Ramage, N. Amin, B. Schwikowski, and T. Ideker (2003). Cytoscape: a software environment for integrated models of biomolecular interaction networks. *Genome Research* **13**, 2498–504.

Sigala, I., M. Koutroumani, A. Koukiali, T. Giannakouros, and E. Nikolakaki (2021). Nuclear translocation of SRPKs is associated with 5-FU and cisplatin sensitivity in HeLa and T24 cells. *Cells* **10**, 759.

Simon, J. A. (2001). Yeast as a model system for anticancer drug discovery. *Expert Opinion on Therapeutic Targets* **5**, 177–95.

Siperstein, M. D. and V. M. Fagan (1966). Feedback control of mevalonate synthesis by dietary cholesterol. *The Journal of Biological Chemistry* **241**, 602–9.

Skalnik, D. G., H. Narita, C. Kent, and R. D. Simoni (1988). The membrane domain of 3-hydroxy-3-methylglutaryl-coenzyme A reductase confers endoplasmic reticulum localization and sterol-regulated degradation onto beta-galactosidase. *The Journal of Biological Chemistry* **263**, 6836–41.

Snoek, I. S. I. and H. Y. Steensma (2006). Why does *Kluyveromyces lactis* not grow under anaerobic conditions? Comparison of essential anaerobic genes of *Saccharomyces cerevisiae* with the *Kluyveromyces lactis* genome. *Federation of European Microbiological Societies Yeast Research* **6**, 393–403.

Soetaert, K. (2019). *CRAN - package plot3D.*

Soltis, D. A., G. McMahon, S. L. Caplan, D. A. Dudas, H. A. Chamberlin, A. Vattay, D. Dottavio, M. L. Rucker, R. G. Engstrom, and S. A. Cornell-Kennon (1995). Expression, purification, and characterization of the human squalene synthase: use of yeast and baculoviral systems. *Archives of biochemistry and biophysics* **316**, 713–23.

Song, B.-L., N. B. Javitt, and R. A. DeBose-Boyd (2005). Insig-mediated degradation of HMG CoA reductase stimulated by lanosterol, an intermediate in the synthesis of cholesterol. *Cell Metabolism* **1**, 179–89.

Sørensen, B. S. and M. R. Horsman (2020). Tumor hypoxia: impact on radiation therapy and molecular pathways. *Frontiers in Oncology* **10**, 562.

Stefely, J. A. and D. J. Pagliarini (2017). Biochemistry of mitochondrial coenzyme Q biosynthesis. *Trends in Biochemical Sciences* **42**, 824–843.

Stein, C. M., N. Brown, M. G. Carlson, P. Campbell, and A. J. Wood (1997). Coadministration of glyburide and minoxidil, drugs with opposing effects on potassium channels. *Clinical Pharmacology and Therapeutics* **61**, 662–8.

Steinberg, D. (2006). Thematic review series: the pathogenesis of atherosclerosis. An interpretive history of the cholesterol controversy, part V: the discovery of the statins and the end of the controversy. *Journal of Lipid Research* **47**, 1339–51.

Sterner, D. E., X. Wang, M. H. Bloom, G. M. Simon, and S. L. Berger (2002). The SANT domain of Ada2 is required for normal acetylation of histones by the yeast SAGA complex. *The Journal of Biological Chemistry* **277**, 8178–86.

Stolz, A., R. S. Schweizer, A. Schäfer, and D. H. Wolf (2010). Dfm1 forms distinct complexes with Cdc48 and the ER ubiquitin ligases and is required for ERAD. *Traffic* **11**, 1363–9.

Strandberg, T. E., K. Pyörälä, T. J. Cook, L. Wilhelmsen, O. Faergeman, G. Thorgeirsson, T. R. Pedersen, J. Kjekshus, and 4S Group (2004). Mortality and incidence of cancer during 10-year follow-up of the Scandinavian Simvastatin Survival Study (4S). *Lancet* **364**, 771–7.

Subramanian, A., P. Tamayo, V. K. Mootha, S. Mukherjee, B. L. Ebert, M. A. Gillette, A. Paulovich, S. L. Pomeroy, T. R. Golub, E. S. Lander, et al. (2005). Gene set enrichment analysis: a knowledge-based approach for interpreting genome-wide expression profiles. *Proceedings of the National Academy of Sciences of the United States of America* **102**, 15545–50.

Sudlow, C., J. Gallacher, N. Allen, V. Beral, P. Burton, J. Danesh, P. Downey, P. Elliott, J. Green, M. Landray, et al. (2015). UK biobank: an open access resource for identifying the causes of a wide range of complex diseases of middle and old age. *PLoS Medicine* **12**, e1001779.

Sun, W., P. E. Sanderson, and W. Zheng (2016). Drug combination therapy increases successful drug repositioning. *Drug Discovery Today* **21**, 1189–95.

Sun, X., W.-D. Chen, and Y.-D. Wang (2017). DAF-16/FOXO transcription factor in aging and longevity. *Frontiers in Pharmacology* **8**, 548.

Sundqvist, A., M. T. Bengoechea-Alonso, X. Ye, V. Lukiyanchuk, J. Jin, J. W. Harper, and J. Ericsson (2005). Control of lipid metabolism by phosphorylation-dependent degradation of the SREBP family of transcription factors by SCF(Fbw7). *Cell Metabolism* **1**, 379–91.

Suzuki, K. (2013). Selective autophagy in budding yeast. *Cell Death and Differentiation* **20**, 43–8.

Swanson, R., M. Locher, and M. Hochstrasser (2001). A conserved ubiquitin ligase of the nuclear envelope/endoplasmic reticulum that functions in both ER-associated and Matalpha2 repressor degradation. *Genes & Development* **15**, 2660–74.

Swerdlow, D. I., D. Preiss, K. B. Kuchenbaecker, M. V. Holmes, J. E. L. Engmann, T. Shah, R. Sofat, S. Stender, P. C. D. Johnson, R. A. Scott, et al. (2015). HMG-coenzyme A reductase inhibition, type 2 diabetes, and bodyweight: evidence from genetic analysis and randomised trials. *Lancet* **385**, 351–61.

Szklarczyk, D., A. Franceschini, S. Wyder, K. Forslund, D. Heller, J. Huerta-Cepas, M. Simonovic, A. Roth, A. Santos, K. P. Tsafou, et al. (2015). STRING v10: protein-protein interaction networks, integrated over the tree of life. *Nucleic Acids Research* **43**, D447–52.

Takaguri, A., K. Satoh, M. Itagaki, Y. Tokumitsu, and K. Ichihara (2008). Effects of atorvastatin and pravastatin on signal transduction related to glucose uptake in 3T3L1 adipocytes. *Journal of Pharmacological Sciences* **107**, 80–9.

Talarek, N., E. Gueydon, and E. Schwob (2017). Homeostatic control of START through negative feedback between Cln3-Cdk1 and Rim15/Greatwall kinase in budding yeast. *eLife* **6**, e26233.

Tan, P., S. Wei, L. Yang, Z. Tang, D. Cao, L. Liu, J. Lei, Y. Fan, L. Gao, and Q. Wei (2016a). The effect of statins on prostate cancer recurrence and mortality after definitive therapy: a systematic review and meta-analysis. *Scientific Reports* **6**, 29106.

Tan, Q., M. Wang, M. Yu, J. Zhang, R. G. Bristow, R. P. Hill, and I. F. Tannock (2016b). Role of autophagy as a survival mechanism for hypoxic cells in tumors. *Neoplasia* **18**, 347–55.

Tan, S.-X., M. Teo, Y. T. Lam, I. W. Dawes, and G. G. Perrone (2009). Cu, Zn superoxide dismutase and NADP(H) homeostasis are required for tolerance of endoplasmic reticulum stress in *Saccharomyces cerevisiae*. *Molecular Biology of the Cell* **20**, 1493–508.

Tang, C., J. Wang, Q. Wei, Y.-P. Du, H.-P. Qiu, C. Yang, and Y.-C. Hou (2018). Tropomyosin-1 promotes cancer cell apoptosis via the p53-mediated mitochondrial pathway in renal cell carcinoma. *Oncology Letters* **15**, 7060–7068.

Taylor, M. B. and I. M. Ehrenreich (2015). Higher-order genetic interactions and their contribution to complex traits. *Trends in Genetics* **31**, 34–40.

Taylor, R. C. (2016). Aging and the UPR(ER). *Brain Research* **1648**, 588–593.

Tchen, T. T. (1958). Mevalonic kinase: purification and properties. *The Journal of Biological Chemistry* **233**, 1100–3.

Theesfeld, C. L. and R. Y. Hampton (2013). Insulin-induced gene protein (INSIG)-dependent sterol regulation of Hmg2 endoplasmic reticulum-associated degradation (ERAD) in yeast. *The Journal of Biological Chemistry* **288**, 8519–8530.

Thomas, L. L., A. M. N. Joiner, and J. C. Fromme (2018). The TRAPPIII complex activates the GTPase Ypt1 (Rab1) in the secretory pathway. *The Journal of Cell Biology* **217**, 283–298.

Thomlinson, R. H. and L. H. Gray (1955). The histological structure of some human lung cancers and the possible implications for radiotherapy. *British Journal of Cancer* **9**, 539–49.

Thorsness, M., W. Schafer, L. D'Ari, and J. Rine (1989). Positive and negative transcriptional control by heme of genes encoding 3-hydroxy-3-methylglutaryl coenzyme A reductase in *Saccharomyces cerevisiae*. *Molecular and Cellular Biology* **9**, 5702–12.

Tobert, J. A., G. D. Bell, J. Birtwell, I. James, W. R. Kukovetz, J. S. Pryor, A. Buntinx, I. B. Holmes, Y. S. Chao, and J. A. Bolognese (1982a). Cholesterol-lowering effect of mevinolin, an inhibitor of 3-hydroxy-3-methylglutaryl-coenzyme a reductase, in healthy volunteers. *The Journal of Clinical Investigation* **69**, 913–9.

Tobert, J. A., G. Hitzenberger, W. R. Kukovetz, I. B. Holmes, and K. H. Jones (1982b). Rapid and substantial lowering of human serum cholesterol by mevinolin (MK-803), an inhibitor of hydroxymethylglutaryl-coenzyme A reductase. *Atherosclerosis* **41**, 61–5.

Toepfer, N., C. Childress, A. Parikh, D. Rukstalis, and W. Yang (2011). Atorvastatin induces autophagy in prostate cancer PC3 cells through activation of LC3 transcription. *Cancer Biology & Therapy* **12**, 691–9.

Tong, A. H., M. Evangelista, A. B. Parsons, H. Xu, G. D. Bader, N. Pagé, M. Robinson, S. Raghibizadeh, C. W. Hogue, H. Bussey, et al. (2001). Systematic genetic analysis with ordered arrays of yeast deletion mutants. *Science* **294**, 2364–8.

Tong, A. H. Y. and C. Boone (2006). Synthetic genetic array analysis in *Saccharomyces cerevisiae*. *Methods in Molecular Biology* **313**, 171–92.

Tong, A. H. Y., G. Lesage, G. D. Bader, H. Ding, H. Xu, X. Xin, J. Young, G. F. Berriz, R. L. Brost, M. Chang, et al. (2004). Global mapping of the yeast genetic interaction network. *Science* **303**, 808–13.

Toyama, E. Q., S. Herzig, J. Courchet, T. L. Lewis, O. C. Losón, K. Hellberg, N. P. Young, H. Chen, F. Polleux, D. C. Chan, et al. (2016). Metabolism. AMP-activated protein kinase mediates mitochondrial fission in response to energy stress. *Science* **351**, 275–281.

Trocha, P. J. and D. B. Sprinson (1976). Location and regulation of early enzymes of sterol biosynthesis in yeast. *Archives of Biochemistry and Biophysics* **174**, 45–51.

Trzaskos, J. M., R. L. Magolda, M. F. Favata, R. T. Fischer, P. R. Johnson, H. W. Chen, S. S. Ko, D. A. Leonard, and J. L. Gaylor (1993). Modulation of 3-hydroxy-3-methylglutaryl-CoA reductase by 15 alpha-fluorolanost-7-en-3 beta-ol. A mechanism-based inhibitor of cholesterol biosynthesis. *The Journal of Biological Chemistry* **268**, 22591–9.

Trzaskos, J. M. (1995). Oxylanosterols as modifiers of cholesterol biosynthesis. *Progress in Lipid Research* **34**, 99–116.

Tsukada, M. and Y. Ohsumi (1993). Isolation and characterization of autophagy-defective mutants of *Saccharomyces cerevisiae*. *Federation of European Biochemical Societies Letters* **333**, 169–74.

Tsvetanova, N. G. (2013). The secretory pathway in control of endoplasmic reticulum homeostasis. *Small GTPases* **4**, 28–33.

Tutuncuoglu, B. and N. J. Krogan (2019). Mapping genetic interactions in cancer: a road to rational combination therapies. *Genome Medicine* **11**, 62.

Tutuska, K., L. Parrilla-Monge, E. Di Cesare, A. Nemajerova, and U. M. Moll (2020). Statin as anti-cancer therapy in autochthonous T-lymphomas expressing stabilized gain-of-function mutant p53 proteins. *Cell Death & Disease* **11**, 274.

Unger, R. H. (1995). Lipotoxicity in the pathogenesis of obesity-dependent NIDDM. Genetic and clinical implications. *Diabetes* **44**, 863–70.

UniProt Consortium (2021). UniProt: the universal protein knowledgebase in 2021. *Nucleic Acids Research* **49**, D480–D489.

Urbano, F., M. Bugliani, A. Filippello, A. Scamporrino, S. Di Mauro, A. Di Pino, R. Scicali, D. Noto, A. M. Rabuazzo, M. Averna, et al. (2017). Atorvastatin but not pravastatin impairs mitochondrial function in human pancreatic islets and rat β-cells. Direct effect of oxidative stress. *Scientific Reports* **7**, 11863.

Vannini, N., V. Campos, M. Girotra, V. Trachsel, S. Rojas-Sutterlin, J. Tratwal, S. Ragusa, E. Stefanidis, D. Ryu, P. Y. Rainer, et al. (2019). The NAD-booster nicotinamide riboside potently stimulates hematopoiesis through increased mitochondrial clearance. *Cell Stem Cell* **24**, 405–418.e7.

Voynova, N. S., C. Roubaty, H. M. Vazquez, S. K. Mallela, C. S. Ejsing, and A. Conzelmann (2015). *Saccharomyces cerevisiae* isdependent on vesicular traffic between the Golgi apparatus and the vacuole when inositolphosphorylceramide synthase Aur1 is inactivated. *Eukaryotic Cell* **14**, 1203–16.

Wagih, O. and L. Parts (2014). gitter: a robust and accurate method for quantification of colony sizes from plate images. *Genes, Genomes, Genetics* **4**, 547–52.

Wagih, O., M. Usaj, A. Baryshnikova, B. VanderSluis, E. Kuzmin, M. Costanzo, C. L. Myers, B. J. Andrews, C. M. Boone, and L. Parts (2013). SGAtools: one-stop analysis and visualization of array-based genetic interaction screens. *Nucleic Acids Research* **41**, W591–6.

Waliullah, T. M., A. M. Yeasmin, A. Kaneko, N. Koike, M. Terasawa, T. Totsuka, and T. Ushimaru (2017). Rim15 and Sch9 kinases are involved in induction of autophagic degradation of ribosomes in budding yeast. *Bioscience, biotechnology, and biochemistry* **81**, 307–310.

Walker, M. E., T. D. Nguyen, T. Liccioli, F. Schmid, N. Kalatzis, J. F. Sundstrom, J. M. Gardner, and V. Jiranek (2014). Genome-wide identification of the Fermentome; genes required for successful and timely completion of wine-like fermentation by *Saccharomyces cerevisiae*. *BMC Genomics* **15**, 552.

Wang, C. W., J. Kim, W. P. Huang, H. Abeliovich, P. E. Stromhaug, W. A. Dunn, and D. J. Klionsky (2001). Apg2 is a novel protein required for the cytoplasm to vacuole targeting, autophagy, and pexophagy pathways. *The Journal of Biological Chemistry* **276**, 30442–51.

Wang, D., H. Wang, and X. Zou (2017). Identifying key nodes in multilayer networks based on tensor decomposition. *Chaos* **27**, 063108.

Wang, H. J., J. Y. Park, O. Kwon, E. Y. Choe, C. H. Kim, K. Y. Hur, M.-S. Lee, M. Yun, B. S. Cha, Y.-B. Kim, et al. (2015). Chronic HMGCR/HMG-CoA reductase inhibitor treatment contributes to dysglycemia by upregulating hepatic gluconeogenesis through autophagy induction. *Autophagy* **11**, 2089–2101.

Wang, J., C. Tang, C. Yang, Q. Zheng, and Y. Hou (2019a). Tropomyosin-1 functions as a tumor suppressor with respect to cell proliferation, angiogenesis and metastasis in renal cell carcinoma. *Journal of Cancer* **10**, 2220–2228.

Wang, J. and G. S. Wu (2014). Role of autophagy in cisplatin resistance in ovarian cancer cells. *The Journal of Biological Chemistry* **289**, 17163–73.

Wang, K., T. A. Gerke, X. Chen, and M. Prosperi (2019b). Association of statin use with risk of Gleason score-specific prostate cancer: A hospital-based cohort study. *Cancer Medicine* **8**, 7399–7407.

Wang, L., G. Lu, and H.-M. Shen (2020). The long and the short of PTEN in the regulation of mitophagy. *Frontiers in Cell and Developmental Biology* **8**, 299.

Wang, T., S. Seah, X. Loh, C.-W. Chan, M. Hartman, B.-C. Goh, and S.-C. Lee (2016). Simvastatin-induced breast cancer cell death and deactivation of PI3K/Akt and MAPK/ERK signalling are reversed by metabolic products of the mevalonate pathway. *Oncotarget* **7**, 2532–44.

Warde-Farley, D., S. L. Donaldson, O. Comes, K. Zuberi, R. Badrawi, P. Chao, M. Franz, C. Grouios, F. Kazi, C. T. Lopes, et al. (2010). The GeneMANIA prediction server: biological network integration for gene prioritization and predicting gene function. *Nucleic Acids Research* **38**, W214–20.

Waters, D. D., J. E. Ho, S. M. Boekholdt, D. A. DeMicco, J. J. P. Kastelein, M. Messig, A. Breazna, and T. R. Pedersen (2013). Cardiovascular event reduction versus new-onset diabetes during atorvastatin therapy: effect of baseline risk factors for diabetes. *Journal of the American College of Cardiology* **61**, 148–52.

Watson, R. T. and J. E. Pessin (2006). Bridging the GAP between insulin signaling and GLUT4 translocation. *Trends in Biochemical Sciences* **31**, 215–22.

Wei, M., P. Fabrizio, J. Hu, H. Ge, C. Cheng, L. Li, and V. D. Longo (2008). Life span extension by calorie restriction depends on Rim15 and transcription factors downstream of Ras/PKA, Tor, and Sch9. *PLoS Genetics* **4**, e13.

Weir, C. B. and J. K. Le (2021). *Metronidazole.* StatPearls Publishing, 1807–1849.

Wenner Moyer, M. (2010). The search beyond statins. *Nature Medicine* **16**, 150–3.

Wheaton, W. W., S. E. Weinberg, R. B. Hamanaka, S. Soberanes, L. B. Sullivan, E. Anso, A. Glasauer, E. Dufour, G. M. Mutlu, G. S. Budigner, et al. (2014). Metformin inhibits mitochondrial complex I of cancer cells to reduce tumorigenesis. *eLife* **3**, e02242.

Wickham, H. (2016). *ggplot2 - elegant graphics for data analysis.*

Williams, M. L., G. K. Menon, and K. P. Hanley (1992). HMG-CoA reductase inhibitors perturb fatty acid metabolism and induce peroxisomes in keratinocytes. *Journal of Lipid Research* **33**, 193–208.

Winzeler, E. A., D. D. Shoemaker, A. Astromoff, H. Liang, K. Anderson, B. Andre, R. Bangham, R. Benito, J. D. Boeke, H. Bussey, et al. (1999). Functional characterization of the S. cerevisiae genome by gene deletion and parallel analysis. *Science* **285**, 901–6.

Wong, C. C., Y. Qian, X. Li, J. Xu, W. Kang, J. H. Tong, K.-F. To, Y. Jin, W. Li, H. Chen, et al. (2016). SLC25A22 promotes proliferation and survival of colorectal cancer cells with KRAS mutations and xenograft tumor progression in mice via intracellular synthesis of aspartate. *Gastroenterology* **151**, 945–960.e6.

Wong, W. W.-L., J. W. Clendening, A. Martirosyan, P. C. Boutros, C. Bros, F. Khosravi, I. Jurisica, A. K. Stewart, P. L. Bergsagel, and L. Z. Penn (2007). Determinants of sensitivity to lovastatin-induced apoptosis in multiple myeloma. *Molecular Cancer Therapeutics* **6**, 1886–97.

Wong, W. W., M. M. Tan, Z. Xia, J. Dimitroulakos, M. D. Minden, and L. Z. Penn (2001). Cerivastatin triggers tumor-specific apoptosis with higher efficacy than lovastatin. *Clinical Cancer Research* **7**, 2067–75.

Wouters, B. G. and M. Koritzinsky (2008). Hypoxia signalling through mTOR and the unfolded protein response in cancer. *Nature Reviews Cancer* **8**, 851–64.

Xia, J., E. E. Gill, and R. E. W. Hancock (2015). NetworkAnalyst for statistical, visual and network-based meta-analysis of gene expression data. *Nature Protocols* **10**, 823–44.

Xie, Y., E. M. Rubenstein, T. Matt, and M. Hochstrasser (2010). SUMO-independent in vivo activity of a SUMO-targeted ubiquitin ligase toward a short-lived transcription factor. *Genes & Development* **24**, 893–903.

Xie, Z., A. Bailey, M. V. Kuleshov, D. J. B. Clarke, J. E. Evangelista, S. L. Jenkins, A. Lachmann, M. L. Wojciechowicz, E. Kropiwnicki, K. M. Jagodnik, et al. (2021). Gene set knowledge discovery with Enrichr. *Current Protocols* **1**, e90.

Yaluri, N., S. Modi, M. López Rodríguez, A. Stančáková, J. Kuusisto, T. Kokkola, and M. Laakso (2015). Simvastatin impairs insulin secretion by multiple mechanisms in MIN6 cells. *PloS One* **10**, e0142902.

Yan, M.-M., J.-D. Ni, D. Song, M. Ding, and J. Huang (2015). Interplay between unfolded protein response and autophagy promotes tumor drug resistance. *Oncology Letters* **10**, 1959–1969.

Yanae, M., M. Tsubaki, T. Satou, T. Itoh, M. Imano, Y. Yamazoe, and S. Nishida (2011). Statin-induced apoptosis via the suppression of ERK1/2 and Akt activation by inhibition of the

geranylgeranyl-pyrophosphate biosynthesis in glioblastoma. *Journal of Experimental & Clinical Cancer Research* **30**, 74.

Yang, P.-M. and C.-C. Chen (2011). Life or death? Autophagy in anticancer therapies with statins and histone deacetylase inhibitors. *Autophagy* **7**, 107–8.

Yang, P.-M., Y.-L. Liu, Y.-C. Lin, C.-T. Shun, M.-S. Wu, and C.-C. Chen (2010). Inhibition of autophagy enhances anticancer effects of atorvastatin in digestive malignancies. *Cancer Research* **70**, 7699–709.

Ye, Y., M. Fujii, A. Hirata, M. Kawamukai, C. Shimoda, and T. Nakamura (2007). Geranylgeranyl diphosphate synthase in fission yeast is a heteromer of farnesyl diphosphate synthase (FPS), Fps1, and an FPS-like protein, Spo9, essential for sporulation. *Molecular Biology of the Cell* **18**, 3568–81.

Yokoyama, C., X. Wang, M. R. Briggs, A. Admon, J. Wu, X. Hua, J. L. Goldstein, and M. S. Brown (1993). SREBP-1, a basic-helix-loop-helix-leucine zipper protein that controls transcription of the low density lipoprotein receptor gene. *Cell* **75**, 187–97.

Yoo, M., J. Shin, J. Kim, K. A. Ryall, K. Lee, S. Lee, M. Jeon, J. Kang, and A. C. Tan (2015). DSigDB: drug signatures database for gene set analysis. *Bioinformatics* **31**, 3069–71.

Yoon, J., A. Blumer, and K. Lee (2006). An algorithm for modularity analysis of directed and weighted biological networks based on edge-betweenness centrality. *Bioinformatics* **22**, 3106–8.

Yu, H., P. M. Kim, E. Sprecher, V. Trifonov, and M. Gerstein (2007). The importance of bottlenecks in protein networks: correlation with gene essentiality and expression dynamics. *PLoS Computational Biology* **3**, e59.

Yuan, Q., C. D. Dong, Y. Ge, X. Chen, Z. Li, X. Li, Q. Lu, F. Peng, X. Wu, J. Zhao, et al. (2019). Proteome and phosphoproteome reveal mechanisms of action of atorvastatin against esophageal squamous cell carcinoma. *Aging* **11**, 9530–9543.

Zanconato, F., G. Battilana, M. Cordenonsi, and S. Piccolo (2016). YAP/TAZ as therapeutic targets in cancer. *Current Opinion in Pharmacology* **29**, 26–33.

Zavrel, M., S. J. Hoot, and T. C. White (2013). Comparison of sterol import under aerobic and anaerobic conditions in three fungal species, *Candida albicans*, *Candida glabrata*, and *Saccharomyces cerevisiae*. *Eukaryotic Cell* **12**, 725–38.

Zeigerer, A., M. A. Lampson, O. Karylowski, D. D. Sabatini, M. Adesnik, M. Ren, and T. E. McGraw (2002). GLUT4 retention in adipocytes requires two intracellular insulin-regulated transport steps. *Molecular Biology of the Cell* **13**, 2421–35.

Zelcer, N., L. J. Sharpe, A. Loregger, I. Kristiana, E. C. L. Cook, L. Phan, J. Stevenson, and A. J. Brown (2014). The E3 ubiquitin ligase MARCH6 degrades squalene monooxygenase and affects 3-hydroxy-3-methyl-glutaryl coenzyme A reductase and the cholesterol synthesis pathway. *Molecular and Cellular Biology* **34**, 1262–70.

Zeman, E. M., J. M. Brown, M. J. Lemmon, V. K. Hirst, and W. W. Lee (1986). SR-4233: a new bioreductive agent with high selective toxicity for hypoxic mammalian cells. *International Journal of Radiation Oncology, Biology, Physics* **12**, 1239–42.

Zhang, N. and L. Cao (2017). Starvation signals in yeast are integrated to coordinate metabolic reprogramming and stress response to ensure longevity. *Current Genetics* **63**, 839–843.

Zhang, Y. P., X. J. Chen, Y. Y. Li, and H. Fukuhara (1992). *LEU2* gene homolog in *Kluyveromyces lactis*. *Yeast* **8**, 801–4.

Zhang, Z., L. Zhou, N. Xie, E. C. Nice, T. Zhang, Y. Cui, and C. Huang (2020). Overcoming cancer therapeutic bottleneck by drug repurposing. *Signal Transduction and Targeted Therapy* **5**, 113.

Zhang, Z., S. Zhao, Z. Yao, L. Wang, J. Shao, A. Chen, F. Zhang, and S. Zheng (2017). Autophagy regulates turnover of lipid droplets via ROS-dependent Rab25 activation in hepatic stellate cell. *Redox Biology* **11**, 322–334.

Zhao, Y., J. Hu, G. Miao, L. Qu, Z. Wang, G. Li, P. Lv, D. Ma, and Y. Chen (2013). Transmembrane protein 208: a novel ER-localized protein that regulates autophagy and ER stress. *PloS One* **8**, e64228.

Zhou, G., O. Soufan, J. Ewald, R. E. W. Hancock, N. Basu, and J. Xia (2019). NetworkAnalyst 3.0: a visual analytics platform for comprehensive gene expression profiling and meta-analysis. *Nucleic Acids Research* **47**, W234–W241.

Zhou, J., W. Li, Q. Xie, Y. Hou, S. Zhan, X. Yang, X. Xu, J. Cai, and Z. Huang (2014). Effects of simvastatin on glucose metabolism in mouse MIN6 cells. *Journal of diabetes research* **2014**, 376570.

Zhou, J., G. Li, Y. Zheng, H.-M. Shen, X. Hu, Q.-L. Ming, C. Huang, P. Li, and N. Gao (2015). A novel autophagy/mitophagy inhibitor liensinine sensitizes breast cancer cells to chemotherapy through DNM1L-mediated mitochondrial fission. *Autophagy* **11**, 1259–79.

Zhou, T.-Y., L.-H. Zhuang, Y. Hu, Y.-L. Zhou, W.-K. Lin, D.-D. Wang, Z.-Q. Wan, L.-L. Chang, Y. Chen, M.-D. Ying, et al. (2016). Inactivation of hypoxia-induced YAP by statins overcomes hypoxic resistance tosorafenib in hepatocellular carcinoma cells. *Scientific Reports* **6**, 30483.

Zhu, J., X. Jiang, and F. F. Chehab (2014). FoxO4 interacts with the sterol regulatory factor SREBP2 and the hypoxia inducible factor HIF2α at the CYP51 promoter. *Journal of Lipid Research* **55**, 431–42.

Zinnah, K. M. A., J.-W. Seol, and S.-Y. Park (2020). Inhibition of autophagy flux by sertraline attenuates TRAIL resistance in lung cancer via death receptor 5 upregulation. *International Journal of Molecular Medicine* **46**, 795–805.

Zitomer, R. S., M. P. Limbach, A. M. Rodriguez-Torres, B. Balasubramanian, J. Deckert, and P. M. Snow (1997). Approaches to the study of Rox1 repression of the hypoxic genes in the yeast *Saccharomyces cerevisiae*. *Methods* **11**, 279–88.